Pharmacological disruption of RNA splicing inhibits ovarian cancer growth and synergises with PARP inhibitors

Yuewei Xu

Department of Surgery and Cancer

Imperial College London

October 2022

A thesis submitted for the degree of Doctor of Philosophy

Statement of originality

I declare that this thesis is the result of my own work, and any work done in collaboration has been clearly acknowledged.

Copyright declaration

The copyright of this thesis rests with the author. Unless otherwise indicated, its contents are licensed under a Creative Commons Attribution-Non Commercial 4.0 International Licence (CC BY-NC).

Under this licence, you may copy and redistribute the material in any medium or format. You may also create and distribute modified versions of the work. This is on the condition that: you credit the author and do not use it, or any derivative works, for a commercial purpose.

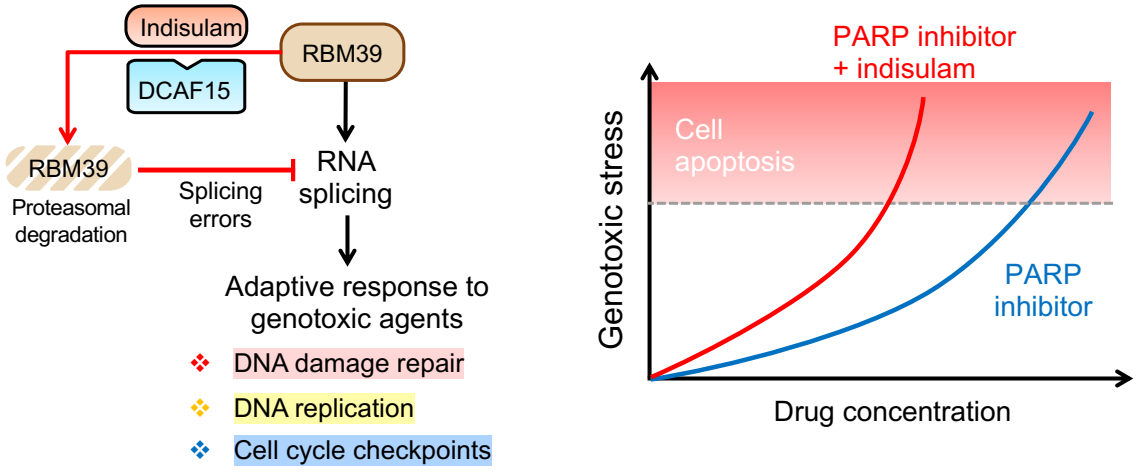
When reusing or sharing this work, ensure you make the licence terms clear to others by naming the licence and linking to the licence text. Where a work has been adapted, you should indicate that the work has been changed and describe those changes.

Please seek permission from the copyright holder for uses of this work that are not included in this licence or permitted under UK Copyright Law.

Abstract

High-grade serous ovarian cancer is the most common and lethal subtype of ovarian cancer with limited therapeutic options. Although PARP inhibitor maintenance therapy has shown considerable clinical benefits in ovarian cancer patients, the emergence of acquired drug resistance is a major challenge. Splicing factors coordinate splicing of pre-mRNAs, and they have been implicated in many biological processes including DNA repair. The splicing factor RBM39, in particular, is a promising cancer target, which can be rapidly depleted using the newly identified molecular glue indisulam. In this thesis, I characterised the role of RBM39 in HGSOC cells and found that RBM39 mediates the adaptive response to PARP inhibitors. Indisulam promotes the recruitment of RBM39 to the DCAF15-associated E3 ubiquitin ligase complex, leading to polyubiquitination and proteasomal degradation of RBM39. In HGSOC cells, loss of RBM39 caused widespread splicing defects and significantly reduced protein expression of many DNA repair genes, leading to growth inhibition and increased sensitivity to PARP inhibition *in vitro* and *in vivo*. Indisulam suppressed olaparib-induced activation of the ATM-Chk2 and Chk1 signalling pathways, resulting in higher levels of DNA damage, replication abnormalities, and apoptosis. Using a variety of HGSOC models, I showed that indisulam synergises with multiple PARP inhibitors in a *DCAF15*-dependent manner regardless of *BRCA* status. Overall, data from this thesis suggest that depleting RBM39 with indisulam is a promising therapeutic strategy to improve PARP inhibitor response in patients with HGSOC, which may benefit a wide range of patients irrespective of *BRCA* status.

Graphical abstract



Acknowledgements

Firstly, I thank my supervisors, Professor Hector Keun and Dr Anke Nijhuis, for giving me the chance to work on this exciting project and for their tremendous support and guidance over the past four years. I also thank all current and past group members, especially Chiharu Wickremesinghe, Michael Gruet, Flora Upton, and Yitao Xu, for critically reviewing my research and helping me during difficult times. My PhD study is funded by a joint scholarship of Imperial College London and China Scholarship Council.

I want to thank Professor Iain McNeish, Dr Sarah Spear, Dr Carmen Aguirre Hernandez, and Fabio Grundland Freile for their support in designing, conducting, and analysing animal studies. Thank you to all animal technicians at the Central Biomedical Services, particularly Roxanne Wood, Bonnie Glen, and Chantelle Day, for supporting the animal studies. I also want to thank Dr Alex Montoya and Dr Holger Kramer (now at the University of Oxford) at the Medical Research Council London Institute of Medical Sciences for carrying out the proteomics analysis.

I owe everything to my parents, who stand by my side all the time. And to my little sisters, thank you for making me laugh when I was feeling down.

Finally, I dedicate this thesis to my lovely wife, Xiaoyu Zhang, for without her support, I would not have had enough energy and sanity to finish my study.

Publications

XU, Y., MA, Y., SPEAR, S., MONTOYA, A., KRAMER, H., DRAGUNAITE, B., GRUET, M., UPTON, F., XU, Y., WICKREMESINGHE, C., MCNEISH, I., NIJHUIS, A. & KEUN, H. C. Pharmacological depletion of RNA splicing factor RBM39 synergizes with PARP inhibitors in ovarian cancer. (In preparation, aiming to submit in December 2022 to the journal Science Translational Medicine.)

NIJHUIS, A., SIKKA, A., YOGEV, O., HERENDI, L., BALCELLS, C., MA, Y., POON, E., ECKOLD, C., VALBUENA, G. N., **XU, Y.,** LIU, Y., DA COSTA, B. M., GRUET, M., WICKREMESINGHE, C., BENITO, A., KRAMER, H., MONTOYA, A., CARLING, D., WANT, E. J., JAMIN, Y., CHESLER, L. & KEUN, H. C. 2022. Indisulam targets RNA splicing and metabolism to serve as a therapeutic strategy for high-risk neuroblastoma. *Nature Communications*, 13, 1380.

XU, Y., NIJHUIS, A. & KEUN, H. C. 2020. RNA-binding motif protein 39 (RBM39): An emerging cancer target. *Br J Pharmacol.*

Contents

Table of Contents

Abstract *3*

Graphical abstract *3*

Acknowledgements *4*

Publications *5*

Abbreviations *15*

Chapter 1. Introduction *18*

1.1. Ovarian cancer **18**

1.1.1. Clinical characteristics of ovarian cancer 18

1.1.2. Subtypes of ovarian cancer 18

1.1.3. Clinical interventions for ovarian cancer 20

1.2. PARP inhibitors **20**

1.2.1. Main mechanisms of action 20

1.2.2. Synthetic lethality between PARP inhibition and HR deficiency 22

1.2.3. PARP inhibitors in the clinic 23

1.2.4. Similarities and differences in PARP inhibitors 28

1.2.5. PARP inhibitor resistance 32

1.2.6. Combination therapies 34

1.3. Alternative splicing **38**

1.3.1. Alternative splicing is an emerging cancer vulnerability 38

1.3.2. RBM39 is a promising cancer target 41

1.3.3. Targeting RBM39 with molecular glues 43

1.4. Hypothesis and aims **46**

1.4.1. Improving PARP inhibitor response by targeting splicing factors 46

1.4.2. Preliminary data 47

1.4.3. Hypothesis and aims 49

Chapter 2. Materials and Methods *50*

2.1. Drug preparation **50**

2.2. Cell lines **50**

2.3. PCR-based alternative splicing analysis **51**

Contents

2.4. Protein Extraction 53

2.5. Western blot 53

2.6. Human phospho-kinase array 54

2.7. Sulforhodamine B cell growth assay 55

2.8. Colony growth assay 55

2.9. Cell apoptosis assays 56

2.9.1. Caspase-Glo 3/7 activation assay 56

2.9.2. Annexin V-Propidium Iodide staining assay 57

2.10. Drug combination and synergy analysis 57

2.10.1. Synergy analysis using the Chou-Talalay method 57

2.10.2. Drug combination screen using the Bliss Independence 58

2.11. *In vivo* studies using the ID8 murine HGSOC model 58

2.12. Immunofluorescence analysis 60

2.13. Single-cell gel electrophoresis (COMET assay) 61

2.13.1. Alkaline COMET assay 61

2.13.2. Neutral COMET assay 62

2.14. Cell cycle analysis 62

2.15. DNA fibre analysis 63

2.16. RNA sequencing and proteomics analysis 65

2.16.1. RNA sequencing 65

2.16.2. Proteomics analysis 65

2.16.3. Venn diagrams, functional annotation, and enrichment analysis 66

2.17. Systematic literature analysis 67

2.17.1. Identifying RBM39-associated alternative splicing events 67

2.17.2. Identifying determinants for PARP inhibitor sensitivity 67

2.18. Statistical analysis 68

Chapter 3. Evaluating the therapeutic value of indisulam in ovarian cancer 70

3.1. RBM39 regulates RNA splicing of DNA damage repair genes 70

3.1.1. Systematic analysis of RBM39-associated alternative splicing events 70

3.1.2. Indisulam causes alternative splicing of DNA damage repair genes in HGSOC 73

3.2. Indisulam synergises with cisplatin in HGSOC cells 77

Contents

3.3. Indisulam synergises with multiple PARP inhibitors in HGSOC cells..... 79

3.3.1. Indisulam and olaparib cause synergistic growth inhibition and cell apoptosis.....79

3.3.2. Indisulam synergises with multiple PARP inhibitors irrespective of *BRCA*-status 83

3.3.3. DCAF15 is necessary for the synergy between indisulam and PARP inhibitors.....86

3.4. A large-scale drug combination screen reveals novel synergy between indisulam and FDA-approved anti-cancer drugs..... 88

3.5. Discussion 92

Chapter 4. Evaluating the combined effect of indisulam and olaparib in the ID8 murine model of HGSOC 96

4.1. Validating the synergy of indisulam and olaparib in ID8 models *in vitro*..... 96

4.2. Investigating the tolerability of indisulam and olaparib *in vivo* 99

4.2.1. Optimising drug formulations for *in vivo* administration 99

4.2.2. The combination of indisulam and olaparib shows signs of tumour suppressive effect in ID8-*Trp53*$^{-/-}$ tumours *in vivo*.....100

4.2.3. Indisulam and olaparib combination perhaps inhibit growth of subcutaneous ID8 tumours. ...103

4.3. Indisulam improves survival benefits of olaparib in mice bearing HR-proficient ID8 tumours.....107

4.4. Discussion 111

Chapter 5. Investigating the synergy mechanisms between indisulam and olaparib. 114

5.1. The combination of indisulam and olaparib leads to DNA damage accumulation.....114

5.1.1. Indisulam partially inhibits olaparib-induced activation of ATM-Chk2 signalling.....114

5.1.2. Combination of indisulam and olaparib leads to a substantial increase in γH2AX levels.....118

5.1.3. Indisulam may exacerbate DNA damaging effect of olaparib 123

5.2. The combination of Indisulam and olaparib causes cell cycle arrest 127

5.3. The combination of Indisulam and olaparib causes replication stress 129

5.3.1. Indisulam and olaparib cause replication fork abnormalities when used in combination 129

5.3.2. The combination of indisulam and olaparib downregulates Chk1 expression 132

5.4. The combination of indisulam and olaparib increases γH2AX and downregulates ATM *in vivo* 134

5.5. Discussion 136

5.5.1. Indisulam reduces PARP inhibitor resistance by exacerbating olaparib-induced genotoxic stress 136

Contents

5.5.2. Indisulam synergises with olaparib by downregulating ATM expression and increasing DNA damage 139

5.5.3. Replication stress also contributes to the synergy between indisulam and olaparib 140

5.5.4. Indisulam, olaparib, and the combination therapy cause cell cycle arrest.....141

5.5.5. Limitations and Future work.....142

5.5.6. Conclusion 146

Chapter 6. Assessing the impact of indisulam and olaparib on HGSOC transcriptome and proteome 147

6.1. Overview of the transcriptomic and proteomic analysis 147

6.2. Indisulam disrupts alternative splicing of DNA repair and replication genes 150

6.2.1. Indisulam treatment leads to mis-splicing in cell cycle and DNA damage repair genes.....150

6.2.2. Most proteins downregulated by indisulam are splicing targets of RBM39.....152

6.2.3. Indisulam may increase PARP inhibitor response by downregulating DNA repair proteins.....153

6.2.4. Indisulam downregulates protein expression of genes modulating PARP inhibitor sensitivity – an untargeted analysis.....158

6.3. The ID8 model recapitulates indisulam-mediated splicing and proteomic changes in human HGSOC cells.....163

6.4. Olaparib may also modulate protein expression through splicing changes.....166

6.5. Protein changes exclusive to the combination of indisulam and olaparib.....168

6.6. Discussion 170

Chapter 7. Final discussion and future directions 175

7.1. Current model for the synergy between indisulam and PARP inhibitor 175

7.2. Gaps and future directions 179

7.2.1. What markers may predict the response of indisulam and its synergy with PARP inhibitors? ..179

7.2.2. Does indisulam reduce DNA damage repair capacity? 180

7.2.3. Does the combination of indisulam and olaparib cause replication catastrophe? 180

7.2.4. How important are ATM and Chk1 changes in the synergy?.....181

7.2.5. Does indisulam-induced splicing errors generate novel protein isoforms and neoantigens?....181

7.2.6. Does RBM39 interact directly with PARP1?.....182

7.2.7. Could indisulam increase PARP inhibitor response by depleting the nucleotide pool? 183

7.2.8. Does the synergy involve RBM39 as a transcriptional coregulator? 183

7.2.9. Other limitations and future works 184

7.3. Concluding remarks 185

Contents

References *187*

Appendix *232*

1. Appendix Figures and Tables **232**

2. Appendix Materials and Methods **234**

2.1. Proteomics analysis 234

3. Appendix Discussion **237**

3.1. Rationale for drug combination therapy 237

3.2. Bliss independence model 238

3.3. Loewe additivity 239

3.4. Chou-Talalay method 241

3.5. Re-defining synergy with advanced models 242

3.6. Challenges in synergy analysis 244

4. Copyright permissions **245**

List of Figures

Figure 1.1. Classification of ovarian cancer. 19

Figure 1.2. PARP inhibitor treatment is synthetically lethal with homologous recombination deficiency. 23

Figure 1.3. Mechanisms of alternative pre-mRNA splicing. 39

Figure 1.4. RBM39 is a member of the U2AF-like family protein. 42

Figure 1.5. Anti-cancer aryl sulphonamides cause selective RBM39 degradation by DCAF15. 44

Figure 1.6. DCAF15 amplification is common in ovarian cancer and correlates with higher indisulam sensitivity. 48

Figure 3.1. Pathway enrichment analysis of commonly mis-spliced genes after RBM39 depletion. 72

Figure 3.2. Indisulam causes RBM39 degradation and splicing errors of DNA repair genes in HGSOC. 76

Contents

Figure 3.3. Indisulam increases cisplatin response in cisplatin-resistant HGSOC cells. 78

Figure 3.4. Indisulam synergises with olaparib in HGSOC cells. 80

Figure 3.5. Indisulam and olaparib synergistically inhibit OVSAHO colony growth..... 82

Figure 3.6. Indisulam synergises with multiple PARP inhibitors in HGSOC cells..... 84

Figure 3.7. Indisulam synergises with PARP inhibitors irrespective of *BRCA2* status. 85

Figure 3.8. DCAF15 is necessary for the synergy between RBM39 degraders and PARP inhibitors. 87

Figure 3.9. Overview of the screen combining indisulam with a panel of FDA-approved drugs. 90

Figure 3.10. Drug combination screen between indisulam and a panel of FDA-approved drugs. 91

Figure 4.1. ID8 model recapitulates peritoneal metastasis in human HGSOC. 97

Figure 4.2. Indisulam and E7820 synergise with olaparib in ID8 cells. 98

Figure 4.3. Suspensions of olaparib and indisulam under a microscope..... 100

Figure 4.4. The combination of indisulam and olaparib shows signs of anti-tumour effect in the HR-proficient ID8 model..... 102

Figure 4.5. Olaparib reduces subcutaneous tumour formation in the *Brca2*-deficient ID8 model. 106

Figure 4.6. Indisulam and olaparib reduces subcutaneous tumour development in the HR-proficient ID8 model..... 107

Figure 4.7. Indisulam improves olaparib response in HR-proficient ID8 mice. 110

Figure 5.1. Indisulam reduces olaparib-induced Chk2 activation in HGSOC cells. 115

Figure 5.2. Indisulam downregulates ATM expression and partially inhibits activation of the ATM-Chk2 pathway. 117

Figure 5.3. Indisulam leads to the accumulation of γH2AX foci in HGSOC cells. 120

Figure 5.4. The combination of Indisulam and PARP inhibitors leads to increased γH2AX foci formation in HGSOC cells. 121

Contents

Figure 5.5. The combination of indisulam and olaparib increases γH2AX expression. 122

Figure 5.6. Alkaline COMET assay successfully detects doxorubicin-induced DNA damage. 125

Figure 5.7. Indisulam increases olaparib-induced DNA damage in KURAMOCHI cells. 126

Figure 5.8. The combination of indisulam and olaparib causes cell cycle arrest at the S and G2/M phases. 128

Figure 5.9. The addition of indisulam to olaparib causes replication abnormalities. 131

Figure 5.10. The combination of indisulam and olaparib downregulates Chk1 in HGSOC cells. 133

Figure 5.11. The combination of indisulam and olaparib increases γH2AX and reduces Atm expression in the ID8 murine HGSOC model. 135

Figure 5.12. A simple model for the synergy between indisulam and PARP inhibitor(s). 136

Figure 5.13. A detailed model showing indisulam increases PARP inhibitor response in HGSOC cells. 138

Figure 6.1. Overview of the transcriptomic and proteomic analyses in human and mouse HGSOC cells. 149

Figure 6.2. Indisulam causes aberrant splicing in cell cycle and DNA damage repair genes. 151

Figure 6.3. Indisulam downregulates protein expression mainly by inducing splicing errors. 152

Figure 6.4. Many DNA repair genes modulated by indisulam are outside the proteomics coverage. 154

Figure 6.5. Indisulam downregulates protein expression of multiple DNA repair genes. 157

Figure 6.6. Process of identifying articles for the systematic literature review. 160

Figure 6.7. Indisulam downregulates genes known to increase PARP inhibitor response upon depletion. 162

Figure 6.8. Indisulam causes similar effects in murine HGSOC cells as in human HGSOC cells. 164

Figure 6.9. Indisulam downregulates six key DNA repair genes in ID8-*Trp53*$^{-/-}$ cells. 165

Contents

Figure 6.10. Overlap in genes where splicing is disrupted by olaparib and indisulam. 167

Figure 6.11. Olaparib and indisulam regulate different splicing events within the same gene target. 167

Figure 6.12. Identification of proteins exclusively downregulated by the combination of indisulam and olaparib including Chk1. 169

Figure 7.1. Indisulam increases PARP inhibitor response by disrupting RBM39-mediated splicing. 176

List of Tables

Table 1.1 FDA and EMA indications of PARP inhibitors in ovarian cancer[a] 27

Table 1.2. PARP1-trapping potency and target specificity of PARP inhibitors 31

Table 2.1 List of drugs used in this thesis. 50

Table 2.2 Sources and culture conditions for cell lines. 51

Table 2.3 Primers used to validate exon skipping events. 52

Table 2.4 The PCR reaction program. 52

Table 2.5 Antibodies used for western blot. 54

Table 3.1. Characteristics of alternative splicing datasets included for RBM39 splicing analysis 71

Table 3.2. Examples of DNA damage repair genes mis-spliced upon RBM39 depletion. 73

Table 6.1. Functional annotation of the 25 DNA repair genes mis-spliced and downregulated (at protein levels) by indisulam. 155

Table 6.2. Characteristics of dropout CRISPR screens included for the systematic review.. 161

Contents

Lists of Figures, Tables, and Equations in the Appendix

Appendix Figure 1. Indisulam induces aberrant splicing DNA repair genes in HGSOC cells. 232

Appendix Figure 2. Validation of DCAF15-knockout in the PEO1 clones. 233

Appendix Figure 3. Synergistic efficacy and potency. 243

Appendix Figure 4. Index of achievable efficacy by the BRAID synergy model. 244

Appendix Table 1. Phospho-events detected in the human kinase array worth future investigation. 234

Appendix Equation 1 240

Appendix Equation 2 241

Abbreviations

Abbreviation	Definition
RBM39	RNA-binding motif protein 39
a.u.	Arbitrary unit
ABCB1	ATP binding cassette subfamily B member 1
AF488	Alexa Fluor 488 dye
AP-1	Activation protein-1
BPS	Branchpoint residue
BRAID	Bivariate Response to Additive Interacting Doses
BRC	Biomedical Research Centre
BRCA1/2	Breast cancer gene 1/2
BSA	Bovine serum albumin
53BP1	P53 binding protein 1
CA125	Cancer antigen 125
CDK	Cyclin-dependent kinase
CI	Combination index
CQS	Chloroquinoxaline sulphonamide
CtIP	C-terminal binding protein 1 interacting protein
CtIP	Terminal binding protein 1 interacting protein
DCAF15	DDB1- and CUL4- associated factor 15
DMSO	Dimethyl sulfoxide
DSBs	Double-stranded DNA breaks
EC50	Half-maximal effect
EMA	European Medicines Agency
EOC	Epithelial ovarian cancer
FA	Fluorescence anisotropy
FBS	Foetal bovine serum
FDA	U.S. Food & Drug Administration
FDR	False discovery rate
HGSOC	High-grade serous ovarian cancer
HR	Homologous recombination repair
HRD	Homologous recombination deficiency
HRP	Horseradish peroxidase
I.P.	Intraperitoneal injection
I.V.	Intravenous
IAE	Index of achievable efficacy
IC50	Concentration causing 50% growth inhibition
ISE/ESE	Intronic/exonic splicing enhancer
ISS/ESS	Intronic/exonic splicing silencer
KEGG	Kyoto Encyclopedia of Genes and Genomes

Abbreviations

LC-MS/MS	Liquid chromatography-tandem mass spectrometer
LFQ	Label-free quantification
LGSOC	Low-grade serous ovarian cancer
LMA	Low melting point agarose
MuSyc	Multi-dimensional synergy of combinations
NAD	Nicotinamide adenine dinucleotide
NEB	New England Biolabs
NHEJ	Non-homologous recombination repair
NMPA	China's National Medical Products Administration
ns	Not (statistically) significant
ORR	Objective response rate
OS	Overall survival
PAR	Poly-(ADP-ribose)
PARG	PAR glycohydrolase
PARP	poly-(ADP-ribose) polymerase
PBS	Phosphate-buffered saline
PCR	Polymerase chain reaction
PD-L1	Programmed death-ligand 1
PFS	Progression-free survival
PI	Propidium Iodide
Pre-mRNA	Precursor message RNA
PUF60	Poly(U)-binding splicing factor 60
R-loop	DNA-RNA hybrid
RPA	Replication protein A
RRM	RNA recognition motif
RS	Arginine-serine rich
S1981	Serine-1981
T68	Threonine-68
s.c.	Subcutaneous
S0	Artificial within groups variance
SD	Standard deviation
SDS	Sodium dodecyl sulfate
SEM	Standard error of mean
SF1	Splicing factor 1
SF3B1	Splicing factor 3b subunit 1
snRNP	Small nuclear ribonucleoprotein
SRB	Sulforhodamine
SSBs	Single-stranded DNA breaks
ssDNA	Single-stranded DNA
TBST	Tris-buffered saline with 0.1% of Tween-20
TCA	Trichloroacetic acid
TCGA	The Cancer Genome Atlas

Abbreviations

Tm	PCR annealing temperature
TNKS	Tankyrase
TNKS1	Tankyrase 1
TR-FRET	Time-resolved Förster resonance energy
TRIM27	Tripartite motif containing 27
TUDEL	TdT-dUTP DSB end labelling
TYMS	Thymidylate synthetase
U2AF	U2 auxiliary factor
UBCH8	E2 ubiquitin-conjugating enzyme L6
UHM	U2AF homology motif
ULM	UHM ligand motif
VEGF	Vascular endothelial growth factor
γH2AX	Phospho-histone H2A.X (Ser139)

Chapter 1. Introduction

1.1. Ovarian cancer

1.1.1. Clinical characteristics of ovarian cancer

Ovarian cancer is one of the most common and aggressive cancer in females worldwide, with a five-year survival rate of less than 50% (Stewart et al., 2019, Torre et al., 2018). In the United Kingdom, it affects 4% of newly diagnosed female cancer patients but accounts for up to 5% of cancer-related deaths in women, making it the most lethal gynaecological cancer (Cancer-Research-UK). Genetic mutations in the tumour suppressor genes *BReast CAncer gene 1* (*BRCA1*) and *BRCA2* are major genetic risk factors for ovarian cancer, increasing the risk from 2% in the general population to over 50% and 16.5%, respectively (Ingham et al., 2013, Mavaddat et al., 2013). Other risk factors include age (after 45 years old), more ovulation cycles, and endometriosis (Stewart et al., 2019).

No screening method for ovarian cancer is available yet. The cancer antigen 125 (CA125) was historically used as a biomarker for ovarian cancer screening, but it has failed to decrease ovarian cancer mortality due to low sensitivity and specificity (Charkhchi et al., 2020). Early diagnosis of ovarian cancer is also very challenging because the disease is often asymptomatic at stages I and II, and a definitive diagnosis is only possible through biopsies or surgery (ESMO, 2017). As a result, most patients are diagnosed at stage III or IV with a five-year survival rate of 26.9% and 13.4%, respectively (Cancer-research-UK). At the time of diagnosis, tumours may have metastasised to distant organs such as the omentum, liver and lungs (Stewart et al., 2019). Many patients also develop ascitic fluid (ascites) within the peritoneal cavity, which allows tumour cells to move readily throughout the abdominal cavity, leading to peritoneal carcinomatosis and rapid disease progression (Ford et al., 2020).

1.1.2. Subtypes of ovarian cancer

Ovarian cancer is a heterogeneous disease with multiple subtypes, and most tumours do not originate from ovaries (Figure 1.1). Three major histological origins have been identified: epithelial (>90%), germ cell (3%), and sex-cord stromal (<2%) (Stewart et al., 2019). Epithelial ovarian cancer (EOC) can be further stratified into five subtypes: high-grade serous (70% - 80%), low-grade serous (< 5%), clear-cell (10%), endometrioid (10%) and mucinous (3%) (Lisio

et al., 2019). High-grade serous ovarian cancer (HGSOC) is more aggressive than low-grade serous ovarian cancer (LGSOC) and other subtypes. Whilst LGSOC frequently occurs through malignant transformation of ovarian tissues, the origin of most HGSOC is found to be inflammatory fallopian tube epithelial tissues, which then spread to ovaries (Salvador et al., 2009, Kurman and Shih Ie, 2008, Kurman and Shih Ie, 2011, Kurman and Shih Ie, 2016, Kurman, 2013). Alternatively, subtypes of EOC can be divided into two categories based on the model proposed by Kurman and Shih Ie (2008). The type I EOC includes LGSOC, clear-cell and mucinous subtypes, characterised by a stable genome with wild-type *TP53* expression but frequent oncogenic mutations in signalling pathways such as RAS-MAPK and PI3K-AKT pathway (Kurman and Shih Ie, 2016). The type II EOC is dominated by the HGSOC, which harbours ubiquitous *TP53* loss-of-function, frequent defects in DNA repair pathways (Bell et al., 2011), extensive copy-number variations, and genome instability (Cheng et al., 2022, Kurman and Shih Ie, 2016). From a clinical perspective, type II EOCs are usually aggressive tumours with poor survival, while type I EOCs tend to be indolent tumours with a better prognosis (Kurman and Shih Ie, 2016). Overall, HGSOC is the most lethal subtype of ovarian cancer, and novel therapeutic interventions are needed to improve patient survival.

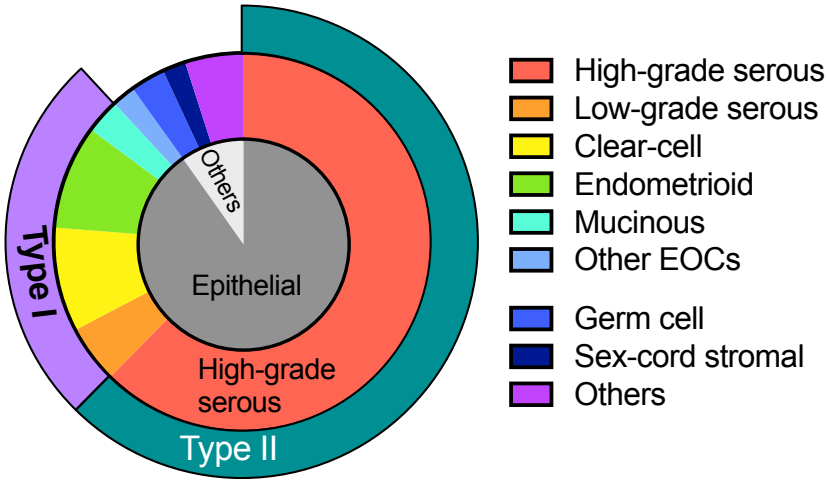


Figure 1.1. Classification of ovarian cancer.
Ovarian cancer contains many subtypes. According to histological features, epithelial ovarian cancer (EOC) is the most common type of ovarian cancer, and it is further divided into five major subtypes: high-grade serous, low-grade serous, clear-cell, endometrioid and mucinous (Lisio et al., 2019). A dualistic model has also been proposed, dividing epithelial ovarian cancer into type I and type II tumours (Kurman and Shih Ie, 2016). HGSOC is the most common form of type II EOC tumour, and abundant evidence suggests it mostly originates from the fallopian tube before disseminating to ovaries and other organs (Kurman, 2013).

1.1.3. Clinical interventions for ovarian cancer

Clinical interventions for ovarian cancer are influenced by the disease stages, age, and health status of patients. The first-line treatment for ovarian cancer typically involves surgical removal of tumour deposits and chemotherapies of platinum agents and taxanes (ESMO, 2017, Matulonis, 2018, Tsibulak et al., 2019). Cisplatin and carboplatin are classic examples of platinum-derived DNA damaging agents that crosslink DNA strands, interfering with DNA replication and inhibiting the proliferation of cancer cells (Dasari and Tchounwou, 2014). Taxanes such as paclitaxel and docetaxel are drugs that block cell division by disrupting microtubule function (Abal et al., 2003). The primary treatment is effective for approximately 70% of patients, but the disease often relapses within two years (Banerjee et al., 2021, Stewart et al., 2019). For recurrent ovarian cancer, chemotherapies and poly-(ADP-ribose) polymerase (PARP) inhibitors are commonly used, and some patients also receive a combination of chemotherapy and antiangiogenesis agents such as bevacizumab (Garcia and Singh, 2013, Lisio et al., 2019). Immunotherapies repeatedly failed to demonstrate satisfactory anti-cancer activities in ovarian cancer (Varga et al., 2019, Disis et al., 2019, Barber and Matei, 2021), despite the fact that immune checkpoint inhibitors have shown remarkable benefits in a broad range of cancer types (Esfahani et al., 2020). Overall, the lack of targeted therapies is one of the main drivers of the high case-mortality rate of ovarian cancer, which has only improved marginally since the introduction of platinum and taxanes in the clinic (Sopik et al., 2015), highlighting the urgent need for novel therapies.

1.2. PARP inhibitors

1.2.1. Main mechanisms of action

PARP inhibitors are small molecular inhibitors targeting PARP1- and PARP2-mediated sensing and repair of single-stranded DNA breaks (SSBs) [reviewed in (Rouleau et al., 2010, Konecny and Kristeleit, 2016)]. SSBs can arise spontaneously due to replication errors or DNA damaging agents such as radiation and cisplatin. The DNA binding domain of PARP1/2 allows rapid recruitment of PARPs to the damage site, and DNA binding activates their enzymatic function – catalysing the synthesis of poly-(ADP-ribose) chains (PARylation) using nicotinamide adenine dinucleotide^{+} (NAD^{+}) as a substrate (Durkacz et al., 1980, Alemasova and Lavrik, 2019). Targets of PARylation not only include downstream DNA damage repair factors but

also include PARP1 and PARP2 themselves (Vyas et al., 2014, Jungmichel et al., 2013). Low levels of auto-PARylation of PARP1/2 facilitate the recruitment of proteins required for SSBs repair, and further auto-PARylation increases the negative charges of PARPs and drives the dissociation of PARPs from negatively charged DNA strands, exposing the DNA lesion to repair proteins (Alemasova and Lavrik, 2019, Lindahl et al., 1995, Mortusewicz et al., 2007). Overlapping functions of PARP1 and PARP2 have been identified, but PARP1 accounts for 75-90% of PARylation and PARP-mediated DNA damage repair (Shieh et al., 1998, Sallmann et al., 2000).

As NAD^+ mimetics, PARP inhibitors block PARP-mediated DNA damage repair through catalytic inhibition and trapping PARP at the DNA damage site (Figure 1.2) (Murai et al., 2012, Murai et al., 2014, Hopkins et al., 2015, Zandarashvili et al., 2020). Trapped PARP shields the lesion from repair proteins and hinders DNA replication, leading to persistent SSBs and stalled replication forks (Murai et al., 2014, Murai et al., 2012, Hopkins et al., 2019, Hopkins et al., 2015, Wang et al., 2020). Catalytic inhibition and PARP trapping collectively contribute to the accumulation of SSBs that if unrepaired, can deteriorate into double-stranded DNA breaks (DSBs) during DNA replication. PARP inhibitors also induce DSBs by disrupting PARP1/2-mediated replication stress response. PARP1 binds to stalled replication forks and restarts them through MRE11, allowing DNA replication to continue (Bryant et al., 2009, Ying et al., 2012). PARP inhibition or knockdown increases fork stalling and breakage, causing DSBs formation – evidenced by ATM-mediated phosphorylation of H2AX (γH2AX), a marker for DSBs (Burma et al., 2001, Aguilar-Quesada et al., 2007, Bryant et al., 2009).

Persistent DSBs are cytotoxic and can lead to increased genome instability and cell apoptosis (Dale Rein et al., 2015, Ronson et al., 2018). Cells with defective homologous recombination repair (HR), a DSBs repair mechanism with high accuracy, are particularly sensitive to PARP inhibitor treatment (Bryant et al., 2005, Farmer et al., 2005). This synthetic lethal interaction between HR repair and PARP inhibition is discussed in the next section.

1.2.2. Synthetic lethality between PARP inhibition and HR deficiency

HR and non-homologous recombination (NHEJ) are two major DSB repair mechanisms (Scully et al., 2019). DSBs are detected by a protein complex involving DSB repair proteins MRE11, Nbs1 (NBN), and RAD50 (Rose et al., 2020). ATM is a pivotal kinase activated by the MRE11-complex, which then transduces the signal by phosphorylating a wide range of downstream targets such as Chk2, histone H2AX, P53 binding protein 1 (53BP1), and BRCA1 (Awasthi et al., 2015). Phosphorylated Chk2 activates cell cycle checkpoints and triggers cell cycle arrest, allowing time for damage repair (Stolz et al., 2011, Zannini et al., 2014). Phospho-H2AX (γH2AX) at the damage site provides a binding platform for DNA damage repair proteins (Sharma et al., 2012). Activated 53BP1 and BRCA1 compete for the damage sites, and the outcome determines the choice of repair mechanisms (Scully et al., 2019). When sister chromatids are available (during or shortly after DNA replication in the S phase), BRCA1 is preferentially recruited to the damage site, where it initiates high-fidelity repair of DSBs through HR. HR starts with the resection of broken DNA ends by the C-terminal binding protein 1 interacting protein (CtIP), generating overhangs of 3'-ended single-stranded DNA (ssDNA) (Scully et al., 2019). Then, the BRCA2-PALB2 complex is recruited to the DSBs and promotes RAD51 to displace replication protein A (RPA) on ssDNA (Scully et al., 2019). Loading of the RAD51 onto ssDNA overhangs requires the help of the BCDX2 complex consisting of RAD51 paralogs RAD51B, RAD51C, RAD51D, and XRCC2 (Chun et al., 2013, Suwaki et al., 2011). RAD51-coated ssDNA next binds to the complementary strand of the sister chromatid and uses it as a template for the faithful repair of DSBs (Scully et al., 2019). Alternatively, 53BP1 occupies DSBs and initiates the NHEJ pathway to repair DSBs. As NHEJ requires as little as four base pairs of sequence homology for two broken ends to be ligated (Pannunzio et al., 2018), it is susceptible to errors and may cause chromosome rearrangements and increase genome instability (Betermier et al., 2014).

HR-deficient cancer cells are viable but vulnerable to DNA damage, and HR deficiency (HRD) is synthetically lethal with pharmacological disruption of PARP1/2 (Figure 1.2) (Bryant et al., 2005, Farmer et al., 2005). Following PARP inhibitor treatment, SSBs accumulate in cancer cells, which leads to increased DSB formation during DNA replication (Rose et al., 2020, Taglialatela et al., 2017). In the absence of HR, cancer cells have to rely on the error-prone NHEJ pathway to repair DSBs, generating substantial genomic abnormalities and eventually

leading to cell apoptosis (Bryant et al., 2005, Farmer et al., 2005). This synthetically lethal relationship provides a scientific rationale for the clinical development of PARP inhibitors. In ovarian cancer, loss of *BRCA1* and *BRCA2* expression due to mutations or epigenetic silencing are the main sources of HRD, accounting for up to 23% and 11% of all HGSOC cases, respectively (Bowtell et al., 2015, Bell et al., 2011). Deleterious mutations in other genes, including *ATM* (1%), *ATR* (<1%), Fanconi amenia genes (<6%), and *PTEN* (7%), also contribute to HRD (Bell et al., 2011). Overall, approximately 50% of ovarian cancer patients have tumours with defective HR repair and may benefit from the synthetic lethality with PARP inhibitor treatment.

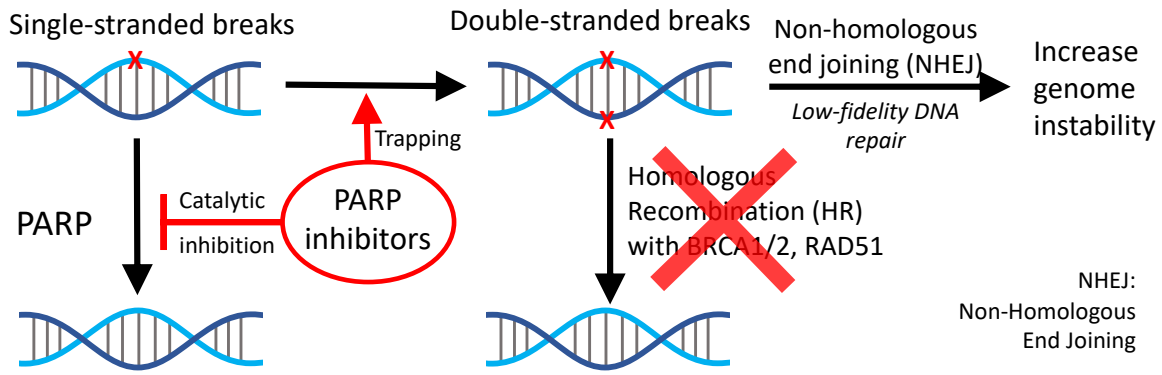


Figure 1.2. PARP inhibitor treatment is synthetically lethal with homologous recombination deficiency.
PARP inhibitors inhibit PARP-mediated repair of single-stranded breaks (SSBs) through catalytic inhibition, leading to persistent SSBs that may deteriorate into double-stranded breaks (DSBs) during DNA replication. Meanwhile, PARP inhibitors trap PARP at the site of DNA damage and the resultant PARP-DNA complex shields SSBs from DNA repair factors and cause replication stress, eventually leading to DSBs formation. Cells can repair DSBs accurately using the sister chromatid as a template via BRCA1/2- and RAD51-mediated homologous recombination (HR). Alternatively, DSBs can be repaired through the low-fidelity non-homologous end joining (NHEJ). Because NHEJ does not require a template, broken ends of DSBs may not be joined correctly, leading to chromosome rearrangements and increased genome instability. In tumours with HR deficiency (HRD), high levels of DSBs caused by PARP inhibitor treatment are repaired through the error-prone NHEJ, resulting in overwhelming genome instability and cell apoptosis.

1.2.3. PARP inhibitors in the clinic

Currently, three PARP inhibitors, including olaparib, niraparib, and rucaparib, have been approved as monotherapies or maintenance therapies for advanced ovarian cancer (Table 1.1). Olaparib (LYNPARZA®) was the first PARP inhibitor approved by the US Food & Drug Administration (FDA) in 2014 as a treatment for heavily-treated ovarian cancer patients with germline mutation of BRCA1 and BRCA2 (FDA, 2014). Study 42 was the key clinical trial that

led to the approval (Kim et al., 2015, AstraZeneca, 2014). This open-label, nonrandomised phase II trial recruited 193 patients who either had platinum-resistant ovarian cancer or were not suitable for further platinum therapy. Primary data found that the olaparib administration led to an objective response rate (ORR) of 31.1% in patients (Kaufman et al., 2015). After filtering for germline BRCA-mutated participants (137/193), olaparib treatment achieved an ORR of 46% in platinum-sensitive patients and achieved an ORR of 30% in platinum-resistant patients, demonstrating considerable anti-tumour activities (Domchek et al., 2016, Kim et al., 2015). In 2014, olaparib was also approved by the European Medicines Agency (EMA) as maintenance therapy for platinum-sensitive recurrent ovarian cancer with *BRCA1/2* mutations (EMA, 2014). This decision was made because olaparib significantly improved the median PFS of platinum-sensitive HGSOC patients from 4.3 months (placebo) to 11.2 months in the phase II clinical trial Study 19 (Ledermann et al., 2012, Ledermann et al., 2014). The same trend of improvements was reproduced in a more recent phase III trial (SOLO-2) (Pujade-Lauraine et al., 2017). In the SOLO-2 trial, olaparib maintenance therapy showed substantial survival benefits in *BRCA*-mutated patients with platinum-sensitive recurrent ovarian cancer, improving the overall survival (OS) from 38.8 months (placebo) to 51.7 months in the treatment group (Poveda et al., 2021, Poveda et al., 2020). As for newly diagnosed patients, olaparib was evaluated in a randomised, double-blinded phase III trial (SOLO-1) as the first-line maintenance therapy for newly diagnosed patients with *BRCA*-mutated stage III or IV ovarian cancer (95% were HGSOC). It reduced the risk of the three-year relapse rate by 70% (Moore et al., 2018) and improved the median progression-free survival (PFS) of patients from 13.8 months (placebo) to 56 months (Banerjee et al., 2021). As a result, olaparib was further approved by FDA (2018), EMA (2019), and China's National Medical Products Administration (NMPA, 2019) as first-line maintenance therapy for platinum-sensitive *BRCA*-mutated advanced ovarian cancer after completing the primary chemotherapy (FDA, 2018a, EMA, 2019a, AstraZeneca, 2019).

In 2020, niraparib (ZEJULA) became the second PARP inhibitor approved by both FDA and EMA as a first-line maintenance therapy for ovarian cancer under the same indication as olaparib (EMA, 2020, FDA, 2020). Niraparib was also approved by NMPA as a first-line maintenance therapy for newly diagnosed ovarian cancer patients and a maintenance treatment for patients with relapsed ovarian cancer (ZaiLab, 2020). These approvals were

primarily based on data from the PRIMA phase III trial, in which niraparib was used as a front-line maintenance therapy and improved median PFS from 10.4 months (placebo) to 21.9 months in HRD patients, and from 8.2 months (placebo) to 13.8 months when considering all participants regardless of their HRD status (Gonzalez-Martin et al., 2019).

Other PARP inhibitors have not been approved as first-line maintenance therapy for newly diagnosed patients. Rucaparib (RUBRACA) was approved by FDA as a monotherapy for BRCA-mutated ovarian cancer patients after two or more lines of chemotherapy (FDA, 2016) and it was approved by EMA as maintenance therapy for platinum-sensitive ovarian cancer (EMA, 2018). To the date of writing (July 2022), the only approval for Pamiparib in ovarian cancer was in 2021 by NMPA as a treatment for ovarian cancer patients with germline BRCA-mutations who have had two or more lines of chemotherapies (NMPA, 2021). Talazoparib (Talzenna) has been approved by FDA (FDA, 2018b) and EMA (EMA, 2019b) for HER2-negative and BRCA-mutated breast cancer, but not yet in ovarian cancer. Veliparib is in advanced clinical trials and has not received any official approval yet.

Multiple systematic reviews and network meta-analyses of clinical trials have shown that PARP inhibitors (olaparib, niraparib and rucaparib) offer substantial benefits in BRCA-mutated or HRD-positive ovarian cancer patients, in terms of prolonging PFS (Wang et al., 2021a, Xu et al., 2020a, Lin et al., 2021, Hao et al., 2021, Tomao et al., 2019, Staropoli et al., 2018) and extending overall survival (Yang et al., 2020, Luo et al., 2022). This is not surprising given the synthetic lethality between PARP inhibition and HRD. Interestingly, accumulating clinical evidence has revealed that PARP inhibitors are also beneficial for HRD-negative patients, albeit to a lesser extent than for HRD-positive patients (Wethington et al., 2021, Wang et al., 2021a, Yang et al., 2020, Lin et al., 2021). Four clinical trials (PRIMA, PAOLA-1, VELIA, and SOLO-1) reported that PARP inhibitors significantly improved the PFS in newly diagnosed ovarian cancer patients, not only in those with BRCA mutations and HRD (hazard ratio = 0.35 and 0.43, respectively), but also in those without BRCA mutations or HRD (hazard ratio = 0.72 and 0.83, respectively) (Lin et al., 2021). In the PRIMA study, niraparib treatment prolonged the median PFS of patients with HR-proficient tumours to 8.1 months, in comparison with 5.4 months in the placebo group (Gonzalez-Martin et al., 2019). Another example is the phase III VELIA trial, in which newly diagnosed HGSOC patients received veliparib as a part of the primary treatment and continued to receive it as a maintenance therapy (Coleman et al.,

2019). The data showed that veliparib improved median PFS to 15 months in patients with HR-proficient ovarian cancer, in comparison with 11.5 months in the control group (Coleman et al., 2019). A similar trend was observed in relapsed patients, where meta-analysis of PARP inhibitors in clinical trials revealed significant improvements in PFS in HRD-negative patients with hazard ratios ranging from 0.49-0.58 (Tomao et al., 2019, Wang et al., 2021a). The exact mechanism underlying the intriguing response of HR-proficient patients to PARP inhibitors is still undefined. Possible explanations include inaccurate characterisation of HRD status in patients, or off-target effects of PARP inhibitors – which will be discussed in the next section.

Chapter 1 – Introduction

Table 1.1 FDA and EMA indications of PARP inhibitors in ovarian cancer[a]

	FDA indications	EMA indications
Olaparib (LYNPARZA)	(1) As **first-line maintenance treatment** for ○ newly diagnosed ovarian cancer, ○ (and) germline or somatic *BRCA1/2*-mutated ○ (and) completed front-line chemotherapy with complete or partial response to platinum. (2) As **maintenance treatment** for ○ platinum-sensitive relapsed ovarian cancer, ○ (and) in complete or partial response to platinum (3) As **monotherapy treatment** for ○ heavily treated ovarian cancer patients (≥ 3 lines), ○ (and) germline *BRCA1/2*-mutated (4) (Olaparib + bevacizumab) as **fist-line maintenance treatment** for ○ newly diagnosed ovarian cancer, ○ (and) HRD-positive[b] ○ (and) completed front-line chemotherapy + bevacizumab with complete or partial response.	(1) As **first-line maintenance treatment** for ○ newly diagnosed ovarian cancer, ○ (and) germline or somatic *BRCA1/2*-mutated ○ (and) completed front-line chemotherapy with complete or partial response to platinum. (2) As **maintenance treatment** for ○ platinum-sensitive relapsed ovarian cancer, ○ (and) in complete or partial response to platinum (3) (Olaparib + bevacizumab) as **fist-line maintenance treatment** for ○ newly diagnosed ovarian cancer, ○ (and) HRD-positive[b] ○ (and) completed front-line chemotherapy + bevacizumab with complete or partial response.
Rucaparib (RUBRACA)	(1) As **maintenance treatment** for ○ platinum-sensitive relapsed ovarian cancer, ○ (and) in complete or partial response to platinum.	(1) As **maintenance treatment** for ○ platinum-sensitive relapsed ovarian cancer, ○ (and) in complete or partial response to platinum. (2) As **monotherapy treatment** for ○ heavily treated ovarian cancer patients (≥ 2 lines), ○ (and) platinum-sensitive, relapsed or progressive, ○ (and) BRCA mutated (germline and/or somatic).
Niraparib (ZEJULA)	(1) As **first-line maintenance treatment** for ○ newly diagnosed ovarian cancer, ○ (and) completed front-line chemotherapy with complete or partial response. (2) As **maintenance treatment** for ○ relapsed ovarian cancer, ○ (and) in complete or partial response to platinum (3) As **monotherapy treatment** for ○ heavily treated ovarian cancer patients (≥ 3 lines), ○ (and) HRD positive[b]	(1) As **first-line maintenance treatment** for ○ newly diagnosed ovarian cancer, ○ (and) completed front-line chemotherapy with complete or partial response. (2) As **maintenance treatment** for ○ platinum-sensitive relapsed ovarian cancer, ○ (and) in complete or partial response to platinum

Note: [a]The indications also extend to fallopian tube and primary peritoneal cancer. [b]HRD status is tested based on the approved companion diagnostic method. FDA, U.S. Food and Drug Administration; EMA, European Medicines Agency.

1.2.4. Similarities and differences in PARP inhibitors

Comparing the clinical efficacy of PARP inhibitors is difficult due to the distinct designs of clinical trials, and only indirect comparisons are available. Meta-analysis studies have shown that olaparib, niraparib and rucaparib, offer substantial benefits in prolonging PFS with no statistical difference (Wang et al., 2021a, Xu et al., 2020a, Staropoli et al., 2018, Luo et al., 2022). Regarding safety profiles, no statistical difference in toxicity-driven therapy discontinuation rate was found among these three PARP inhibitors (Xu et al., 2020a, Cai et al., 2021). However, PARP inhibitor treatment is associated with higher rates of grade 3-4 adverse events (severe or even life-threatening events) than the placebo group (Staropoli et al., 2018, Wang et al., 2021a, Xu et al., 2020a, Cai et al., 2021, Hao et al., 2021). Olaparib is relatively better tolerated than niraparib and rucaparib because the risk of developing high-grade adverse effects is significantly lower (Wang et al., 2021a, Xu et al., 2020a, Staropoli et al., 2018, Hao et al., 2021, Luo et al., 2022). For example, niraparib is associated with a higher risk of high-grade haematological toxicities, including thrombocytopenia and neutropenia, and rucaparib is linked to a higher rate of severe vomiting and sometimes abdominal pain (Staropoli et al., 2018, Wang et al., 2021a).

Safety profiles of veliparib and talazoparib have also been characterised. In the VELIA trial, the tolerability of veliparib was evaluated when it was in combination with chemotherapy (Coleman et al., 2019). The addition of veliparib was found to increase the risk of haematological and gastrointestinal disorders more than what was observed with olaparib, niraparib or rucaparib, which might be caused by additive toxicity of veliparib and chemotherapy (Hao et al., 2021). Talazoparib treatment has been associated with a trend of higher adverse event rates and more frequent dose-reduction or therapy discontinuation when compared with olaparib, niraparib, and rucaparib (Cai et al., 2021). No pair-wise comparison between veliparib and talazoparib is available yet.

The differential safety profiles of PARP inhibitors seen in the clinic may be determined by varying target specificity and PARP-trapping capacities (Table 1.2) besides differences in dosing schedule and pharmacokinetics. Although PARP1 and PARP2 are preferential targets of all six PARP inhibitors, three out of them (rucaparib, pamiparib and talazoparib) exhibited off-target engagement with other PARP family proteins such as tankyrase 1 (TNKS1) and

TNKS2, with IC50 values less than 1 μM (Table 1.2) (Antolin et al., 2020, Antolín and Mestres, 2014, Sandhu et al., 2022, Xiong et al., 2020, Knezevic et al., 2016, Carney et al., 2018, Wahlberg et al., 2012). TNKS1 and TNKS2 have similar catalytic domains as PARP1/2. They have been implicated in multiple cellular activities, including cell mitosis, the Wnt signalling pathway, and telomere elongation [reviewed in (Kim, 2018)]. TNKS1 and TNKS2 have also been associated with DNA-PK- and the mediator of DNA damage checkpoint protein 1 (MDC1)-mediated DSBs repair (Dregalla et al., 2010, Nagy et al., 2016). It is possible that the off-target engagement with TNKS1 and TNKS2 impacts clinical response and safety profiles of PARP inhibitors.

Meanwhile, off-target interactions between PARP inhibitors (rucaparib, veliparib, and niraparib) and multiple kinases and transporters have also been documented (Table 1.2) (Antolín and Mestres, 2014, Knezevic et al., 2016, Sandhu et al., 2022). Among PARP inhibitors in clinical development (not enough data for pamiparib), rucaparib is the least specific PARP inhibitor, which inhibits at least 11 kinases (PIM1, PIM2, PIM3, PRKD2, DYRK1A, DYRK1B, cyclin-dependent kinase 1 (CDK1), CDK9, CDK16, HIPK2, CK2) and three transporters (MATE1, MATE2 and OCT1) with most IC50 values less than 2 μM (Antolín and Mestres, 2014, Knezevic et al., 2016, Sandhu et al., 2022), a concentration readily achievable in xenografts (Murray et al., 2014) and patients (Shapiro et al., 2019, Grechko et al., 2021). On the other hand, olaparib is the most selective PARP inhibitor, which inhibits PARP1-4 with nanomolar affinity and does not inhibit most kinases and reporters tested so far (Antolín and Mestres, 2014, Knezevic et al., 2016, Sandhu et al., 2022). The selective nature of olaparib could be the reason for its superior tolerance in patients to other PARP inhibitors.

Another distinction among PARP inhibitors is the PARP trapping activity (Table 1.2). PARP trapping potency can be ranked as talazoparib >> olaparib = rucaparib > veliparib (Hopkins et al., 2019, Hopkins et al., 2015, Murai et al., 2014, Murai et al., 2012). The efficacy of niraparib-mediated PARP trapping varies depending on experimental conditions. Murai et al. (2012) reported that niraparib is a stronger PARP trapper than olaparib, but Hopkins et al. (2015) observed that niraparib traps PARP to a similar level as the weak PARP trapper veliparib. Pamiparib is reported as a potent PARP trapper, but it has not been directly compared with other PARP inhibitors (Xiong et al., 2020).

Structural analysis of PARP1 retention on DNA demonstrates that PARP trapping is a combined effort of catalytic inhibition and allosteric alteration of DNA binding affinity of PARP (Zandarashvili et al., 2020). Zandarashvili et al. (2020) divided PARP inhibitors (including non-clinical drugs) into three categories: type 1 inhibitors – allosterically alter the helical domain of PARP1 and stabilise the PARP-DNA complex; type 2 inhibitors – minor to no allosteric effect; and type 3 inhibitor – having the opposite effect of type 1 inhibitors and decreases DNA-binding affinity of PARP. Type 1 PARP inhibitors only include drugs in preclinical development. Olaparib and talazoparib are type 2 inhibitors with similar allosteric effects, and PARP-trapping potency is determined by the potency of catalytic inhibition (Zandarashvili et al., 2020). Niraparib, rucaparib and veliparib are type 3 inhibitors, and their catalytic inhibitory effect plays a major role in overcoming the reduced DNA-binding affinity of PARP and stabilising the PARP-DNA complex (Zandarashvili et al., 2020).

PARP trapping is widely considered as the major contributor to anti-cancer activities of PARP inhibitors *in vitro*, because it is better correlated with cytotoxicity in cancer cells than catalytic inhibitory effects (Murai et al., 2014, Murai et al., 2012, Murai and Pommier, 2019). However, in animal models, comparable therapeutic tumour growth inhibition can be achieved using olaparib, veliparib, or talazoparib, regardless of PARP trapping differences (Hopkins et al., 2019, Hopkins et al., 2015). A similar trend is also observed in clinical trials in which the weakest PARP trapper, veliparib, demonstrated a similar ORR as other PARP inhibitors in patients with platinum-sensitive or BRCA-mutated ovarian cancer (reviewed in (Rose et al., 2020)), implying that PARP trapping efficacy does not necessarily determine therapeutic response, especially in animals and in patients. On the other hand, PARP trapping has been associated with more serious adverse effects. As the strongest PARP trapper, talazoparib is substantially more toxic to human bone marrow cells than olaparib, rucaparib and veliparib, and it has the worst tolerability in mice (Hopkins et al., 2019, Hopkins et al., 2015). This could explain the association between talazoparib therapy and a significantly higher risk of dose reduction in clinical trials (Cai et al., 2021), as discussed earlier in this section.

Taken together, PARP inhibitors have shown comparable benefits in the clinic but differential safety profiles in patients. Olaparib is the most selective PARP inhibitor and has demonstrated better tolerability than other PARP inhibitors. Distinctions in target specificity and PARP trapping potency may underly the differences in side effects.

Table 1.2. PARP1-trapping potency and target specificity of PARP inhibitors

			Olaparib	Rucaparib	Niraparib	Veliparib[a]	Talazoparib	Pamiparib
PARP1 trapping EC50 by TR-FRET			5 ± 1.2 nM	Not tested[b]	14 ± 4 nM	19 ± 7 nM	2.7 ± 0.6 nM	Not tested
PARP1 trapping EC50 by FA-binding asay			300 - 1000 nM	Not tested[b]	300 - 1000 nM	> 3000 nM	30 - 100 nM	13 nM
PARP family		PARP1	0.42 - 19 nM	0.8 - 80 nM	2 - 35 nM	3.0 - 10.3 nM	0.6 - 3 nM	1.3 nM
		PARP2	1 - 251 nM	28 - 83 nM	2 - 15.3 nM	High affinity	4.1 nM	0.92 nM
		PARP3	46 - 230 nM	460 - 512 nM	296 - 1,300 nM	High affinity	63 nM	68 nM
		PARP4	410 nM	839 nM	330 - 446 nM	Medium affinity	254 nM	Not tested
		TNKS1	1230 - 3534 nM	25 - 144 nM	570 - 2,355 nM	No interaction	322 nM	230 nM
		TNKS2	1700 - 2340 nM	14 - 890 nM	5130 nM	No interaction	108 nM	140 nM
		PARP10	1250 - 9300 nM	570 - 1433 nM	1900 nM	No interaction	7800 nM	11000 nM
		PARP12	10050 nM	6650 nM	437 - 790 nM	No interaction	Not tested	2400 nM
		PARP14	No inhibition	8830 nM	17300 nM	No interaction	25500 nM	Not tested
		PARP15	17600 nM	32600 nM	29200 nM	No interaction	47400 nM	Not tested
		PARP16	5100 nM	No inhibition	n.d.	No interaction	1900 nM	Not tested
Transporters	DAT	Dopamine transporter	Not tested	Not tested	51 nM	Not tested	Not tested	Not tested
	NET	Norepinephrine transporter	Not tested	Not tested	239 nM	Not tested	Not tested	Not tested
	SERT	Serotonine transporter	Not tested	Not tested	363 nM	Not tested	Not tested	Not tested
	OCT1	organic cation transporter 1	> 10000 nM	4300 nM	n.d.	Not tested	Not tested	Not tested
	MATE1	Multidrug and toxin extrusion protein 1	5500 nM	630 nM	> 10000 nM	Not tested	Not tested	Not tested
	MATE2	Multidrug and toxin extrusion protein 2	> 10000 nM	190 nM	n.d.	Not tested	Not tested	Not tested
Kinases	DYRK1A	Dual specificity tyrosine phosphorylation regualted kinase 1A	> 30000 nM	1400 nM	297 nM	> 30000 nM	> 10000 nM	Not tested
	DYRK1B	Dual specificity tyrosine phosphorylation regualted kinase 1B	> 10000 nM	747 nM	254 nM	Not tested	> 10000 nM	Not tested
	PIM1	Serine/threonine-protein kinase PIM1	> 30000 nM	1200 nM	Not tested	17000 nM	Not tested	Not tested
	PIM2	Serine/threonine-protein kinase PIM2	> 30000 nM	7700 nM	Not tested	> 30000 nM	Not tested	Not tested
	PIM3	Serine/threonine-protein kinase PIM3	> 10000 nM	436 nM	Not tested	Not tested	> 10000 nM	Not tested
	PRKD2	Protein kinase D2	> 30000 nM	9700 nM	Not tested	> 30000 nM	Not tested	Not tested
	CDK1	Cyclin dependent kinase 1	> 30000 nM	1400 nM	Not tested	> 30000 nM	Not tested	Not tested
	CDK9	Cyclin dependent kinase 9	> 30000 nM	2700 nM	Not tested	8200 nM	Not tested	Not tested
	CDK16	Cyclin dependent kinase 16	> 10000 nM	381 nM	> 10000 nM	Not tested	> 10000 nM	Not tested
	HIPK2	Homeodomain Interacting Protein Kinase 2	> 30000 nM	4400 nM	Not tested	> 30000 nM	Not tested	Not tested
	CK2	Casein kinase 2 alpha 1	> 30000 nM	7800 nM	Not tested	> 30000 nM	Not tested	Not tested
	CDC7	Cell division cycle 7	> 30000 nM	> 30000 nM	Not tested	> 30000 nM	Not tested	Not tested
	STK17A	Serine/Threonine Kinase 17A	> 30000 nM	> 30000 nM	Not tested	> 30000 nM	Not tested	Not tested
	ALK	ALK receptor tyrosine kinase	> 30000 nM	18000 nM	Not tested	> 30000 nM	Not tested	Not tested
	DCK	Deoxycytidine kinase	No inhibition	No inhibition	67000 nM	No inhibition	Not tested	Not tested
H6PD		Hexose-6-phosphate dehydrogenase	No inhibition	18000 nM	No inhibition	No inhibition	Not tested	Not tested

IC50 values	Thermal shift ΔTm
< 100 nM	ΔTm > 10
100 - 1000 nM	7 < ΔTm < 9.99
1000 - 10000 nM	4 < ΔTm < 6.99
> 10000 nM	ΔTm < 0.99

Note: [a]The interaction between veliparib with PARP family proteins (except PARP1) was determined by thermal shift assay (Wahlberg et al., 2012). [b]In western blot analysis, rucaparib showed comparable PARP1-trapping with olaparib (Murai et al., 2014). TR-FRET (time-resolved Förster resonance energy transfer) PARP trapping EC50 (Hopkins et al., 2015), FA (fluorescence anisotropy)-binding assay PARP trapping EC50 (Murai et al., 2014, Murai et al., 2012), and IC50 values (Antolin et al., 2020, Antolín and Mestres, 2014, Sandhu et al., 2022, Wahlberg et al., 2012) were obtained from the literature.

1.2.5. PARP inhibitor resistance

Restoring HR repair activity

Drug resistance is a common challenge for clinical drugs, and PARP inhibitors are no exception. The most well-characterised resistance mechanism in the clinic is the restoration of HR activity by reversion mutations (Barber et al., 2013, Gornstein et al., 2018, Kondrashova et al., 2017, Quigley et al., 2017, Weigelt et al., 2017, Goodall et al., 2017, Lin et al., 2019, Mayor et al., 2017, Christie et al., 2017). In *BRCA*-mutated cells, a single point mutation is sufficient to correct the nonsense mutation in *BRCA1 or BRCA2*, resulting in partial or complete restoration of BRCA expression and HR repair activity, thereby acquiring resistance to PARP inhibitors (Sakai et al., 2009, Sakai et al., 2008, Tobalina et al., 2021). Secondary insertions and deletions can also restore the open reading frame of *BRCA* and confer PARP inhibitor resistance (Tobalina et al., 2021). In patients, reversion mutations in *BRCA1* and *BRCA2* (Christie et al., 2017, Lin et al., 2019, Mayor et al., 2017, Quigley et al., 2017, Weigelt et al., 2017, Tobalina et al., 2021), as well as other DNA repair genes such as *RAD51C* and *RAD51D* (Kondrashova et al., 2017), have been correlated with acquired PARP inhibitor resistance and significantly shorter PFS (Lin et al., 2019, Hu et al., 2022). Meta-analysis of *BRCA* sequencing data revealed that approximately 21.4% and 27.5% of ovarian cancer patients harbour reversion mutations in *BRCA1* and *BRCA2*, respectively (Tobalina et al., 2021). The actual reversion mutation rate is likely higher as most patients are not genetically tested during and after PARP inhibitor treatment (Rose et al., 2020).

Besides reversion mutations, HR activities can be restored by suppressing the competitive repair pathway NHEJ, which is selectively effective in BRCA1 deficient tumours (Bunting et al., 2010, Bouwman et al., 2010). As discussed earlier (Section 1.2.2), BRCA1 and 53BP1 compete for occupancy at DSBs, and the result determines the choices of repair pathways. One key event in this process is the resection of DSBs, which is a necessary step for HR repair but is inhibited by 53BP1 and other NHEJ proteins (Scully et al., 2019). Inhibition of 53BP1 allows end resection in *BRCA1*-mutated cells, enabling *BRCA1*-independent activation of HR repair (Bunting et al., 2010) and PARP inhibitor resistance *in vivo* (Jaspers et al., 2013, Duarte et al., 2018). This has been observed in the clinic, where 53BP1 deficiency significantly correlates with increased PARP inhibitor resistance in HRD ovarian cancer patients (Hurley et al., 2019).

Depletion of downstream effectors of 53BP1, such as RIF1 and the Shieldin protein complex, phenocopies the loss of 53BP1 in BRCA1-mutated cells (Chapman et al., 2013, Zimmermann et al., 2013, Noordermeer et al., 2018, Dev et al., 2018, Gupta et al., 2018). Similar effects can also be achieved in 53BP1-independent manners, for example, by depleting either DYNLL1 (He et al., 2018) or HELB (Tkáč et al., 2016), two enzymes inhibiting nucleases required for DSBs processing before HR.

Reducing PARP trapping

Decreasing PARP trapping is another approach to acquiring PARP inhibitor resistance. PAR glycohydrolase (PARG) is an enzyme modulating the dynamics of PARylation by degrading PAR chains generated by PARPs (dePARylation) (Harrision et al., 2020). Depletion of PARG allows the accumulation of PAR chains, which reduces PARP trapping and partially restores the PARylation-dependent DNA damage repair mechanism, thereby leading to decreased PARP inhibitor response (Gogola et al., 2018, Chand et al., 2017). However, PARG inhibition does not always lead to PARP inhibitor resistance because PARG inhibitors have been reported to overcome PARP inhibitor resistance (Chen and Yu, 2019, Pillay et al., 2019, Gravells et al., 2017, Coulson-Gilmer et al., 2021). It is still unclear what determines the impact of PARG inhibition on PARP inhibitor sensitivity.

Besides PARG loss, PARP inhibitor resistance may arise through point mutations or deletions in *PARP1* that affect trapping (Pettitt et al., 2018). For example, the R591C mutation in PARP1 completely abrogated PARP-trapping by talazoparib in cancer cells, and it is a suspected mechanism of olaparib resistance in some patients (Pettitt et al., 2018, Zandarashvili et al., 2020).

Stabilising stalled replication forks

Thirdly, PARP inhibitor resistance can be acquired through the stabilisation of stalled replication fork. Following PARP inhibitor treatment, accumulating SSBs and trapped PARP-DNA complexes are obstacles that sterically hinder the progression of DNA replication forks. Stalled replication forks can have detrimental effects when they are degraded or collapsed, leading to the formation of DSB (Taglialatela et al., 2017, Saleh-Gohari et al., 2005). Downregulation of factors mediating fork degradation, such as EZH2 (Rondinelli et al., 2017)

and PTIP (Ray Chaudhuri et al., 2016), prevents fork degradation and promotes PARP inhibitor resistance.

Upregulating drug efflux pumps

The fourth resistance mechanism to PARP inhibitors is by upregulating drug efflux pumps to reduce the cellular concentration of PARP inhibitors. The most well-characterised efflux pump is the ATP binding cassette subfamily B member 1 (ABCB1, also known as MDR1 or P-glycoprotein) transporter. Both olaparib and talazoparib are substrates of the efflux pump (Lawlor et al., 2014, FDA, 2018b). Overexpression of *ABCB1* is frequent in chemotherapy-resistant patients (Christie et al., 2019), and it causes PARP inhibitor resistance in several *in vitro* and *in vivo* cancer models (Rottenberg et al., 2008, Vaidyanathan et al., 2016, Jaspers et al., 2015). It is worth highlighting that overexpression of efflux pumps can lead to multi-drug resistance, and tumours may acquire cross-resistance to PARP inhibitors during chemotherapies (Vaidyanathan et al., 2016, Jaspers et al., 2015, Lombard et al., 2019). This has encouraged the development of additional PARP inhibitors, such as veliparib (Lawlor et al., 2014) and pamiparib (Deng et al., 2022), that are not affected by ABCB1.

Overall, tumours may acquire PARP inhibitor resistance through several approaches. Restoration of HR has been well-characterised in the clinic, and investigations of other resistance mechanisms in patients are ongoing.

1.2.6. Combination therapies

PARP inhibitor + First-line chemotherapy

As PARP inhibition facilitates the accumulation of DNA lesions, adding PARP inhibitors to conventional chemotherapy is an attractive combination strategy. Myelosuppression is a major concern when DNA damaging agents are combined with PARP inhibitors, especially for those PARP inhibitors with a strong PARP trapping effect, such as rucaparib and talazoparib (Rose et al., 2020, Veneris et al., 2020). In the phase III VELIA trial, the combination of veliparib, a weak PARP trapper, and chemotherapy (followed by veliparib maintenance) significantly improved the median PFS of newly diagnosed HGSOC patients in comparison with chemotherapy alone (Coleman et al., 2019). However, patients who received the veliparib and chemotherapy are more likely to experience adverse events such as anaemia and

thrombocytopenia than patients only treated with chemotherapy (Coleman et al., 2019), highlighting the potential risks of combining PARP inhibitors with chemotherapy. The clinical efficacy of other PARP inhibitors in combination with front-line chemotherapy for patients with newly diagnosed ovarian cancer has not been reported at the time of writing.

PARP inhibitor + angiogenesis inhibitor

Bevacizumab is an antiangiogenic antibody frequently used as part of the front-line therapy for newly diagnosed ovarian cancer patients. Patients often receive bevacizumab in combination with chemotherapy, followed by bevacizumab alone as maintenance therapy (Tsibulak et al., 2019). Considering the success of PARP inhibitors in delaying disease progression, it is attractive to combine bevacizumab with PARP inhibitors as a dual-agent maintenance treatment. The scientific rationale for this combination strategy is twofold. Firstly, hypoxia in tumours caused by antiangiogenic drugs inhibits HR repair by downregulating the normoxia-dependent expression of HR genes such as *BRCA1*, *BRCA2* and *RAD51* (Bindra et al., 2004, Bindra et al., 2005, Fanale et al., 2013, Kaplan et al., 2019, Veneris et al., 2020). This leads to an increased response to PARP inhibitors, even in tumours with acquired PARP inhibitor resistance (Kaplan et al., 2019). Secondly, targeting two distinct pathways could reduce the chance of drug resistance and improve treatment efficacy.

Positive outcomes have been reported in the PAOLA-1 trial, in which ovarian cancer patients received olaparib or a placebo in combination with bevacizumab, after completing the front-line therapy of platinum, taxanes and bevacizumab (Ray-Coquard et al., 2019). Adding olaparib to bevacizumab significantly improved median PFS from 16.6 months in the placebo group to 22.1 months (Ray-Coquard et al., 2019). The combination maintenance therapy is most effective in patients with BRCA-mutated tumours, but a beneficial effect was also observed in patients with HRD-negative tumours, albeit to a lesser extent (Ray-Coquard et al., 2019). Similar benefits in PFS were observed in a phase II trial where olaparib was combined with an antiangiogenic drug, cediranib, to treat patients with recurrent HGSOC cancer (Liu et al., 2014). However, due to a lack of an olaparib-only arm in these two trials, it is still unclear if PARP inhibitors synergise with antiangiogenic agents or are merely additive. Clinical trials are ongoing to test the combination of rucaparib with bevacizumab, which may provide further evidence supporting the combination strategy (Lorusso et al., 2021).

PARP inhibitor + Immunotherapy

The clinical performance of immune checkpoint inhibitors has been disappointing in ovarian cancer. When used as monotherapy, the overall response rate of immunotherapy was less than 15% [reviewed in (Veneris et al., 2020)]. In two phase III clinical trials (JAVELIN-200 and IMagyn500), the programmed death-ligand 1 (PD-L1) inhibitory antibody avelumab in combination with chemotherapy failed to demonstrate significant benefits in PFS and overall survival in patients who had recurrent or newly diagnosed ovarian cancer (Pujade-Lauraine et al., 2021, Moore et al., 2021).

Evidence suggests that tumours with HRD may be prone to immunotherapy due to a higher mutation burden and an increase in the expression of mutation-driven neoantigens (Birkbak et al., 2013, Strickland et al., 2016). It has been reported that genotoxic stress caused by PARP inhibitors results in the release of DNA fragments and activation of the antigen-resenting cells, thereby improving the efficacy of immunotherapy in xenograft models of ovarian cancer (Ding et al., 2018, Shen et al., 2019). These observations suggest that PARP inhibitors may enhance immunotherapy response in ovarian cancer patients. In phase I and II trial TOPACIO, the addition of niraparib to the PD-1 inhibitor pembrolizumab showed an overall response rate of 45% in heavily treated ovarian cancer patients with *BRCA*-mutated tumours and an overall response rate of 20% in patients without *BRCA* mutations (Konstantinopoulos et al., 2019). Similar findings were observed in several other phase I or II clinical trials [reviewed in (Musacchio et al., 2022)], suggesting that the combination treatment consisting of PARP inhibitors and immune checkpoint inhibitors is effective in ovarian cancer. However, phase III trials with control groups and more participants are needed to ascertain if these two classes of drugs are better in combination than monotherapies.

PARP inhibitor + DNA damage repair inhibitor

Restoration of HR repair activity is the most common mechanism of acquired PARP inhibitor resistance in the clinic (Section 1.2.5). Combining PARP inhibitors with targeted therapies inhibiting HR repair is therefore expected to reduce or overcome PARP inhibitor resistance. Several kinases modulate HR repair activity, such as CDK4/6, PI3K, and Wee1. Preclinical evidence has shown that inhibitors targeting CDK4/6 (Yi et al., 2019) or PI3K (Ibrahim et al.,

2012) lead to downregulated expression of BRCA1/2 and reduced RAD51 recruitment, thereby reducing HR repair and synergises with PARP inhibitors *in vitro* and in mouse xenografts. Wee1 inhibitor reduces HR repair in cancer cells and sensitises cells to PARP inhibitors (Krajewska et al., 2013). Multiple clinical trials are ongoing to test the clinical efficacy of PARP inhibitors in combination with these DNA damage repair inhibitors [reviewed in (Bonadio and Estevez-Diz, 2021)].

PARP inhibitor + replication stress response inhibitor

Increased tolerance of replication stress is another key mechanism for PARP inhibitor resistance. ATR and Chk1 are two pivotal kinases sensing replication stress and regulating replication fork stability. Inhibiting the ATR-Chk1 pathway disrupts the replication stress response and may sensitise tumours to PARP inhibitors by increasing replication fork abnormalities and preventing cancer cells from acquiring drug resistance via stabilising replication forks (Parmar et al., 2019, Kim et al., 2020, Brill et al., 2017, Kim et al., 2017). Several ATR inhibitors and Chk1 inhibitors are in early clinical development [reviewed in (Veneris et al., 2020)].

Challenges for combination strategies

In addition to the combination therapies mentioned above, several other strategies have been proposed to improve the clinical efficacy of PARP inhibitors, and the number is growing (Bonadio and Estevez-Diz, 2021). However, most of them are limited to scientific investigations and have not been translated to clinical studies. Even for those combination treatments in clinical evaluation, it has been difficult to conclude whether the drug combination is superior to monotherapies due to a lack of control arms. Overall, PARP inhibitor maintenance therapy remains the main option for most ovarian cancer patients after completing the front-line chemotherapy. There is an urgent need for combination therapies or alternative targeted therapies to tackle the emerging PARP inhibitor resistance.

Chapter 1 – Introduction

1.3. Alternative splicing

1.3.1. Alternative splicing is an emerging cancer vulnerability

RNA splicing is a crucial step in gene expression. It requires the coordination of many RNA-binding proteins and splicing factors to form the spliceosome complex. During RNA splicing, non-coding introns from the precursor message RNA (pre-mRNA) are removed, and the flanking exons are ligated, producing mature mRNAs ready for protein translation [reviewed in (Stanley and Abdel-Wahab, 2022)]. Three conserved sequences in the intron are crucial for the spliceosome assembly and RNA splicing, including the GU dinucleotide at the 5' splice site, the polypyrimidine tract followed by AG dinucleotide at the 3' splice site, and the branch point adenosine between 5' and 3' splice sites (Figure 1.3A). The GU dinucleotide at the 5' splice site is firstly recognised by the U1 small nuclear ribonucleoprotein (snRNP), followed by splicing factor 1 (SF1), which recognises the adenosine at the branch site sequence. At the 3' splice site, the polypyrimidine tract and AG dinucleotide sequence allow the binding of the U2 auxiliary factor (U2AF) complex, consisting of U2AF65 and U2AF35, which then promotes the displacement of SF1 at the branch point sequence by the U2 snRNP complex. A fully functional spliceosome is completed by the addition of the U4/U6.U5 tri-snRNP complex, enabling a two-step transesterification reaction that removes the intron from the transcript (Figure 1.3B).

Interestingly, splicing of pre-mRNAs can occur in different ways due to alternative splice site recognition, resulting in multiple mRNA transcripts with distinct combinations of exons (Figure 1.3C). There are five main events of alternative splicing, including cassette exon (exon skipping), intron retention, alternative 5' or 3' splice site in the exon, and mutually exclusive exons (Wang and Aifantis, 2020). It is estimated that alternative splicing impacts the expression of over 95% of multi-exon genes in human, contributing to the diverse transcriptome and proteome (Wang et al., 2008). One of the most well-known examples of alternative splicing is the *BCL2L1* gene, which has two splicing variants depending on whether exon 2 is fully or partially included in the final mRNA. Recognition of the splice site within exon 2 causes partial exon loss and generates a truncated protein isoform BCL-xS that promotes apoptosis, whilst ignoring the site leads to a long protein isoform BCL-xL that inhibits apoptosis and is associated with tumour progression and chemotherapy resistance (Trisciuoglio et al., 2017, Stevens and Oltean, 2019).

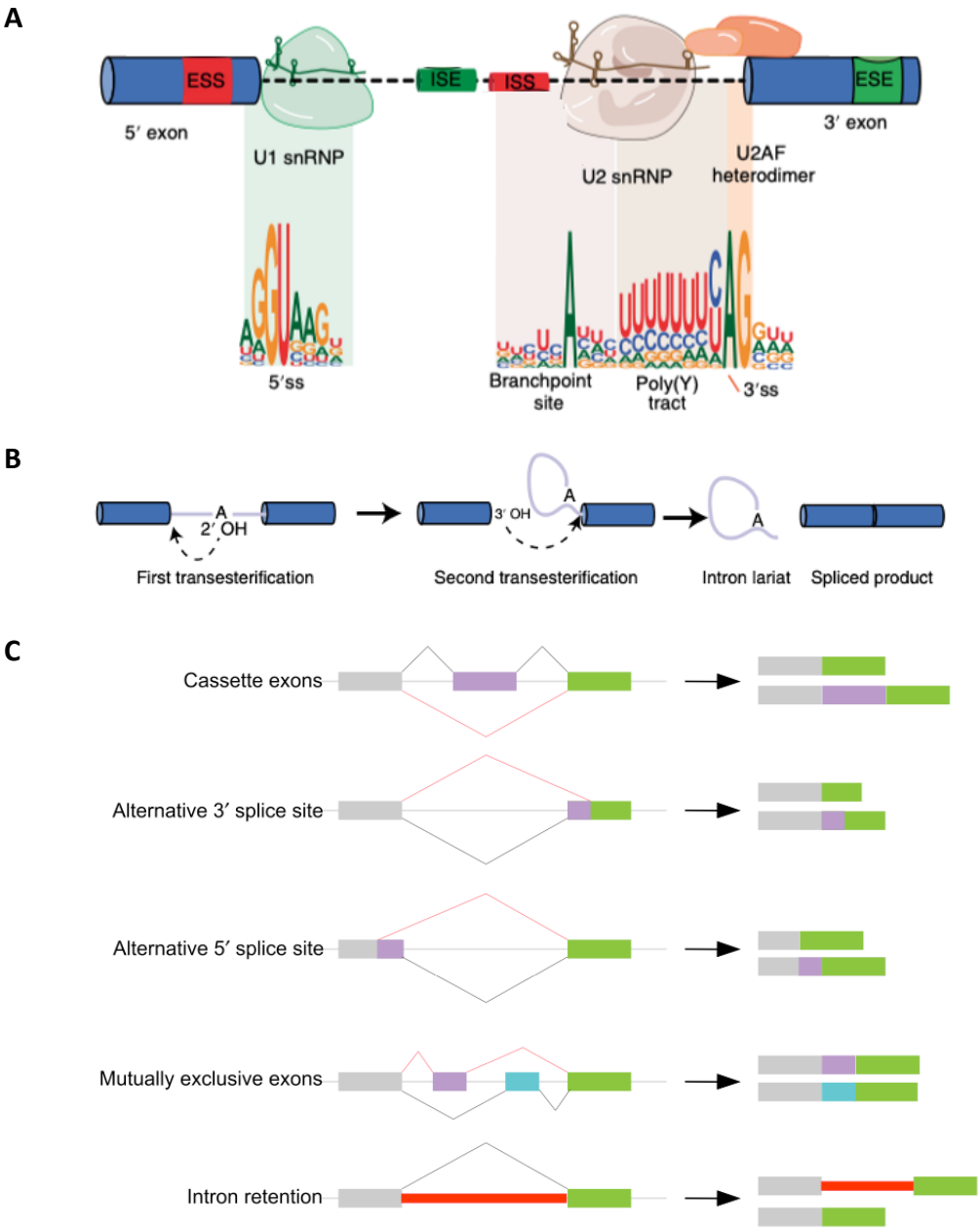


Figure 1.3. Mechanisms of alternative pre-mRNA splicing.
(A) Splicing pre-mRNAs requires sequential recognition of the 5′ splice site (5′ ss) by the U1 snRNP, polypyrimidine tract [poly(Y)tract] and the 3′ splice site (3′ss) by the U2AF heterodimer (orange), and the branchpoint adenine/A by the U2 snRNP complex. Splicing activities are subject to modulation by enhancers (ISE/ESE, intronic/exonic splicing enhancer) and silencers (ISS/ESS, intronic/exonic splicing silencer). **(B)** Introns (grey line) are spliced out, and exons (blue cylinders) are joined following a two-step transesterification. The branch site adenine/A firstly reacts with the 5′ss guanine, leading to 5′ss cleavage and formation of a lariat structure. It also exposes a 3′ exonic hydroxyl (-OH) group, which then reacts with the first nucleotide of the next exon, thereby ligating two exons and removing the lariat intron. **(C)** Diagrams showing five major forms of alternative splicing events, including cassette exons (exon skipping), alternative 5′ or 3′ splice site (partial exon loss or intron retention), mutually exclusive exons, and intron retention. A and B are adapted from Stanley and Abdel-Wahab (2022), and C is taken from Wang and Aifantis (2020) with permission.

Chapter 1 – Introduction

Splicing factors are frequently mutated or dysregulated in cancer, resulting in reprogrammed splicing machinery that promotes tumour growth and progression (El Marabti and Younis, 2018, Stanley and Abdel-Wahab, 2022, Xu et al., 2020b, Kim et al., 2008). Besides upregulating anti-apoptotic BCL-xL expression, cancer cells can acquire resistance to anti-cancer drugs through upregulating drug-resistant splicing isoforms of therapeutic targets and altering splicing of genes required for drug uptake and activation [reviewed in (Sciarrillo et al., 2020)]. Inactivation of tumour suppressor genes through intron retention has also been reported in cancer patients [reviewed in (Wang and Aifantis, 2020)].

In HGSOC, pathway enrichment analysis reveals that spliceosome is significantly upregulated in tumours, and overexpression of splicing factors is associated with poor patient prognosis (Wang et al., 2021b, Zhao et al., 2021). Meanwhile, several studies have identified alternative splicing signatures that could serve as prognostic indicators for ovarian cancer (Yue et al., 2022, Ouyang et al., 2021, Yao et al., 2022, Liu et al., 2021, Zhu et al., 2018, Zhang et al., 2021a, Gusev et al., 2019). Splicing variants promoting chemotherapy resistance have also been identified (Wang et al., 2016, Paul et al., 2015, Zhang et al., 2013), indicating that splicing factors are important for tumour progression and therapy response.

For example, the splicing factor 3b subunit 1 (SF3B1) is a core component of the U2 snRNP complex and is a putative oncogene frequently mutated in multiple haematological cancers and solid tumours (Seiler et al., 2018). SF3B1 mutations are clustered in the domains responsible for intronic branch point residue recognition, which mutated SF3B1 displayed aberrant branch site binding and alternative splicing at non-canonical 3’ splice sites, resulting in mRNA variants with frameshifts (Seiler et al., 2018, Darman et al., 2015, DeBoever et al., 2015). Both positive (Kanagal-Shamanna et al., 2021) and negative correlations (Dalton et al., 2020, Fu et al., 2017) between SF3B1 mutation and cancer patient prognosis have been reported, suggesting context-dependent roles of SF3B1 in tumour progression. Multiple small molecular inhibitors have been developed to target SF3B1 in spliceosome-mutated cancer and have demonstrated promising preclinical activities [reviewed in (Sette and Paronetto, 2022)].

However, the clinical translation of SF3B1 inhibitors has been difficult. Two phase I clinical trials for the first-generation inhibitor E7107 were terminated because of unexpected

toxicities (Eskens et al., 2013, Hong et al., 2014). Although the second-generation inhibitor H3B-8800 was better tolerated in patients, it failed to achieve a partial or complete response in a phase I trial (Steensma et al., 2021).

Taken together, dysregulated alternative splicing is an emerging vulnerability and therapeutic target in cancer. However, the current understanding of splicing factors in cancer development and progression is still limited, and clinical translation of splicing factor inhibitors has not been successful in the clinic. While additional trials of SF3B1 inhibitors are ongoing, it is vital to explore other splicing factors as cancer targets.

1.3.2. RBM39 is a promising cancer target

The RNA-binding motif protein 39 (RBM39, also known as HCC1, CAPER, or CAPERα) is a transcriptional coactivator and a splicing factor (Xu et al., 2020b). In 2020, I published the first review article in the field summarising the latest understanding of RBM39 in transcriptional coregulation and alternative splicing of pre-mRNAs (Xu et al., 2020b). The majority of the literature review in this section and the next section has been published in the British Journal of Pharmacology (Xu et al., 2020b).

Although evidence suggests RBM39 enhances transcriptional activities of multiple transcription factors, such as oestrogen receptors and progesterone receptors, the mechanisms and clinical relevance of RBM39 as a transcriptional coregulator in cancer are still poorly characterised. On the other hand, RBM39 has been recognised as a promising cancer target owing to its role in alternative pre-mRNA splicing and the fact that loss of RBM39 causes transcriptome-wide splicing abnormalities and reduces cancer cell viability (Mai et al., 2016a, Han et al., 2017b, Uehara et al., 2017).

Structurally, RBM39 belongs to the U2AF-like protein family, which also include U2AF65, poly(U)-binding splicing factor 60 (PUF60) and RBM23 (Figure 1.4A) (Dowhan et al., 2005). Except RBM23 (Ting et al., 2019), U2AF-family proteins are splicing factors (Hastings et al., 2007, Prigge et al., 2009). RBM39 contains an arginine-serine rich (RS) domain, two canonical RNA recognition motifs (RRM1-2) and one U2AF homology motif (UHM) (Figure 1.4) (Loerch et al., 2014, Stepanyuk et al., 2016). The RS domain is important for nuclear localisation of RBM39 and interaction with other splicing factors containing the RS domain; the RRM

domains are involved in various interactions with transcription factors, splicing factors and RNAs; and the UHM domain is critical for RBM39 to interact with essential splicing factors such as U2AF65 and SF3B1 via the UHM-UHM ligand motif (ULM) interaction (Figure 1.4B) (Loerch et al., 2014, Stepanyuk et al., 2016, Xu et al., 2020b, Ellis et al., 2008, Tari et al., 2019). Evidence from RBM39 interactome and structural analysis suggests a model that, during pre-mRNA splicing, RBM39 recognises the polypyrimidine tract at the intronic 3' splice site through the RRM1 and RRM2 domains, where it interacts with U2AF65 directly and facilitates SF3B1-mediated branch site recognition of the U2 snRNP complex (Figure 1.4) (Xu et al., 2020b). As SF3B1 has five ULM domains, two RBM39 molecules and other UHM-containing splicing factors such as PUF60 may be recruited as well to complete the assembly of the spliceosome (Loerch et al., 2014, Xu et al., 2020b, Huang et al., 2017). This model is supported by the findings that RBM39-regulated splicing events overlap partially with that of U2AF65 and PUF60 (Mai et al., 2016a, Kralovicova et al., 2018).

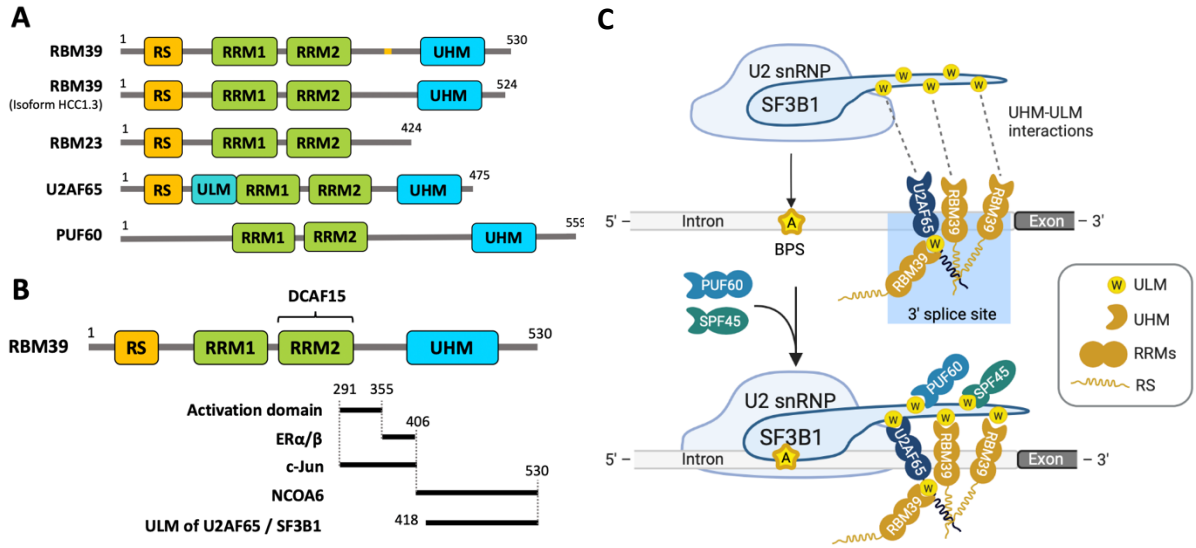


Figure 1.4. RBM39 is a member of the U2AF-like family protein.
(A) The U2AF-like family protein contains four members, including RBM39, RBM23, U2AF65 and PUF60. They share similar arginine-serine rich (RS) domains and RNA recognition motifs (RRMs). Except for RBM23, U2AF-like proteins contain a U2AF homology motif (UHM), mediating interactions with other splicing factors. **(B)** Experimentally validated interaction domains of RBM39 with transcription factors, splicing factors and the DDB1- and CUL4- associated factor 15 (DCAF15)-associated E3 ubiquitin ligase complex (requires molecular glues). **(C)** A model for RBM39-medicated pre-mRNA splicing. RBM39 recognises the 3' splice site together with U2AF65, promoting the recruitment of SF3B1 to the branchpoint residue (BPS). The interaction between UHM-ligand motifs (ULMs) and UHMs is essential for spliceosome assembly. This figure is taken from my review paper with permission (Xu et al., 2020b).

RBM39-mediated transcriptional coregulation and splicing modulation have been implicated in cancer cell proliferation, angiogenesis, hypoxia response and tumour growth in preclinical studies [reviewed in (Xu et al., 2020b)]. Overexpression of RBM39 has also been detected in breast cancer (Campbell et al., 2018, Mercier et al., 2009), non-small cell lung cancer (Chai et al., 2014), and gastric cancer (Lu et al., 2021a), suggesting that RBM39 is important for tumorigenesis. As a downstream target of the oncogene MYC, RBM39 maintains tumour metabolism and survival in MYC-driven neuroblastoma (Singh et al., 2021, Nijhuis et al., 2022). It also promotes the expression of other oncogenes, such as *tripartite motif containing 27* (*TRIM27*) in colorectal cancer (Han et al., 2017b) and *HOXA9* target genes in acute myeloid leukaemia (Wang et al., 2019). Furthermore, CRISPR knock-out and RNA interference screens found that RBM39 is essential in over 70% of cancer cell lines tested (Dempster et al., 2019, DepMap, 2020, McFarland et al., 2018, Meyers et al., 2017, Xu et al., 2020b). In line with these findings, therapies targeting RBM39 have demonstrated promising (preclinical) anti-cancer activities in a diverse array of cancers including acute myeloid leukaemia (Wang et al., 2019, Han et al., 2017b, Hsiehchen et al., 2020), colorectal cancer (Han et al., 2017b, Owa et al., 1999, Ozawa et al., 2001, Sillars-Hardebol et al., 2012, Uehara et al., 2017, Ting et al., 2019, Wu et al., 2019), breast cancer (Campbell et al., 2018, Chilewski et al., 2020, Mercier et al., 2009, Mercier et al., 2014, Puvvula et al., 2021), non-small cell lung cancer (Chai et al., 2014, Fukuoka et al., 2001, Ozawa et al., 2001), melanoma (Lu et al., 2021b), gastric cancer (Lu et al., 2021a), and neuroblastoma (Nijhuis et al., 2022, Singh et al., 2021). Taken together, RBM39 is a valuable cancer target and RBM39-targeted therapy may benefit a wide range of cancer patients.

1.3.3. Targeting RBM39 with molecular glues

Targeting RBM39 in cancer cells had been challenging until the recent discovery of RBM39 degraders. In 2017, two research groups revealed that a panel of anti-cancer aryl sulphonamides act as molecular glues promoting a neo-interaction between RBM39 and DCAF15 – a receptor of the E3 ubiquitin ligase complex (Figure 1.5) (Han et al., 2017b, Uehara et al., 2017). Formation of the RBM39-sulphonamide-DCAF15 ternary complex lead to polyubiquitination and subsequently proteasomal degradation of RBM39 (Figure 1.5B-C) (Bussiere et al., 2020, Du et al., 2019, Faust et al., 2020, Han et al., 2017b, Uehara et al., 2017). Depletion of RBM39 in this manner results in transcriptome-wide splicing abnormalities and

remarkable growth inhibition of tumours *in vivo* (Han et al., 2017b, Nijhuis et al., 2022, Singh et al., 2021), consistent with the effect of RBM39 knock-down or knock-out (Ting et al., 2019, Uehara et al., 2017, Wang et al., 2019). Besides RBM39, RBM23 is another neo-substrate of DCAF15 in the presence of anti-cancer aryl sulphonamides due to high sequence homology in the second RRM domain with RBM39 (Faust et al., 2020, Bussiere et al., 2020, Ting et al., 2019). Interestingly, current evidence indicates that RBM39 is exclusively responsible for splicing abnormalities and cytotoxicity in response to the anti-cancer aryl sulphonamides, evidenced by the findings that the point mutation G268V in the RRM2 domain of RBM39 abrogated DCAF15-mediated RBM39 degradation, rescued splicing errors and conferred strong resistance to anti-cancer aryl sulphonamides (Han et al., 2017b, Ting et al., 2019, Wang et al., 2019).

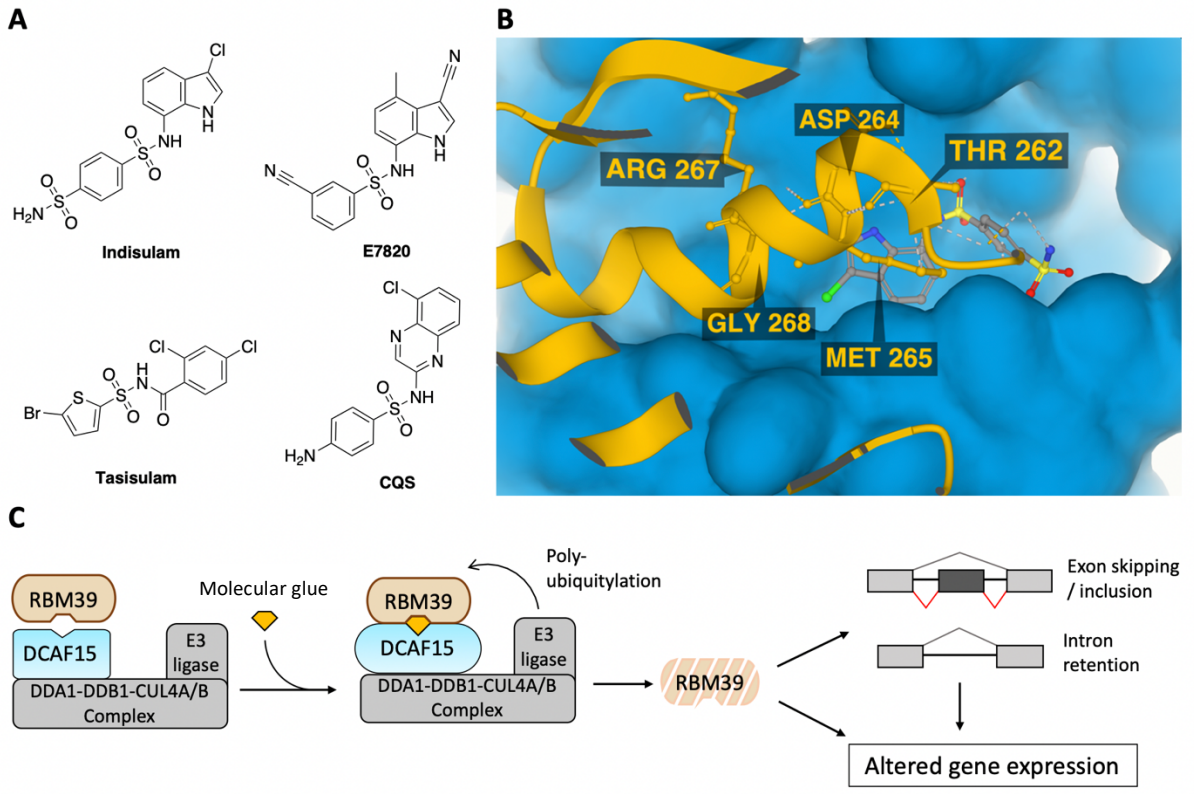


Figure 1.5. Anti-cancer aryl sulphonamides cause selective RBM39 degradation by DCAF15.
(A) Structure of anti-cancer aryl sulphonamides re-discovered as a novel class of molecular glues targeting RBM39. **(B)** Crystal structure of RBM39 (RRM2)-indisulam-DCAF15 complex (PDB ID: 6U7D). Indisulam (shown as ball-and-stick) induces conformational changes of DCAF15 (shown as blue Gaussian surface), generating a shallow but extensive binding pocket for the RRM2 domain of RBM39 (in yellow). Indisulam directly interacts with both RBM39 and DCAF15. Mutations in RRM2 residues (highlighted) can abrogate this interaction, conferring strong resistance to indisulam. **(C)** Mechanism of RBM39 degradation induced by anti-cancer aryl sulphonamides. RBM39 is not a natural substrate of the DCAF15-associated E3 ubiquitin ligase complex, but it is recruited to DCAF15 in the presence of

molecular glues. Consequently, RBM39 is polyubiquitinylated and degraded through proteosomes. Loss of RBM39 causes splicing abnormalities across the transcriptome and alters gene expression. This figure is taken from my review paper with permission (Xu et al., 2020b).

Four anti-cancer aryl sulphonamides have been identified as molecular glues promoting RBM39 degradation, including indisulam (or E7070), E7820, chloroquinoxaline sulphonamide (CQS) and tasisulam (Figure 1.5A). They all degrade RBM39 through DCAF15 but with varying efficiency. According to RBM39 degradation potency, they can be ranked as E7820 ≈ indisulam >> CQS ≈ tasisulam, which positively correlates with their cytotoxicity and efficiency in modulating RNA splicing (Han et al., 2017b, Uehara et al., 2017, Coomar et al., 2021). Before being re-discovered as molecular glues, these aryl sulphonamides had been independently investigated in preclinical studies and demonstrated promising anti-tumour activities both *in vitro* and *in vivo* [reviewed in (Xu et al., 2020b)]. Historically, indisulam was developed as a cell cycle inhibitor downregulating the expression of cyclin A, B1, H and CDK1 (Fukuoka et al., 2001, Owa et al., 1999, Ozawa et al., 2001, Yokoi et al., 2002); E7820 was characterised as an antiangiogenesis agent reducing integrin α2 expression (Funahashi et al., 2002, Hülskamp et al., 2021, Semba et al., 2004); CQS was known as a drug targeting topoisomerase IIα and IIβ (Gao et al., 2000, Gao et al., 2003); and tasisulam was documented as an agent targeting cell cycle and angiogenesis (Haritunians et al., 2008, Meier et al., 2011). Although indisulam, E7820, CQS, and tasisulam showed seemingly differential effects in early studies, it is likely that all of these phenotypes are downstream effects of RBM39 degradation via DCAF15 because either RBM39-G268V mutation or DCAF15 depletion conferred strong resistance to all four anti-cancer aryl sulphonamides (Han et al., 2017b, Uehara et al., 2017). In addition, exon skipping events of *TOP2A* and *TOP2B* genes have been identified in RNA sequencing data of cancer cells treated with RBM39 degraders (Nijhuis et al., 2022, Wang et al., 2019), which may account for the observed impact of CQS on topoisomerase IIα and IIβ. RBM39 also regulates the splicing of vascular endothelial growth factor (VEGF) isoforms (Dowhan et al., 2005, Uehara et al., 2017, Mai et al., 2016a) and many cell cycle genes (Nijhuis et al., 2022, Wang et al., 2019, Mai et al., 2016a, Singh et al., 2021), which may explain previously observed antiangiogenic and cell cycle inhibitory effect of indisulam, E7820 and tasisulam.

Between 1989 to 2020, indisulam, E7820, CQS and tasisulam were evaluated as monotherapy for cancer treatment in 13, 2, 6, and 10 clinical trials, respectively [reviewed in (Xu et al.,

2020b)]. Contrary to the strong anti-tumour effect in preclinical studies, only minor to moderate clinical benefits were observed in small numbers of patients, and none of the anti-cancer aryl sulphonamides progressed beyond phase III trials (Xu et al., 2020b). Because all clinical trials were designed before the aryl sulphonamides were known as molecular glues, no predictive marker was available and little to no patient stratification was performed, which could be the main reasons for disappointing clinical performance. Re-evaluating these agents as RBM39 degraders and identifying cancer patients with increased RBM39 or spliceosome dependency are expected to improve the clinical outcome (Wang et al., 2019, Singh et al., 2021, Nijhuis et al., 2022, Hsiehchen et al., 2020).

1.4. Hypothesis and aims

1.4.1. Improving PARP inhibitor response by targeting splicing factors

Splicing factors are recognised as important players in DNA damage response by coordinating expression and alternative splicing of DNA damage repair proteins (Sciarrillo et al., 2020, Rahmutulla et al., 2014, Meng et al., 2019). For example, the expression of key DNA damage repair factors, such as ATM, RAD51 and Chk1, requires the functional U2 snRNP complex, and inhibiting this complex results in defective DNA damage response (Tanikawa et al., 2016). Similar inhibitory effects were observed in SF3B1-mutated cancer cells, where abnormal splicing of many DNA damage repair genes was observed (Lappin et al., 2022). In agreement with these findings, loss of splicing factors SF3B1 and U2AF65 phenocopy *BRCA1*-deficiency and sensitise BRCA-proficient cancer cells to PARP inhibitors and chemotherapy (Lappin et al., 2022, Savage et al., 2014). Furthermore, spliceosome inhibition overcomes chemotherapy resistance in *BRCA1*-mutated breast cancer and ovarian cancer cells by downregulating the expression of the BRCA1-Δ11q splicing variant (Wang et al., 2016). These studies demonstrate that targeting spliceosome components is a promising approach to improve cancer cell response to chemotherapy and PARP inhibitors.

RBM39 is a splicing factor interacting closely with SF3B1 and U2AF65 [reviewed in (Xu et al., 2020b)]. Transcriptomic analysis suggests that RBM39 may regulate the splicing of DNA damage repair factors (Mai et al., 2016a), but the exact mechanism and clinical significance of this finding have not been investigated. It is reasonable to predict that by inducing splicing errors in DNA repair genes, loss of RBM39 would compromise DNA damage response and

increase the sensitivity of cancer cells to platinum and PARP inhibitors. This is particularly interesting in the context of ovarian cancer, where PARP inhibitor resistance is an emerging challenge, and the therapeutic potential of spliceosome-targeted therapy has not been explored.

1.4.2. Preliminary data

In our recent publication, we performed RNA-sequencing analysis using the human neuroblastoma cell line IMR-32 after indisulam treatment, which revealed aberrant splicing in many DNA damage repair genes such as *ATM*, *BRCA1*, *RAD51D* and *TP53BP1* (Nijhuis et al., 2022). I hypothesised indisulam may cause similar splicing abnormalities in ovarian cancer as it did in IMR-32, because a series of indisulam-induced alternative splicing events in neuroblastoma cells were validated in ovarian cancer cells (unpublished data from Dr Anke Nijhuis, personal communication, 10 January 2019).

The frequent somatic focal amplification of chromosome 19p13 in HGSOC increases copy numbers of many genes including DCAF15 (genomic location 19p13.12) (Sung et al., 2014). In-house analysis of public datasets revealed that over 50% of serous ovarian cancer tumours had increased copy numbers of *DCAF15*, correlating with increased DCAF15 mRNA abundance and higher sensitivity to indisulam (Figure 1.6). Preliminary analysis in our lab confirmed that indisulam is cytotoxic to ovarian cancer cells and causes RBM39 degradation in a DCAF15-dependent manner (Figure 1.6). These data encourage further investigation of RBM39-targeted therapy in ovarian cancer.

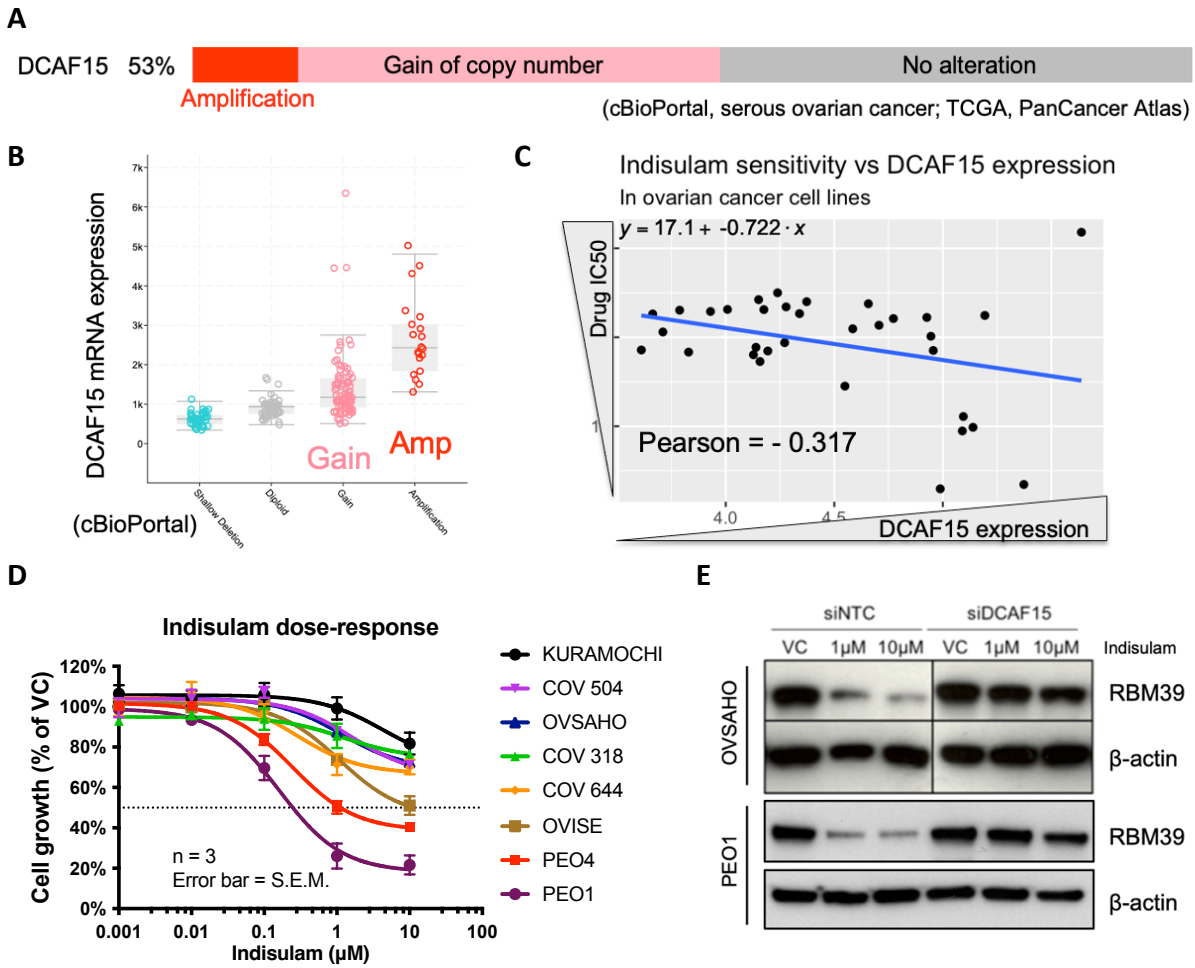


Figure 1.6. DCAF15 amplification is common in ovarian cancer and correlates with higher indisulam sensitivity.

(A-C) Up to 53% of patients with serous ovarian cancer have increased copy numbers of DCAF15 in ovarian cancer patients (a), which correlates with increased *DCAF15* mRNA expression (b) and higher sensitivity to indisulam (c). The findings were originally found by Dr Anke Nijhuis and I reperformed the analysis to generate these figures. Gain, gain of *DCAF15* copy number (three to four copies). Amp, amplified *DCAF15* (more than five copies). Patient data in (a-b) were acquired from the Cancer Genome Atlas PanCancer dataset of serous ovarian cancer and plotted using the cBioPortal (Gao et al., 2013, Cerami et al., 2012). Drug sensitivity data and the DCAF15 expression data in ovarian cancer cell lines were obtained from the Cancer Target Discovery and Development Network (Rees et al., 2016) and the Cancer Cell Line Encyclopaedia (https://sites.broadinstitute.org/ccle), respectively. **(D)** Ovarian cancer cells were treated with the molecular glue indisulam for 72 hours with indicated doses, and cell growth was estimated using the SRB assay. Data were generated by Dr Anke Nijhuis (n = 3). **(E)** Western blot data show that indisulam induced RBM39 degradation in OVSAHO and PEO1 cells, which was rescued when DCAF15 expression was knocked down by siRNA (n = 3). Data of OVSAHO cells and OVISE cells were generated by master students Anushana Shukla and Demi A. Wiskerke, respectively.

1.4.3. Hypothesis and aims

Based on literature evidence and preliminary data, I hypothesised that RBM39 degraders, such as indisulam, induce mis-splicing of DNA damage repair genes in ovarian cancer cells, leading to increased susceptibility to DNA damaging agents including PARP inhibitors. The aims of each results chapter were:

Chapter 3: Examining whether indisulam synergises with DNA damaging agents in ovarian cancer cell lines from two perspectives: growth inhibition and induction of cell apoptosis.

Chapter 4: Evaluating the tolerability and combination effect of indisulam and PARP inhibitor olaparib in the ID8 murine HGSOC model.

Chapter 5: Investigating the impact of indisulam on genotoxic stress (DNA damage and replication stress) caused by PARP inhibitors.

Chapter 6: Assessing the impact of indisulam on transcriptome and proteome in ovarian cancer cells.

Chapter 2. Materials and Methods

2.1. Drug preparation

The following drugs were used to treat cells (Table 2.1). They were prepared according to manufacturers' instructions.

Table 2.1 List of drugs used in this thesis.

Drugs	Source	Identifier	Vehicle solutions
Indisulam	Sigma-Aldrich	SML1225	Dimethyl sulfoxide (DMSO, *in vitro*) Saline (0.9% NaCl) containing 3.5% DMSO and 6.5% Tween-80 (*in vivo*)
E7820	Sigma-Aldrich	SML2950	DMSO
Olaparib	Selleckchem	S1060	DMSO (*in vitro*) Saline containing 3.5% DMSO and 6.5% Tween-80 (*in vivo*)
Rucaparib phosphate	Selleckchem	S1098	DMSO
Veliparib	Selleckchem	S1004	DMSO
Niraparib	Selleckchem	S2741	DMSO
IdU	Sigma-Aldrich	I7125	1M NH_4OH
BrdU	Sigma-Aldrich	B5002	DMSO
Z-VAD-FMK	APExBIO (a gift from Professor Iain McNeish)	A1902	DMSO

2.2. Cell lines

Sources and culture conditions of cell lines used in this thesis are shown below (Table 2.2). Cells were cultured at 37°C with 5% CO_2 and regularly tested for mycoplasma contamination. To avoid genetic drift, fresh stocks of human cell lines were thawed every two to three months, and murine cell lines were cultured for no more than ten passages. KURAMOCHI, COV318, COV504, COV644 and PEO1 (the parental line used for *DCAF15* editing) cell lines were authenticated by the European Collection of Authenticated Cell Culture (operated by the Public Health England, case #112332). The rest of human HGSOC cell lines were authenticated by the supplier. The CRISPR-edited murine ovarian cancer ID8-*Trp53*$^{-/-}$ and ID8-*Trp53*$^{-/-}$;*Brca2*$^{-/-}$ clones were generous gifts from Professor Iain McNeish, whose team generated these clones (Walton et al., 2016).

Table 2.2 Sources and culture conditions for cell lines.

Cell lines	Sources	Culture conditions[a]
KURAMOCHI	A kind gift from Dr Haonan Lu, Imperial College London	DMEM medium (5.6 mM glucose) + 10% FBS + 2 mM L-glutamine + 100 units/mL of penicillin-streptomycin
COV318	European Collection of Authenticated Cell Culture	DMEM medium (5.6 mM glucose) + 10% FBS + 2 mM L-glutamine + 100 units/mL of penicillin-streptomycin
COV504	European Collection of Authenticated Cell Culture	DMEM medium (5.6 mM glucose) + 10% FBS + 2 mM L-glutamine + 100 units/mL of penicillin-streptomycin
COV644	European Collection of Authenticated Cell Culture	DMEM medium (5.6 mM glucose) + 10% FBS + 2 mM L-glutamine + 100 units/mL of penicillin-streptomycin
OVSAHO	Japanese Collection of Research Bioresources	RPMI-1640 medium + 10% FBS + 2 mM L-glutamine + 100 units/mL of penicillin-streptomycin
OVISE	Japanese Collection of Research Bioresources	RPMI-1640 medium + 10% FBS + 2 mM L-glutamine + 100 units/mL of penicillin-streptomycin
PEO1	Public Health England	RPMI-1640 medium + 10% FBS + 2 mM L-glutamine + 100 units/mL of penicillin-streptomycin + 2 mM sodium pyruvate
PEO4	Public Health England	RPMI-1640 medium + 10% FBS + 2 mM L-glutamine + 100 units/mL of penicillin-streptomycin + 2 mM sodium pyruvate
PEO1-*DCAF15*^{WT}; PEO1-*DCAF15*^{KO}	Generated by Dr Anke Nijhuis[a].	RPMI-1640 medium + 10% FBS + 2 mM L-glutamine + 100 units/mL of penicillin-streptomycin + 2 mM sodium pyruvate
ID8-*Trp53*$^{-/-}$; ID8-*Trp53*$^{-/-}$;*Brca2*$^{-/-}$	Professor Iain McNeish	DMEM medium (25 mM glucose) + 4% FBS + 2 mM L-glutamine + 100 units/mL of penicillin-streptomycin + 1mM sodium pyruvate + 1x Insulin-Transferrin-Selenium solution.

Note: [a]FBS, foetal bovine serum, was sourced from Gibco™ and FirstLink. The rest reagents were products of Gibco™. [b]*DCAF15*-knockout in the PEO1 cells was validated by Dr Anke Nijhuis. The knockout clones showed small deletion in *DCAF15* and strong resistance to indisulam, consistent with previous studies (Uehara et al., 2017, Han et al., 2017b). The loss of DCAF15 at the protein level was not validated due to the lack of specific antibodies. The parental PEO1 cell line was a kind gift from Professor Bob Brown. It acquired a mis-sense mutation (5192A>T) in *BRCA2* because of long-term culturing, which partially restores the BRCA2 function (Sakai et al., 2009). The PEO1 cell line purchased from the Public Health England did not have the *BRCA2* reversion mutation.

2.3. PCR-based alternative splicing analysis

Total RNA from cells was extracted using the miRNeasy Mini Kit (Qiagen, #217004) or RNeasy® Mini Kit (Qiagen, #74106) with DNase digestion step according to the manufacturer's instructions. Yield from each extraction was quantified using a NanoDrop with the "RNA-40"

function. Then, an equal amount of RNA was reverse-transcribed into cDNA using the High-Capacity RNA-to-cDNA™ Kit (Applied Biosystems). To detect exon skipping events, primers flanking the skipped exons were designed and synthesised by Eurofins Scientific. Table 2.3 shows a list of all primers used in this thesis. Exon annotations were based on the human reference genome GRCh37 (https://grch37.ensembl.org/index.html). The optimal annealing temperature (Tm) for each pair of primers was determined using the New England Biolabs (NEB) Tm Calculator (https://tmcalculator.neb.com/#!/main). The Q5® High-Fidelity PCR Kit (NEB) was used to prepare polymerase chain reaction (PCR) mixtures, and samples were run on a DNA Engine TETRAD2 Peltier Thermal Cycler (MJ Research, PTC-240) following the program shown below (Table 2.4). The amplified products were mixed with the Purple Gel Loading Dye (NEB) and electrophoresed for 45 to 60 minutes in 2-3% agarose (Sigma-Aldrich) gels supplemented with 1:10,000 SYBRsafe DNA gel stain (Invitrogen) or GelRed. After electrophoresis, the gels were imaged using a Gel Doc. Fiji V2.0.0 was used for densitometry analysis. The abundance of each splicing variant was normalised to the combined abundance of all splicing isoforms detected in the sample.

Table 2.3 Primers used to validate exon skipping events.

Gene	Exon skipping	Primer sequence (5' to 3')		Tm
GAPDH	No skipping	Forward Reverse	GGCTGCTTTTAACTCTGG GGAGGGATCTCGCTCC	66
BRCA1	Exons 8 and 9	Forward Reverse	AACTCTGAGGACAAAGCAGC CTGTAATGAGCTGGCATGAGT	66
RAD51D	Exons 4 and 5	Forward Reverse	TGGCTCAGTTCTCGGCTTT AGATGTCAAATGCATGCACCA	66
TP53BP1	Exon 17	Forward Reverse	GCTGTTGCTGAGTCTGTTGC TGCGTACTTCCCGGATTGTT	68
RIF1	Exon 7	Forward Reverse	AGGTGGGCAAAACTGGTCAT TGGGTGCTCCACTACGAAAT	67
ATM	Exons 52 and 53	Forward Reverse	TGCCTCTTATGTACCAATTGGCT AATTGGCTGGTCTGCTGGAA	67

Table 2.4 The PCR reaction program.

PCR steps	Temperature	Duration
Initial Denaturation	98°C	30 seconds
35 Cycles	98°C 60-70°C 72°C	10 seconds 30 seconds 20 seconds
Final Extension	72°C	2 minutes
Hold	4°C	Unlimited

Chapter 2 – Materials and Methods

2.4. Protein Extraction

To extract proteins from cultured cells, cells were lysed in RIPA lysis buffer (#R0278, Sigma-Aldrich) supplemented with 1% HALT protease inhibitor (Thermo Scientific, #78429) or 1% HALT protease and phosphatase inhibitor cocktail (Thermo Scientific, #78442). When extracting proteins from tumour tissues, 10 to 30 mg tissues were mixed with 500-600 µL RIPA lysis buffer supplemented with 3% Halt Protease and Phosphatase Inhibitor Cocktail. Glass grinding beads were added, and the tissue was homogenised using the Precellys Evolution tissue homogeniser with activated Cryolys Evolution cooling system (10,000 rpm, 20s*5 with 15s pause, two cycles). To facilitate protein extraction, the tissue suspensions were sonicated for 10 minutes in an iced-water bath, followed by a 30-minute incubation on ice. Protein supernatants were collected after high-speed centrifugation (20,000xg at 4°C for 20 minutes). The concentration of extracted proteins was determined using the Pierce BCA protein assay (Thermo Scientific #23225) with a standard curve included every time.

2.5. Western blot

For electrophoresis, protein samples were mixed with the 1x Laemmli Sample Buffer (BIO-RAD, supplemented with 10% 2-mercaptoethanol) and heated at 95°C for 10 minutes. For protein samples extracted using urea, the heating step was skipped. Next, samples were loaded onto 4-20% tris-glycine Mini-PROTEAN® Precast Gel and electrophoresed at 200V for 35 to 50 minutes in the running buffer. After electrophoresis, proteins were transferred onto nitrocellulose membranes using the wet-transfer (100V for one hour). The standard sodium dodecyl sulfate (SDS) running buffer (25 mM Tris, 190 mM glycine, and 0.1% SDS) and transfer buffer (25 mM Tris, 190 mM Glycine, 20% Methanol, pH 8.3) were used.

Membranes were blocked for one hour in the blocking buffer, which consisted of 5% skimmed milk in tris-buffered saline with 0.1% of Tween-20 (TBST). After blocking, membranes were incubated with primary antibodies overnight at 4°C. The next day, membranes were washed three times with TBST (five minutes each) and incubated with horseradish peroxidase (HRP)-conjugated secondary antibodies. Afterwards, the membrane was washed three times with TBST, and the membrane-bound HRP-conjugated antibodies were detected using the SuperSignal™ West Pico PLUS Chemiluminescent Substrate (Thermo Scientific™). The chemiluminescent signal was captured using Amersham Hyperfilm ECL (GE Healthcare) films.

Densitometry analysis of protein band intensities was performed using Fiji V2.0.0, and the values were normalised to the loading control β-actin unless otherwise indicated.

A list of antibodies is shown in Table 2.5. Primary antibodies were prepared in the blocking buffer or TBST containing 5% bovine serum albumin (BSA) when the target protein was phosphorylated. Secondary antibodies were prepared in the blocking buffer. Membranes might be stripped once with the Restore WB stripping buffer (Thermo Scientific #21059) and re-probed with additional antibodies.

Table 2.5 Antibodies used for western blot.

Antibodies	Source	Identifier	Dilutions
Rabbit anti-RBM39	Sigma-Aldrich	HPA001591	1:250 – 1:500
Mouse anti-β-actin	Abcam	Ab6276	1:10,000 – 1:50,000
Mouse anti-phospho-Histone H2A.X (S139)	Sigma-Aldrich	05-636	1:1,000
Rabbit anti-phospho-Chk2 (T68)	R&D system	AF1626	1:300
Rabbit anti-Chk2	R&D system	MAB1358	1:500
Rabbit anti-phospho-ATM (S1981)	Abcam	Ab81292	1:2,000
Mouse anti-ATM	GeneTex	GTX70103	1:1,000
Rabbit anti-phospho-Chk1 (S345)	Cell Signaling Technology	CST2348	1:1,000
Mouse anti-Chk1		CST2360	1:1,000
HRP-conjugated goat anti-rabbit	Invitrogen	31460	1:2,500 - 1:5,000
HRP-conjugated goat anti-mouse	Invitrogen	31340	1:2,500 - 1:5,000

2.6. Human phospho-kinase array

KURAMOCHI cells were treated with 10 μM indisulam and 30 μM olaparib either individually or in combination for 48 hours, and total proteins were extracted using the RIPA lysis buffer (Sigma-Aldrich, #R0278) supplemented with 1x Halt Protease and Phosphatase Inhibitor Single-Use Cocktail (Thermo Scientific, #78442). Protein concentration was estimated using Pierce BCA Protein Assay Kit (Thermo Scientific #23225). An equal amount of protein (185 μg) was used for each Proteome Profiler Human Phospho-Kinase Array (R&D system, ARY003B) following manufacturer's instructions. SuperSignal West Pico PLUS Chemiluninescent Substrate (Thermo Scientific, #34579) and Amersham Hyperfilm ECL (GE Healthcare) were used to visualise signals of kinase phosphorylation (around five minutes of exposure). Image Studio Lite (LI-COR) was used for densitometry analysis. Kinases with visible signals in at least one array were included for downstream analysis (n = 27) and ranked based on densitometry intensities in the vehicle control. Then, phosphorylation changes of each kinase were calculated relative to vehicle control. Kinases with differential relative phosphorylation

changes (≥50% difference relative to vehicle control) between monotherapy and the combination therapy.

2.7. Sulforhodamine B cell growth assay

Cell growth was measured using the sulforhodamine (SRB) assay as previously described (Vichai and Kirtikara, 2006). SRB powder was purchased from Sigma-Aldrich. In brief, cells were counted using a haemocytometer (Hawksley) and seeded in 96-well plates at the following densities: 500 cells/well (ID8 clones), 2000 cells/well (OVISE, COV318, and COV504), 2500 cells/well (PEO1 and PEO4), 4000 cells/well (COV644 and KURAMOCHI), and 5000 cells/well (OVSAHO). Cells were allowed to attach overnight before drug treatment. Drugs of desired concentration were always prepared fresh in the culture medium. At the end of drug treatment, cells were fixed with 10% (w/v) trichloroacetic acid (TCA) solution at 4 °C for one hour, and then gently rinsed under tap water. Fixed plates were air-dried on the bench overnight. The next day, cells were stained with 0.4% SRB solution (in 1% acetic acid) for 30 min at room temperature. Stained cells were washed with 1% acetic acid four times to remove the unbound dye and air-dried on the bench. Afterwards, protein-bound SRB was solubilised in 10 mM Tris-base for 30 minutes with gentle agitation. To quantify cell growth, absorbance at 565 nm or 510nm was measured using a microplate reader (OPTImax Molecular Devices or ClarioStar from BMG Labtech). Cell-free blank controls were always included for background correction. Relative cell growth was calculated by normalising to the vehicle control (0.1% - 0.2% DMSO). Each biological repeat included at least three technical replicates unless otherwise specified. Dose-response curves and the dose causing 50% growth inhibition (IC50) were generated using the Prism V9.4.1 using nonlinear regression function [inhibitor] vs. response (three parameters).

2.8. Colony growth assay

Adherent cells were detached from the culture flasks using TrypLE Express Enzyme (1X, no phenol red, Gibco #12604013), and single-cell suspensions were generated by passing cells through a 40 µm cell strainer (Corning). Appropriate numbers of cells were seeded into 6-well plates and incubated for 16 days before staining and counting. The medium in each well was refreshed every two to three days.

For OVSAHO colony growth assay, cells were seeded at a density of 3000/well, and the drug treatment started five days post-seeding. At the end of 48- or 72-hour treatment, cells were washed twice with phosphate-buffered saline (PBS) and fresh media were added. On day 16, cells were washed once with PBS and fixed in ice-cold methanol for 10 minutes. Fixed cells were stained with 0.5% crystal violet (in 20% methanol) at room temperature for 10 minutes. Stained cells were washed gently under tap water to remove excess dye and air-dried for long-term storage. Colonies were imaged with an Epson Perfection V300 scanner.

Fiji V2.0.0 was used to count OVSAHO colonies. Each well was manually cropped out from the entire image and converted to 8-bit format. Outlines of colonies were highlighted by "Find edges" function and the colour threshold was adjusted to (42;255). Colonies larger than 50 pixels (in 1.35 inches x 1.35 inches, 800 pixel/inch dimension) and circularity between 0.30 to 1.00 were counted automatically using the "Analyse Particle" function. A pilot OVSAHO colony growth assay with increasing seeding density (156/well to 5000/well) was conducted beforehand to optimise parameters for automated colony counting.

2.9. Cell apoptosis assays

2.9.1. Caspase-Glo 3/7 activation assay

Caspase 3/7 activities in cells were measured using the Caspase-Glo 3/7 assay (Promega) following the supplier's instructions. Cells were seeded in clear-bottom 96-well plates at the same density as the SRB assay (Section 2.6). Two parallel plates were seeded and exposed to the same drugs for the same duration. One for caspase 3/7 activity measurement and another for cell growth measurement using the SRB assay. At the end of the drug treatment, conditioned media were removed and replaced with 50 µL fresh culture media. An equal volume of Caspase-Glo 3/7 reagent was added to each well and incubated at room temperature for one hour with agitation. The reaction mixture was next transferred into CulturPlate White Opaque 96-well plates, and luminescence signals were measured using a ClarioStar plate reader (BMG Labtech). Fold changes in caspases activities were background corrected using cell-free controls and normalised to vehicle control and the SRB data (caspases signal relative to vehicle control / cell growth relative to vehicle control). Each biological repeat included three technical replicates.

2.9.2. Annexin V-Propidium Iodide staining assay

KURAMOCHI cells were seeded in 12-well plates (150,000 cells per well) and were treated with 10 µM indisulam, 30 µM olaparib, or their combination (with or without 10 µM Z-VAD-FMK) for 48 hours. At the end of the drug treatment, adherent cells were detached using the TrypLE Express Enzyme and combined with floating cells. Cell suspensions were washed twice with ice-cold PBS and resuspended in 1x binding buffer (0.01M Hepes, 0.14M NaCl, 2.5 mM $CaCl_2$). Cells were passed through cell strainers (30 µm) to generate single-cell suspensions. Next, they were stained in 50 µL binding buffer containing 2.5 µL Cy5.5-conjugated Annexin V (BD Biosciences, #559925) and 2.5 µL eBioscience Propidium Iodide (PI) Staining Solution (Invitrogen, 00-6990-50). After 15 minutes of staining in the dark (room temperature), 300 µL binding buffer was added to each sample and samples were analysed within two hours using a BD FACS Canto analyser. The 488nm laser and PerCP filter were used to detect PI, and 633 nm laser and APC filter were used to detect Cy5.5-conjugated Annexin V staining. Colour compensations were performed each time using untreated cells and single-colour positive controls (cells heated at 60 °C for 4 minutes). Data were analysed using FlowJo V10.6.2, and the same gating was used across biological repeats.

2.10. Drug combination and synergy analysis

2.10.1. Synergy analysis using the Chou-Talalay method

The Chou-Talalay method (Chou and Talalay, 1984, Chou, 2010) and Bliss Independence [reviewed in (Yang et al., 2015)] were used for synergy analysis. The Chou-Talalay method was the preferential choice because it is more accurate than other conventional methods (discussed in the Appendix Discussion). The Bliss Independence was only used for the drug combination screen in Section 2.10.2. The Appendix Discussion critically reviews the advantages and disadvantages of these two methods and other commonly used synergy methods.

For synergy analysis using the Chou-Talalay method, dose-response curves of each drug were acquired through the SRB cell growth assay. Doses of two drugs that cause similar levels of growth inhibition (no more than IC60) were selected for combination treatment, and two agents were mixed at a constant ratio. The combination index (CI) values were calculated

using CompuSyn (Chou and Martin, 2005). CI < 1 indicates synergism; CI = 1 indicates additive; and CI > 1 indicates antagonism.

2.10.2. Drug combination screen using the Bliss Independence

A library of FDA-approved drugs (approved oncology drugs set IX, plates 4891-4892) was acquired from the United States National Cancer Institute Developmental Therapeutics Program (https://wiki.nci.nih.gov/display/NCIDTPdata/Compound+Sets). From the library, I selected all genotoxic agents (n = 54) and taxanes (n = 6) to be combined with either vehicle control (0.1% DMSO) or a sublethal dose of indisulam (10 µM) in a pairwise approach in KURAMOCHI cells. Seven doses of the selected drugs were combined with indisulam, ranging from 8 nM to 20 µM. All drug combinations were tested in parallel, and cell growth was measured using the SRB assay. To adjust for the seeding differences across plates, each plate contained at least three technical replicates of vehicle control for normalisation. Each drug combination had one technical replicate.

The bliss independence was used for synergy analysis in this drug screen because the data did not contain a full-dose response curve of indisulam and therefore did not meet the requirement for the Chou-Talalay method. The Bliss score was calculated as the difference between observed growth inhibition and the expected additive growth inhibition (growth inhibition of indisulam + growth inhibition of the drug of interest – growth inhibition of indisulam*growth inhibition of the drug of interest). Bliss scores > 0 indicate synergism, Bliss scores = 0 indicate additive, and Bliss scores < 0 indicate antagonistic. Drugs were categorised as likely synergistic with indisulam if at least two dose-pairs had Bliss scores ≥ 0.05; and drugs were categorised as likely antagonistic with indisulam if at least five dose-pairs had Bliss scores ≤ -0.05. Drugs were ranked based on the number of dose-pairs having Bliss scores ≥ 0.05 and the average bliss score of all dose-pairs. Drugs were annotated based on the database provided by SelleckChem (https://www.selleckchem.com/screening/fda-approved-drug-library.html).

2.11. *In vivo* studies using the ID8 murine HGSOC model

All animal studies were conducted in accordance with the UK Animals (Scientific Procedures) Act 1986. I was the principal investigator for all studies and registered as a personal license

holder (I26105643) under Professor Iain McNeish's Project License (PA780D61A). Yitao Xu, Flora Upton, Michael Gruet, Dr Sarah Spear and Fabio Grundland Freile supported me in completing animal studies, but I did the majority of the work (from the study design, acquiring data, to analysing the data). C57BL/6 female mice aged between 6-7 weeks were ordered from Charles River Laboratories (UK). Upon arrival, mice were acclimatised for seven days and at day eight, they were intraperitoneally (I.P.) injected with five million ID8-*Trp53*$^{-/-}$ cells in 200 µL warm PBS.

Drug suspensions of indisulam (Sigma-Aldrich) and olaparib (Selleckchem) were prepared in saline containing 3.5% DMSO and 6.5% Tween-80 one week before scheduled drug injections. The optimisation process of the drug formulation is shown in Section 4.2.1. Single-use aliquots were prepared and stored at -20 °C until the injection day. Animals were randomised for drug treatment. Drugs were administrated via I.P. and injection sites were alternated between the left and right abdomen to minimise animal discomfort. Mice were regularly monitored and weighed at least twice a week.

Humane endpoints in the studies were defined in the Project License and following clinical signs were monitored throughout the study: any of over 20% weight loss, abdominal distension greater than late pregnancy, self-mutilation, facial grimace, hunched posture, and reduced activity. For pilot studies (Section 4.2.2 – 4.2.3), mice were sacrificed upon reaching the humane endpoints or 42 days after tumour injection. For the survival studies (Section 4.3), mice were sacrificed upon reaching the humane endpoint or 120 days after tumour injection. To improve consistency and minimise human bias while assessing humane endpoints, researchers were blinded from treatment details after completing all drug injections. The decision of mice reaching the humane endpoint was always discussed with an independent animal technician. After sacrificing the mice, visible omental tumour deposits were collected. Tumour tissues were snap-frozen in liquid nitrogen or dry ice and stored at -80°C.

Notably, data from the survival study in Section 4.3 were acquired through two biological repeats, each containing six mice per treatment group. In the first round, three mice (one received indisulam and two received the combination therapy) remained healthy till day 120. In the second round, one mouse from the vehicle control group and another from the

combination group (15 mg/kg/day of indisulam + 50 mg/kg/day of olaparib) survived till day 120 without any clinical signs. Only one (which received the combination therapy in the first round) of them developed subcutaneous (s.c.) tumours developed during the drug injection, indicating the existence of ascitic tumour cells and successful tumour implantation. The other four mice survived till day 120 without developing s.c. tumours and no tumour deposits were found upon necropsy. All mice were included for the survival analysis.

2.12. Immunofluorescence analysis

Cells were seeded in 96-well plates at the same density as the SRB assay (Section 2.6). After drug treatment, conditioned media were removed and cells were washed once with PBS. Then, cells were fixed with 4% methanol-free formaldehyde (Fisher Scientific #11586711) for 15 minutes at room temperature. Fixed cells were washed twice with PBS before permeabilisation with 0.1% Triton-X-100 (Sigma-Aldrich, #T8787) for 30 minutes at room temperature. After permeabilisation, cells were gently washed with PBS once and were blocked in the blocking buffer (1% BSA and 2% FBS in PBS) for 30 minutes. To detect γH2AX foci, cells were incubated overnight with mouse anti-γH2AX antibody (1:500 in the blocking buffer, Sigma-Aldrich, #05-636) at 4°C. The next day, cells were washed three times with PBS and were incubated with the staining solution containing Alexa Fluor 488 dye (AF488)-conjugated goat anti-mouse antibody (1:500, Invitrogen, #A11001) and 1 μg/mL DAPI (Sigma-Aldrich, #9542) in the blocking buffer for two hours at room temperature. After staining, cells were washed with PBS three times and kept in 200 μL PBS at 4°C until imaging. An INCell Analyzer 1000 with a 20x objective lens was used to image the γH2AX and DAPI staining. Twenty-five fields were captured from each well.

Images were analysed using the speckle counting pipeline by the Cell Profiler V3.1.8 (https://cellprofiler.org/previous-examples#speckle-counting). Image analysis parameters were determined by comparing negative control cells (vehicle control-treated cells) and positive control cells (cisplatin-treated cells). The nuclei were identified with typical diameter 25 – 100 (in pixel unit), global Otsu threshold (two classes, smoothing scale = 1.318, correction factor = 1.0, smoothing filter = 10, suppress local maxima that are closer than 15 pixels in distance). A mask was created based on nuclei and applied to the γH2AX-stained images. Foci were enhanced using the "Speckles" features (size = 10). Foci of γH2AX were defined as

objects with typical objects with typical diameter between 3 and 15 pixels, and the global manual threshold of 0.15 was used (smoothing scale = 1.3488, clumped objects were distinguished and dividing lines were drawn by shape, smoothing filter = 2, suppress local maxima that are closer than 2 pixels in distance). Once parameters were finalised, experimental images were analysed automatically (in an unbiased manner) by Cell Profiler. At least 500 cells from 25 different views were analysed in each group. The maximum foci count was 50 foci per nucleus. Foci numbers for each nucleus were counted and counts from all fields within the same well were pooled together. The data were shown as bar charts with whiskers indicating 10^{th} or 90^{th} percentile. In case more than 90% cells have less than five foci, the data were presented as the proportion of nuclei containing at least five γH2AX foci (Figure 5.3).

2.13. Single-cell gel electrophoresis (COMET assay)

2.13.1. Alkaline COMET assay

The alkaline COMET assay was performed according to a previously published protocol (Lu et al., 2017). One day before the assay started, COMET slides were prepared by coating SuperFrost microscopic slides with 1% agarose in distilled water (Sigma-Aldrich, #4718). The active lysis solution was freshly prepared by adding 1% Triton X-100 (Sigma-Aldrich #T8787) and 10% DMSO to the inactive lysis solution (2.5M NaCl, 100 mM EDTA, 10 mM Trizma base and 200 mM NaOH in distilled water). Cells were treated in 12-well plates and trypsinised to generate single-cell suspensions. After washing twice with ice-cold PBS, around 3000 cells were mixed with 0.7% low melting point agarose (LMA, Sigma #A9414) and cast as a thin layer on COMET slides. These slides were then covered with a round coverslip and left in the cold room for 20 minutes (protected from light). Once the LMA-cell mixture solidified, coverslips were gently removed and another thin layer of 0.7% LMA was added to prevent cell loss during lysis and washes. Cell lysis was performed by submerging the slides in the active lysis solution overnight in cold room (in the dark). After lysis, the slides were washed in distilled water twice and submerged in freshly prepared alkaline electrophoresis solution (200 mM NaOH, 1 mM EDTA, pH>13) to allow DNA to unwind for one hour on ice. Electrophoresis was performed on ice at 0.8V/cm for 10 minutes. Excess electrophoresis solution was neutralised with 0.4M Trizma base and the slides were fixed with ice-cold 70% ethanol for 30min at room

temperature. Fixed slides were dried for 30 minutes at 37 °C before 15-minute staining with SYBR Gold Nucleic Acid Gel Stain (1:1000, Life Technologies #11494). COMET images were taken through a Nikon Eclipse TE2000-U Inverted Microscope with a 10x objective. Tail moments of comets were quantified with TriTek COMETscore 2.0 and at least 100 comets were scored in each condition.

2.13.2. Neutral COMET assay

For the Neutral COMET assay, COMET slides were prepared in the same way as the alkaline COMET assay. Cells were lysed in the active lysis buffer for one hour at 4 °C in the dark. Then, the slides were submerged in the neutral unwinding solution (1X Tris-Borate-EDTA buffer, pH = 8 - 9) for 30 minutes on ice (in the dark). After unwinding, electrophoresis was performed in 1X Tris-Borate-EDTA buffer for 15 minutes at room temperature (avoid light). Then, slides were drained off electrophoresis buffer and incubated in DNA precipitation solution (1M NH_4Ac in 82.27% Ethanol) for 30 minutes at room temperature (avoid light). Afterwards, slides were fixed, stained, and imaged in the same way as the alkaline COMET assay. This protocol is not optimal and it failed to detect doxorubicin-induced DNA damage (Figure 5.6E).

2.14. Cell cycle analysis

Cell cycle analysis was performed as previously described (Au - Cecchini et al., 2012). In the final hour of drug treatment, the culture media was supplemented with nucleotide analogous (10 µM BrdU or 200 µM IdU) to label replicating cells. Then, cells were detached by trypsinisation and washed twice with PBS. After removing PBS, the cell pellet was resuspended in 100 µL PBS, and 1 mL of 70% ethanol was added drop-wise while gentle vortexing to fix cells. After fixation, cells were stored at 4°C overnight. The following day, ethanol was removed by centrifugation (500xg for 5 minutes). The cell pellet was resuspended in 500 µL of denaturing buffer (2M HCl with 0.5% Tx-100) and incubated at room temperature for 30 minutes with gentle agitation. This was followed by centrifugation to remove the supernatant, and the pellet was resuspended with 500 µL neutralisation buffer (0.1M NaB_4O_7, pH 8.5). Five minutes later, the neutralisation buffer was removed and cells were blocked with blocking buffer (PBS containing 1% BSA and 0.2% Tween-20) for 30 minutes at room temperature, during which they were passed through a cell strainer to remove aggregates.

To detect incorporated nucleotide analogous, cells were incubated with the mouse anti-BrdU (1:25 in the blocking buffer, BD Biosciences, BD347580) antibody for one hour with agitation at room temperature, then washed twice with the blocking buffer, and incubated with the AF488-conjugated goat-anti-mouse antibody (1:100 in the blocking buffer, Invitrogen, #A11001) for one hour in the dark with agitation (room temperature). Next, cells were washed twice with the blocking buffer to remove residue antibodies. The DNA was stained with 300 µL FxCycle PI/RNase staining solution (Invitrogen, #F10797) for 15 minutes at room temperature in the dark. Labelled cells were analysed on a BD FACS Canto analyser. AF488 and PI intensities were detected using the FITC filter (530/30) and PerCP filter (682/33), respectively. Colour compensation controls were included for each experiment. The data were analysed using FlowJo V10.6.2 and the same gating was used across biological repeats.

2.15. DNA fibre analysis

The DNA fibre analysis was performed based on methods reported in the literature (Pillay et al., 2019, Cong et al., 2021). In the final hour of the drug treatment, cells were pulse-labelled with 10 µM BrdU for 30 minutes, briefly washed three times with warm PBS, and then pulse-labelled 200 mM IdU for 30 minutes. BrdU and IdU were prepared in media containing drugs. Next, cells were detached by trypsinisation and washed once with ice-cold PBS. Cell numbers were counted using a haemocytometer. After removing PBS, cells were resuspended in freezing media and stored at -80°C until analysis.

To prepare DNA fibres, cells in freezing media were thawed at 37°C and centrifuged at 500xg for 5 minutes to remove the supernatant. The cell pellet was washed once with PBS and resuspended in ice-cold PBS at a density of 1000 cells per µL. Then, 2 µL of cells were spotted at one end of a superfrost slide (Fisher Scientific, #16242171), and each slide contained two spots. After air-drying for five minutes, the drops were mixed with 7 µL of lysis buffer (200 mM Tris-HCl, pH 7.5, 50 mM EDTA, and 0.5% SDS). To release the DNA content, cells were incubated in the lysis buffer for five to seven minutes until the drop edge started to dry. DNA fibres were spread along the slide by tilting the slide at a small angle (15° – 20°). This prompted the DNA mixture to slowly run down the slide, leaving visible threads of DNA behind. The DNA spreads were air-dried for 30 minutes at room temperature and fixed in the

fixation buffer (75% methanol and 25% acetic acid) for 10 minutes. Fixed slides were air-dried for another 30 minutes and stored at 4 °C until staining.

To stain DNA fibres, the slides were rinsed with distilled water, and DNA strands were denatured by placing slides in 2.5M HCl for one hour. This is followed by two PBS washes and one-hour blocking in PBS containing 1% BSA and 0.1% Tween-20. Incorporated BrdU and IdU were probed with antibodies sequentially. Firstly, slides were incubated with the rat anti-BrdU antibody (1:50 in the blocking buffer, Abcam, #ab6326) for 90 minutes at room temperature, washed three times (twice with PBS, once with the blocking buffer, five minutes each), and incubated with the AF647-conjugated goat anti-rat antibody (1:100 in the blocking buffer, Invitrogen, A21247) at room temperature. Next, slides were washed once with PBS and stored in fresh PBS overnight at 4°C. The following day, slides were washed once with the blocking buffer and incubated with the mouse anti-BrdU antibody (1:50 in the blocking buffer, BD Biosciences, BD347580) for one hour at room temperature to detect IdU. After washing twice with PBS and once with the blocking buffer, slides were incubated with the AF488-conjugated goat anti-mouse antibody (1:100 in the blocking buffer, Invitrogen, A11001) for another hour at room temperature. Excess antibodies were removed by washing with PBS twice and the blocking buffer. After draining the excess buffer, slides were mounted with the Fluoromount-G (Invitrogen, #00-4958-02) and covered with coverslips. The gap between the coverslip and slide was sealed with nail polish. Slides were stored at 4°C (in the dark) until imaging. An Aurox laser-free confocal microscope (60x water objective) was used to image slides within 48 hours of staining. In each repeat, at least 50 fields were taken from each group. The coordinates of each field were recorded to avoid accidentally imaging the same fibre twice.

DNA fibre types were manually determined based on the review from Quinet et al. (2017). Fibre track lengths were manually measured using Fiji V2.0.0, and the “ROI manager tool” was used to annotate fibre selections in each field numerically.

Chapter 2 – Materials and Methods

2.16. RNA sequencing and proteomics analysis

2.16.1. RNA sequencing

Dr Anke Nijhuis generated samples for RNA sequencing, and the National Institute for Health and Care Research-funded Imperial Biomedical Research Centre (BRC) Genomics Facility provided the sequencing service. In brief, three biological replicates of the following samples were submitted for sequencing: KURAMOCHI cells treated with vehicle control (0.1% DMSO), 10 µM indisulam, 30 µM olaparib, or 10 µM indisulam in combination with 30 µM olaparib for 24 hours; and ID8-*Trp53*$^{-/-}$ cells treated with vehicle control (0.1% DMSO) or 1 µM indisulam for 24 hours. Total RNA was extracted using the miRNeasy Mini Kit (Qiagen). Sample integrity was assessed by collaborators the Imperial BRC genomics facility and all samples passed the quality control protocol. Mitochondrial and ribosomal RNA was removed via ribodepletion. A Nextseq2000 P2 (200 cycles) sequencer was used to generate 100-base pair (bp) paired-end reads, producing around 50 million reads per sample.

The alternative splicing analysis was performed by Michael Gruet using the SpliceFisher (Han et al., 2017b, Nijhuis et al., 2022). Sequencing reads from KURAMOCHI cells were mapped to the human reference genome GRCh38, and reads from ID8-*Trp53*$^{-/-}$ cells were mapped to the mouse reference genome GRCm39.

2.16.2. Proteomics analysis

To generate protein lysates, five million KURAMOCHI cells were seeded in 15-cm dishes and allowed to attach overnight. The next day, cells were treated with vehicle control (0.1% DMSO), 10 µM indisulam, 30 µM olaparib, or the combination (10 µM indisulam plus 30 µM olaparib) for 48 hours. At the end of the drug treatment, cells were washed once with PBS containing 1% NaF and detached by incubating with 6 mL TrypLE Express Enzyme (supplemented with 1% NaF) at 37°C for 10 minutes. Another 6 mL of fresh medium (supplemented with 1% NaF) was added immediately after trypsinisation. Cell suspension was harvested and washed twice with ice-cold PBS (supplemented with 1% NaF). After the final PBS wash, the cell pellet was resuspended in 200 µL lysis buffer consisting of 8M urea in 20 mM HEPES, pH 8.0, supplemented with 1.5X phosphatase inhibitor cocktail (ActiveMotif, #37492). Cells in lysis buffer were incubated on ice for 10 minutes and then sonicated in an ice bath for a total of ten minutes (five minutes on and one minute off, two cycles). Cell debris

were removed by centrifuging at 20,000xg for 20 minutes at 4°C and the supernatant was collected. In case the genomic DNA and cell debris were loose, the lysates might be centrifuged again to improve yield. The concentration of protein samples was determined using the Pierce BCA protein assay. According to the BCA results, concentrations of protein samples were adjusted to 2.2 μg/μL and snap-frozen on dry ice. Protein Lo-Bind tubes (Thermo Scientific) were used throughout the process to maximise protein yield.

For ID8-*Trp53*$^{-/-}$ samples, 130,000 cells were seeded in 60 mm dishes. The next days, cells were treated with vehicle control or 1 μM indisulam for 48 hours. Total proteins were extracted by Dr Anke Nijhuis following the same steps as above.

Snap-frozen protein samples containing 50 μg of protein were delivered to the laboratory of Dr Holger Kramer and Dr Alex Montoya for liquid chromatography-tandem mass spectrometer (LC-MS/MS) analysis. A detailed proteomics method is available in Appendix Materials and Methods. In brief, protein samples were pre-processed and analysed using an LC-MS/MS. Raw data were processed using the MaxQuant software platform (v16.10.43), and the label-free quantification (LFQ) was analysed using the Perseus V1.6.15.0. In Perseus, LFQ was log2 transformed and rows with at least four valid readings were included for differential expression analysis. Significantly up- or down-regulated proteins were determined by student's t-test (two-tailed) with thresholds of false discovery rate (FDR) less than 0.05 and the artificial within groups variance (S0) = 0.1.

2.16.3. Venn diagrams, functional annotation, and enrichment analysis

Lists of genes (duplicates removed) were overlapped using the online tool Venny V2.1.0 (Oliveros, 2007) (https://bioinfogp.cnb.csic.es/tools/venny/) and Venn diagrams were drawn in Microsoft PowerPoint for Mac V16.66.1. The Database for Annotation, Visualization and Integrated Discovery (DAVID) (Huang da et al., 2009, Sherman et al., 2022) was used for functional annotation and enrichment analysis (https://david.ncifcrf.gov/summary.jsp). Gene ontology biological processes (DIRECT), Kyoto Encyclopedia of Genes and Genomes (KEGG), REACTOME, and WIKIPATHWAY databases were selected for enrichment analysis. Customised background gene lists were used whenever possible and specified in figure legends. Pathways with FDR < 0.1 were considered significantly enriched. To compare mouse and human gene lists, the "Human and Mouse Homology Classes with Sequence information"

file was downloaded from the Mouse Genome Informatics (http://www.informatics.jax.org/downloads/reports/index.html). The "DB Class Key" was used to match mouse genes to their human equivalent.

2.17. Systematic literature analysis

2.17.1. Identifying RBM39-associated alternative splicing events

To identify common exon skipping and intron retention events in RBM39-depleted cancer cells, I performed a literature search in the PubMed database using "RBM39" as the key word on 10 August 2022. Inclusion criteria were (1) publications that performed RNA-sequencing analysis using RBM39-depleted cancer cells (via knockdown, knockout, or through molecular glues), (2) and conducted alternative splicing analysis, (3) and published the list of alternatively spliced genes. Exclusion criteria were (1) studies did not use human cancer cells, or (2) publications without publicly available lists of mis-spliced genes. Review articles were also excluded. The studies were read in detail to assess eligibility. Five studies were included for analysis (Nijhuis et al., 2022, Singh et al., 2021, Wang et al., 2019, Lu et al., 2021b, Mai et al., 2016a), and lists of exon-skipped or intron-retained genes were downloaded from their supplementary information online. Occurrence of genes across lists were counted in R studio v2022.07.2 using the group_by() and summarise() functions of the dyplr package. Exon skipped genes detected in at least six lists and intron retained genes detected in at least six lists were categorised as common splicing targets of RBM39. Exon skipped genes and intron retained genes were pooled together (duplicates removed) and pathway enrichment analysis was carried out as described in the Section 2.16.3. Pathway enrichment analysis was also performed using the exon skipped genes only. The FDR cut-off was set as 0.1.

2.17.2. Identifying determinants for PARP inhibitor sensitivity

To identify genes that sensitise cells to PARP inhibitors upon depletion, I carried out a PubMed literature search on 10 October 2022 using the advanced terms: (((PARPi or PARP inhibitor) AND (sensitivity)) AND (CRISPR)) AND (screen). Inclusion criteria were publications that performed drop-out CRISPR sensitivity screens for PARP inhibitor sensitivity and with the screen results available online. Review articles and studies that used knockdown screens were excluded. All included publications were read in detail to assess eligibility. Screen outputs from eligible publications were downloaded from supplementary information online or

extracted from main figures. Six eligible publications (Zimmermann et al., 2018, Verma et al., 2021, Su et al., 2020, Juhász et al., 2020, Hewitt et al., 2021, Fang et al., 2019a) plus eight other eligible publications (did not match the key terms but matched the inclusion criteria) (Jamal et al., 2022, Tsujino et al., 2022, Noordermeer et al., 2018, Olivieri et al., 2020, DeWeirdt et al., 2020, Su et al., 2020, Blanck et al., 2020) were included for downstream analysis. In the drop-out CRISPR screen, depleted sgRNA indicates knocking out the target gene sensitise cells to PARP inhibitors (Zimmermann et al., 2018). The same cut off was applied to all datasets: log10(negative selection score) $\leq$ -2 and log2(fold change) $\leq$ -0.05. Genes (sgRNA-depleted) that were detected in at least two drop-out screens were categorised as high-confidence genes that sensitise cells to PARP inhibitors upon depletion. Pathway enrichment analysis was conducted as described in Section 2.16.3.

2.18. Statistical analysis

Except for the proteomics data (Section 2.16.2), statistical analysis was performed using the GraphPad Prism 9 for macOS (V9.4.1). Fisher's exact test was performed (2X2 contingency tables) for enrichment analysis. Student's t-test was used to compare statistical differences between two groups. For western blot data with systematic variations across biological repeats, a paired student's t test was used. One-way ANOVA followed by multiple comparisons tests were used to measure statistical differences among three or more groups. Two-way ANOVA followed by multiple comparisons tests were used to analyse statistical differences when the data included multiple combination doses. For heavily skewed data, such as γH2AX foci counts, Kruskal-Wallis test and multiple comparisons test were used to calculate p-values. Except (Figure 4.7), statistical results were annotated in figures as: ns = not significant, *p < 0.05, **p < 0.01, ***p < 0.001, and ****p < 0.0001. For the Kaplan-Meier survival curves in Figure 4.7, the Log-rank (Mantel-Cox) test was performed to calculate the statistical differences between groups. Bonferroni correction was used to correct the significance threshold for multiple comparisons. The family-wide significance level was 0.05. Since six comparisons were made, the Bonferroni-corrected significance threshold was 0.05/6 = 0.0083. The p-values less than 0.0083 were considered significant and annotated with *.

Sample sizes for animal studies were determined following the guidelines published by Charan and Kantharia (2013). The resource equation method was used to determine sample

sizes for the pilot studies and the first round of the survival analysis. The E values (number of animals – number of groups) between 10 to 20 were considered optimal (Charan and Kantharia, 2013). The E value was 12 (for pilot studies which included 18 mice, six groups) and 20 (for the first round of the survival analysis which included 24 mice, four groups). Data from the first survival analysis was used to calculate the sample size for the second survival analysis. I used the sample size calculator (https://sample-size.net/sample-size-survival-analysis/) (Schoenfeld, 1983) and following parameters were used: significance threshold = 0.0083, statistical power = 75%, proportions of subjects in each group = 1:1, relative hazard ratio olaparib vs. combination = 7.09, attrition rate = 10%). The calculations return the minimal sample size as 12, and therefore six mice were included in each group for the second biological repeat.

Chapter 3

Chapter 3. Evaluating the therapeutic value of indisulam in ovarian cancer

3.1. RBM39 regulates RNA splicing of DNA damage repair genes

3.1.1. Systematic analysis of RBM39-associated alternative splicing events

RBM39 is an important splicing factor for the 3' splice site recognition, and loss of RBM39 causes transcriptome-wide splicing abnormalities in multiple types of cancers (Han et al., 2017b, Nijhuis et al., 2022, Singh et al., 2021, Ting et al., 2019, Uehara et al., 2017, Wang et al., 2019, Mai et al., 2016a, Lu et al., 2021b). Although RBM39 may have cancer or cell line-specific roles, the splicing of some genes may be regulated by RBM39 consistently across cancer types. One way to identify such genes is to consolidate splicing events from previously reported datasets. To this end, I performed a systematic literature search in PubMed database to identify genes alternatively spliced in RBM39-depleted cells. I identified 52 results related to the term "RBM39", and 11 of them reported RNA sequencing analysis in RBM39-depleted cells. After removing two studies that did not use human cancer cell lines (Kralovicova et al., 2018, Faherty et al., 2016) and four papers that did not publish full lists of alternative splicing events (Han et al., 2017b, Ting et al., 2019, Uehara et al., 2017, Puvvula et al., 2021), five studies containing 11 lists of transcriptome-wide alternative splicing events were eligible for further analysis (Table 3.1) (Nijhuis et al., 2022, Singh et al., 2021, Wang et al., 2019, Lu et al., 2021b, Mai et al., 2016a).

I focused on exon skipping and intron retention events because these two events are the most abundant alternative splicing events detected in RBM39 deficient cells (Han et al., 2017b, Wang et al., 2019, Mai et al., 2016a), and they could have direct impact on protein function by introducing premature stop codons or skipping of essential exons. Common splicing targets of RBM39 were defined by any gene mis-spliced in at least six datasets. Since the maximum number of datasets per cancer type was five, this cut-off would require candidate genes to be exon skipped (or intron retained) in at least two cancer types. The results showed that, in RBM39 deficient cells, 1774 (out of 9368) genes were commonly exon skipped, and 629 (out of 6201) genes displayed intron retention events.

Chapter 3

Table 3.1. Characteristics of alternative splicing datasets included for RBM39 splicing analysis

	First author	Year	Disease	Cell line	Method of RBM39 depletion	Sequencer	Alternative splicing analysis	Exon skipped genes	Intron retained genes	References
1	Nijhuis, A.	2022	Neuroblastoma	IMR-32	5 µM Indisulam for 16 hours	HiSeq4000, 75bp pair-ended, 45 million reads	SpliceFisher	2753	2336	(Nijhuis et al., 2022)
2	Singh, S.	2021	Neuroblastoma	BE2C	shRBM39 (#188) for 72 hours	Hiseq platform, 100bp pair-ended	rMATS v4.1.0	4714	1924	(Singh et al., 2021)
3	Singh, S.	2021	Neuroblastoma	BE2C	shRBM39 (#190) for 72 hours	Hiseq platform, 100bp pair-ended	rMATS v4.1.0	5276	1559	(Singh et al., 2021)
4	Singh, S.	2021	Neuroblastoma	SKNAS	shRBM39 (#188) for 72 hours	Hiseq platform, 100bp pair-ended	rMATS v4.1.0	5097	1997	(Singh et al., 2021)
5	Singh, S.	2021	Neuroblastoma	SKNAS	shRBM39 (#190) for 72 hours	Hiseq platform, 100bp pair-ended	rMATS v4.1.0	4539	1762	(Singh et al., 2021)
6	Lu, S. X.	2021	Melanoma	501-MEL-ES	1 µM indisulam for 96 hours	Hiseq2000, 101bp paired end, 100 million reads	MISO v2.0	3511	3887	(Lu et al., 2021b)
7	Lu, S. X.	2021	Melanoma	A375	1 µM indisulam for 96 hours	Hiseq2000, 101bp paired-end, 100 million reads	MISO v2.0	2349	1397	(Lu et al., 2021b)
8	Lu, S. X.	2021	Melanoma	SK-MEL-239	1 µM indisulam for 96 hours	Hiseq2000, 101bp paired-end, 100 million reads	MISO v2.0	2894	2239	(Lu et al., 2021b)
9	Wang, E.	2019	Acute myeloid leukaemia	MOLM-13	CRISPR knockout, 6 days post-transduction	HiSeq4000, 150 cycles paired-end	MATS v4.0.2	1624	131	(Wang et al., 2019)
10	Wang, E.	2019	Acute myeloid leukaemia	THP-1	CRISPR knockout, 6 days post-transduction	HiSeq4000, 150 cycles paired-end	MATS v4.0.2	1600	268	(Wang et al., 2019)
11	Mai, S.	2016	Breast cancer	MCF-7	RBM39 knockdown for 48 hours	Hiseq2000, 100bp pair-ended	MAQ software	222	8	(Mai et al., 2016a)

Functional annotation and enrichment analysis revealed that commonly mis-spliced genes following RBM39-depletion were significantly enriched in cell cycle-related pathways (fold enrichment = 1.34 – 2.05, FDR = 0.019 – 0.086), which is expected because RBM39 has been implicated in cell cycle progression (Abbate et al., 2004, Owa et al., 1999, Ozawa et al., 2001, Yokoi et al., 2002, Wang et al., 2019, Singh et al., 2021). Interestingly, DNA repair pathways were also significantly enriched (fold enrichment values between 1.45 to 1.55, FDR between 0.066 to 0.068), which included genes essential for DNA damage recognition (*ATM*, *ATR*, *CHEK1*, and *CHEK2*), HR repair (*BRCA1* , *RAD51C* and *RAD51D*), Fanconi Anaemia (*FANCI*, *FANCD2*, and *FANCA*) and NHEJ repair pathways (*TP53BP1*, and *RIF1*) (Table 3.2). In particular, the ATM-mediated DSB repair pathway was significantly enriched among the common exon skipped genes in RBM39 deficient cells (fold enrichment = 2.5, FDR = 0.03). Most of these alternative splicing events have not been appreciated in previous studies and the role of RBM39 in DNA damage response is largely unknown. This systematic analysis uncovered novel insights into RBM39 biology and suggests that RBM39 has conserved roles in modulating cell cycle and DNA damage response through alternative splicing.

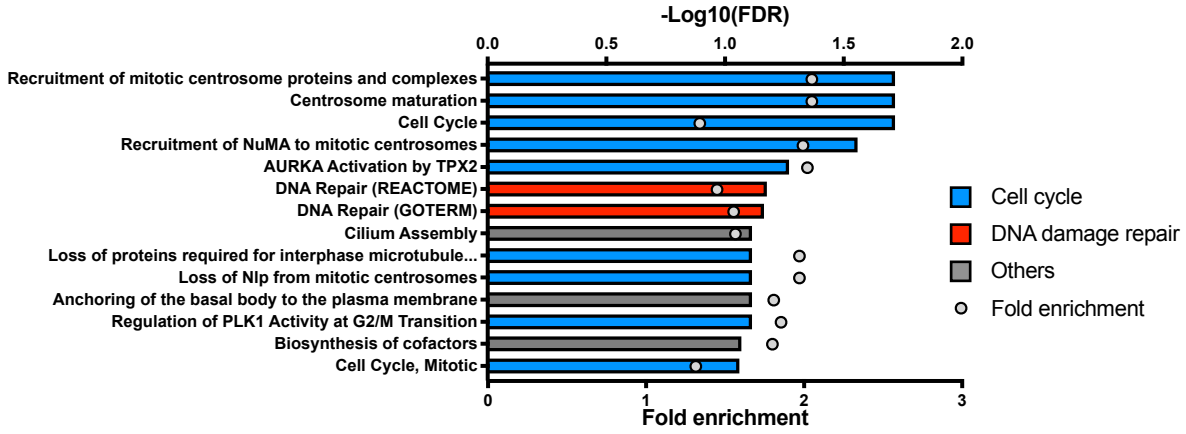


Figure 3.1. Pathway enrichment analysis of commonly mis-spliced genes after RBM39 depletion. Common exon skipping and intron retention targets of RBM39 were identified by examining transcriptome-wide alternative splicing analysis in RBM39-depleted cells. Significantly enriched pathways or gene ontology terms (fold enrichment > 1) are ranked according to their false discovery rate (FDR). FDR < 0.1 was considered significantly enriched. The top x-axis indicates -Log_{10}(FDR), and the bottom x-axis indicates fold enrichment (open circles in grey).

Table 3.2. Examples of DNA damage repair genes mis-spliced upon RBM39 depletion.

RBM39 depleted cell lines		Exon skipping or intron retention events						
		ATM	*ATR*	*FANCI*	*BRCA1*	*RAD51D*	*RIF1*	*TP53BP1*
Neuroblastoma	IMR-32	+	+	+	+	+	+	+
	BE2C (shRBM39#188)	+	+	+	+	+	-	+
	BE2C (shRBM39#190)	+	+	+	+	+	+	+
	SKNAS (shRBM39#188)	+	+	+	+	+	+	+
	SKNAS (shRBM39#190)	+	+	+	+	+	+	+
Melanoma	501-MEL-ES	+	+	+	+	-	+	+
	A375	+	+	+	-	+	+	+
	SK-MEL-239	+	+	+	-	+	+	+
Acute myeloid leukemia	MOLM-13	-	-	+	+	+	-	-
	THP-1	-	+	+	-	-	-	-
Breast cancer	MCF-7	-	-	+	-	-	+	-
Total number of occurrence		8	9	11	7	8	8	8

3.1.2. Indisulam causes alternative splicing of DNA damage repair genes in HGSOC

Given the *in silico* finding that RBM39 may modulate DNA damage repair genes, I hypothesised that RBM39 degraders might sensitise HGSOC cells to DNA damaging agents. Among human ovarian cancer cell lines, KURAMOCHI and OVSAHO are considered two of the most representative cell lines of HGSOC tumours from the perspectives of copy number variation and genetic mutations (Domcke et al., 2013). KURAMOCHI and OVSAHO are *BRCA2*-deficient due to a nonsense mutation and homozygous deletion in *BRCA2*, respectively (Domcke et al., 2013). Tumiati et al. (2018) confirmed that KURAMOCHI is HR-deficient using a functional HR assay (based on RAD51 foci formation). To the best of my knowledge, HR repair activity in OVSAHO cells has not been quantified. PEO1 (HR-deficient due to *BRCA2* nonsense mutation) and PEO4 cells (HR-proficient due to acquired *BRCA2* reversion mutation) are two HGSOC cell lines derived from the same patient before and after acquiring chemo-resistance, respectively (Langdon et al., 1988, Sakai et al., 2009). These two cell lines were used as sensitive and resistant models to platinum and PARP inhibitors. I found that, despite loss of *BRCA2* expression, KURAMOCHI and OVSAHO showed intrinsic resistance to both cisplatin and olaparib to a similar level as PEO4 cells, rather than similar to *BRCA*-mutated PEO1 cells (Figure 3.2A). Similar findings have been reported in the literature (Coulson-Gilmer et al., 2021, Pillay et al., 2019, Kim et al., 2020), demonstrating that KURAMOCHI and OVSAHO are valuable models for PARP inhibitor-resistant HGSOC.

Preliminary data from our lab showed that indisulam caused RBM39 degradation in ovarian cancer cell lines and inhibited ovarian cancer growth (Figure 1.6). Interestingly, RBM39

degradation was detected not only in indisulam-sensitive ovarian cancer cell lines, but also in indisulam-resistant cell lines, such as OVSAHO (Figure 1.6). I ascertained that indisulam treatment degrades RBM39 in KURAMOCHI and OVSAHO cells in a dose-dependent manner (Figure 3.2B). To study whether RBM39 degradation leads to splicing errors in HGSOC cells, I selected five core DNA repair genes from the common splicing targets of RBM39 (Table 3.2), including *ATM* (mediates DSB recognition), *BRCA1* and *RAD51D* (mediates HR repair), and *TP53BP1* and *RIF1* (mediates NHEJ) (Figure 3.2C). Positions of skipped exons were predicted based on our recently published alternative splicing analysis in the neuroblastoma IMR-32 cells (Nijhuis et al., 2022). Primers were designed to flank the skipped exons, allowing the detection of exon skipped variants based on PCR product sizes.

PCR-based exon skipping analysis showed that indisulam treatment caused exon skipping of all five DNA damage repair genes in KURAMOCHI and OVSAHO cells (Figure 3.2D). More specifically, a *BRCA1* variant with exon 9 (77bp) skipping was detected. Because the length of exon 9 is not dividable by three (length of codons), skipping of this exon would introduce frameshifts and premature stop codons. Transcripts with premature stop codons are known to trigger the nonsense-mediated decay and have a short half-life [reviewed in (Lykke-Andersen and Jensen, 2015)]. As for *RAD51D*, exon 5 is essential for its protein function (Gruver et al., 2009), and the two mRNA variants without this exon are therefore unlikely to produce functional proteins. The exon 17 (484bp) skipping in *TP53BP1* variant is predicted to cause frameshift, which also causes truncation of a domain necessary for 53BP1 activation and interaction with other NHEJ proteins (Bothmer et al., 2011, Escribano-Díaz et al., 2013). In *RIF1*, the exon 7 (93bp) translates to amino acid (a.a.) 232-262, which is a part of the DNA binding domain (Fontana et al., 2018). As a result, the *RIF1* mRNA isoform without exon 7 might not be able to function properly. Indisulam also induced skipping of exon 52 (159bp, a.a. 2544-2596) and exon 53 (47bp, a.a. 2597-2642) in *ATM*, affecting the dimerisation domain and the kinase domain, which are important for ATM activation and signalling (Choi et al., 2016). In addition, exons 52 and 53 of *ATM* also contain multiple mutation sites (such as Ser2546) that have been associated with loss of protein function and hereditary ataxia-telangiectasia (A-T) syndrome (Choi et al., 2016, Telatar et al., 1998). Therefore, it is possible that the *ATM* splice variants may lead to reduced protein expression or translate to truncated ATM with impaired catalytic function. Notably, the increase in aberrant splicing variants was

correlated with the decrease in canonical mRNAs (Figure 3.2D), implying that loss of RBM39 could also reduce the protein expression of these genes by reducing the abundance of correctly spliced transcripts. Indisulam-mediated ATM reduction will be described in Chapter 5, and the downregulation of other genes at protein levels were confirmed in our recent proteomics analysis (will be described in Chapter 6).

In summary, RBM39 depletion by indisulam disrupted the splicing of key DNA repair genes in HGSOC cells, potentially affecting ATM-mediated DNA damage recognition, BRCA1- and RAD51D-mediated HR repair, and 53BP1- and RIF1-mediated NHEJ repair (Figure 3.2C). These findings confirm HGSOC as an additional cancer in which DNA damage response seems to be modulated by RBM39. At the time of writing this chapter, RNA sequencing and alternative splicing analyses were ongoing to systematically characterise splicing changes in RBM39-depleted HGSOC cells and will be described in Chapter 6.

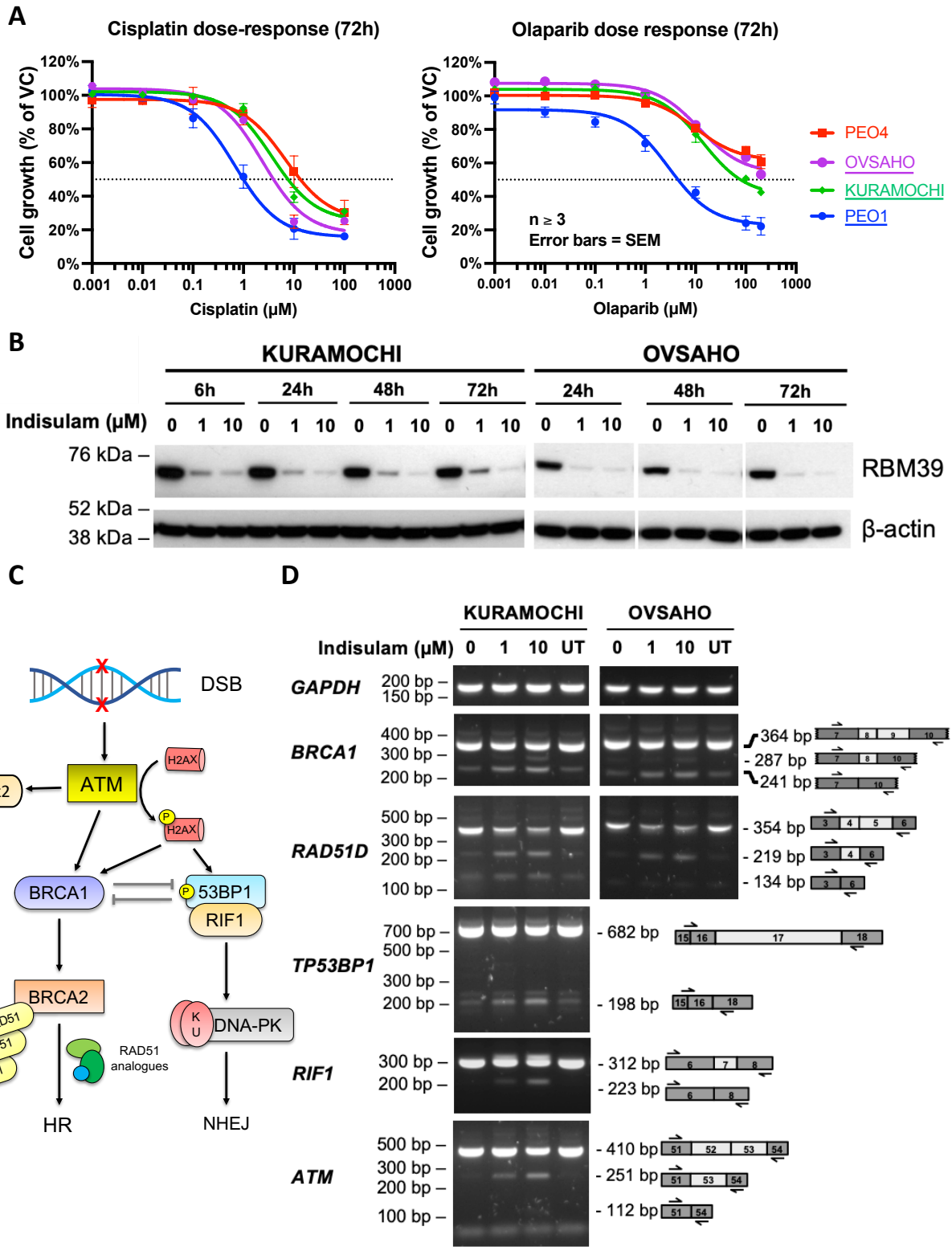


Figure 3.2. Indisulam causes RBM39 degradation and splicing errors of DNA repair genes in HGSOC. **(A)** Cisplatin and olaparib dose-response curves of four HGSOC cell lines. Cells were treated with vehicle control (VC) or increasing doses of cisplatin (or olaparib) for 72 hours (72h). Cell proliferation was measured using the SRB assay. Error bar = SEM and n ≥ 3 (except n = 2 for the PEO4 cisplatin dose-response curve). HR-deficient cell lines are underlined. The cisplatin dose-response curves were acquired with help from Dr Anke Nijhuis. **(B)** KURAMOCHI (n = 1) and OVSHAO (n = 1) were treated with vehicle control (0.1% DMSO) or indisulam (1μM or 10 μM) for 6 to 72 hours. The abundance of RBM39 was assessed using western blot, and β-actin was used as a loading control. Indisulam-

mediated RBM39 degradation in KURAMOCHI cells was also observed in Figure 5.2. **(C)** A simplified diagram showing key proteins involved in DSB repair. ATM functions as a sensor for DSBs. BRCA1 and 53BP1 compete for the DSBs, and the result determines repair pathway choices. **(D)** KURAMOCHI and OVSAHO cells were untreated (UT, culture media only) or treated with indicated doses of indisulam for 24 hours before PCR-based exon skipping analysis. Splicing variants detected are annotated on the right. Exons that might be skipped are highlighted in light grey. The same splicing changes were observed at other time points (6, 48, and 72 hours) (Appendix Figure 1) and in (Figure 6.11).

3.2. Indisulam synergises with cisplatin in HGSOC cells

Platinum agents are ubiquitous components of front-line chemotherapy in ovarian cancer, which has been in clinical use since the late 1970s (Lisio et al., 2019, Sopik et al., 2015). One classic example of platinum-based anti-cancer drugs is cisplatin, which damages DNA by causing intrastrand and interstrand crosslinks (Wang and Lippard, 2005). Intrastrand DNA crosslinks are repaired by the nucleotide excision repair, and interstrand crosslinks are resolved by the Fanconi anaemia pathway with the help from HR repair proteins (Dietlein et al., 2014, Reardon et al., 1999). Unrepaired DNA crosslinks hinder DNA replication and deteriorate into more detrimental DSBs upon replication fork collapse, eventually leading to increased genome instability and cell death (Frankenberg-Schwager et al., 2005).

Given the findings that indisulam causes mis-splicing of DNA damage repair genes in HGSOC cells, I hypothesised that indisulam-treated cells might have higher sensitivity to platinum agents such as cisplatin. To explore this hypothesis, the combination effect of indisulam and cisplatin was assessed using the Chou-Talalay synergy method (Chou and Martin, 2005). Indisulam was combined with cisplatin at a constant ratio to achieve equal potency, and the CI values were calculated as described in the Materials and Method. CI < 1 indicates synergism and CI > 1 indicates antagonism (Chou and Martin, 2005). In both KURAMOCHI and OVSAHO cells, the combination of indisulam and cisplatin showed significantly stronger anti-proliferative effects than monotherapies, and combination index values consistently less than 1, indicating indisulam is synergistic with cisplatin (Figure 3.3A-B). Next, the impact of indisulam, cisplatin and their combination on cell apoptosis was assessed using the caspases 3/7 activation assay. While indisulam alone had a minor impact on cell apoptosis, it considerably elevated cell apoptosis caused by cisplatin, suggesting a strong synergy between indisulam and cisplatin in triggering cell apoptosis (Figure 3.3C-D).

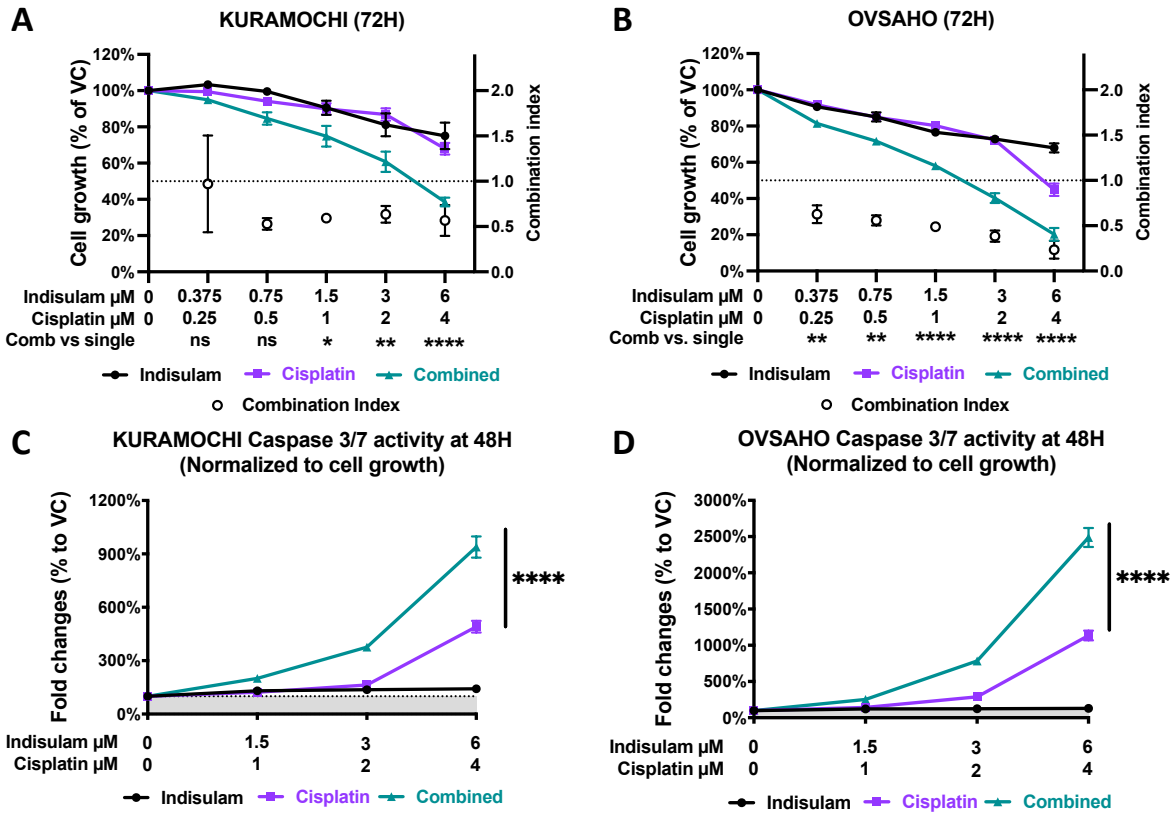


Figure 3.3. Indisulam increases cisplatin response in cisplatin-resistant HGSOC cells.

(A-B) KURAMOCHI (a) and OVSAHO (b) cells were treated with indisulam, cisplatin, or the combination of these two drugs for 72 hours and cell growth was measured by the SRB assay (n = 3, error bar = SEM). The left y-axis shows the cell growth relative to the vehicle, and the right y-axis shows the combination index values (CI) calculated by the Chou-Talalay method (open circles, error bar = SD). CI < 1 indicates synergism. **(C-D)** Cells were treated with indisulam and cisplatin either alone or in combination for 48 hours, and cell apoptosis was measured using the caspase 3/7 activation assay (n = 3, error bar = SEM). Statistical significance between monotherapy and combination therapy in (a-d) was determined using 2-way ANOVA followed by Dunnett's multiple comparisons test (*p < 0.05, **p < 0.01, *** p < 0.001, **** p < 0.0001).

Chapter 3

3.3. Indisulam synergises with multiple PARP inhibitors in HGSOC cells

3.3.1. Indisulam and olaparib cause synergistic growth inhibition and cell apoptosis

Combining indisulam and PARP inhibitors is another valuable strategy because PARP inhibitors have been used as a front-line maintenance therapy for ovarian cancer patients. I used olaparib, the most widely prescribed PARP inhibitor (Sandhu et al., 2022), to investigate the combined effect between indisulam and PARP inhibitors in HGSOC cells. The Chou-Talalay method was used to evaluate the combined effect. As expected, indisulam synergised with olaparib in both KURAMOCHI and OVSAHO cells, leading to a stronger anti-proliferative effect than individual drugs (Figure 3.4A-B).

I hypothesised that the observed growth inhibition was a result of cell apoptosis, which may peak at an earlier time point. I speculated that combination doses causing 40% to 50% growth inhibition at 72 hours might be able to elicit strong apoptosis at 48 hours. Therefore, cell apoptosis analysis was analysed by treating cells with up to 10 µM indisulam and 30 µM olaparib for 48 hours. I investigated cell apoptosis using two methods: caspase 3/7 activation assay and annexin V-based flow cytometry analysis. While indisulam and olaparib alone only showed a minor increase in caspase 3/7 activation, the combination of these two drugs caused a substantial increase in cell apoptosis, indicating synergistic cytotoxicity (Figure 3.4C-D). In the flow cytometry-based cell apoptosis analysis, annexin V staining was used as a marker for apoptotic cells and propidium iodide was included as a cell viability dye. This dual-labelling technique allows the detection of early apoptotic cells (Annexin V^+ & PI^-) and late apoptotic cells (Annexin V^+ & PI^+). In accordance with increased caspase 3/7 activation, the proportion of apoptotic KURAMOCHI cells was significantly increased only when indisulam and olaparib were combined, but not when they were used individually (Figure 3.4E). The increase of both early and late apoptotic cells by the drug combination was effectively rescued by the addition of the pan-caspase inhibitor Z-VAD-FMK, indicating cell necrosis was not involved (Figure 3.4E).

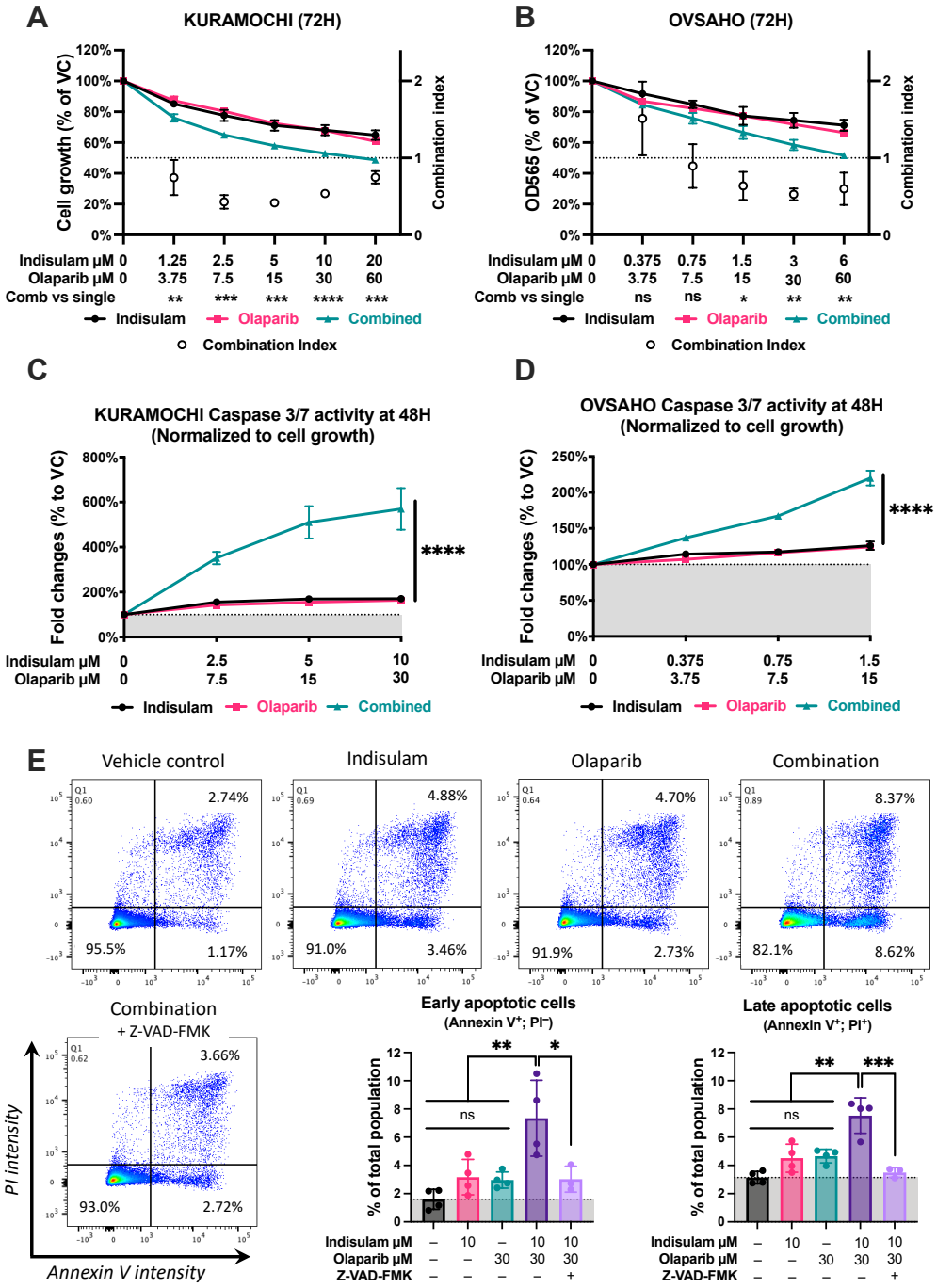


Figure 3.4. Indisulam synergises with olaparib in HGSOC cells.
(A-B) Cell growth after 72-hour treatment of indisulam and olaparib individually or in combination (n = 3, error bar = SEM). The right y-axis indicates CI values calculated by the Chou-Talalay method (error bar = SD). CI < 1 indicates synergism. **(C-D)** Cell apoptosis (caspase 3/7 activation) was assessed after treatment with indisulam, olaparib, or their combination for 48 hours. The grey region indicates basal caspases activities. Two-way ANOVA with Dunnett's multiple comparison test was used in (a-d) to determine the statistical significance between combination treatment and individual treatment. **(E)** KURAMOCHI cells were treated with vehicle control, indisulam, olaparib, the drug combination, or the combination plus 10 µM Z-AVD-FMK for 48 hours before flow cytometry analysis. Representative data from at least three biological repeats were shown, and the same gating was used across repeats. Proportions of early and late apoptotic cells were quantified (error bar = SD). Ordinary one-way ANOVA and Tukey's multiple comparisons test were used for statistical analysis in (e). ns = not significant, *p < 0.05, ** p < 0.01, *** p < 0.001, ****p < 0.0001.

Chapter 3

The impact of indisulam and olaparib combination therapy on colony growth was investigated using the two-dimensional colony growth assay. A pilot experiment showed that colonies of KURAMOCHI, COV504 and OVISE were hard to quantify due to fuzzy outline and frequent merging of colonies (Figure 3.5A). On the other hand, OVSAHO colonies were easy to count because they were compact and discrete from each other. Subsequent optimisation identified 3000 cells per well in 6-well plates was the optimal seeding density for OVSAHO colony growth assay, and the image processing pipeline I established could count colonies semi-automatically with high accuracy (r^2 = 0.9942) (Figure 3.5A-B). To assess the inhibitory effect on OVSAHO colony growth, cells were allowed to grow for five days to form small colonies, followed by a 48-hour or 72-hour pulse of indisulam and olaparib individually or in combination (Figure 3.5C). Afterwards, the drugs were washed away and fresh media were added. Colonies were incubated until 16 days post-seeding. The data showed that the drug combination resulted in a significantly stronger suppressive effect on colony growth than individual treatment (Figure 3.5D-E). The observation that washout of indisulam and olaparib after 48- or 72-hour exposure did not lead to recovered colony growth till day 16 implies that short-term exposure to indisulam and olaparib may be sufficient for the synergy to occur, which is a desirable characteristic for future clinical translation.

Taken together, above findings provide strong evidence that adding indisulam to olaparib treatment is a promising therapeutic approach in ovarian cancer, which can cause synergistic growth inhibition and induction of cell apoptosis.

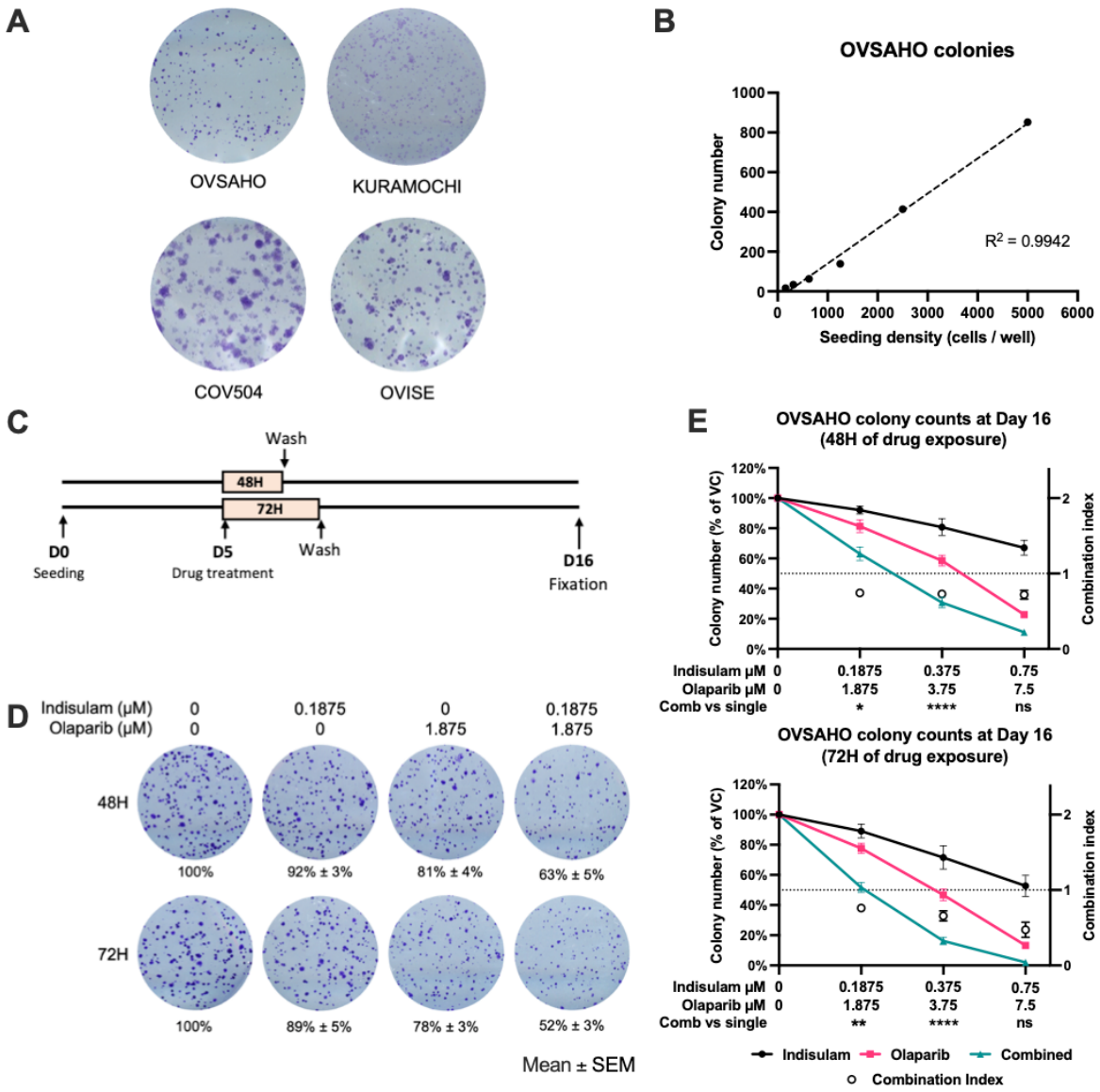


Figure 3.5. Indisulam and olaparib synergistically inhibit OVSAHO colony growth.
(A) Representative images showing shapes of ovarian cancer cell colonies. Unlike other ovarian cancer cell lines tested, the OVSAHO cells formed discrete colonies and were ideal for colony counting. **(B)** A standard curve showing a linear correlation between OVSAHO cell seeding density and colony counts. Colonies were counted semi-automatically as described in the Methods and Materials (Section 2.8). **(C)** Diagrams showing the design of the colony growth assay used in (d-e). **(D)** Representative fields of OVSAHO colonies (at day 16) after receiving 48-hour or 72-hour pulses of indisulam, olaparib, or indisulam plus olaparib. The numbers below each image are mean ± SEM from three biological repeats. **(E)** Quantification of OVSAHO colonies after pulse treatment of indisulam, olaparib, or their combination for 48 or 72 hours and incubating in fresh media until day 16 (n = 3, error bar = SEM). The right y-axis indicates CI values calculated by the Chou-Talalay method (open circles, error bar = SD). CI < 1 indicates synergism. Statistical differences between the combination therapy and the monotherapies were calculated by two-way ANOVA and Dunnett's multiple comparisons test (ns, not significant; *p < 0.05; **p < 0.01; ****p < 0.0001).

3.3.2. Indisulam synergises with multiple PARP inhibitors irrespective of *BRCA*-status

The strong synergy observed between indisulam and olaparib motivated me to investigate if the same benefit could be achieved with other PARP inhibitors because they share similar mechanisms of action. Besides olaparib, rucaparib and niraparib have also been approved to treat ovarian cancer patients, and I tested their combination effect with indisulam. As expected, the combination of indisulam with either rucaparib or niraparib showed consistent trends of synergy in both KURAMOCHI and OVSAHO cells (Figure 3.6A-B), indicating that indisulam synergises with multiple PARP inhibitors.

An increasing number of studies have found that PARP trapping is an important characteristic of PARP inhibitors, and clinical PARP inhibitors have shown varying degrees of PARP trapping potency [reviewed in (Murai and Pommier, 2019)]. To investigate if PARP trapping is an important factor in the synergy, I examined the combined effect of indisulam with veliparib, the weakest PARP trapper in clinical development (Hopkins et al., 2015, Murai et al., 2012). In KURAMOCHI cells, indisulam and veliparib combination led to synergistic growth inhibition and induction of cell apoptosis (Figure 3.6C), similar to what was observed when indisulam was combined with olaparib (Figure 3.4A-D). These data suggest that strong PARP-trapping ability is not essential for PARP inhibitors to act synergistically with indisulam.

It is interesting to notice that the synergy (between indisulam and olaparib or rucaparib) was effective in COV318 and COV504 cells (Figure 3.7A-B) (Domcke et al., 2013). According to Domcke et al. (2013), neither COV318 (likely HGSOC) nor COV504 (possibly HGSOC) harbour BRCA1/2 mutations. In addition, COV318 has been validated as a HR-proficient cell line (Tumiati et al., 2018). This led to a hypothesis that indisulam might be able to reduce or overcome PARP inhibitor resistance caused by reversion mutations that restores *BRCA1/2* expression, which accounts for most acquired PARP inhibitor resistance in the clinic (Noordermeer and van Attikum, 2019). To investigate this hypothesis, PEO1 and PEO4 cells were selected because PEO4 has almost the same genomic features as PEO1, except the *BRCA2*-mutation in PEO1 was reverted to wild-type *BRCA2* (Sakai et al., 2009). Similar levels of synergistic growth inhibition were found in PEO1 and PEO4 cells treated with indisulam and olaparib (Figure 3.7C). Meanwhile, PEO1 and PEO4 cells showed similar levels of cell apoptosis in response to the combination of indisulam and olaparib (Figure 3.7D). However,

the synergy was not strong enough to render PEO4 cells as sensitive as PEO1 cells to PARP inhibitor treatment (Figure 3.7C). These findings suggest that although indisulam does not fully overcome PARP inhibitor resistance caused by reversion mutations, it is able to improve the performance of PARP inhibitors regardless of *BRCA*-status.

Overall, above findings demonstrate that indisulam synergises with PARP inhibitors in HGSOC irrespective of genomic *BRCA*-status, and a wide range of ovarian cancer patients may benefit from the combination therapy.

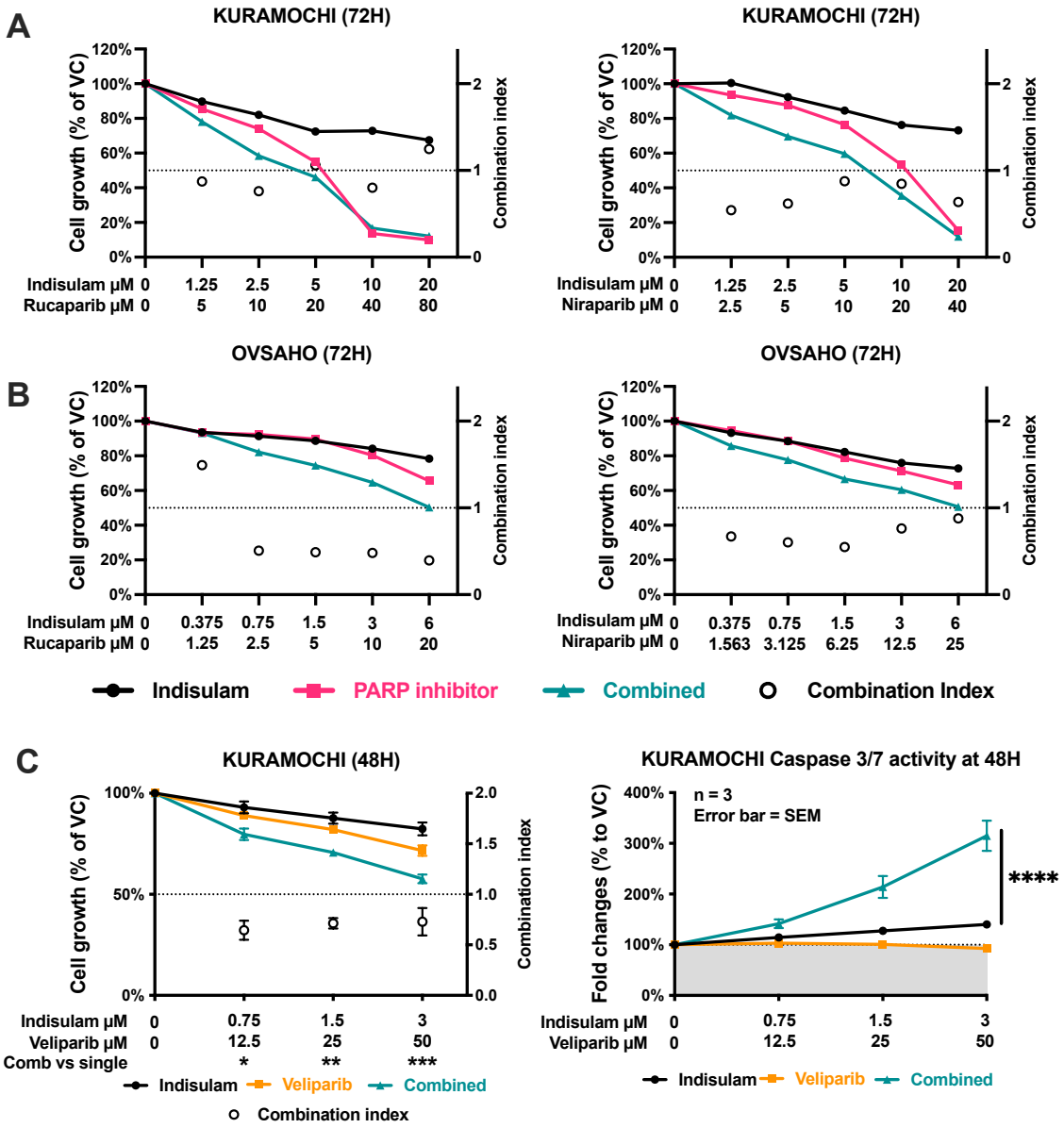


Figure 3.6. Indisulam synergises with multiple PARP inhibitors in HGSOC cells.
(A-B) The proliferation of ovarian cancer cells after 72-hour treatment of indisulam and PARP inhibitor (rucaparib or niraparib) individually or in combination (n = 1). CI values (right y-axis) were calculated by the Chou-Talalay method. **(C)** Cell growth and apoptosis (by caspase 3/7 activation, normalised to the cell growth) measurements of KURAMOCHI cells treated with indisulam, veliparib, or their

combination for 48 hours (n = 3, error bar = SEM). Error bars of CI values = SD. Statistical significance between combination therapy and monotherapies was calculated by two-way ANOVA and Dunnett's multiple comparisons test (ns, not significant; *p < 0.05; **p < 0.01; ***p < 0.001).

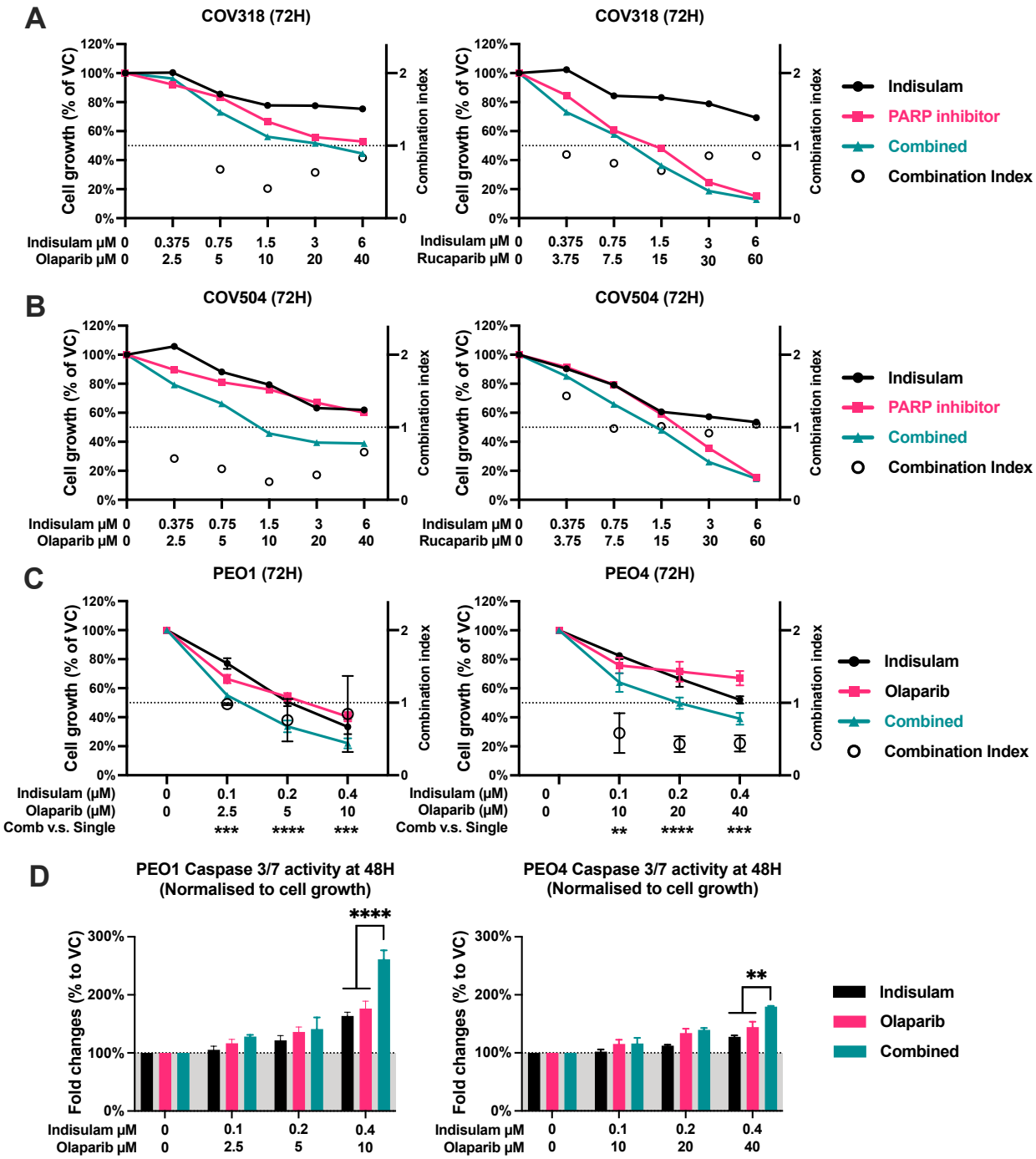


Figure 3.7. Indisulam synergises with PARP inhibitors irrespective of *BRCA2* status.
(A-B) The proliferation of *BRCA*-proficient COV318 and COV504 cells after 72-hour treatment of indisulam and PARP inhibitor (olaparib or rucaparib) individually or in combination (n = 1). CI values were calculated by the Chou-Talalay method. **(C)** SRB assay showing cell growth of PEO1 and PEO4 cells in response to 72-hour treatment of indisulam and olaparib either alone or in combination (n = 3, error bar = SEM). CI values were shown as open circles to the right y-axis (error bar = SD). Data were collected with the help of the master student Madelen Shepherd under my supervision. **(D)** Caspase 3/7 activation assay showing cell apoptosis in PEO1 and PEO4 cells after 48-hour treatment of

indisulam and olaparib individually or in combination. Statistical differences between individual drugs and the combination treatment were calculated by two-way ANOVA and Dunnett's multiple comparisons test (**p < 0.01, ***p < 0.001, **** p < 0.0001).

3.3.3. DCAF15 is necessary for the synergy between indisulam and PARP inhibitors

It is well-established that indisulam degrades RBM39 and causes splicing errors in a DCAF15-dependent manner (Han et al., 2017b, Nijhuis et al., 2022, Singh et al., 2021, Ting et al., 2019, Uehara et al., 2017, Wang et al., 2019). However, data from cell-free systems suggests that indisulam may act independently of DCAF15 by directly inhibiting carbonic anhydrases (Abbate et al., 2004, Del Prete et al., 2020, Oda et al., 2003). Our recent publication also documented some DCAF15-independent metabolic changes in indisulam-treated neuroblastoma IMR-32 cells (Nijhuis et al., 2022).

To investigate if indisulam enhances PARP inhibitor response in a DCAF15-dependent manner, I used the *DCAF15*-knockout PEO1 clones previously generated in our laboratory through CRISPR-Cas9 editing. *DCAF15* knockout was ascertained by DNA sequencing (deletions in *DCAF15*), rescued RBM39 degradation and downstream splicing errors (unpublished data from Dr Anke Nijhuis, Appendix Figure 2). Due to a lack of DCAF15-specific antibodies, knockout efficiency at protein levels has not been confirmed. In the future, *DCAF15* knockout specificity in these clones will be verified by restoring *DCAF15* expression in knockout clones, and the knockout efficiency will be estimated by measuring *DCAF15* mRNA expression using qPCR or quantifying DCAF15 peptide expression using targeted protein mass-spectrometry. As expected, the combination treatment of indisulam plus olaparib synergistically inhibited proliferation of the control clone without *DCAF15* editing (PEO1-$DCAF15^{WT}$) (Figure 3.8A). On the other hand, the PEO1-$DCAF15^{KO}$ clone showed strong resistance to indisulam treatment, and the addition of indisulam to olaparib was not more anti-proliferative than olaparib monotherapy (Figure 3.8A), suggesting that loss of DCAF15 abrogates the synergy between indisulam and olaparib.

E7820 is another RBM39-targeting anti-cancer aryl sulphonamides. There has been no evidence suggesting that E7820 inhibits carbonic anhydrase like indisulam, and we did not observe any *DCAF15*-independent metabolic effect in E7820-treated neuroblastoma cells (Nijhuis et al., 2022). I found that E7820 and olaparib combination led to synergistic growth inhibition and induction of cell apoptosis in KURAMOCHI and OVSAHO cells (Figure 3.8B-C),

which recapitulates what was observed between indisulam and olaparib (Figure 3.4A-D). Therefore, carbonic anhydrase inhibition or other *DCAF15*-independent metabolic changes are unlikely to be involved in the synergy in HGSOC.

Taken together, above findings demonstrate that the synergy between indisulam (or E7820) and PARP inhibitors are downstream of *DCAF15*-mediated RBM39 degradation and presumably mis-splicing events.

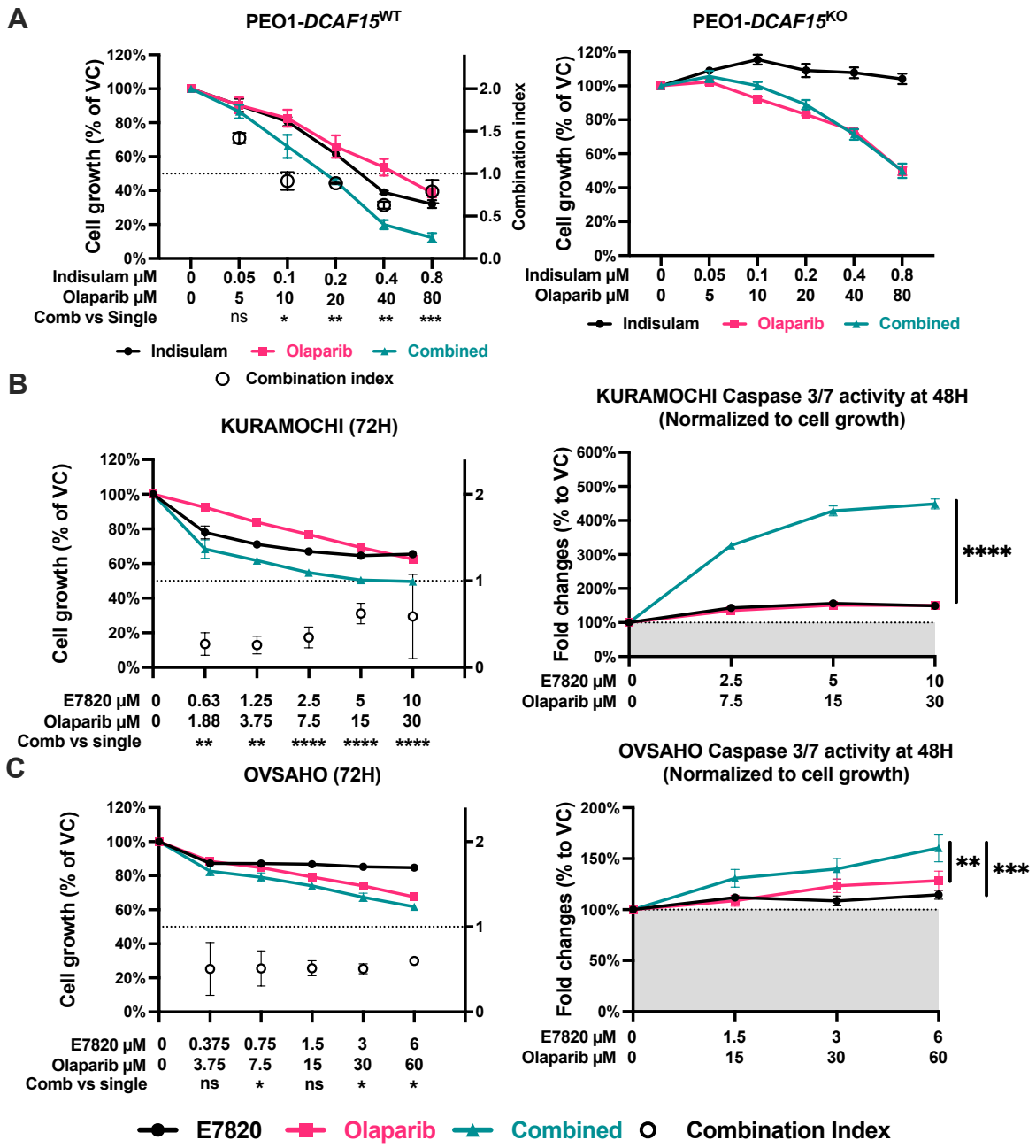


Figure 3.8. DCAF15 is necessary for the synergy between RBM39 degraders and PARP inhibitors.
(A) A CRISPR-edited *DCAF15*-knockout PEO1 clone (PEO1-DCAF15^{KO}) were previously generated in-house by Dr Anke Nijhuis, along with a control clone without DCAF15 editing (PEO1-DCAF15^{WT}). Cells

were treated with indicated doses of indisulam and olaparib either individually or in combination for 72 hours before cell growth measurement via the SRB assay (n = 3, error bar = SEM). **(B-C)** Cell growth (SRB assay, left panels) and apoptosis (caspase 3/7 assay, right panels) measurements of KURAMOCHI (b) and OVSAHO cells (c) in response to E7820 and olaparib treatment as monotherapies or in combination (n = 3, error bar = SEM). CI values were calculated by the Chou-Talalay method and shown as open circles to the right y-axis (error bar = SD). Two-way ANOVA followed by Dunnett's multiple comparisons test was performed to determine the statistical significance between combination therapy and individual drugs (ns, not significant; *p < 0.05, **p < 0.01, ***p < 0.001, ****p < 0.0001). Data were collected with help from master students Madelen Shepherd (a) and Yurui Ma (b-c) under my supervision.

3.4. A large-scale drug combination screen reveals novel synergy between indisulam and FDA-approved anti-cancer drugs

The strong synergy between indisulam and cisplatin or PARP inhibitor motivated me to investigate if indisulam renders cells susceptible to other DNA damaging agents. To systematically evaluate this hypothesis, I carried out a drug combination screen combining indisulam with a panel of FDA-approved genotoxic agents, including 22 alkylating agents, 18 nucleotide synthesis inhibitors or nucleotide analogous, nine topoisomerase inhibitors, four PARP inhibitors (olaparib, niraparib, rucaparib, and talazoparib), and one DNA methyltransferase inhibitor (Figure 3.9A). I also included six taxanes/microtubule inhibitors (Figure 3.9A), because they are often administrated together with platinum agents in ovarian cancer (ESMO, 2017). The cell line KURAMOCHI was selected for this screen due to its high similarity to human HGSOC tumours (Domcke et al., 2013).

In brief, DNA damaging agents were serial diluted (ranging from 8 nM to 20 µM, seven doses) and combined with either vehicle control or 10 µM indisulam – a dose that causes approximately 20% growth inhibition in KURAMOCHI cells (Figure 3.9B). The Bliss independence was used as a readout for the synergy (or antagonism) between the FDA-approved drugs and indisulam. The Chou-Talalay method was not used because a full dose-response curve of indisulam was not included in the screen and therefore the data did not meet the requirement for the Chou-Talalay method. In addition, one dose pair is sufficient for the Bliss independence analysis. The Bliss scores were calculated as the difference between the observed growth inhibitory effect and the expected effect (Figure 3.9B). Bliss scores > 0 indicate synergism and Bliss scores < 0 indicate antagonism. Drugs showed Bliss score $\geq$ 0.05 in at least two (out of seven) dose-pairs with indisulam were defined as likely

synergistic with indisulam, and drugs showed Bliss score ≤ -0.05 in at least five dose-pairs with indisulam were defined as likely antagonistic with indisulam (Figure 3.9B).

As shown in Figure 3.10, 27% (15 out of 54) of FDA-approved genotoxic agents were likely synergistic with indisulam, including six alkylating agents (such as temozolomide, carboplatin, and oxaliplatin), two topoisomerase inhibitors (irinotecan and dexrazoxane), four DNA/RNA synthesis inhibitors (such as hydroxyurea), one PARP inhibitor (olaparib), and one DNA methyltransferase inhibitor (azacytidine). Although the Fisher's exact test did not find any significant trend of enrichment, this screen successfully identified olaparib as likely synergistic with indisulam, in accordance with earlier findings (Section 3.3). The synergy between indisulam and carboplatin or oxaliplatin were also expected because they are derivatives of cisplatin [reviewed in (Dasari and Tchounwou, 2014)]. One previous study also reports that indisulam synergises with the topoisomerase inhibitor irinotecan (Ozawa et al., 2012). In addition, Teixeira et al. (2021) have shown that indisulam synergises with temozolomide in glioblastoma *in vitro* and *in vivo*. Other synergistic interactions are novel and worth validating in future studies.

It is worth noting that cisplatin has shown strong synergy with indisulam in previous experiments (Figure 3.3), but in this drug combination screen, it only showed weak Bliss synergism with indisulam at few doses and did not meet the criteria for "likely synergistic". This suggests that the combination doses used in this drug combination screen may not be optimal for cisplatin to synergise with indisulam. Therefore, it is possible that those drugs with similar ranks as cisplatin might also synergise with indisulam if more doses were tested.

On the other end of the spectrum, the screen identified a subset of drugs that are likely antagonistic with indisulam (Figure 3.10). These drugs are significantly enriched for taxanes/microtubule inhibitors such as paclitaxel (Fisher's exact test, p-value < 0.001). In light of this new observation, it is reasonable to argue that indisulam should not be added to the chemotherapy for ovarian cancer patients because the benefit of synergy with platinum agents may be diminished by the antagonism with taxanes. Several topoisomerase inhibitors (such as doxorubicin) and DNA/RNA synthesis inhibitors were also likely antagonistic with indisulam, but they were not significantly enriched (Fisher's exact test, $p >> 0.05$). Future

analysis is needed to validate these antagonism interactions and decipher the underlying mechanisms.

Overall, indisulam showed trends of synergy with some but not all DNA damaging agents, suggesting that loss of RBM39 renders HGSOC cells susceptible to specific types of genotoxic stress. Although this drug combination screen was performed with limited technical replicates, it revealed several intriguing drug-drug interactions for further validation.

A

Drugs of interest	#
Alkylating agent	22
DNA/RNA synthesis inhibitor	18
Taxane/microtubule inhibitor	6
Topoisomerase inhibitor	9
PARP inhibitor	4
DNA methyltransferase inhibitor	1

B

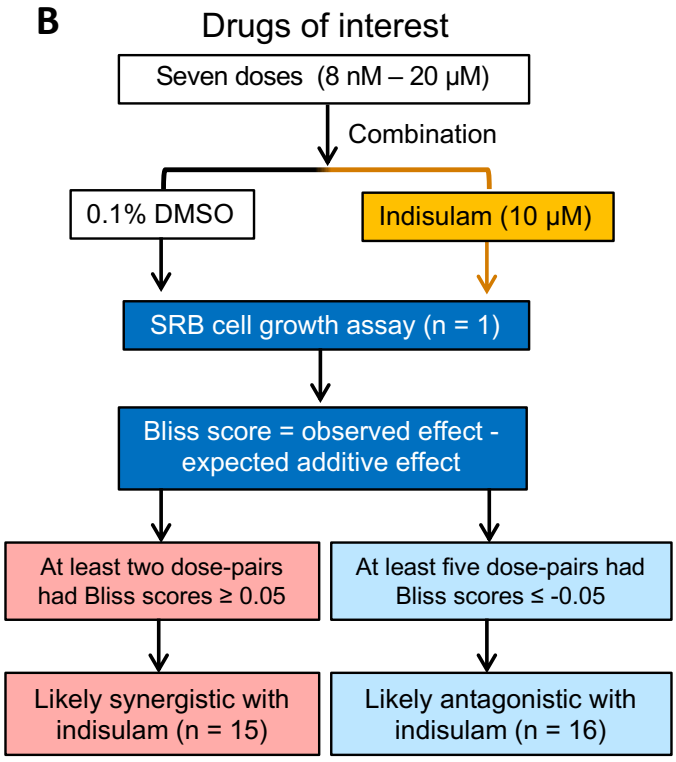


Figure 3.9. Overview of the screen combining indisulam with a panel of FDA-approved drugs.
(A) Indisulam was combined (pairwise) with 54 FDA-approved genotoxic agents from five major classes, and six microtubule inhibitors. **(B)** The drugs in (a) were serial diluted (8 nm to 20 µM, seven doses) and combined with either vehicle control (0.1% DMSO) or 10 µM indisulam. The growth inhibitory effect of individual drugs and the combinations were tested in KURAMOCHI cells using a 72-hour SRB cell proliferation assay (n = 1 with one technical replicate). The Bliss scores were calculated as the difference between the observed growth inhibition and the expected additive growth inhibition. Each drug has seven Bliss scores because each was combined with indisulam (10 µM) at seven different concentrations (dose-pairs). Drugs were categorised as "likely synergistic" or "likely antagonistic" with indisulam based on the indicated criteria.

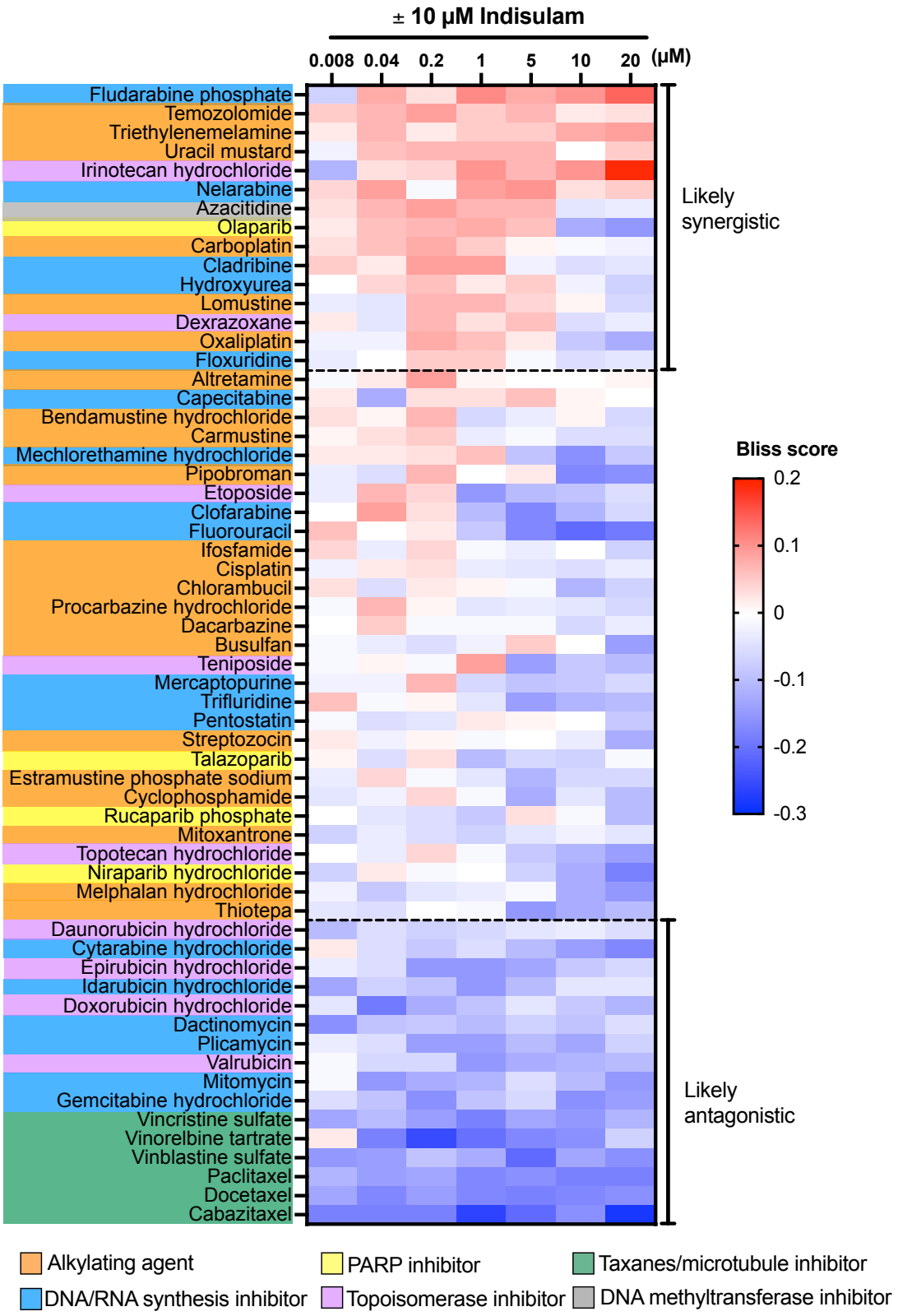


Figure 3.10. Drug combination screen between indisulam and a panel of FDA-approved drugs. Heatmap showing bliss scores of the previously described drug combinations screen (Figure 3.9), where KURAMOCHI cells were treated with indicated doses of drugs with or without 10 μM indisulam. Drugs were ranked based on the number of dose-pairs (with indisulam) showing Bliss scores ≥ 0.05 and average bliss scores. The criteria for defining drugs that are likely synergistic or likely antagonistic with indisulam are shown in Figure 3.9B.

Chapter 3

3.5. Discussion

HGSOC is a refractory disease with limited therapeutic options and is a leading cause of death in women (Stewart et al., 2019, Torre et al., 2018, ESMO, 2017). PARP inhibitors including olaparib, niraparib, and rucaparib have demonstrated substantial clinical benefits, especially in patients with HRD tumours due to the synthetic lethality between PARP inhibition and HR deficiency (Bryant et al., 2005, Wethington et al., 2021, Yang et al., 2020, Wang et al., 2021a, Lin et al., 2021, Farmer et al., 2005). PARP inhibitor therapy usually lasts for years and this long-term administration has increased the chance of acquired PARP inhibitor resistance. Reversion mutations that restore HR proficiency were the most common form of resistance mechanism in clinical settings, and several other mechanisms have also been documented in preclinical studies [reviewed in (Noordermeer and van Attikum, 2019)]. It remains a challenge to improve PARP inhibitor efficacy and reduce drug resistance.

Targeting splicing factors such as SF3B1 and U2AF65 has been shown to increase cancer cell response to PARP inhibitors (Lappin et al., 2022, Savage et al., 2014). In this chapter, I show that RBM39 is another splicing factor which can be targeted to increase cancer cell response to PARP inhibitors. The combination of indisulam-mediated RBM39 degradation and olaparib causes synergistic growth inhibition and induction of apoptosis in HGSOC cell lines. The synergy has been observed in multiple HGSOC cell lines including *BRCA*-mutated (PEO1), *BRCA*-reversion (PEO4), and *BRCA*-wild-type (COV318 and COV504) cell lines. The synergy was also effective in KURAMOCHI and OVSAHO cells, two *BRCA2*-deficient cell lines with intrinsic PARP inhibitor resistance through unknown mechanisms (Pillay et al., 2019, Kim et al., 2020, Ingham et al., 2013). I also found that indisulam synergised with the weak PARP trapper (veliparib) as well as strong PARP trappers (olaparib, rucaparib and niraparib) , suggesting that catalytic inhibition of PARP may play a major role in the synergy. Collectively, these data suggest that the combination therapy of RBM39 degraders and PARP inhibitors may have a broad therapeutic application. It may benefit many ovarian cancer patients irrespective of their *BRCA*-status and which PARP inhibitor they are taking. However, HRD and DCAF15-amplified patients may have a wider therapeutic window as lower doses of RBM39 degraders and PARP inhibitors would be needed to achieve the synergy.

Another important finding is that the synergy between indisulam and PARP inhibitors occurs in a *DCAF15*-dependent manner, despite some indications that indisulam may act independently from DCAF15-mediated RBM39 degradation (Abbate et al., 2004, Del Prete et al., 2020, Nijhuis et al., 2022). Knock out of *DCAF15* not only conferred strong indisulam resistance in PEO1 cells, but also abrogated the combination benefit of indisulam and olaparib. In addition, E7820 recapitulated the effect of indisulam in the synergy with olaparib, further indicating that the synergy is downstream of DCAF15-mediated RBM39 degradation. This is consistent with results from another in-house drug combination screen, where indisulam showed *DCAF15*-dependent synergy with a panel of chemotherapy drugs in the HCT116 colorectal cancer cells. However, whether *DCAF15* abundance in cancer cells could influence the synergy efficacy remain to be investigated in the future.

The synergy between RBM39 degraders and PARP inhibitors is compatible with the hypothesis that loss of RBM39 causes splicing errors in DNA damage repair genes, thereby attenuating DNA damage response. The systematic analysis (Section 3.1.1) of alternative splicing events in neuroblastoma (Nijhuis et al., 2022, Singh et al., 2021), melanoma (Lu et al., 2021b), acute myeloid leukaemia (Wang et al., 2019), and breast cancer (Mai et al., 2016a) showed that the common splicing changes upon RBM39 depletion is not random. There is a significant enrichment for G2/M DNA damage checkpoint and DSB repair pathways. I have validated RBM39-dependent splicing of several key DNA repair genes. In HGSOC cells, indisulam treatment caused deleterious exon skipping events affecting multiple DSB repair pathways, including DNA damage recognition (*ATM*), HR repair (*BRCA1* and *RAD51D*), and NHEJ repair (*TP53BP1* and *RIF1*). This finding suggests a consistent role of RBM39 in modulating alternative splicing of DNA repair genes across various cancer backgrounds. Given that multiple components of DSB repair pathways are affected simultaneously, RBM39 depletion is likely to disrupt both HR- and NHEJ-mediated DSB repair, leading to increased susceptibility to additional genotoxic stress. This could explain the trends of synergy between indisulam and many DNA damaging agents tested, and the combination benefit of indisulam and PARP inhibitors in cell lines with or without functional BRCA1/2.

Interestingly, several antagonistic interactions were also noticed in the drug combination screen. In the screen, indisulam showed a consistent trend of antagonism with anthracycline-based topoisomerase II inhibitors such as doxorubicin. Nevertheless, not all topoisomerase

inhibitors were antagonistic with indisulam. For example, irinotecan and dexrazoxane showed strong trends of synergism with indisulam. Since doxorubicin and other anthracyclines have alternative mechanisms of action apart from topoisomerase inhibition [reviewed in (Nitiss, 2009)], it is possible that the antagonism with indisulam may be a result of topoisomerase-independent effects.

Another interesting antagonism is between indisulam and taxanes, which discourages the combination of indisulam with this chemotherapy in ovarian cancer. One possible explanation is that taxanes cause cell cycle arrest at mitosis (reviewed in(Škubník et al., 2021)), during which gene expression and pre-mRNA splicing are silenced (Palozola et al., 2017), thereby negating the effect of indisulam on alternative splicing and leading to antagonism. In addition, indisulam can arrest cells at the G1/S phase (Yokoi et al., 2002, Fukuoka et al., 2001, Owa et al., 1999) and decrease the number of cells reaching mitosis, thereby attenuating the effect of taxanes.

These antagonistic interactions are as informative as the synergistic interactions identified between indisulam and clinical drugs. Collectively, they provide valuable insights into RBM39 biology and highlight combination strategies worth investigating.

It is worth noting that 30 µM olaparib was used in some functional assays, which is more than sufficient to inhibit PARylation and might have induced non-specific interactions with other targets such as TNKS1/2 (Table 1.2). Although this dose is clinically relevant and achievable in patient plasma (Yamamoto et al., 2012, Roth et al., 2014, Pilla Reddy et al., 2018), it may cause off-target interactions and lead to unintended functional consequences. For example, TNKS-dependent cell mitosis might be inhibited and thus the observed anti-proliferative effect was not solely caused by PARP1/2 inhibition (Wu et al., 2022). Current evidence cannot rule out the involvement of TNKS1/2 inhibition in the synergy between olaparib and indisulam. Future research would be necessary to assess if 30 µM olaparib causes strong TNKS inhibition in HGSOC cells. If so, it would be important to examine if TNKS inhibitors synergise with indisulam in the same way as PARP inhibitors, and whether knocking down *TNKS1* and *TNKS2* protects cells from the synergy.

Chapter 3

To sum up, findings from this chapter revealed an important and hitherto unreported role of RBM39 in modulating DNA damage response, and that RBM39 degrader renders cells more susceptible to DNA damaging agents. In particular, the combination of indisulam and PARP inhibitors showed promising synergy in HGSOC cells irrespective of genomic *BRCA*-status. This suggests that combining indisulam with PARP inhibitor therapy may benefit a wide range of ovarian cancer patients. However, the exact events leading to the synergy are still unclear and will be investigated further in Chapter 5.

Chapter 4

Chapter 4. Evaluating the combined effect of indisulam and olaparib in the ID8 murine model of HGSOC

4.1. Validating the synergy of indisulam and olaparib in ID8 models *in vitro*

The promising therapeutic potential of indisulam in improving olaparib response in HGSOC cell lines motivated me to investigate the synergistic interaction in animal models of HGSOC. I decided to use the syngeneic ID8 model, established in 2000 from ovarian surface epithelial cells of a C57BL/6 mouse (Roby et al., 2000). In 2016, the research team led by Professor Iain McNeish improved ID8 models by introducing the *Trp53* deletion (ID8-*Trp53*$^{-/-}$) to recapitulate the universal loss of p53 in human HGSOC tumours (Walton et al., 2016). Additional ID8 clones were generated with CRISPR/Cas9-mediated knockout of additional genes, such as *Brca2* (ID8-*Trp53*$^{-/-}$;*Brca2*$^{-/-}$), producing a series of isogenic murine models for HGSOC research (Walton et al., 2017, Walton et al., 2016). One major advantage of ID8-derived syngeneic models over xenograft is the use of immunocompetent mice, which offers a physiologically relevant tumour microenvironment. In addition, mice bearing ID8 tumours usually develop bloody peritoneal ascites and exhibit preferential metastasis to the omentum, recapitulating the process of peritoneal metastasis observed in many ovarian cancer patients (Figure 4.1) (Walton et al., 2016, Ford et al., 2020). Therefore, the ID8 model was selected to study the efficacy of indisulam and olaparib combination therapy *in vivo*.

Prior to *in vivo* investigation, the effect of indisulam and olaparib *in vitro* was assessed in the laboratory using two ID8 clones: ID8-*Trp53*$^{-/-}$ and ID8-*Trp53*$^{-/-}$;*Brca2*$^{-/-}$. Since RBM39 is highly conserved between human and mouse, I expected that indisulam treatment would affect ID8 cells in the same way as human HGSOC cell lines. Indeed, western blot analysis demonstrated that indisulam treatment induced a dose-dependent degradation of Rbm39 in ID8 cells (Figure 4.2A). Cell proliferation analysis showed that the ID8-*Trp53*$^{-/-}$;*Brca2*$^{-/-}$ clone (IC50 = 0.62 µM, 95% confidence interval = 0.46 – 0.83 µM) was over ten times more sensitive to olaparib than the ID8-*Trp53*$^{-/-}$ clone (IC50 = 8.8 µM, 95% confidence interval = 6.62 – 11.75 µM) (Figure 4.2B), which is consistent with their HR status demonstrated in the original publication (Walton et al., 2016). On the other hand, both ID8 clones showed similar sensitivity to indisulam and E7820 (Figure 4.2C). The combination of either indisulam or E7820

with olaparib led to synergistic growth inhibition in both ID8 clones, regardless of their *Brca2* status (Figure 4.2D-E). This is consistent with previous observations with human HGSOC cell lines, supporting previous conclusion that pharmacological depletion of RBM39 improves PARP inhibitor response irrespective of BRCA status.

In summary, these findings indicate that indisulam synergises with olaparib in ID8 cells in the same way as in human HGSOC cell lines. Furthermore, the HR-proficient ID8-*Trp53*$^{-/-}$ clone is a useful model for HR-proficient tumours, which are less responsive to PARP inhibitors than HR-deficient tumours.

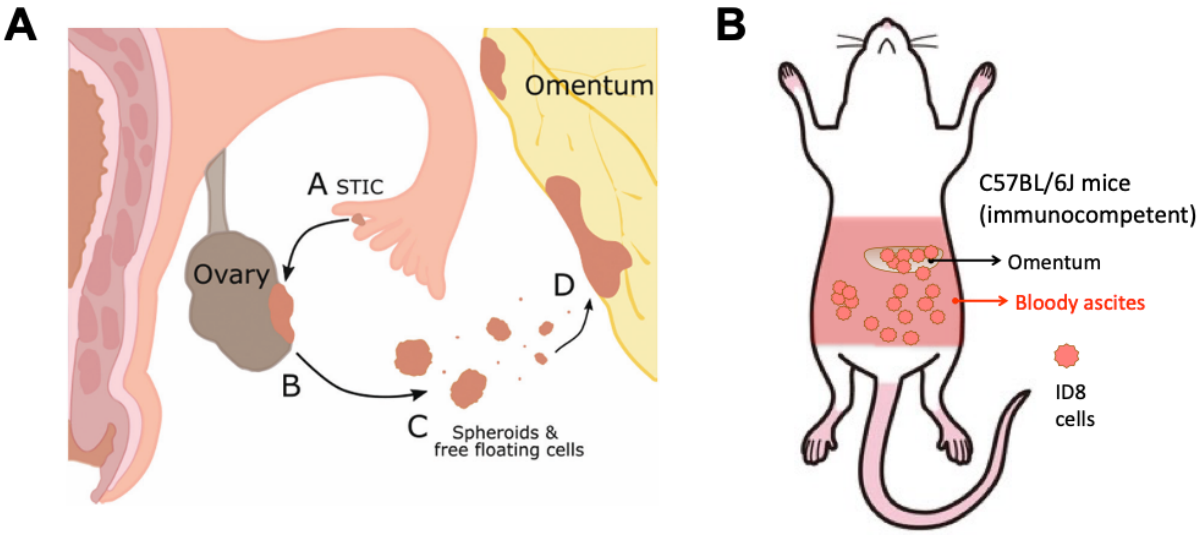


Figure 4.1. ID8 model recapitulates peritoneal metastasis in human HGSOC.
(A) Diagram showing the peritoneal metastasis of HGSOC in patients. Current studies suggest that most HGSOC originates from the fallopian tube as a premalignant lesion (STIC, serous tubal intraepithelial carcinoma) before disseminating to the ovary. As HGSOC tumour burden increases, the primary tumour may shed floating cancer cells or spheroids, leading to peritoneal metastasis to the omentum and later to other organs. In addition, patients may develop ascites when tumour deposits block the abdominal lymphatic drainage system and increase leakage from blood vessels. This diagram is taken from Lusk et al. (2021) with permission. **(B)** Diagram showing the ID8 murine HGSOC model. ID8 cells are commonly injected intraperitoneally into the peritoneal cavity. Similar to disease progression in patients, omentum is the preferential site for ID8 metastasis, and the tumour-bearing mice eventually develop ascites.

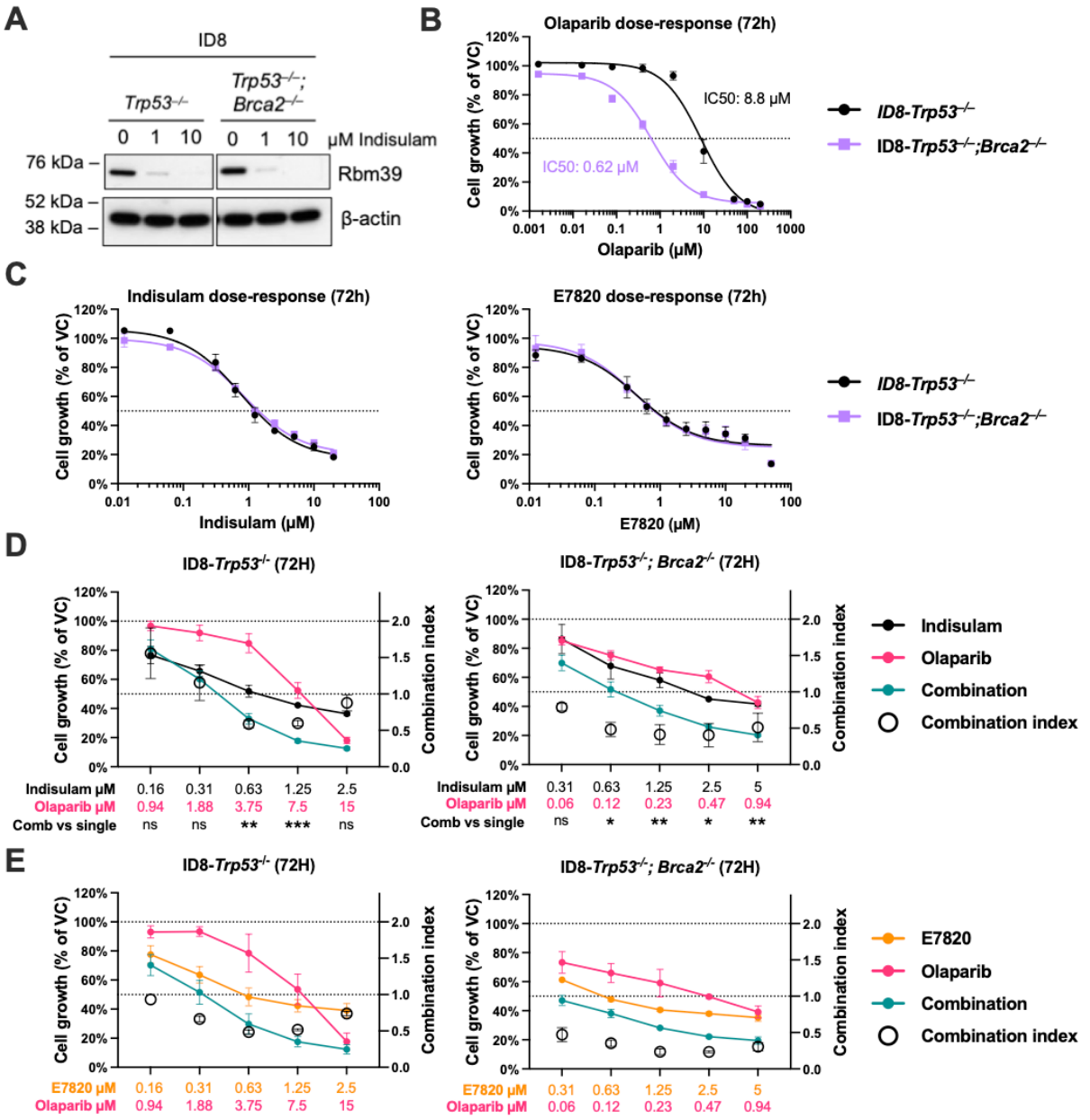


Figure 4.2. Indisulam and E7820 synergise with olaparib in ID8 cells.
(A) ID8-*Trp53*$^{-/-}$ and ID8-*Trp53*$^{-/-}$;*Brca2*$^{-/-}$ cells were treated with indicated doses of indisulam for 6 hours before western blot analysis (n = 1). **(B-C)** Cell growth of ID8 cells after 72-hour treatment of olaparib, indisulam or E7820. Data were collected from at least two independent experiments, and the error bar = SEM (n=3 for ID8-*Trp53*$^{-/-}$). **(D)** Cell growth of ID8 cells following 72-hour treatment of indisulam and olaparib as monotherapies or in combination (n = 3, error bar = SEM). CI values were calculated by the Chou-Talalay method and shown as open circles to the right y-axis (n = 3, error bar = SD). Statistical difference between combination therapy and monotherapies was determined by the two-way ANOVA and Dunnett's multiple comparisons test (ns, not significant; *p < 0.05; ** p < 0.01; ***p < 0.001). **(E)** ID8 cells were treated with E7820 and olaparib individually or in combination for 72 hours and cell growth was measured (n = 2, error bar = SEM). CI index values were shown to the right y-axis (n = 2, error bar = SD). Cell growth in (a-e) was measured by the SRB assay.

Chapter 4

4.2. Investigating the tolerability of indisulam and olaparib *in vivo*

4.2.1. Optimising drug formulations for *in vivo* administration

Many small molecular drugs have low solubility in water. Thus, emulsifiers, surfactants, or hydrophilic co-solvents are often included in the formulation to increase drug solubility. Indisulam is commonly administrated intravenously (I.V.) in saline (0.9% NaCl) containing 3.5% DMSO and 6.5% Tween-80 (Ozawa et al., 2001, Han et al., 2017b, Nijhuis et al., 2022). Although orally (in tablets) available for patients, olaparib is frequently administrated in mice via intraperitoneal (I.P.) injection and several formulations have been used, including 4% DMSO plus 30% polyethylene glycols 300 (PEG300) (Wang et al., 2020), 10% 2-hydroxypropyl-β-cyclodextrin (HBC) (Yi et al., 2019, Bajrami et al., 2014, Ding et al., 2018), or 10-20% captisol (Karakashev et al., 2017, Karakashev et al., 2020).

In this study, I decided to use the same formulation for indisulam and olaparib, which allows simultaneous administration of both drugs and reduces animal suffering. Since olaparib is compatible with various vehicles, I hypothesised that it could be prepared in the same formulation as indisulam (3.5% DMSO and 6.5% Tween-80 in saline). Surprisingly, neither indisulam nor olaparib was able to dissolve completely in this formulation, but repeated sonication was able to reduce particle size and generate drug suspensions. Under the microscope, undissolved particles of indisulam and olaparib looked no larger than average mammalian cells (Figure 4.3) (Hoogduijn et al., 2013). Although such drug suspensions are not suitable for I.V. delivery, they can be used for I.P. injections (Di and Kerns, 2016). HBC was also tested as an alternative co-solvent. However, up to 20% of HBC was not sufficient to dissolve powders of indisulam and olaparib even after repeated sonication and overnight agitation. As a result, indisulam and olaparib were prepared in 3.5% DMSO plus 6.5% Tween-80 in saline for I.P. injection.

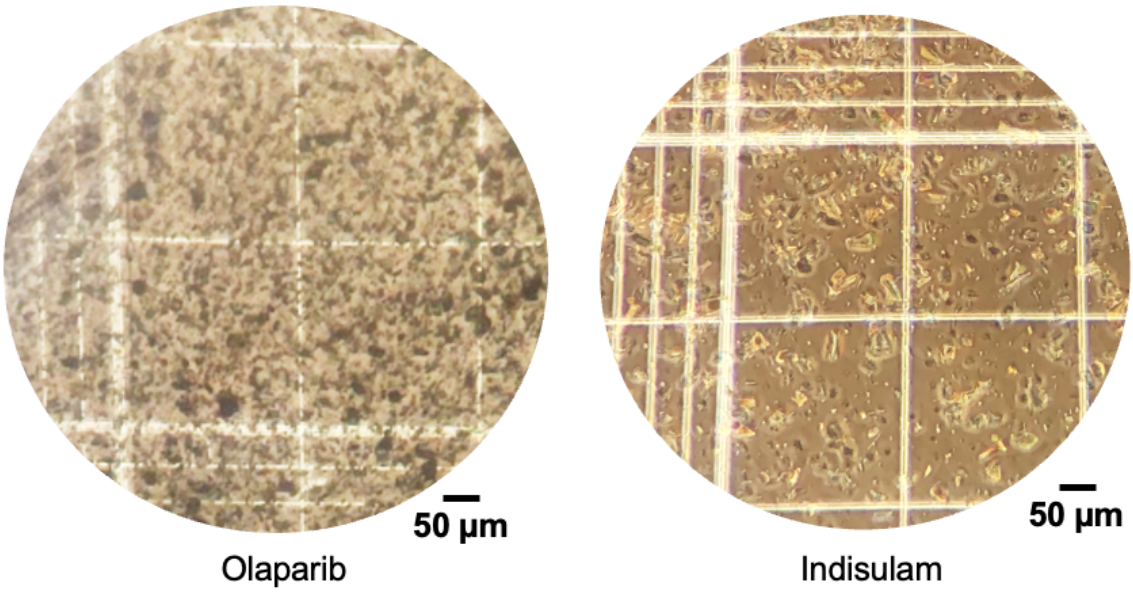


Figure 4.3. Suspensions of olaparib and indisulam under a microscope.
Olaparib (left, 12.5 mg/mL) and indisulam (right, 6.25 mg/mL) were dissolved in saline containing 3.5% DMSO and 6.5% Tween-80 as described in the Materials and Method. Representative images of undissolved particles of olaparib and indisulam are shown here. Haemocytometer was used to estimate particle diameters. Scale bar = 50 µm. Olaparib particles were needle-shaped crystals and occasionally formed dense 'clouds' due to high concentration. Indisulam particles had irregular shapes and appeared larger than particles of olaparib. Both types of particles were no larger than the size of a typical mouse stem cell (average diameters are around 28 µm) (Hoogduijn et al., 2013).

4.2.2. The combination of indisulam and olaparib shows signs of tumour suppressive effect in ID8-*Trp53*$^{-/-}$ tumours *in vivo*

The first *in vivo* study was designed to examine the tolerability of indisulam and olaparib combination therapy in mice. In brief, ID8-*Trp53*$^{-/-}$ cells were injected into the peritoneal cavity of female C57Bl/6J mice and allowed to form tumours for 35 days (Figure 4.4A). Then, mice were randomised into six groups (n = 3) and received vehicle control or increasing doses of the combination therapy (indisulam + olaparib) daily for up to seven days. Each group included three mice, except one group (n = 2, one mouse dropped out of the study before drug injection). Significant loss of body weight (> 10%) and signs of suffering were used as primary indicators for animal health.

Up to 25 mg/kg/day indisulam (Ozawa et al., 2001, Han et al., 2017b, Nijhuis et al., 2022, Wang et al., 2019) or 50 mg/kg/day olaparib (Karakashev et al., 2020, Wang et al., 2020) have been used in mice with no reports of toxicities. Therefore, in this pilot study, indisulam was combined with olaparib at a constant ratio of 1:2. The highest administrated dose combination was 25 mg/kg/day indisulam plus 50 mg/kg/day olaparib, and the lowest

combination dose was 1.56 mg/kg/day indisulam plus 3.13 mg/kg/day olaparib. Twenty-four hours after the final dosing, all mice were sacrificed and omental tumours were collected as a marker for overall tumour burden.

No significant weight loss or signs of distress were observed in mice receiving up to 12.5 mg/kg/day indisulam plus 25 mg/kg/day olaparib (Figure 4.4B), suggesting that the combination therapy is well tolerated at these doses. On the other hand, 100% of mice (n = 2) experienced diarrhoea and substantial weight loss after five injections of the combination therapy at the highest dose (25 mg/kg/day indisulam and 50 mg/kg/day olaparib), and the drug treatment was thus discontinued (Figure 4.4B). Due to a lack of control arms with monotherapies, it was not possible to determine whether the adverse events were driven by one of the drugs or potentially additive toxicity between indisulam and olaparib.

None of the mice formed visible ascites during the study, but they all had tumour deposits in the omentum. Interestingly, in the two mice that showed adverse events to 25 mg/kg/day indisulam plus 50 mg/kg/day olaparib, a trend of reduction in omental tumour weight was observed, implying a partial response to the combination therapy (Figure 4.4C). No omental tumour weight reduction was observed at other doses (Figure 4.4C). Nonetheless, western blot analysis using omental tumour proteins revealed that as low as 6.25 mg/kg/day indisulam was able to induce RBM39 degradation in tumours, confirming successful target engagement of indisulam (Figure 4.4D).

Overall, this pilot study suggests that indisulam at a dose higher than 6.25 mg/kg/day induces RBM39 degradation in ID8 tumours, and its combination with olaparib has the potential to inhibit tumour growth, but with a risk of adverse events when 25 mg/kg/day indisulam was combined with 50 mg/kg/day olaparib.

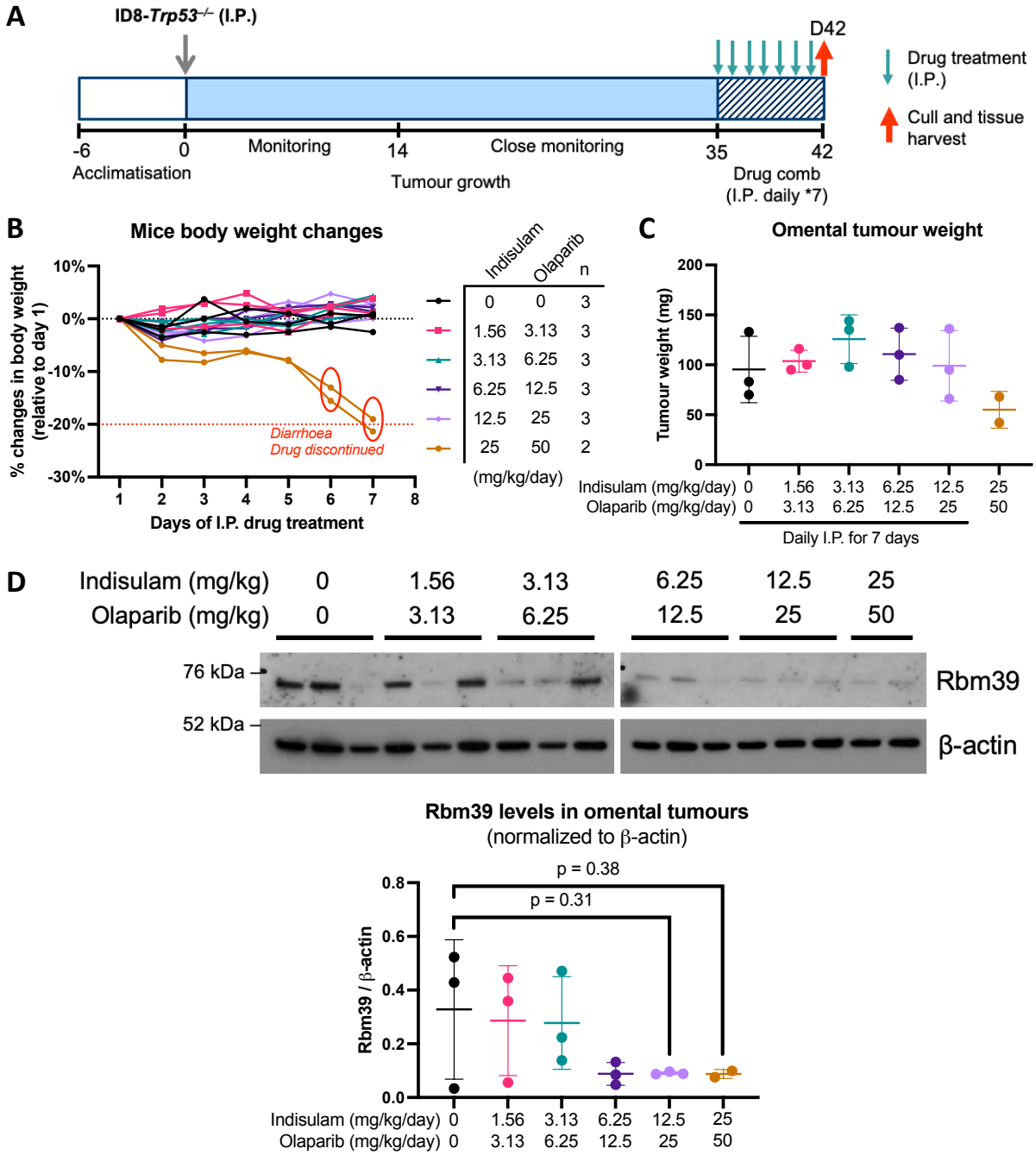


Figure 4.4. The combination of indisulam and olaparib shows signs of anti-tumour effect in the HR-proficient ID8 model.

(A) Timeline of the pilot study showing that the ID8-*Trp53*$^{-/-}$ cells were injected intraperitoneally (I.P.) into C57BL/6J mice and allowed to grow for 35 days before treating with indisulam and olaparib in combination daily for seven days. **(B)** Relative body weight changes of mice during drug administration. Two mice receiving the highest doses of the combination therapy experienced diarrhoea and weight loss, leading to treatment discontinuation after five days (highlighted by red circles). **(C)** Omental tumours were harvested at the end of the study and used as an indicator for overall tumour burden in mice. Error bar = SD. **(D)** Total protein from omental tumour samples was extracted, and Rbm39 levels were measured through western blot. β-actin was used as a loading control. The bottom chart shows the densitometry analysis of Rbm39 band intensities after normalisation to β-actin. The one-way ANOVA and Dunnett's multiple comparisons test were used to calculate statistical differences among groups.

4.2.3. Indisulam and olaparib combination perhaps inhibit growth of subcutaneous ID8 tumours.

A follow-up study was conducted to optimise the dosing schedules of indisulam and olaparib in mice. Due to ethical concerns, FDA-approved clinical doses of olaparib cannot be changed in unapproved combination strategies (such as with indisulam). Therefore, one reasonable approach to reduce adverse effects from combination therapy is to lower the dose of preclinical drugs such as indisulam. To this end, mice bearing ID8-*Trp53*$^{-/-}$ tumours were randomised into seven groups and received the following treatment: vehicle control, olaparib (50 mg/kg/day), indisulam (20 mg/kg/day), or combinations of 50 mg/kg/day olaparib and indisulam (at doses of 8.4, 11.3, 15, or 20 mg/kg/day). The daily drug treatment started on day 28 after the tumour injection, and the duration increased from 7 days to 13 days (Figure 4.5A), because I hypothesised that lower doses of indisulam may need a longer exposure to achieve the same efficacy (as the 25 mg/kg/day indisulam). At the same time, four additional mice were injected with ID8-*Trp53*$^{-/-}$*;Brca2*$^{-/-}$ cells and treated with either vehicle control or 50 mg/kg/day olaparib for 13 days (Figure 4.5A). These two groups of *Brca2*-deficient mice were included as a positive control to examine whether the combination therapy could improve olaparib response in HR-proficient ID8-*Trp53*$^{-/-}$ tumours to a similar level as that of HR-deficient ID8 tumours (ID8-*Trp53*$^{-/-}$*;Brca2*$^{-/-}$). All mice were sacrificed at day 42, and omental tumours were harvested as a primary indicator for tumour burden (Figure 4.5A).

In mice bearing ID8-*Trp53*$^{-/-}$*;Brca2*$^{-/-}$ tumours, 50 mg/kg/day olaparib was well tolerated with no signs of toxicity (Figure 4.5B). Surprisingly, olaparib treatment did not reduce the omental tumour burden compared to the vehicle control (Figure 4.5C). This finding was unexpected because HR-deficient tumours are theoretically sensitive to olaparib treatment. Possible causes include small sample sizes (n = 2) and natural variation in omental tumour sizes. Another probable explanation is that, based on the historical data provided by Dr Sarah Spear and Dr Carmen Aguirre Hernandez (personal communication, 5 July 2021) (Figure 4.5D), the omental tumour may have passed the exponential growth phase by the start of olaparib administration (day 28), and therefore the suppressive effect of olaparib on tumour proliferation was not obvious.

Apart from the omental tumour, I found that the subcutaneous (s.c.) tumour deposits could be used as an alternative marker for disease progression. In ID8 mice with ascites, I.P.

injection sometimes causes small leakage of malignant ascites, and tumour cells may be trapped under the skin, leading to the formation of s.c. tumour deposits. Therefore, I reasoned that they could reflect the tumorigenic potential of ascitic ID8 cells. These s.c. tumour deposits could be found on both sides of the abdomen of mice as I.P. injection sites alternated between the left and right sides of the abdomen (Figure 4.5E). They were usually small and only noticeable via palpation, so I designed a scoring system to estimate the overall s.c. tumour burden semi-quantitatively (Figure 4.5F). The data showed that in comparison with vehicle control, olaparib treatment reduced the development of s.c. tumour deposits in ID8-*Trp53*$^{-/-}$;*Brca2*$^{-/-}$ mice, implying possible tumour suppressive effect of olaparib *in vivo* (Figure 4.5G).

For mice implanted with ID8-*Trp53*$^{-/-}$cells, olaparib-treatment alone (50 mg/kg/day) did not cause any adverse events, and up to 15 mg/kg/day indisulam plus olaparib was well tolerated (Figure 4.6A-B). However, indisulam monotherapy at 20 mg/kg/day caused substantial weight loss in mice (2/2) after six days and reached the humane endpoint soon after (Figure 4.6B). Adverse events were also observed in two out of three mice treated with the combination of indisulam (20 mg/kg/day) and olaparib (50 mg/kg/day) after eight days of drug injections (Figure 4.6B). These findings indicate that there is little to no additive toxicity between indisulam and olaparib, and indisulam is predominantly responsible for toxicities observed in drug combinations.

Omental tumour weight and s.c. tumour scores of ID8-*Trp53*$^{-/-}$ mice were used as indicators for anti-tumour activities. Omental tumour burden showed no significant differences across treatment groups (Figure 4.6C). Interestingly, three mice had healthy-looking omentum without visible tumours, including one mouse (out of two) received indisulam (20 mg/kg/day) and two (out of three) mice received 11.3 mg/kg/day indisulam and 50 mg/kg/day olaparib (Figure 4.6C). Due to the small sample size and a lack of a non-invasive method to check tumour growth before drug treatment, it is unclear whether these three mice experienced complete tumour regression or rejected the tumour implantation. On the other hand, the s.c. tumour scores were lower in olaparib-treated mice than in vehicle-treated mice (Figure 4.6D), suggesting a trend of growth inhibition. The addition of indisulam to olaparib further reduced the s.c. scores in a dose-dependent manner, indicating possible additive or more than additive effect on suppressing s.c. tumour development (Figure 4.6D).

Chapter 4

The differential effects of drug treatment on omental tumours and s.c. tumours support the hypothesis olaparib and indisulam are more effective in inhibiting tumour growth than shrinking tumour sizes. Drug treatment in this pilot study was commenced at day 28, when substantial omental tumour burden exists, and this may be too advanced to achieve a therapeutic effect (Figure 4.5D). Thus, an earlier start of drug treatment is likely to improve the efficacy of the combination therapy, which also better models the clinical use of PARP inhibitors as maintenance therapy (after completing chemotherapy and surgery) when the disease burden is low.

Overall, the above findings suggest that when used at 15mg/kg/day, indisulam might improve olaparib response without causing overt toxicity, and further investigation with a larger sample size was warranted.

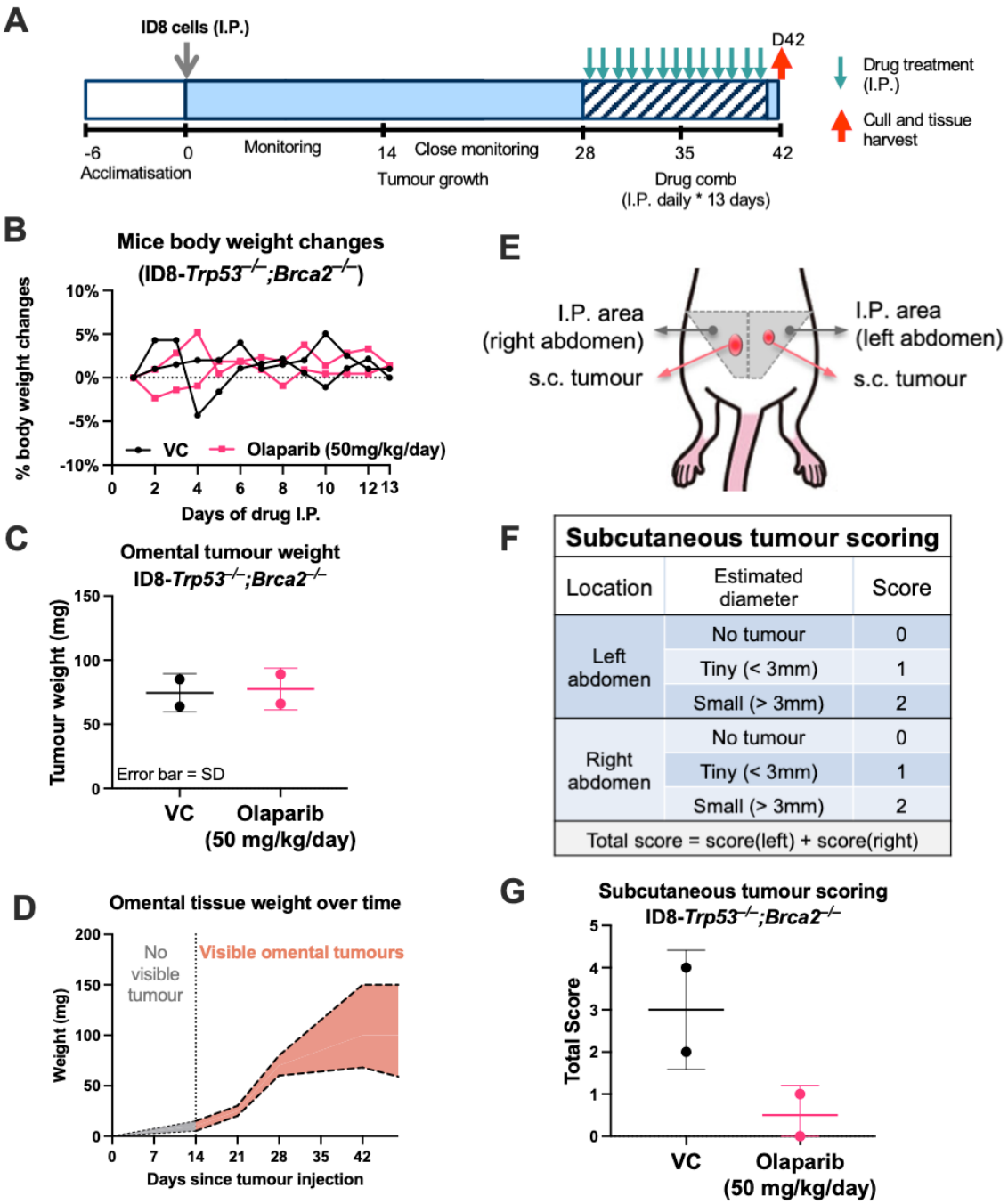


Figure 4.5. Olaparib reduces subcutaneous tumour formation in the *Brca2*-deficient ID8 model. **(A)** Timeline of the *in vivo* study. HR-deficient (ID8-*Trp53*$^{-/-}$;*Brca2*$^{-/-}$) ID8 cells were injected via I.P. into C57BL/6 mice and allowed to form tumours for 28 days before daily drug administration for 13 days. Mice were sacrificed on day 42. **(B-C)** Relative changes of body weight (b) and omental tumour weight (c) of mice bearing ID8-*Trp53*$^{-/-}$;*Brca2*$^{-/-}$ tumours. Error bar = SD. **(D)** Historical data indicating the changes of omental tissue weight (upper and lower limit) since the injection of ID8-*Trp53*$^{-/-}$ or ID8-*Trp53*$^{-/-}$;*Brca2*$^{-/-}$ cells. Data points were acquired from personal communication with Dr Sarah Spear and Dr Carmen Aguirre Hernandez on 5 July 2021. **(E)** Schematic showing formation of subcutaneous (s.c.) tumour deposits caused by repeated I.P. injections and leaking of malignant ascites. **(F)** The s.c. tumours were scored semi-quantitatively, and diameters were estimated through palpation because they were not measurable by callipers. **(G)** The s.c. tumours formed in mice implanted with the *Brca2*-deficient ID8 tumours were scored one day before being sacrificed. Error bar = SD.

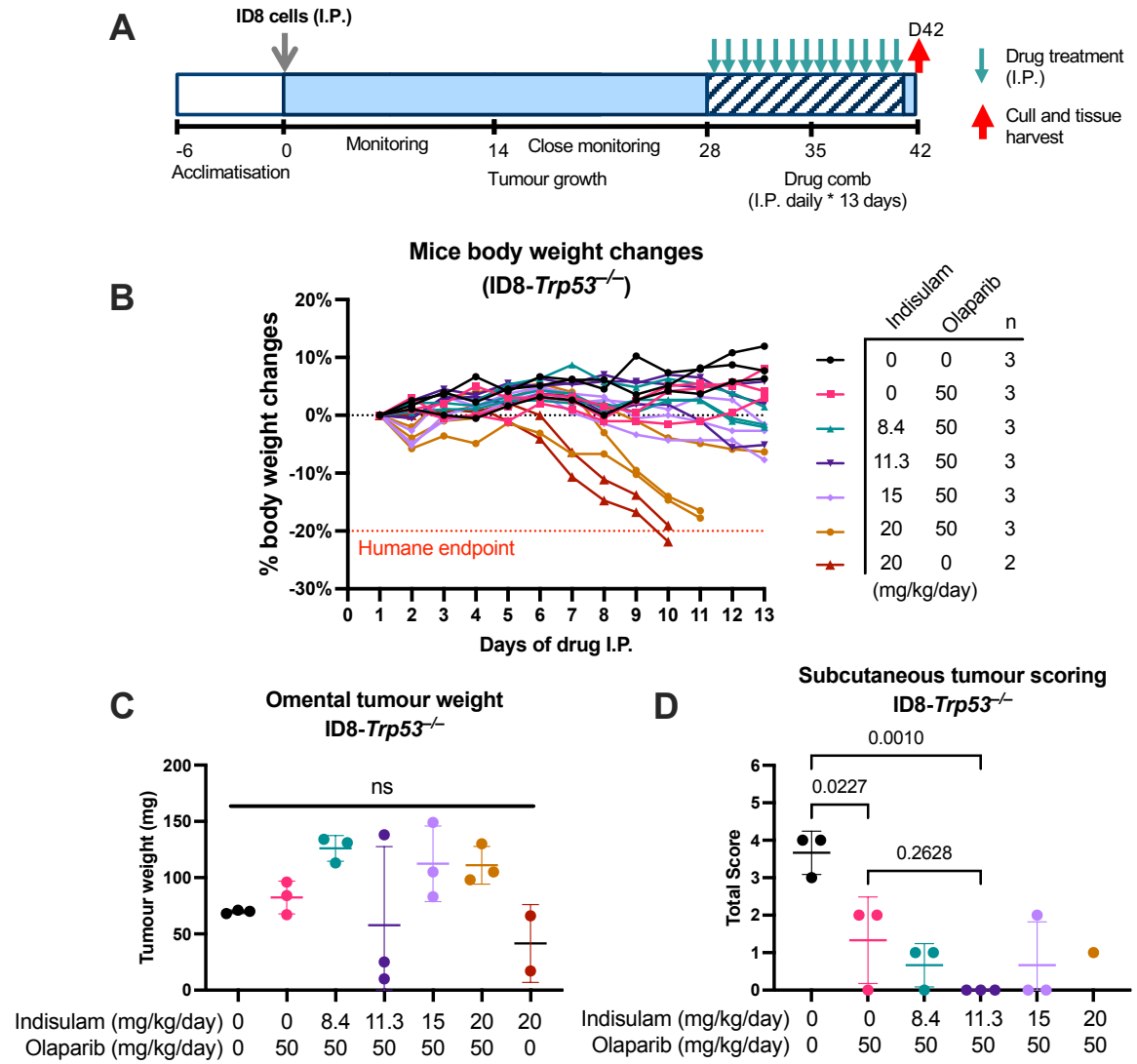


Figure 4.6. Indisulam and olaparib reduces subcutaneous tumour development in the HR-proficient ID8 model.

(A) Diagram showing the timeline of in vivo study with mice implanted with the HR-proficient (ID8-*Trp53*$^{-/-}$) ID8 cells, which was done in parallel with the study of *Brca2*-deficient ID8 tumours in Figure 4.5. The diagram is the same as Figure 4.5A. **(B)** After daily injection of indicated drugs for 13 days, relative body weight changes of mice were recorded. One of the humane endpoints was more than 20% body weight loss. **(C)** Omental tumour weight changes in response to indicated drug treatment. One-way ANOVA followed by Tukey's multiple comparisons test did not find any significant changes (ns, not significant). (D) S.c. ID8-*Trp53*$^{-/-}$ tumours were scored (error bar = SD). One-way ANOVA followed by Šídák's multiple comparisons test was used to calculate the p-values between indicated groups.

4.3. Indisulam improves survival benefits of olaparib in mice bearing HR-proficient ID8 tumours

Pilot studies provided valuable information about drug tolerability and suggested dosing schedules, allowing the design of survival analysis to assess the impact of indisulam and olaparib on the overall survival of HR-proficient ID8-*Trp53*$^{-/-}$ mice. Based on earlier findings, I

speculated that indisulam at 15 mg/kg/day plus olaparib at 50 mg/kg/day was likely to inhibit tumour growth with minimal risks of adverse events. The optimal period of drug administration was between 21-35 days post-tumour inoculation, during which tumours are still growing exponentially (Figure 4.5D). I chose this dosing scheme because it would mimic the clinical use of PARP inhibitors as a maintenance therapy after surgical removal of tumour bulk and chemotherapy. Therefore, ID8-*Trp53*$^{-/-}$ mice were planned to receive drugs daily for 13 days, starting from 21 days after tumour implantation. However, due to unexpected toxicities, the duration of drug administration was reduced from 13 days to 11 days (Figure 4.7A-B).

In this study, 48 mice were injected with ID8-*Trp53*$^{-/-}$ cells and tumours were allowed to grow for 21 days (Figure 4.7A). Then, mice were randomised equally into four groups (n = 12 each) and were treated with vehicle control, indisulam (15 mg/kg/day), olaparib (50 mg/kg/day), or the combination of indisulam (15 mg/kg/day) and olaparib (50 mg/kg/day) for 11 days. After completing the drug treatment, researchers were blinded from drug treatment records for unbiased humane endpoint assessment. Mice were sacrificed when they reached the humane endpoints (listed in the Materials and Methods, Section 2.11) or at the end of the study (day 120).

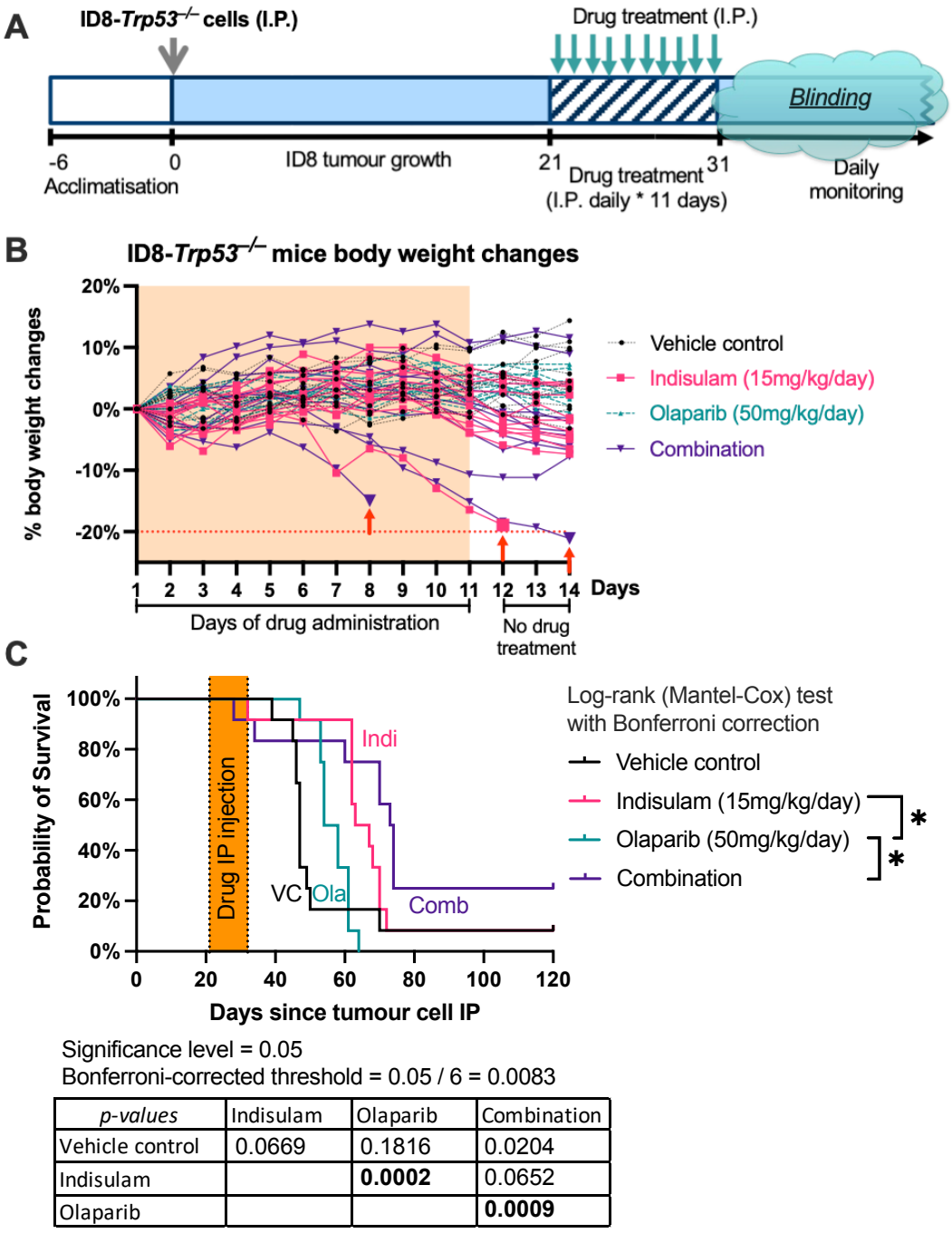
Most mice completed the drug treatment without overt toxicity (Figure 4.7B). However, three mice experienced severe weight loss and reached the humane endpoint during or soon after the drug treatment (Figure 4.7B). All adverse events were indisulam-related, including one received indisulam as monotherapy and two received indisulam in combination with olaparib. Although treatment for these mice was discontinued as soon as unexpected weight loss was noticed (around 10% weight loss), they continued to lose weight and reached the humane endpoint. This finding indicates that although 15 mg/kg/day indisulam is tolerable in most cases, there is a risk of causing adverse events.

In the absence of interventions, ID8-*Trp53*$^{-/-}$ mice showed a median survival of 47 days (Figure 4.7C), which is comparable to previous publications (Walton et al., 2017, Walton et al., 2016). Olaparib treatment showed a moderate survival benefit, increasing the median survival from 47 days to 56 days ($p = 0.1816$, not significant) (Figure 4.7C). The moderate survival benefit from olaparib was expected because the ID8-*Trp53*$^{-/-}$ tumour is resistant to

PARP inhibitor treatment due to HR proficiency. Indisulam-treated mice showed a clear trend of improvement in overall survival when compared with mice treated with vehicle ($p = 0.0669$, not significant) or olaparib ($p = 0.0002$, significant), improving the median survival to 65 days (Figure 4.7C). The combination of indisulam and olaparib exhibited the most survival benefit with the longest median survival of 73.5 days – significantly longer than that of olaparib monotherapy ($p = 0.0009$) and showed a non-significant trend of improvement when compared with vehicle control ($p = 0.0204$) and indisulam monotherapy ($p = 0.06$) (Figure 4.7C).

It is worth noting that five mice survived to day 120 without showing any clinical signs, including mice from following groups: vehicle control ($n = 1$), indisulam ($n = 1$), and the combination of indisulam and olaparib ($n = 3$). Successful tumour implantation could not be confirmed in four of them. However, one of them (received the combination therapy) developed s.c. tumour during drug injection, implying the existence of malignant ascites and successful tumour implantation. This mouse looked healthy throughout the study and there were no visible tumour deposits in the abdominal cavity. This observation implied a possibility that the mouse might have experienced a complete tumour regression. However, this cannot be confirmed due to a lack of non-invasive methods to monitor tumour growth.

Overall, these findings suggest that the indisulam improves olaparib response in HR-proficient tumours.



Significance level = 0.05
Bonferroni-corrected threshold = 0.05 / 6 = 0.0083

p-values	Indisulam	Olaparib	Combination
Vehicle control	0.0669	0.1816	0.0204
Indisulam		**0.0002**	0.0652
Olaparib			**0.0009**

Figure 4.7. Indisulam improves olaparib response in HR-proficient ID8 mice.
(A) Timeline of the survival analysis. Mice with HR-proficient ID8 tumours (ID8-*Trp53*$^{-/-}$) were randomised into four groups for drug treatment. Researchers were blinded from details of treatment for unbiased humane endpoint determination. **(B)** Relative body weight changes of mice during and after the drug treatment. Three mice reached the humane endpoint prematurely due to unexpected toxicities (indicated with red arrows). **(C)** Kaplan-Meier curves showing surviving proportions of ID8-*Trp53*$^{-/-}$ mice since the start of the experiment (48 mice were randomised into four groups, n = 12 each). Data were collected from two biological replicates, with each containing six mice per group. Log-rank test was used to determine statistical differences between survival curves. Bonferroni correction was used for the multiple comparisons test and *p < 0.0083 was considered significant (highlighted in bold).

Chapter 4

4.4. Discussion

The main objective of this chapter was to examine if the indisulam synergises with olaparib in murine models of HGSOC. As KURAMOCHI and OVSAHO cells showed remarkable responses to the combination therapy, I had considered transplanting these two human HGSOC cell lines into mice as xenografts. However, previous literature reported that both cell lines have poor tumorigenicity in athymic mice and are difficult to form xenografts (Mitra et al., 2015, Elias et al., 2015). Tumorigenicity improves with the use of NOD severe combined-immunodeficient gamma mice (Elias et al., 2015), which have impaired T, B and nature killer cell function, but at the cost of reduced clinical relevance due to the lack of a faithful tumour microenvironment.

The orthotopic ID8 murine HGSOC model is a valuable alternative to xenografts, providing a more clinically relevant system using immunocompetent mice. Meanwhile, human RBM39 is highly conserved with murine Rbm39, with 99.8% protein sequence homology (Kang et al., 2015). The only difference is the 23rd amino acid, which changed from asparagine (N) in human RBM39 to serine (S) in mouse Rbm39. As none of the RRM domains is affected, the function of RBM39 is likely conserved between human and mouse.

As expected, ID8 cells responded to indisulam similar to human HGSOC cells, in terms of Rbm39 degradation and synergistic growth inhibition with olaparib *in vitro*. Furthermore, the pharmacodynamic analysis showed that indisulam caused Rbm39 degradation in tumour tissues, confirming the on-target effect of indisulam *in vivo*. Data from the survival analysis showed that the combination of indisulam and olaparib led to significantly better overall survival of mice bearing HR-proficient ID8 tumours than olaparib monotherapy, indicating that adding indisulam to olaparib maintenance therapy might potentially extend the PFS of HGSOC patients. Unfortunately, when indisulam was used at 15 mg/kg/day, it only showed a near additive effect with olaparib. Further studies are therefore needed to optimise the mixing ratio of indisulam and olaparib, which may achieve a strong anticancer effect.

An important observation is that the combination therapy perhaps inducing strong tumour inhibitory effect in ID8-*Trp53*$^{-/-}$ tumours in a small subset of mice. While complete tumour regression is rare with olaparib treatment, it has been reported multiple times with indisulam-

based therapies. In our recent publication, Nijhuis et al. (2022) showed that indisulam treatment at 25 mg/kg/day caused complete regression with a near 100% survival rate in two murine models of neuroblastoma. Another research group used two other murine neuroblastoma models and reported similar findings, with indisulam causing complete tumour regression in over 75% of mice (Singh et al., 2021). It is still unclear why some mice show complete responses while others reach the humane endpoints eventually. The underlying mechanism is particularly elusive for the ID8 models because it is not possible to track tumour progression across time and the tumour burden was only directly measurable during necropsy. Liao et al. (2015) reported an alternative version of the ID8 model tagged with non-immunogenic luciferase, enabling precise monitoring of tumour progression and metastasis upon drug treatment. The same approach should be applicable to the ID8-*Trp53*$^{-/-}$ model used in this study, and a non-immunogenic luciferase-tagged ID8 model would provide valuable insights into the pharmacodynamics of indisulam and olaparib.

Previous studies did not report any indisulam-associated toxicities in C57BL/6 mice (Ozawa et al., 2001, Han et al., 2017b, Nijhuis et al., 2022, Singh et al., 2021, Lu et al., 2021b). It is surprising to find that indisulam at 25 mg/kg/day was poorly tolerated in my studies. Lowering the dose of indisulam to 15 mg/kg/day improved tolerability, but some mice still reached the humane endpoint prematurely, leading to reduced survival benefits. One possible reason for this discrepancy is the different routes of administration. Administrating drugs via I.P. has similar kinetics in drug uptake as I.V (Kim et al., 2011, Fueger et al., 2006), but I.P. injections have a slower rate of drug clearance due to the peritoneal-plasma barrier (Brandl and Prabhu, 2020, Di and Kerns, 2016). The drug clearance rate is probably even lower in mice bearing ID8 tumours because tumour growth obstructs the lymphatic drainage system (Lisio et al., 2019, Sarfarazi et al., 2019). Accumulating drugs in the peritoneal cavity might have irritated the gastrointestinal system, leading to diarrhoea and rapid weight loss in mice. However, my observations suggest that I.V. delivery is not suitable for indisulam at high doses because the drug was not entirely soluble in the previously described formulation (Ozawa et al., 2001), and I.P. administration is a preferable option for drug suspensions. An alternative method to improve indisulam tolerability is by including drug holidays in the dosing schedule to avoid drug accumulation in mice. It has been reported that when administrated following the schedule of 5 days on & 2 days off, 25 mg/kg/day indisulam is well tolerated in mice without

causing haematological toxicities and significant animal weight loss (Wang et al., 2019, Singh et al., 2021). This dosing scheme is worth evaluating in future studies, and it may improve the survival benefits of the combination therapy (indisulam plus olaparib) by preventing mice from reaching the humane endpoint early. It is worth noting that olaparib is well tolerated in mice, and there has been no evidence suggesting its combination with indisulam causes additive toxicity.

The epithelial origin is a limitation of the ID8 model since many HGSOCs originate from the fallopian tube (Roby et al., 2000, Walton et al., 2016). Thus, future studies are necessary to evaluate the combination therapy of indisulam and olaparib in other HGSOC models, such as genetically engineered mouse models (Maniati et al., 2020) or patient-derived ovarian cancer models (Coulson-Gilmer et al., 2021). Nevertheless, the origin of ID8 does not preclude its value in HGSOC research because it faithfully replicates the peritoneal metastasis of HGSOC in patients and expresses several HGSOC markers (Walton et al., 2016). In addition, ID8 model is particularly valuable for approximately 5% of HGSOC patients with tumours originating from the ovarian surface epithelial cells (Lawrenson et al., 2019).

In summary, evidence from this chapter demonstrates that indisulam treatment significantly improves olaparib response in HR-proficient HGSOC tumours. Although indisulam only showed a near-additive effect with olaparib, further optimisation in the dosing schedule probably will improve the drug combination efficacy by reducing indisulam-related toxicities.

Chapter 5

Chapter 5. Investigating the synergy mechanisms between indisulam and olaparib

5.1. The combination of indisulam and olaparib leads to DNA damage accumulation

5.1.1. Indisulam partially inhibits olaparib-induced activation of ATM-Chk2 signalling

Cancer cells depend on cancer-specific intracellular signalling networks for survival. Understanding the changes in signalling pathways could provide valuable insights into the synergy between indisulam and olaparib in HGSOC cells. To this end, human phospho-kinase arrays were used to screen the phosphorylation levels of 43 kinases in KURAMOCHI cells after a 48-hour exposure of indisulam (10 μM) or olaparib (30 μM) as monotherapies or in combination (Figure 5.1). Densitometry analysis revealed differential phosphorylation in at least six kinases, including c-Jun (S63), Src (Y419), Chk2 (T68), PYK2 (Y402), PLC-γ1 (Y783), and MSK1/2 (S376/S370) (Figure 5.1). Among these kinases, Chk2 is an outstanding target because of its involvement in the DNA damage response and was thus selected for western blot validation in this project. The other five kinases are also interesting for future analysis (annotated in Appendix Table 1).

In response to DSBs, ATM activates Chk2 by phosphorylating on T68 (Ahn et al., 2000), and activated Chk2 coordinates DSB repair response by activating HR repair and cell cycle arrest at G1/S and G2/M phases (Matsuoka et al., 1998, Falck et al., 2001, Alkema et al., 2014, Matsuoka et al., 2000, Zannini et al., 2014). In contrast to the low levels of T68-phosphorylated Chk2 (pChk2-T68) in cells treated with vehicle control and indisulam, olaparib treatment caused a substantial increase in pChk2-T68, which is consistent with previous findings (Bryant and Helleday, 2006, YI et al., 2015) and indicates the activation of ATM-mediated DSB repair pathways (Figure 5.1). The combination of indisulam and olaparib also increased pChk2-T68, but to a lesser extent than olaparib monotherapy (Figure 5.1). Western blot analysis confirmed that indisulam did not affect the total levels of Chk2 in KURAMOCHI cells, but partially inhibited Chk2 phosphorylation in response to olaparib, suggesting reduced Chk2 activities (Figure 5.2A-C).

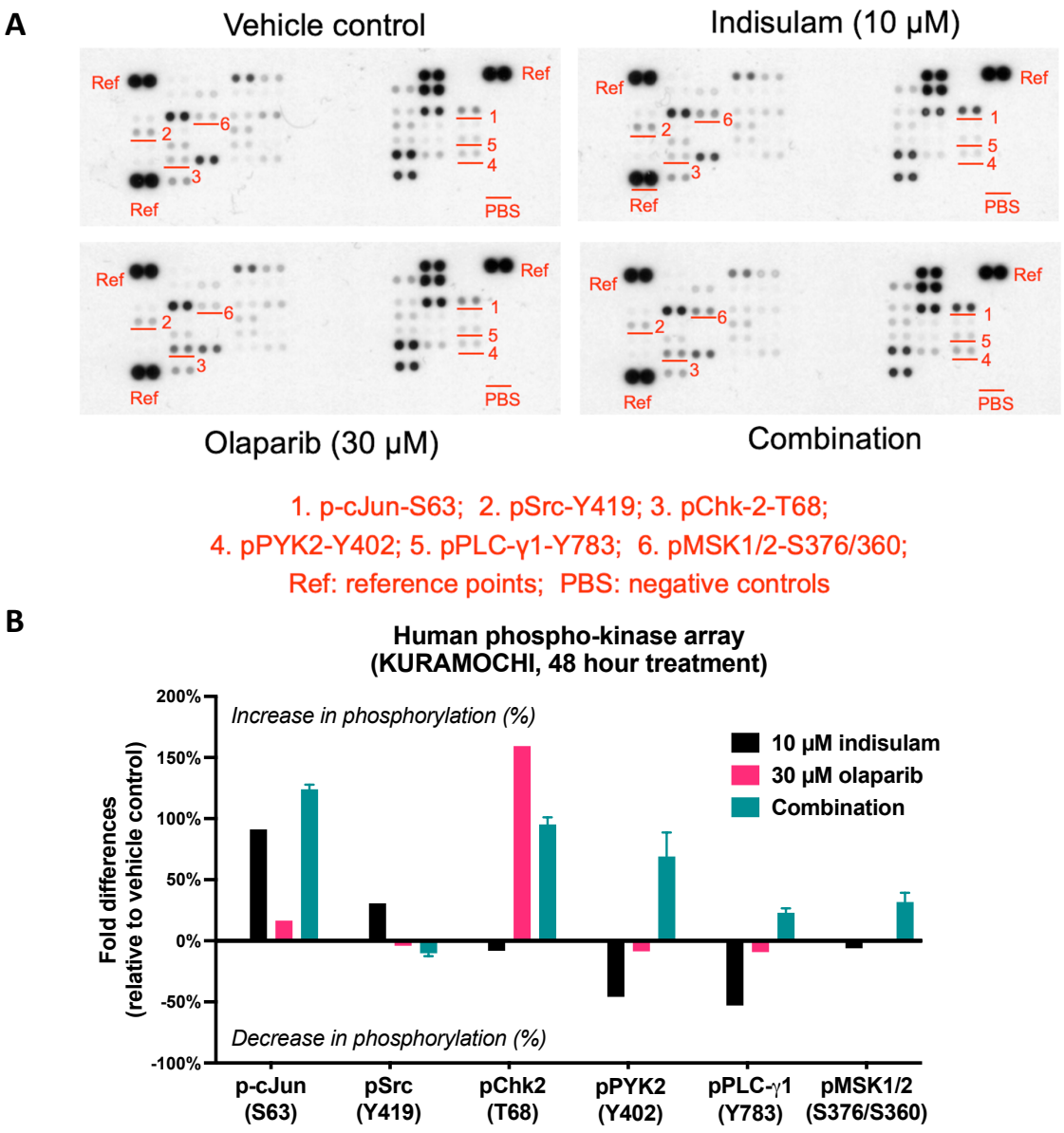


Figure 5.1. Indisulam reduces olaparib-induced Chk2 activation in HGSOC cells.
(A) KURAMOCHI cells were treated with vehicle control, 10 μM indisulam, 30 μM olaparib, or 10 μM indisulam in combination with 30 μM olaparib for 48 hours. Total proteins were extracted for analysis using human phospho-kinase arrays (n = 1). Each kinase has two technical replications (shown as two paired dots). The top six kinases differentially phosphorylated between monotherapies and combination therapies are underlined and annotated. **(B)** Dot intensities in (a) were quantified using image J. Mean differences in phosphorylation levels relative to vehicle control (baseline at 0%) were shown as bar charts (error bar = SD, n = 1 with duplicates). Positive values suggest higher phosphorylation levels than vehicle control, and negative values indicate less phosphorylation than vehicle control. Kinases were ranked from left to right based on descending order of raw densitometry intensities.

Chapter 5

ATM is the main kinase upstream of Chk2, and the lower pChk2-T68 expression indicates reduced ATM catalytic activity. Since earlier findings (Chapter 3) had shown that indisulam causes aberrant skipping in *ATM* and reduces the abundance of the canonical transcript, I hypothesised that indisulam-induced splicing errors might decrease protein expression of ATM or produce dominant negative isoforms of ATM, thereby leading to attenuated phosphorylation of downstream targets such as Chk2. As predicted, western blot analysis found that indisulam monotherapy and the combination therapy (indisulam and olaparib) significantly reduced total levels of ATM in KURAMOCHI cells, whilst olaparib monotherapy had a minor impact (Figure 5.2A and D). The reduced ATM expression is likely to be a result of indisulam-induced splicing errors, such as skipping of exon 52-53 (Figure 3.2), which would cause a 289bp deletion and frameshift. Autophosphorylation of ATM at the S1981 (pATM-S1981) is essential for ATM activation and is commonly used as a marker for its catalytic activities (So et al., 2009, Kozlov et al., 2006). I found that, like pChk2-T68, absolute pATM-S1981 (relative to β-actin) was increased with olaparib treatment but to a lesser extent in cells treated with the combination therapy (Figure 5.2E), indicating that the indisulam-induced downregulation of total and phospho-ATM are plausible reasons for reduced Chk2 activation. Interestingly, while the absolute amount of pATM-S1981 decreases, the combination of indisulam and olaparib led to a higher pATM-S1981/total ATM ratio than olaparib alone (Figure 5.2F), implying a higher level of DSB and increased demand for ATM-mediated DNA damage repair response. An alternative explanation is that after 48-hour exposure to the combination therapy, KURAMOCHI cells with high levels of DNA damage had died due to apoptosis, and the remaining fraction of cells had not accumulated high levels of DNA damage, resulting in reduced activation of the ATM-Chk2 pathway. The amount of DNA damage in cells is thus assessed in the next section.

Overall, these findings suggest that indisulam suppresses olaparib-mediated activation of the ATM-Chk2 pathway in HGSOC cells by downregulating ATM expression. The addition of indisulam to olaparib may therefore reduce ATM-mediated DSB repair and increase DNA damage, leading to increased genotoxic stress and cell apoptosis.

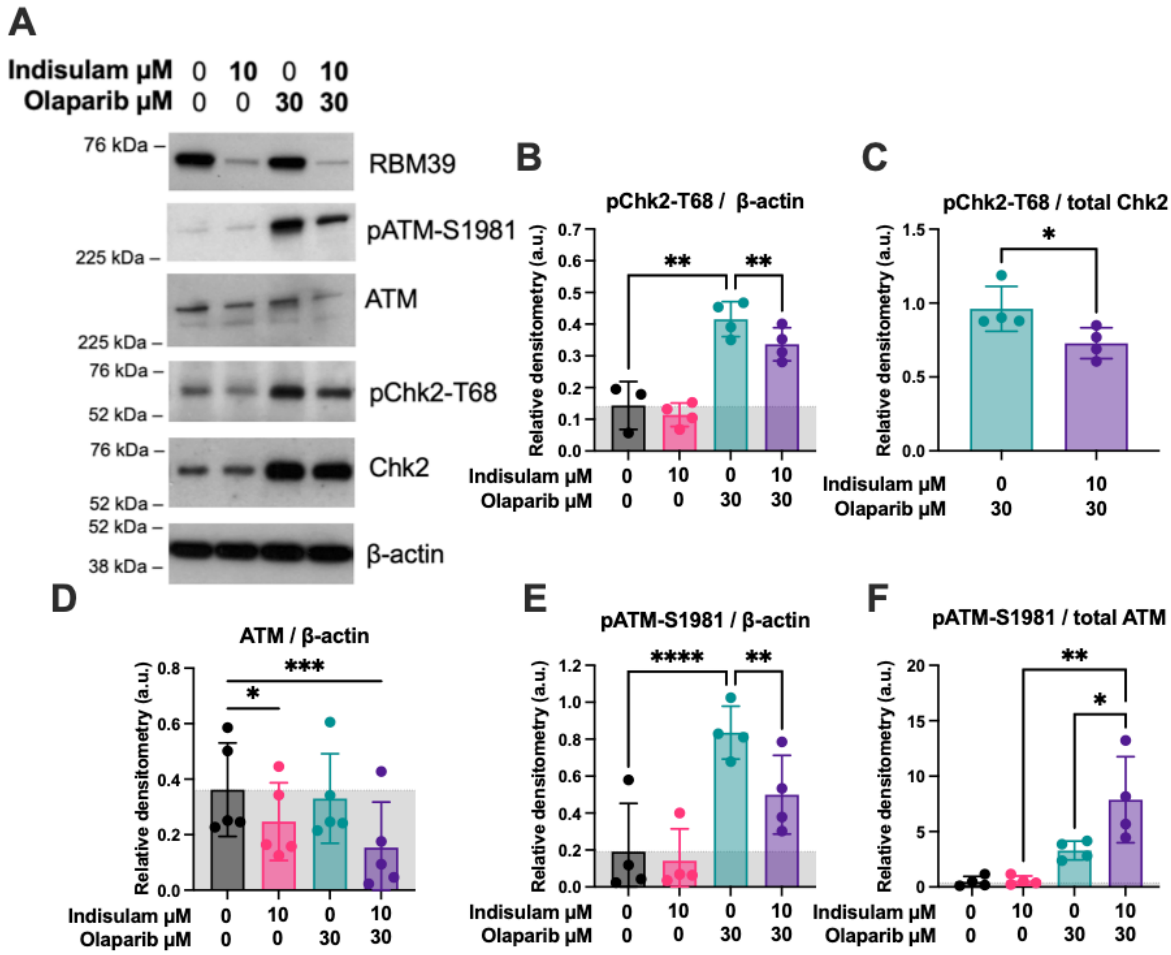


Figure 5.2. Indisulam downregulates ATM expression and partially inhibits activation of the ATM-Chk2 pathway.

(A) KURAMOCHI cells were treated with vehicle control, indisulam, olaparib, or the combination for 48 hours before western blot analysis. Representative blots from four biological replicates are shown here. **(B-C)** Densitometry quantification of pChk2-T68 bands intensities after normalisation to β-actin (b) or total Chk2 (c). Mixed-effect analysis (paired) and Tukey's multiple comparisons were used to determine statistical differences of pChk2-T68/β-actin among groups. A paired t-test was used to compare the statistical difference of pChk2-T68/total Chk2 between olaparib monotherapy and the combination therapy. **(D)** Densitometry analysis of ATM bands intensities relative to β-actin. **(E-F)** Densitometry analysis of pATM-S1981 bands intensities relative to β-actin (e) and total ATM (f). Mean values in arbitrary units (a.u.) from at least four independent repeats are shown (error bar = SD). Statistical differences among groups in (d-f) were calculated by paired one-way ANOVA and Tukey's multiple comparisons test (*p < 0.05, ** p < 0.01, *** p < 0.0001, **** p < 0.0001). Paired analysis was used to control for variations between western blot repeats.

5.1.2. Combination of indisulam and olaparib leads to a substantial increase in γH2AX levels

I next hypothesised that by reducing ATM expression, indisulam might disrupt ATM-mediated DNA damage repair response, leading to increased DNA damage and genotoxic stress. To test this hypothesis, I firstly investigated whether indisulam increases the γH2AX foci formation in PARP inhibitor-resistant HGSOC cell lines KURAMOCHI and OVSAHO. Although commonly used as a marker for DSBs, γH2AX does not necessarily indicate the presence of DSBs, because H2AX can be phosphorylated by ATM upon DSBs, and by ATR and DNA-PK at sites of stalled replication forks (Sedelnikova et al., 2002, Cleaver, 2011, de Feraudy et al., 2010, Sharma et al., 2012). Therefore, γH2AX is in fact an ambiguous marker for genotoxic stress. Immunofluorescence analysis showed that indisulam treatment caused a moderate but significant increase in proportions of γH2AX-positive cells (with at least five foci) in a dose- and time-dependent manner (Figure 5.3), suggesting that indisulam increases genotoxic stress in HGSOC cells.

I next investigated whether indisulam sensitises HGSOC cells to genotoxic stress induced by PARP inhibitors. In comparison with indisulam and olaparib individually, the combination of indisulam and olaparib led to significantly higher numbers of γH2AX foci per cell in KURAMOCHI cells, indicating increased levels of genotoxic stress (Figure 5.4A-B). Similar trends of changes were observed when indisulam was combined with rucaparib or veliparib (Figure 5.4C-D). In OVSAHO cells, the combination of indisulam and PARP inhibitor (olaparib, rucaparib, niraparib, or veliparib) also caused more γH2AX foci formation than monotherapies (Figure 5.4E-H). These findings indicate that a significant increase in genotoxic stress is commonly associated with the synergy between indisulam and PARP inhibitors in HGSOC cells.

I also assessed γH2AX expression in KURAMOCHI and OVSAHO cells using western blot. I found that the combination of indisulam and olaparib led to substantially higher levels of γH2AX than each drug individually (Figure 5.5). The more-than-additive increase in γH2AX could be explained by the presence of strong genotoxic stress or DNA fragmentation during cell apoptosis (Figure 3.4) (Lu et al., 2006, Rogakou et al., 2000). Different sources of γH2AX

can be distinguished in the future by measuring γH2AX expression in apoptotic and non-apoptotic cells using flow cytometry.

In summary, above findings suggest that indisulam exacerbates the genotoxic stress caused by PARP inhibitors.

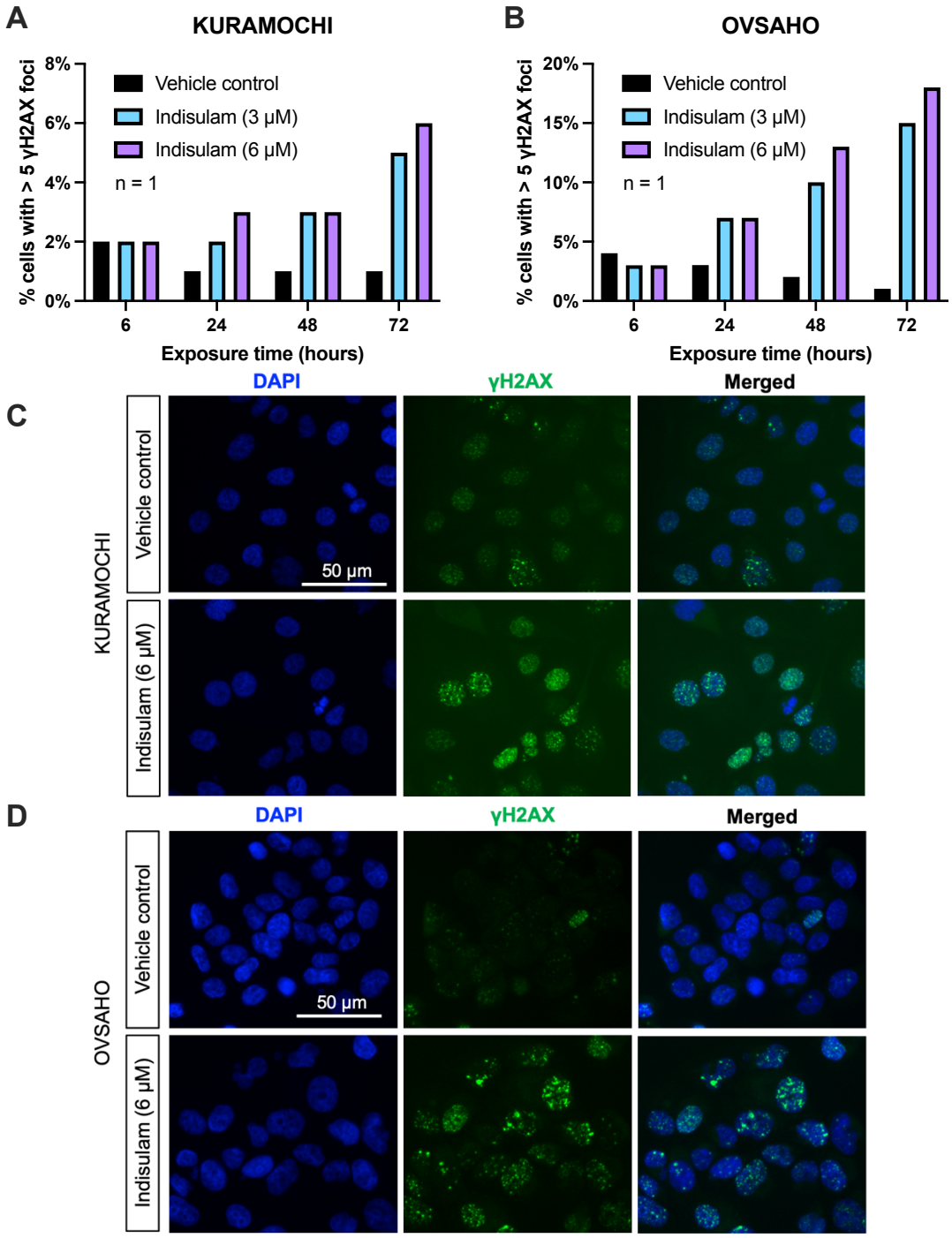


Figure 5.3. Indisulam leads to the accumulation of γH2AX foci in HGSOC cells.
KURAMOCHI or OVSAHO cells were treated with vehicle control or indisulam (3 μM or 6 μM) for 6 to 72 hours before fixation. Fixed cells were immunofluorescence-stained with anti-γH2AX antibody and the foci numbers of γH2AX were counted. **(A)** Bar chart showing proportions of KURAMOCHI cells with more than five γH2AX foci (n = 1). **(B)** Bar chart showing proportions of OVSAHO cells with more than five γH2AX foci (n = 1). **(C-D)** Representative images showing DAPI and γH2AX staining of KURAMOCHI (c) and OVSAHO (d) cells after 72 hours of vehicle or indisulam (6 μM) treatment. Images are at the same scale (scale bar = 50 μm). Similar trends of changes were observed in indisulam-treated cells in Figure 5.4. The reason why data in (a-b) were shown as bar charts, instead of foci per cells in box plots

like in Figure 5.4, was because the majority of cells had no γH2AX foci and the box plots were compressed to the x-axis and were not visible.

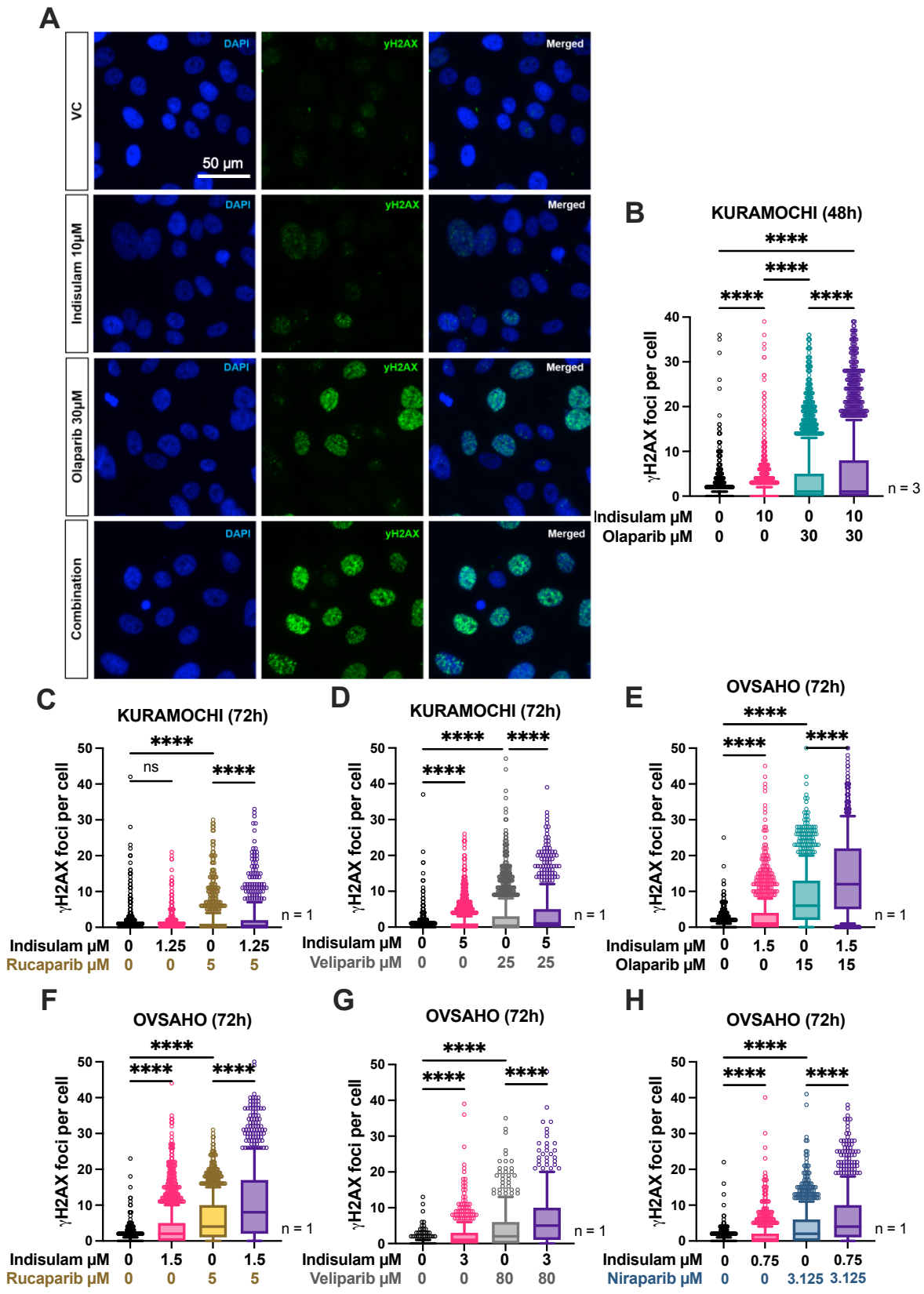


Figure 5.4. The combination of Indisulam and PARP inhibitors leads to increased γH2AX foci formation in HGSOC cells.

(A) KURAMOCHI cells were treated with indisulam (10 µM) and olaparib (30 µM) as monotherapies or in combination for 48 hours before immunostaining γH2AX. Stained cells were imaged and representative images from three biological repeats are shown here. Images are at the same scale (scale bar = 50 µm). **(B)** Box plots (whiskers indicating 10-90 percentiles) showing numbers of γH2AX foci per cell with pooled data from three biological repeats. Data in (a-b) were collected by Dr Anke Nijhuis. **(C-D)** KURAMOCHI cells were treated with indisulam in combination with either rucaparib (c) or veliparib (d) for 72 hours before γH2AX foci counting. **(E-H)** OVSAHO cells were treated with indicated combinations of indisulam and PARP inhibitor(s) for 72 hours before γH2AX foci counting. Data in (c-f) are shown in box plots with whiskers indicating 10-90 percentiles (n = 1 with duplicating replicates). Similar trends of changes were observed in the other two doses of drug combinations. Since data are heavily skewed, the (non-parametric) Kruskal-Wallis test and Dunn's multiple comparisons test were used for statistical tests among groups (****p < 0.0001).

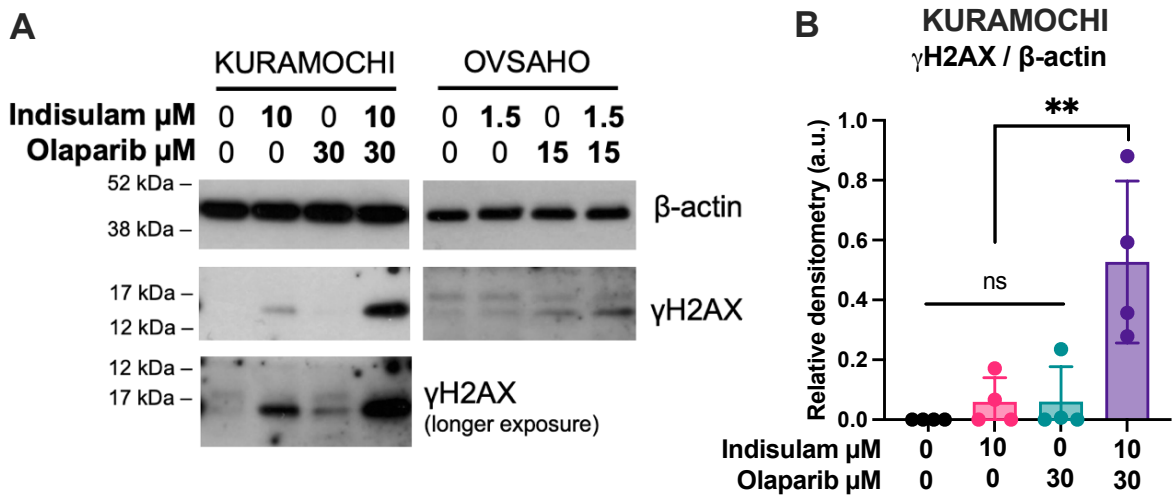


Figure 5.5. The combination of indisulam and olaparib increases γH2AX expression.
(A) KURAMOCHI (n = 4) or OVSAHO (n = 1) cells were treated with indisulam and olaparib either individually or in combination for 48 hours before western blot analysis. β-actin was used as a loading control. **(B)** Densitometry analysis of γH2AX bands intensities relative to β-actin (a.u. arbitrary unit). Ordinary one-way ANOVA and Tukey's multiple comparisons test were used to determine statistical differences among groups (ns, not significant; ** p < 0.01).

5.1.3. Indisulam may exacerbate DNA damaging effect of olaparib

To investigate whether the increase in genotoxic stress involves the accumulation of DNA damage, I quantified DNA strand breaks directly through the single-cell electrophoresis (also known as the COMET assay). To perform COMET assay, cells were immobilised in a thin layer of low-melting point agarose on microscopic slides before being lysed to remove cellular proteins and the nuclear membrane (Figure 5.6A). This was followed by an unwinding step to separate the linked DNA strands. Because intact DNA retains supercoiled loop structures, it has limited mobility under electric fields (Klaude et al., 1996, Afanas'eva et al., 2009). In contrast, DNA strand breaks relax the local torsional stress and generate linear DNA fragments, leading to higher mobility during electrophoresis (Klaude et al., 1996, Afanas'eva et al., 2009). After staining with DNA dyes, nucleoids with DNA damage would shape like a comet with a head and tail (Figure 5.6B). The 'comet head' contains intact DNA in the nucleoli, whilst the 'comet tail' contains the damaged DNA (Figure 5.6B). The length and intensity of the tail positively correlate to the extent of DNA damage and can be quantified as tail moments, calculated as the proportion of tail DNA multiplied by the tail length (Olive and Banáth, 2006, Lu et al., 2017, Au - Nowsheen et al., 2012) (Figure 5.6B).

The COMET assay can be performed under either neutral or alkaline (pH > 13) conditions, depending on which buffer was used for DNA unwinding and electrophoresis. The neutral comet assay detects mostly DSBs (Olive et al., 1991, Olive and Banáth, 2006), whilst the alkaline comet assay detects most types of DNA lesions, including SSBs, DSBs, intermediates of DNA repair, and alkaline-labile sites (apurinic or apyrimidinic sites that are prone to break) (Collins, 2004). I attempted to validate both types of comet assays in HGSOC cells using the genotoxic agent doxorubicin as a positive control, following protocols published by Lu et al. (2017). After overcoming several technical challenges, the alkaline comet assay was successfully optimised for KURAMOCHI cells, evidenced by the observation that doxorubicin induced a dose-dependent increase of tail moment (Figure 5.6C-D). Unfortunately, the neutral comet assay was not fully optimised despite multiple attempts. It failed to detect DNA damage caused by doxorubicin, and a high tail moment was observed in untreated cells (Figure 5.6E). Due to the time limitation, I was not able to test other DSB-inducing agents and optimise the neutral comet assay further. Therefore, only the alkaline comet assay was used to quantify DNA damage levels in HGSOC cells.

Chapter 5

To investigate whether the addition of indisulam increases olaparib-mediated DNA damage, KURAMOCHI cells were treated with indisulam and olaparib individually or in combination for 24 to 72 hours. Data from the alkaline comet assay revealed that at 24 hours, the tail moment was significantly increased in cells treated with olaparib (30 µM), but not indisulam (10 µM) (Figure 5.7). Notably, the addition of indisulam to olaparib significantly increased tail moments when compared with olaparib alone, suggesting higher levels of DNA damage (Figure 5.7). Similar trends were observed at 48 and 72 hours, but the effects were not as strong as 24 hours (Figure 5.7B). Only one biological repeat was conducted due to the time limit, and future replications would be necessary to ascertain the findings.

Overall, above data indicate that the combination of indisulam and olaparib causes more DNA damage than individual treatment.

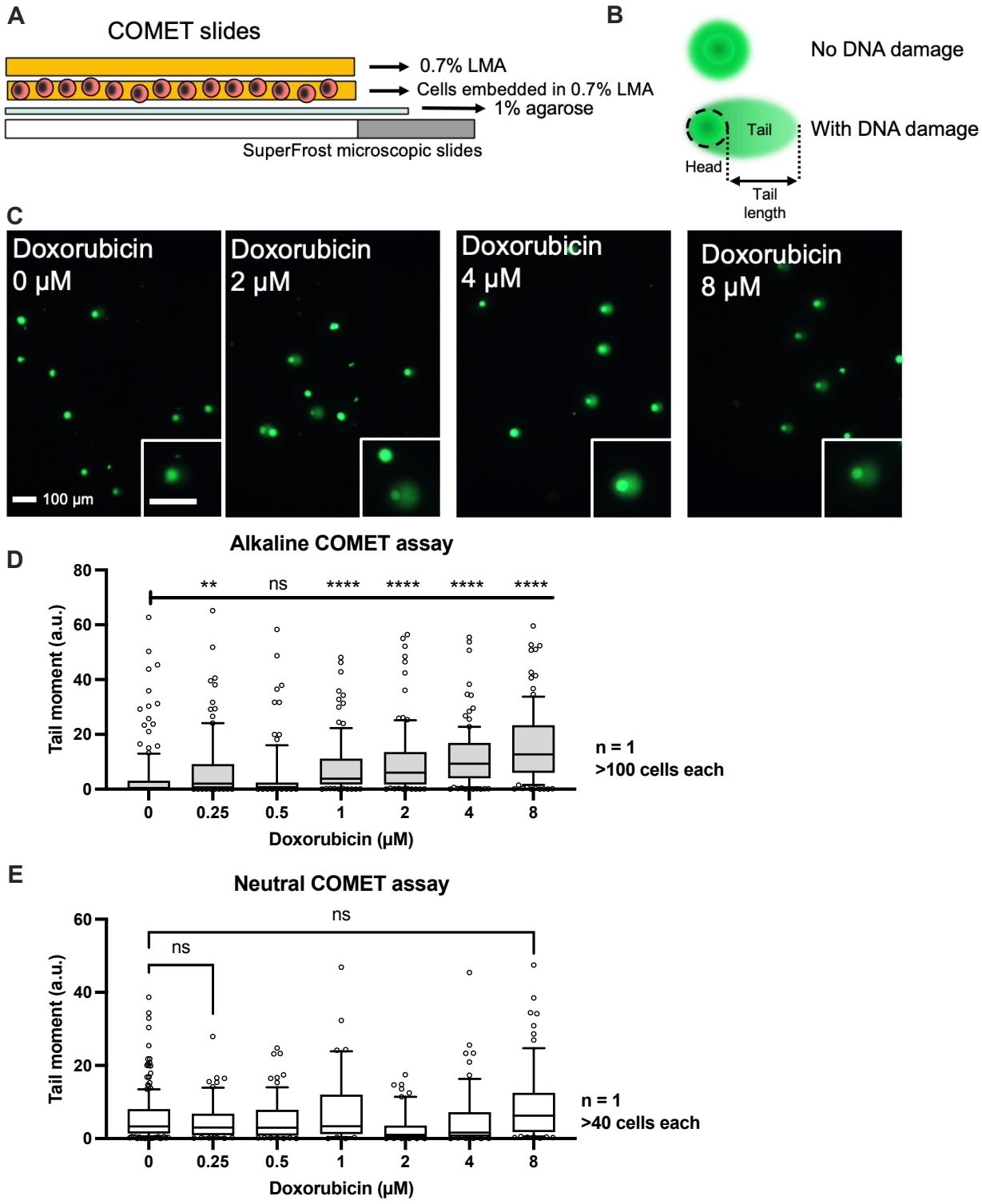


Figure 5.6. Alkaline COMET assay successfully detects doxorubicin-induced DNA damage.
(A) Schematic showing the comet slides containing cells immobilised in 0.7% low-melting point agarose (LMA). **(B)** Schematic showing two examples of nucleoli after comet assay. The shape of nucleoids with little to no DNA damage would stay round. On the other hand, nucleoids with DNA damage would shape like a comet with tails containing damaged DNA. The extent of DNA damage is quantified by calculating the tail moment = % tail DNA * tail length. **(C)** KURAMOCHI cells were treated with increasing doses of doxorubicin for 24 hours before alkaline comet assay. Representative images are shown here with a zoomed view at the bottom right (scale bar = 100 µm). **(D)** Box plots (whiskers indicating the 10^{th} – 90^{th} percentiles) showing quantification of the alkaline comet tail moments of

KURAMOCHI cells after doxorubicin treatment (a.u. arbitrary unit). More than 100 cells were analysed (n = 1). **(E)** KURAMOCHI cells were treated with doxorubicin for 24 hours and analysed with the neutral comet assay. The tail moment from at least 40 cells was quantified and shown as box plots with the 10th – 90th percentiles (n = 1). Kruskal-Wallis test and Dunn's multiple comparisons test were used for statistical analysis (ns, not significant; **p < 0.01; **** p < 0.0001).

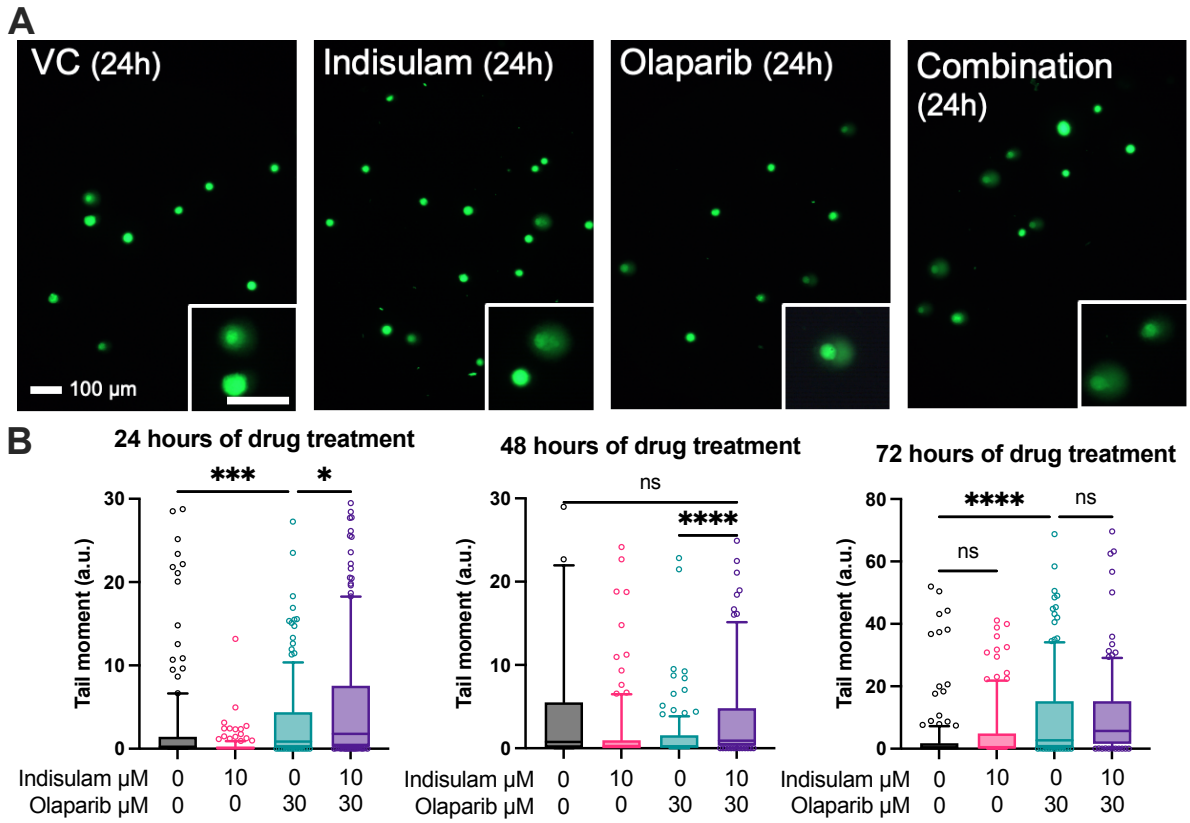


Figure 5.7. Indisulam increases olaparib-induced DNA damage in KURAMOCHI cells.
(A) KURAMOCHI cells were treated with vehicle control (VC), 10 µM indisulam, 30 µM olaparib, or the combination of indisulam and olaparib for 24 hours, followed by the alkaline comet analysis. Representative images are shown here with zoomed views at the bottom right (scale bar = 100 µm). **(B)** Box plot (whiskers indicate the 10th – 90th percentiles) showing tail moments of KURAMOCHI cells after treatment with indicated drugs for 24 to 72 hours. Tail moment (in an arbitrary unit, a.u.) was calculated as % tail DNA multiplied by tail length. At least 130 cells from technical duplicates were analysed (n = 1). Statistical differences were calculated by the Kruskal-Wallis test and Dunn's multiple comparisons test (ns, not significant; *p < 0.05; ***p < 0.001; **** < 0.0001).

Chapter 5

5.2. The combination of Indisulam and olaparib causes cell cycle arrest

Both indisulam (Xu et al., 2020b, Singh et al., 2021) and olaparib (Lloyd et al., 2020, Riches et al., 2020, Sahin et al., 2019) have been implicated in modulating cell cycle progression. This motivated me to investigate the impact of the combination therapy on cell cycle progression using flow cytometry. A dual-labelling technique was applied to distinguish the S phase cells from G1 and G2/M phases by labelling replicating cells with nucleotide analogues (BrdU or IdU). In comparison with the vehicle control, the proportion of KURAMOCHI cells in the S phase and the G2/M phases were significantly increased in cells treated with indisulam and olaparib individually and in combination (Figure 5.8A-B). In addition, the combination of indisulam and olaparib caused higher proportions cells at S phase (mean = 53.8%, $p < 0.01$) than individual treatment of indisulam (mean = 38.5%) or olaparib (mean = 42.9%) (Figure 5.8A-B). Quantification of cells at early, middle, or late stages of the S phase showed that while indisulam did not change the S phase cell distribution, olaparib predominantly arrested cells at late-S (Figure 5.8A, C and D), which might be a result of Chk2-mediated activation of cell cycle checkpoints (Figure 5.2). Interestingly, the addition of indisulam to olaparib caused S phase arrest at earlier stages (mid-S) than olaparib individually, which may imply activation of the intra-S checkpoint (Figure 5.8A, C and D). This is compatible with the hypothesis that indisulam sensitises cells to olaparib by accelerating accumulation of genotoxic stress, thereby activating of cell cycle checkpoints at earlier stages.

Another interesting finding was that the combination treatment consistently reduced DNA replication activities in KURAMOCHI cells, as shown by decreased levels of BrdU/IdU incorporation (Figure 5.8A and E). A similar reduction BrdU/IdU labelling was also observed in cells treated with indisulam or olaparib, albeit to a lesser extent (Figure 5.8A and E).

Overall, these data suggest that the combination of indisulam and olaparib causes cell cycle arrest to a greater level than monotherapies, particularly at the S phase.

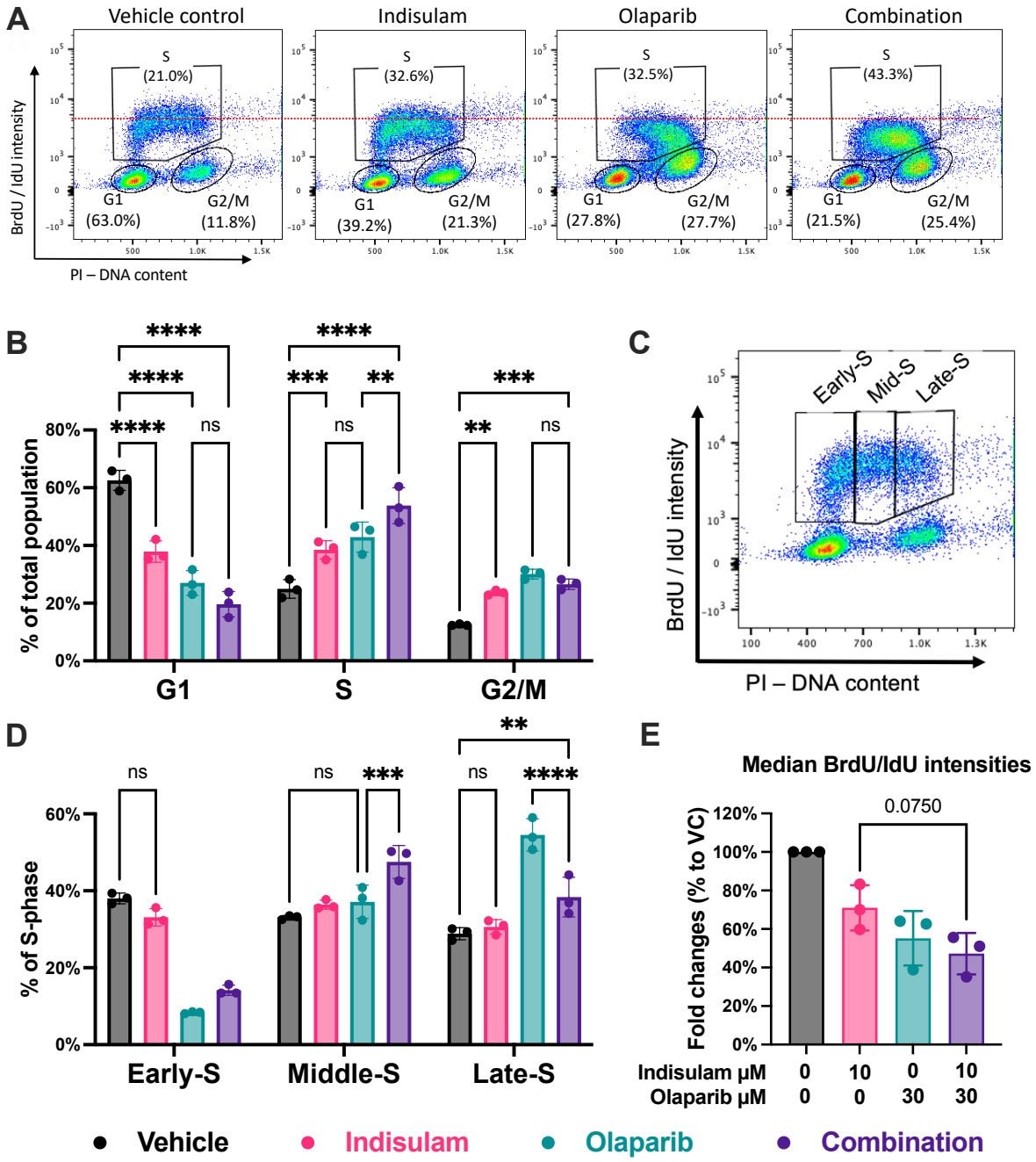


Figure 5.8. The combination of indisulam and olaparib causes cell cycle arrest at the S and G2/M phases.

Asynchronous KURAMOCHI cells were treated with vehicle control, 10 μM indisulam, 30 μM olaparib, or 10 μM indisulam in combination with 30 μM olaparib for 48 hours. During the final hour of drug treatment, cells in S phase were labelled with BrdU or IdU for 60 minutes. After fixation and staining for BrdU/IdU, cells were also stained with propidium iodide (PI) to quantify the DNA content. **(A)** Representative flow cytometry data from three biological repeats are shown here. The same gating was used for all samples. The dotted line in red indicates median BrdU/IdU intensities in cells treated with the vehicle control. **(B)** Bar chart showing mean proportions of cells in each phase of the cell cycle (error bar = SD). **(C-D)** Proportions of cells at early, middle, or late stages of S phases (relative to S phase) were quantified and shown as mean with SD. **(E)** Bar chart showing the median BrdU/IdU intensities of KURAMOCHI cells relative to vehicle control (error bar = SD). Ordinary one-way ANOVA

and Šídák's multiple comparisons test were used for statistical analysis (p-value is shown). Although no significant differences were found, the combination of indisulam and olaparib consistently showed lower levels of BrdU/IdU incorporation than monotherapies. Two-way ANOVA and Tukey's multiple comparisons test were used for statistical analysis in (b) and (d). ns, not significant; *p < 0.05; **p < 0.01; ***p < 0.001; ****p < 0.0001.

5.3. The combination of Indisulam and olaparib causes replication stress

5.3.1. Indisulam and olaparib cause replication fork abnormalities when used in combination

Unrepaired DNA damage directly impedes DNA replication, leading to stalled replication forks that may collapse if not restarted. Many DNA repair proteins, including PARP1, HR repair factors, and NHEJ repair proteins, are involved in removing DNA lesions and restarting stalled replication forks (Zhang et al., 2021b, Gaillard et al., 2015, Maya-Mendoza et al., 2018, Hanzlikova et al., 2018). Replication fork abnormalities could be consequences of DNA damage as well as sources of DSB. The collapse of replication forks is considered a major source of DSB caused by PARP inhibitors, and the stabilisation of replication fork contributes to PARP inhibitor resistance (Rondinelli et al., 2017, Ray Chaudhuri et al., 2016). I hypothesised that the synergy between indisulam and olaparib might also involve replication stress, because earlier findings had shown that the combination therapy causes DNA damage accumulation.

To investigate whether the synergy between indisulam and olaparib involves DNA replication stress, I studied the dynamics of replication fork progression using the DNA fibre analysis (also known as the DNA combing assay). Briefly, KURAMOCHI cells were treated with indisulam, olaparib, or indisulam in combination with olaparib for 48 hours, and in the final hour of drug treatment, cells were pulse labelled (30 minutes each) sequentially with two distinct nucleotide analogues, BrdU and IdU, in the presence of drug treatment (Figure 5.9A). In replicating cells, the synthesis of DNA incorporates BrdU or IdU into the newly synthesised strands. The length of BrdU and IdU labelling indicates the replication fork activities. After immunostaining, three main types of DNA fibres structures could be found: progressing forks (BrdU followed by IdU), new origin fired during the BrdU labelling (BrdU fibre flanked by two IdU fibre), and new origin fired during the IdU labelling phase (IdU fibres only) (Figure 5.9A).

After multiple rounds of troubleshooting, I successfully optimised the DNA fibre analysis for HGSOC cells based on protocols in previous studies (Pillay et al., 2019, Cong et al., 2021). The data (n = 1) showed that in KURAMOCHI cells treated with vehicle control, most DNA fibres were progressing forks (84.14%), and the proportions of new origin firing during BrdU or IdU labelling phases were similar (7.57% - 8.81%) (Figure 5.9B). A similar profile of DNA fibres was observed in cells treated with indisulam (Figure 5.9B). In KURAMOCHI cells treated with olaparib, the proportion of progressing forks (79.36%) was comparable with vehicle control- and indisulam-treated cells, but a lower proportion of new origins were fired during the BrdU labelling (4.83%) than the IdU labelling phase (15.82%) (Figure 5.9B). A more profound change was observed in cells treated with indisulam and olaparib simultaneously, with the fraction of progressing forks reduced to 61.59% (Figure 5.9B). It also caused a dramatic increase in the proportion of new origins fired during the IdU labelling phase (35.33%) (Figure 5.9B). Despite the puzzling imbalance between new origins fired in BrdU and IdU labelling, the reduction of progressing forks in combination therapy-treated cells indicates replication abnormalities. The considerable increase in new origins could be a source of replication stress (Toledo et al., 2013, Toledo et al., 2017), but future studies are needed to assess this possibility.

To examine if the combination of indisulam and olaparib reduces replication fork progression, I quantified the IdU fibre length as an indicator for fork progression (n = 2). The BrdU fibres were not quantified because their staining was more fragmented, making it difficult to define the start and the end of BrdU fibres. It was found that indisulam or olaparib monotherapy had a minor impact on the formation of IdU fibres (Figure 5.9C-D). In contrast, combining indisulam and olaparib significantly reduced the length of IdU fibres (Figure 5.9C-D), indicating replication fork arrest or delayed restart of stalled replication forks.

Taken together, indisulam and olaparib shows a clear trend of more-than-additive interaction in causing replication abnormalities in HGSOC cells, evidenced by excess new origin firing and reduced fork progression. However, future replication is needed to ascertain if the observed trends are reproducible.

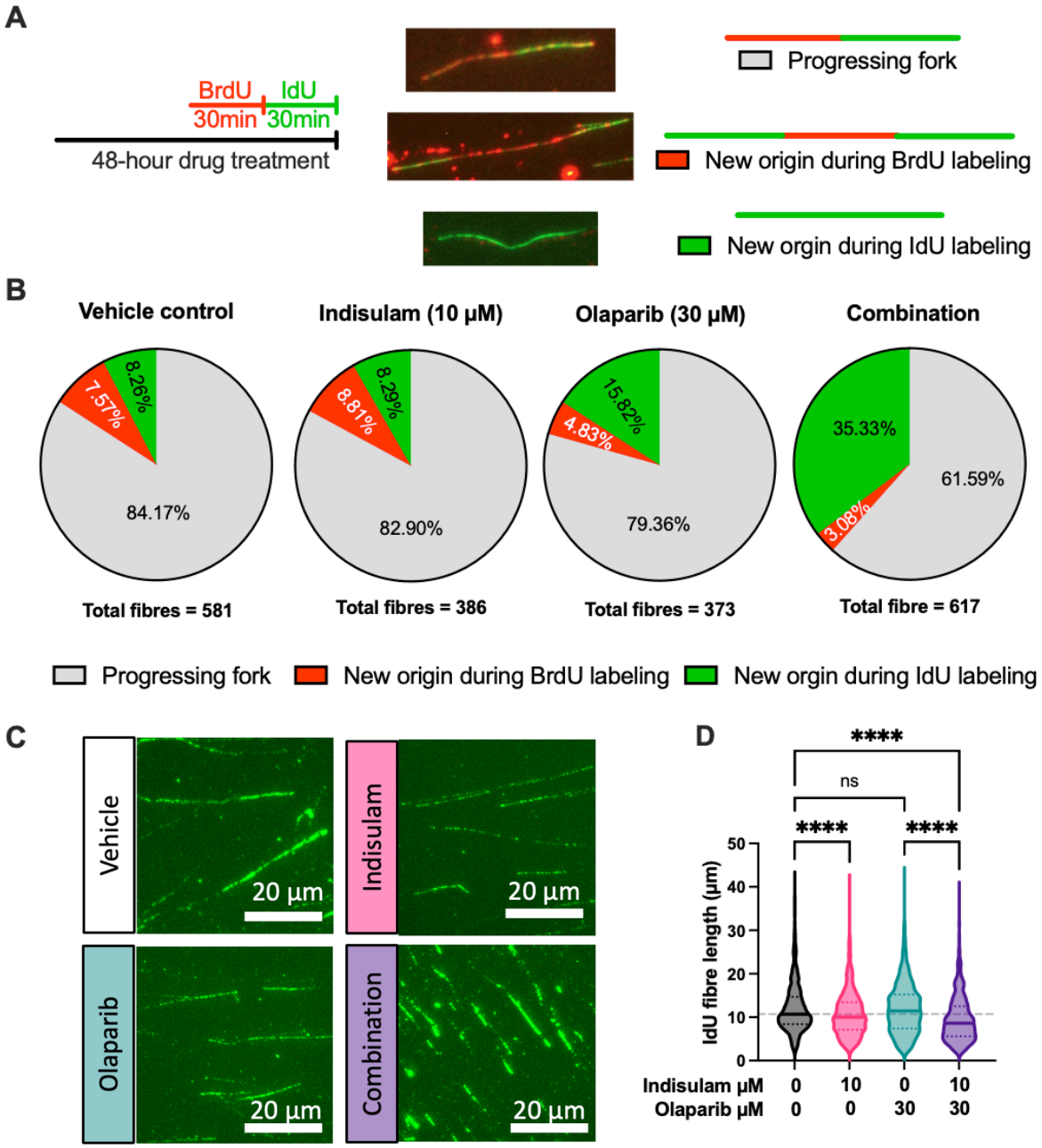


Figure 5.9. The addition of indisulam to olaparib causes replication abnormalities.
KURAMOCHI cells were treated with 10 µM indisulam and 30 µM of olaparib individually or in combination for 48 hours. In the final hour of drug treatment, cells were pulse-labelled with BrdU for 30 minutes, followed by IdU labelling for another 30 minutes. DNA fibre analysis was used to visualise DNA replication fork dynamics. **(A)** Schematic of the experimental design and representative images of progressing forks and new origins fired during pulse labelling. BrdU staining is in red and IdU staining is in green. The diagrams were inspired by Quinet et al. (2017). **(B)** Distribution of three main types of fibres (n = 1). **(C)** Representative images of IdU-labelled DNA fibres from two biological repeats. Scale bar = 20 µm. Cells were pulse labelled with both BrdU and IdU, but only IdU staining is shown here. **(D)** IdU fibre lengths were measured and shown as violin plots. At least 700 fibres from two biological repeats were quantified. Kruskal-Wallis test and Dunn's multiple comparisons test were used for statistical analysis (ns = not significant; ****p < 0.0001).

5.3.2. The combination of indisulam and olaparib downregulates Chk1 expression

ATR is the primary sensor for replication fork abnormalities, which activates Chk1 by phosphorylation at S317 and S345 (Liu et al., 2000, Zhao and Piwnica-Worms, 2001). In the presence of stalled replication forks, activated Chk1 protects and restarts the stalled forks, and inhibits unscheduled firing of dormant replication origins (Ge and Blow, 2010, Toledo et al., 2013, Petermann et al., 2010). I hypothesised that the combination of indisulam and olaparib might negatively impact Chk1 signalling, leading to unscheduled firing of replication origins.

To investigate this hypothesis, I quantified the level of total Chk1 and activated Chk1 (pChk1-S345) in KURAMOCHI cells treated with indisulam (10 μM) and olaparib (30 μM) individually or in combination for 48 hours. Western blot analysis showed that concurrent treatment of indisulam and olaparib led to a significant reduction of total Chk1, which was not seen when indisulam or olaparib was used individually (Figure 5.10A-B). The reduction in total Chk1 was associated with a proportional decrease in pChk1-S345 expression (relative to β-actin) when compared to olaparib monotherapy (Figure 5.10C); thus, the pChk1-S345/total Chk1 ratio was comparable (Figure 5.10D).

Overall, these findings support a hypothesis that concomitant exposure of indisulam and olaparib downregulates Chk1 expression, which may lead to defective replication response and render cells susceptible to replication fork abnormalities and unscheduled firing of dormant replication origins.

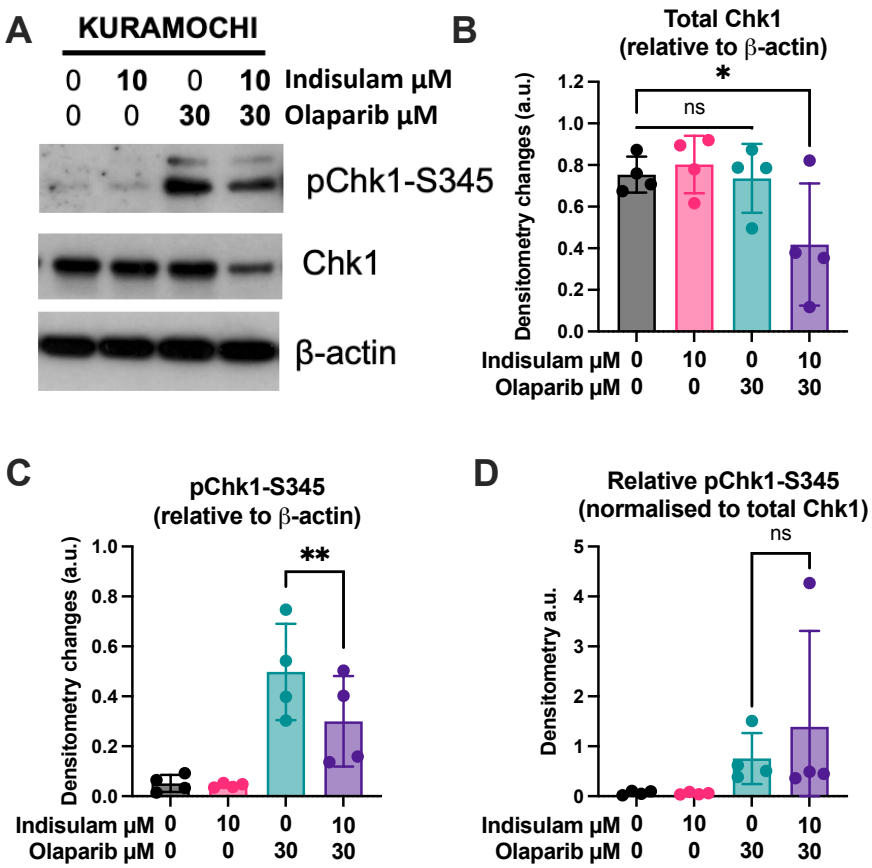


Figure 5.10. The combination of indisulam and olaparib downregulates Chk1 in HGSOC cells.
(A) KURAMOCHI cells were treated with indicated doses of indisulam and olaparib either as monotherapies or in combination for 48 hours before western blot analysis. Representative blots from four biological repeats are shown here. β-actin was used as a loading control. **(B-D)** Densitometry intensities of total Chk1 and pChk1-S354 bands were quantified and shown as total Chk1/β-actin (b), pChk1-S345/β-actin (c), and pChk1-S345/total Chk1 (d). Error bar = SD. Row-matched one-way ANOVA and Tukey's multiple comparisons test were used to calculate the statistical difference in (b). Statistical calculations in (c-d) were performed using the paired one-way ANOVA and Šídák's multiple comparisons test (ns, not significant; *p < 0.05; **p < 0.01).

Chapter 5

5.4. The combination of indisulam and olaparib increases γH2AX and downregulates ATM *in vivo*

In vitro data so far have associated the synergy between indisulam and olaparib with an accumulation of γH2AX and downregulation of ATM and Chk1 at protein levels. This motivated me to investigate if these changes could be detected in ID8 tumours from the pilot *in vivo* study (Figure 4.4). In this study, mice were injected with the ID8-*Trp53*$^{-/-}$ cells and treated with combinations of indisulam and olaparib at various dose combinations daily for five to seven days (Figure 4.4). Western blot analysis showed that the combination therapy caused a significant increase of γH2AX in ID8 tumours in a dose-dependent manner (Figure 5.11A-B). A reduction in Atm protein was also observed, and the 1.56 mg/kg/day indisulam was sufficient to downregulate Atm (Figure 5.9A and C). Variable levels of Chk1 expression were detected across tumours, and the changes did not follow a specific pattern (Figure 5.9A).

In summary, these data provide evidence that the combination therapy of indisulam and olaparib causes genotoxic stress *in vivo*, consistent with findings *in vitro*. However, due to a lack of mice treated with indisulam and olaparib individually, it is still unclear how strong was the drug-drug interaction. Future pharmacodynamic studies would be necessary to better characterise the interaction between indisulam and olaparib *in vivo*. In addition, it is still unclear why ATM degradation was observed before Rbm39 degradation was noticeable in western blot (6.25 mg/kg/day indisulam was needed, Figure 4.4D). Examining the abundance of Atm and Rbm39 in tumour cells using immunohistochemistry, instead of total protein from tumour tissues using western blot, will provide further insights.

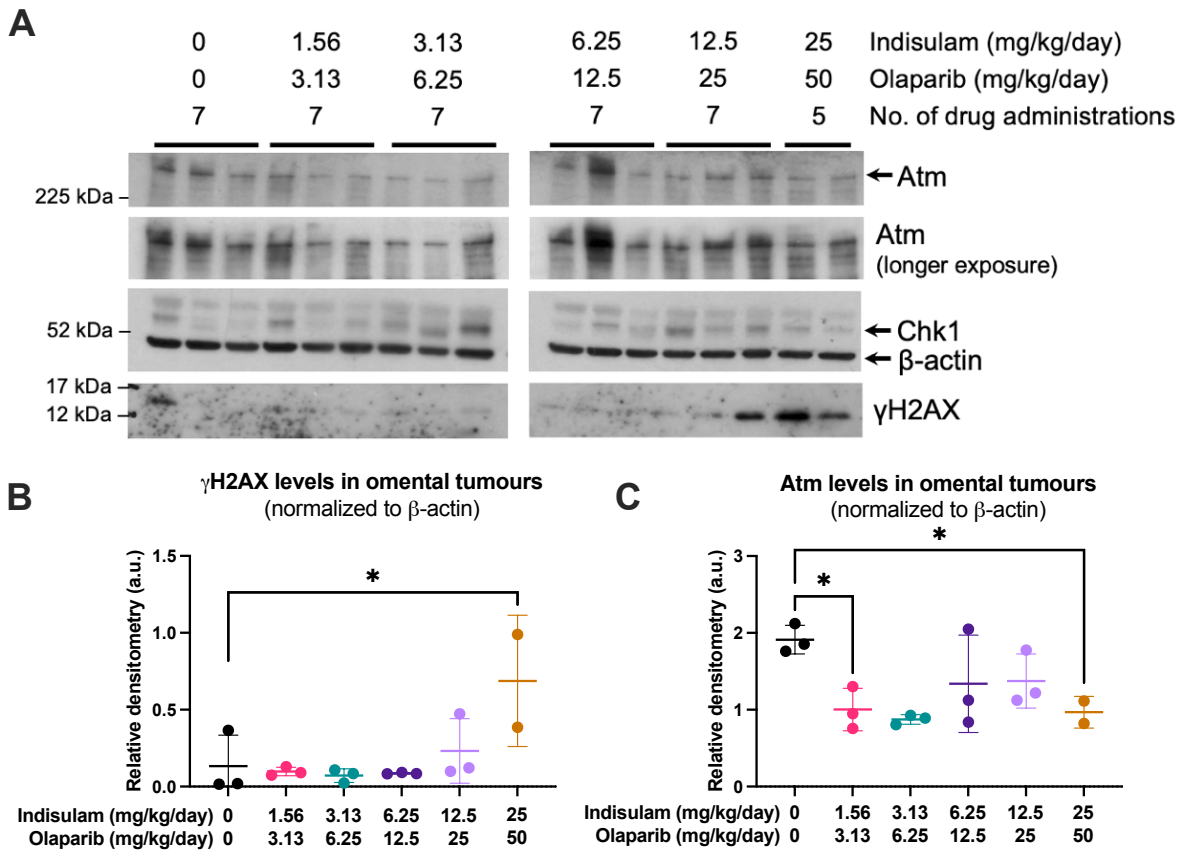


Figure 5.11. The combination of indisulam and olaparib increases γH2AX and reduces Atm expression in the ID8 murine HGSOC model.

(A) Omental tumour samples (ID8-*Trp53*$^{-/-}$ tumours) from the pilot study (Section 4.2.2) were used for western blot analysis. Protein levels of Atm, Chk1, and γH2AX were measured. β-actin was used as a loading control. **(B-C)** Densitometry quantification of γH2AX (b) and Atm (c) bands intensities relative to β-actin (error bar = SD). Ordinary one-way ANOVA with Dunnett's multiple comparisons test was used for statistical analysis (*$p < 0.05$).

Chapter 5

5.5. Discussion

5.5.1. Indisulam reduces PARP inhibitor resistance by exacerbating olaparib-induced genotoxic stress

Data from earlier chapters have shown that indisulam synergises with olaparib in multiple *in vitro* models of HGSOC (Chapter 3) and in the ID8 murine HGSOC model (Chapter 4). In addition, I have validated that indisulam depletes RBM39 in HGSOC cells and causes mis-splicing in a panel of DNA damage repair genes such as *ATM*, *TP53BP1*, *RIF1*, *BRCA1*, and *RAD51D*, suggesting a possibility that indisulam may improve PARP inhibitor response through disrupting splicing of DNA repair genes. In this chapter, I tested this hypothesis by assessing the impact of indisulam, olaparib, and their combination on cellular genotoxic stress from three perspectives: DNA damage response, cell cycle distribution, and DNA replication stress response. Findings from this Chapter suggest a model that indisulam exacerbates genotoxic stress caused by olaparib, thereby leading to synergistic induction of cell apoptosis (Figure 5.12).

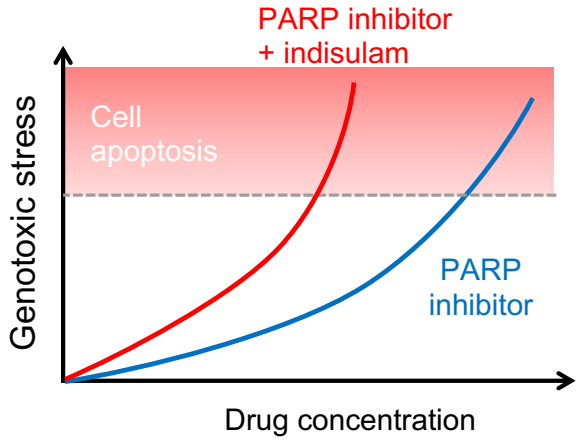


Figure 5.12. A simple model for the synergy between indisulam and PARP inhibitor(s).
Current findings suggest that indisulam exacerbates the genotoxic stress caused by PARP inhibitors such as olaparib, leading to higher levels of DNA damage and replication abnormalities, which may contribute to increased cell apoptosis and synergistic growth inhibition.

More specifically (Figure 5.13A), despite deleterious *BRCA2* mutation (Domcke et al., 2013) and being HRD (Tumiati et al., 2018), KURAMOCHI cells tolerated olaparib-induced DNA damage (Figure 5.4 and Figure 5.7) without causing substantial replication fork abnormalities (Figure 5.9) and cell apoptosis (Chapter 3). The survival of KURAMOCHI cells was associated with profound phosphorylation of ATM, Chk2, and Chk1, implying activation of the DNA damage response and the replication stress response. As summarised in Figure 5.13B, current evidence indicates that indisulam increases PARP inhibitor response in KURAMOCHI cells by downregulating ATM expression and suppressing olaparib-induced activation of the ATM-Chk2 pathway (Figure 5.2), leading to increased DNA damage (Figure 5.4 and Figure 5.7). Meanwhile, the combination of indisulam and olaparib downregulates Chk1 expression through an unknown mechanism, resulting in reduced Chk1 phosphorylation, increased DNA replication abnormalities (Figure 5.9 and Figure 5.10), and possible activation of the intra-S checkpoint (Figure 5.8). As a result, indisulam weakens the DNA damage response and the replication stress response, rendering KURAMOCHI cells susceptible to olaparib-induced genotoxic stress, eventually leading to increased genome instability and cell apoptosis (Chapter 3). While the cell cycle arrest caused by olaparib alone could be transient, the increase in genotoxic stress by the combination of indisulam and olaparib probably causes prolonged cell cycle arrest and reduces cell proliferation. Several mechanistic questions in this model have not been answered, such as the involvement of replication catastrophe, and the duration of cell cycle arrest. They are further discussed in section 5.5.5 (Limitations and Future work).

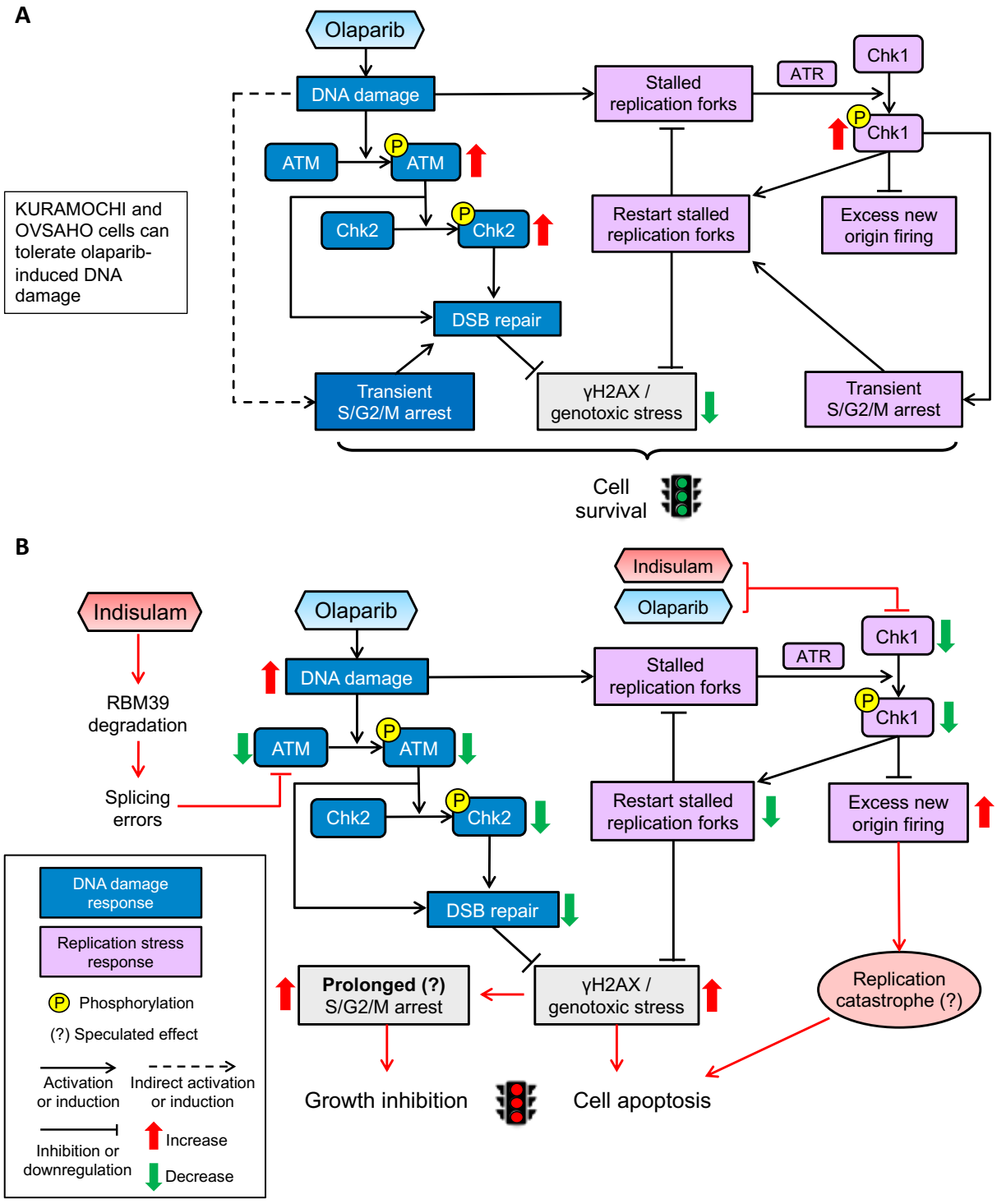


Figure 5.13. A detailed model showing indisulam increases PARP inhibitor response in HGSOC cells. **(A)** Despite loss of *BRCA2* expression, KURAMOCHI and OVSAHO cells can tolerate olaparib-induced DNA damage without substantial cell apoptosis (shown in Chapter 3). Data from this chapter demonstrate that, in KURAMOCHI cells, olaparib treatment activates ATM, Chk2, and Chk1, which coordinate DNA damage response and replication response, thus preventing cell apoptosis. The cell cycle arrest may be transient, allowing cells to resolve the genotoxic stress. **(B)** The addition of indisulam reduces protein expression of ATM through splicing errors and limits signalling activities of the ATM-Chk2 pathway in response to olaparib treatment. This leads to reduced DSB repair, increased genotoxic stress and cell apoptosis. Meanwhile, the combination of indisulam and olaparib downregulates Chk1 expression through an unknown mechanism, resulting in increased replication

fork abnormalities and unscheduled firing of replication origins – a potential source for genome instability and replication catastrophe (Toledo et al., 2013). The cell cycle arrest caused by the combination of indisulam and olaparib might be prolonged since cells may need more time to resolve the increased genotoxic stress, leading to a reduced proliferation rate. The legend in the bottom left corner applies to both (a) and (b).

5.5.2. Indisulam synergises with olaparib by downregulating ATM expression and increasing DNA damage

I found evidence that indisulam causes genotoxic stress in KURAMOCHI cells, demonstrated by increased γH2AX foci count and higher tail moments in the alkaline COMET assay. Meanwhile, indisulam downregulates ATM expression, which is likely to be a consequence of *ATM* mis-splicing following indisulam-mediated RBM39 degradation (Figure 3.2). Apart from HGSOC, mis-splicing and downregulation of ATM have also been documented in neuroblastoma cells after indisulam treatment (Singh et al., 2021), but the authors did not measure DNA damage levels in indisulam-treated cells. Another study in triple-negative breast cancer (MDA-MB-231) reported that RBM39 depletion significantly increased γH2AX expression in western blot, accompanied by a reduction in the HR repair protein RAD51 (Campbell et al., 2018). I have not tested the impact of indisulam on RAD51 expression in KURAMOCHI cells. RAD51 expression may not determine DSB repair capacity in these cells because they are already HR-deficient (Tumiati et al., 2018, Kim et al., 2020, Domcke et al., 2013). In addition, ATM is upstream of RAD51-mediated repair and loss of ATM would cause a more profound impact on DNA damage response (Helt et al., 2005, Blackford and Jackson, 2017, Beucher et al., 2009, Shibata and Jeggo, 2021). Therefore, reduced ATM expression is likely to be an important factor contributing to indisulam-mediated accumulation of DNA damage and genotoxic stress.

When used in combination with PARP inhibitors, indisulam phenocopies the effect of ATM inhibitors. The addition of indisulam partially inhibited olaparib-mediated activation of the ATM-Chk2 pathway, shown by reduced pATM-S1981 and pChk2-T68 expression. It also increases γH2AX expression and foci formation, elevates DNA damage in the alkaline COMET assay, and causes cell cycle arrest in S and G2/M phases. These observations are consistent with findings in other studies which showed more-than-additive induction of DNA damage and cell cycle arrest by combining olaparib with ATM inhibitors such as AZD0156 (Lloyd et al., 2020, Riches et al., 2020, Pike et al., 2018) and KU55933 (Hong et al., 2016, Wang et al., 2017).

In addition, a recent study demonstrated that PARP1 is a substrate of Chk2 (Hsu et al., 2019). Chk2 phosphorylates PARP1 at multiple sites, thereby enhancing PARylation and promoting the nuclear localisation of PARP1 upon DNA damage (Hsu et al., 2019). As a result, Chk2 inhibition reduces PARP1-mediated PARylation and DNA damage repair (Hsu et al., 2019) and sensitises ovarian cancer cells to olaparib (Xu et al., 2021, Anderson et al., 2011). It is worth investigating if indisulam synergises with PARP inhibitors through the same mechanism.

Notably, the combination of indisulam and olaparib causes γH2AX accumulation and ATM reduction in the ID8 tumours, indicating that reduced ATM activity and genotoxic stress accumulation may contribute to the anti-tumour effect *in vivo*. This further support the hypothesis that indisulam-mediated inhibition of ATM-Chk2 signalling plays an important role in the synergy with olaparib.

5.5.3. Replication stress also contributes to the synergy between indisulam and olaparib

In addition to DNA damage accumulation, the combination therapy also involves a substantial increase in the replication stress. I found that indisulam and olaparib showed a more-than-additive effect in reducing the number of progressing replication forks, slowing DNA synthesis, and increasing new origin firing, which were not seen in cells treated with either monotherapy. These observations may be explained by the increase in DNA damage and thus more obstacles to replication fork progression.

The increase in new origin firing can be a result of licensing of dormant replication origins near the sites of stalled replication forks, which is a well-characterised adaptive response to replication stress (Woodward et al., 2006, McIntosh and Blow, 2012, Ge et al., 2007, Ge and Blow, 2010), and the observed downregulation of Chk1 expression and reduced Chk1 activation. The firing of dormant origin is a highly regulated process and is normally inhibited by the ATR-Chk1 pathway (Ge and Blow, 2010, Toledo et al., 2013, Petermann et al., 2010). An increase in active replication origins causes a larger region of ssDNA that needs protection from RPA coating (Toledo et al., 2013). Excess new origin firing may generate an overwhelming amount of ssDNA and deplete the nuclear RPA pool, resulting in unprotected ssDNA that is prone to damage (Ge and Blow, 2010, Toledo et al., 2013, Petermann et al., 2010). Exhaustion of the RPA pool causes irreversible replication catastrophe – cell death at the S phase (Toledo et al., 2013). Previous studies have shown that Chk1 inhibition increases

new origin firing during replication stress (Ge and Blow, 2010, Toledo et al., 2013, Petermann et al., 2010) and reduces the rate of DNA replication (Petermann et al., 2006), which are consistent the effect of indisulam and olaparib in combination. Several recent studies have also demonstrated that ATR inhibitors and Chk1 inhibitors sensitise cancer cells to PARP inhibitors (Kim et al., 2017, Lloyd et al., 2020, Brill et al., 2017, Smith et al., 2020, Di Giulio et al., 2021, Kim et al., 2020). Therefore, the replication stress induced by the combination of indisulam and olaparib may be a combined effort of DNA damage accumulation and Chk1 depletion.

5.5.4. Indisulam, olaparib, and the combination therapy cause cell cycle arrest

One interesting finding is that indisulam-treated cells showed a differential cell cycle profile in HGSOC cells compared with previous studies. Indisulam was initially discovered as a drug causing cell cycle arrest in the G1 phase (Ozawa et al., 2001, Owa et al., 1999, Haddad et al., 2004). Prolong exposure to indisulam also lead to cell cycle arrest in the G2/M phases (Fukuoka et al., 2001, Ozawa et al., 2001, Owa et al., 1999, Wang et al., 2019, Singh et al., 2021). Indisulam treatment is also associated with hypo-phosphorylation of the protein retinoblastoma in patient samples, indicating G1/S blockade (Haddad et al., 2004). In KURAMOCHI cells, indisulam treatment increased fractions of cells in the S and G2/M phases, and reduced G1 phase cells. While my observation of the G2/M arrest is consistent with previous reports, the impact of indisulam on G1/S progression is contradictory. Since the G1/S checkpoint is p53-dependent (Hyun and Jang, 2015), it is possible that the loss of p53 expression in KURAMOCHI cells (Domcke et al., 2013) abrogates the G1/S checkpoint, leading to more cells entering the S phase (Deng et al., 1995). However, I have not investigated this in my project and future investigations would be necessary to assess if p53 deficiency contributes to the indisulam-mediated S phase arrest.

On the other hand, the cell cycle profile of olaparib-treated cells is consistent with previous findings in non-small cell lung cancer (Lloyd et al., 2020, Riches et al., 2020) and ovarian cancer (Sahin et al., 2019). Following olaparib treatment, KURAMOCHI cells are arrested in the late-S and G2/M phases. Because olaparib-treated cells showed increased DNA damage but no significant changes in replication fork behaviours, I speculate that the cell cycle arrest caused by olaparib may be transient in KURAMOCHI cells, and it may be mostly driven by DNA

damage accumulation. The ability of KURAMOCHI cells to tolerate olaparib-induced DNA damage without causing cell apoptosis might be the reason why it is resistant to PARP inhibitors.

Some studies have suggested that inhibiting either Chk1 or Chk2 abrogates the intra-S and G2/M cell cycle checkpoints, leading to a premature entry of mitosis and cell death (Alkema et al., 2014, Niida et al., 2005, Zhang et al., 2008, Lloyd et al., 2020, Kim et al., 2017). However, I found that the combination of indisulam and olaparib caused cell cycle arrest at intra-S, late-S and G2/M phases, despite a reduction in Chk1 and Chk2 activation. One possible explanation is that the residual activities of Chk1 and Chk2 might be sufficient to activate the intra-S and G2/M checkpoints. Alternatively, the replication stress in these cells may be intense enough to cause persistent cell cycle arrest and induce replication catastrophe – cell death in the S phase. These hypotheses are worth investigating in the future, and several strategies are proposed in the next section.

5.5.5. Limitations and Future work

One of the limitations is that the exact level of DSB has not been determined. Although many studies use γH2AX as a marker for DSBs, it is in fact an ambiguous marker for genotoxic stress and does not necessarily suggest DSBs formation. Multiple studies have shown that γH2AX is increased in response to DSBs and arrested replication forks (Sedelnikova et al., 2002, Cleaver, 2011, de Feraudy et al., 2010, Sharma et al., 2012). The increase of γH2AX at the sites of stalled replication forks is mediated by ATR or DNA-PK (Ward and Chen, 2001, Burdak-Rothkamm et al., 2007, Chanoux et al., 2009, Gagou et al., 2010, Ward et al., 2004, Moeglin et al., 2019, Hanasoge and Ljungman, 2007, Toledo et al., 2013, de Feraudy et al., 2010). Some researchers proposed that DSBs-induced γH2AX is commonly shown as discrete foci, whilst γH2AX induced by replication stress tends to form pan-nuclear staining (Coulson-Gilmer et al., 2021, Moeglin et al., 2019). However, this method is only indicative and not very accurate. DNA replication inhibitors, such as hydroxyurea, have shown to increase γH2AX expression and foci formation prior to DSBs formation (Toledo et al., 2013, Petermann et al., 2010, Ward and Chen, 2001, Sirbu et al., 2011). In addition, the definition of pan-nuclear staining is often subjective and may be influenced by the signal intensity and exposure time during image acquisition. Nevertheless, the pan-nuclear staining is still widely recognised as a sign of

replication catastrophe as long as images are analysed in an unbiased approach (set parameters using negative and positive controls, then analyse experimental images blindly) and experimental variations are minimised (use the same microscope with the same exposure).

Therefore, it is still uncertain if DSB formation is involved in the synergy between indisulam and olaparib. In particular, the combination of indisulam and olaparib causes DNA damage accumulation, replication stress, and cell apoptosis, all of which may contribute to the increase in γH2AX. The exact source of γH2AX could be determined in future studies by inhibiting potential upstream kinases of γH2AX, namely ATM (Burma et al., 2001, Stiff et al., 2004), ATR (Stiff et al., 2004, Burdak-Rothkamm et al., 2007, Chanoux et al., 2009, Ward et al., 2004, Ward and Chen, 2001), and DNA-PK (Stiff et al., 2004, Park et al., 2003, Mukherjee et al., 2006, An et al., 2010). Combining γH2AX and other markers, such as 53BP1 (Rappold et al., 2001, de Feraudy et al., 2010, Ward and Chen, 2001, Harding et al., 2011, Ward et al., 2003), RPA (Toledo et al., 2017, Toledo et al., 2013), and Annexin V staining can also suggest the type of genotoxic stress. A neutral COMET assay is ideal to quantify the number of DSB directly (Olive et al., 1991, Olive and Banáth, 2006, Lu et al., 2017, Au - Nowsheen et al., 2012). Unfortunately, despite multiple attempts, I was not able to establish this assay and thus future optimisation is needed. Alternative methods can also be used to detect DSBs accurately, such as the TdT-dUTP DSB end labelling (TUDEL) assay (Lutze et al., 2022).

Another potential criticism is the cell cycle analysis, which only provides one snapshot at 48 hours and cannot differentiate transient cell cycle arrest from persistent cell cycle arrest. Future analysis should synchronise the cell population and examine cell cycle distribution at various time points. Alternatively, the cell cycle progression of individual cells may be tracked using the cell fate profiling assay, which has been used in multiple HGSOC cell lines, including KURAMOCHI and OVSAHO (Pillay et al., 2019, Coulson-Gilmer et al., 2021). Replicating cells can also be labelled with nucleotide analogous, which allows tracking of cell cycle progression after the initial S phase (Lloyd et al., 2020). The activation status of cell cycle checkpoint proteins downstream of Chk1 and Chk2 are also worth investigating in the future, such as Cdc45 (Guo et al., 2015, Liu et al., 2006) and Cdc25A (Xiao et al., 2003, Falck et al., 2001).

Another gap is that I have not confirmed that the reduction in ATM expression and Chk1 expression directly contributes to the increase in DNA damage and replication stress, respectively. Although the causal relationship is plausible based on literature evidence, a rescue experiment would be appropriate to examine whether ATM and Chk1 downregulation determine the synergy between indisulam and olaparib. Plasmids or viral particles containing cDNAs of ATM and Chk1 should be used to bypass any indisulam-mediated splicing errors. Overexpression of ATM or Chk1 is expected to rescue cells from DNA damage accumulation and replication stress, leading to reduced cytotoxicity from the combination therapy. A partial rescue would imply the involvement of additional molecular changes in the synergy between RBM39 depletion and PARP inhibition. In addition, the underlying mechanisms of Chk1 downregulation by indisulam and olaparib should also be investigated.

An additional drawback is the lack of direct evidence showing that indisulam impairs DNA damage repair. Quantifying DNA damage repair capacities using the DR-GFP (for HR repair) and EJ5-GFP (for NHEJ repair) reporter assays have been scheduled in our laboratory (Pierce et al., 1999, Bennardo et al., 2008, Gunn and Stark, 2012). Briefly, the cells of interest are transduced with reporter plasmids that contain a GFP gene disrupted by tandem sites of the endonuclease *I-SceI*. *I-SceI* is a bacteria endonuclease that recognises a very rare sequence, allowing highly selective induction of DSB in the reporter plasmid (Monteilhet et al., 1990, Siegl et al., 2010). Repairing the *I-SceI*-induced DSBs generates a functional GFP gene. The repair efficiency could be easily quantified through flow cytometry. DR-GFP and EJ5-GFP plasmids differ in the design of *I-SceI* sites, which only permit HR or NHEJ repair, respectively.

The current understanding of the replication stress caused by indisulam and olaparib is still preliminary. Only one or two biological replicates are available so far, and future replications are necessary to ascertain if the trend of changes is reproducible. More importantly, it is still unclear how vital is the replication stress to the synergy between indisulam and olaparib. Future studies should investigate if the combination therapy causes replication catastrophe and leads to cell apoptosis at the S phase. The replication catastrophe can be tested by assessing the level of RPA availability in the nucleus and the cell cycle distribution of apoptotic cells using immunofluorescence or flow cytometry (Toledo et al., 2017, Toledo et al., 2013). Overexpressing RPA components is also a good way to ascertain if RPA exhaustion contributes to DNA damage and replication catastrophe (Toledo et al., 2013). It is also important to study

how the combination of indisulam and olaparib reduces progressing forks. There are three possible explanations: increased fork stalling, reduced restarting of stalled forks, and slowed fork progression. Increased fork stalling can be assessed by measuring the asymmetry of IdU fibres in bi-directional forks as previously described (Pillay et al., 2019). To study whether the combination therapy inhibits fork restarting, cells can be sequentially treated with the drug combination and then a short pulse of hydroxyurea (to induce fork stalling). The kinetics of fork restarting can be investigated by monitoring the fork progression after hydroxyurea treatment as previously described (Kumar et al., 2020). Fork progression speed can be quantified by measuring IdU fibre length before and after exposure to the combination therapy (Nieminuszczy et al., 2016). Shorter fibres after the drug treatment suggests slowed fork progression.

As for the DNA fibre analysis, it is still unclear why there was an imbalanced ratio of new origin firing during two consecutive labelling phases. While vehicle control or indisulam caused a comparable number of new origins during two sequential pulse labelling phases (BrdU and IdU), olaparib treatment and the combination therapy caused a higher rate of new origin firing during the IdU labelling (2^{nd} pulse phase) than the BrdU labelling (1^{st} pulse phase) (Figure 5.9B). The imbalanced ratio of new origins might be biologically meaningful. But to the best of my knowledge, no literature has discussed this. Alternatively, this might be caused by technical issues. It is possible that the washing step between the two labelling phases was not fast enough (although it was done within 3 minutes), and the transient withdrawal of cytotoxic drugs might have stimulated DNA replication. If this was the case, washing cells faster using fresh culture media containing the drugs of interest should be able to minimise the issue. Alternatively, it could be due to the detection bias during manual image analysis. The bi-directional DNA fibre caused by origin firing during BrdU labelling (1^{st} phase) is always a rare event and challenging to find. Moreover, the BrdU was poorly labelled by antibodies and often shown as fragmented fibres. Thus, some bi-directional DNA fibres might have been mistaken for progressing forks (uni-directional fibres), especially in cells with replications tress. Other studies have also observed fragmented labelling of DNA fibres (Pillay et al., 2019, Stanojcic et al., 2017, Marheineke et al., 2005). The labelling efficiency could be improved by replacing the BrdU with the Click-iT EdU labelling kit, because the click-it chemistry is a faster

and more efficient fluorescence labelling technic than traditional antibody-based immunostaining (Krishan and Hamelik, 2010).

PARP inhibitors can inhibit PARylation within 30 minutes, though it takes days to show growth inhibition (Murai et al., 2012, Murai et al., 2014). One additional limitation of this chapter is that all experiments were conducted at 48 hours, and thus the interaction between PARylation inhibition and indisulam-mediated splicing abnormalities is still unclear. As RNA splicing changes take time to manifest at protein levels, pre-treating cells with indisulam (24 or 48 hours) before adding olaparib (30 minutes to 48 hours) is a scientifically valid strategy to differentiate short-term impact from long-term consequences of PARP inhibition. Western blot analysis can be used to assess the signalling changes in PARylation, DNA damage response, replication stress response, and cell apoptosis. Immunofluorescence analysis can be used to monitor the recruitment of DNA damage repair factors to damage sites or stalled replication forks. For example, olaparib-induced ATM activation and recruitment might be slowed or reduced in indisulam-treated cells because indisulam downregulates ATM expression. These experiments will provide valuable insights into the interaction between indisulam and olaparib.

5.5.6. Conclusion

In conclusion, I found evidence that the synergy between indisulam and olaparib involves both DNA damage accumulation and replication stress. By downregulating ATM expression, indisulam suppresses olaparib-induced activation of the ATM-Chk2 signalling pathway, potentially impairs DNA repair activities in HGSOC cells and increases susceptibility to PARP inhibitors. The combination of indisulam and olaparib also causes a more-than-additive reduction of Chk1 expression, which may contribute to the increased replication fork abnormalities and excess new origin firing. These findings provide valuable mechanistic insights into the synergistic interaction between indisulam and olaparib and facilitate the identification of genes or pathways that may determine the synergy potential of the combination therapy.

Chapter 6

Chapter 6. Assessing the impact of indisulam and olaparib on HGSOC transcriptome and proteome

6.1. Overview of the transcriptomic and proteomic analysis

Multiple studies have shown that indisulam causes genome-wide splicing changes in cancer cells (Mai et al., 2016a, Faherty et al., 2016, Han et al., 2017b, Kralovicova et al., 2018, Wang et al., 2019, Ting et al., 2019, Puvvula et al., 2021, Nijhuis et al., 2022, Lu et al., 2021b, Singh et al., 2021, Uehara et al., 2017), but the impact of indisulam on HGSOC cell transcriptome and proteome has not been studied. Therefore, we conducted transcriptomic and proteomic analyses to investigate how indisulam affects gene expression in HGSOC cells and how it may improve PARP inhibitor response.

A flowchart of the transcriptomic and proteomic analyses is shown in Figure 6.1A. In brief, KURAMOCHI cells were treated with vehicle control (0.1% DMSO), 10 μM indisulam, 30 μM olaparib, or combination therapy (10 μM indisulam plus 30 μM olaparib). After 24-hour exposure, total RNA was extracted from cells and sent for RNA-sequencing (n = 3). KURAMOCHI cells were treated the same way for 48 hours, and total protein was extracted for (total) proteomic analysis (n = 5). In parallel, the murine HGSOC ID8-*Trp53*$^{-/-}$ cells were treated with vehicle control (0.1% DMSO) or 1 μM indisulam. Total RNA (at 24 hours, n = 3) and total protein (at 48 hours, n = 5) were extracted and sent for RNA sequencing and proteomic analysis. While analyses of these data are ongoing, a summary of key findings to date is presented in this chapter (Figure 6.1B).

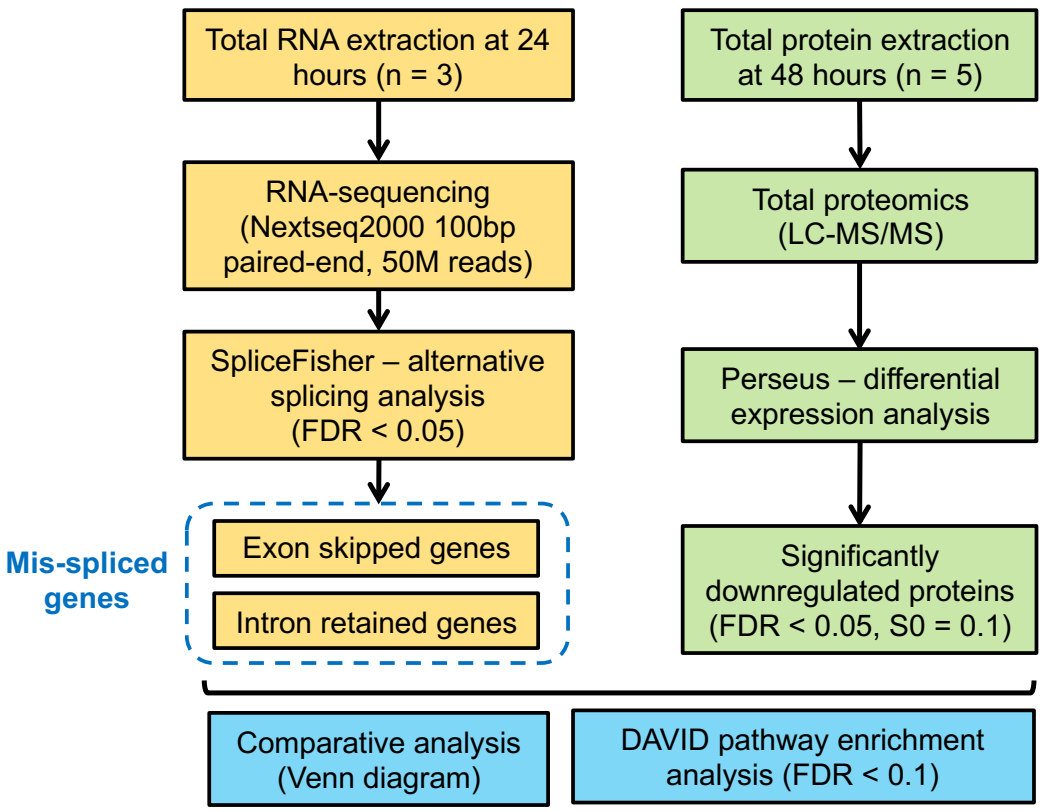
The data were generated and analysed with support from other group members and external collaborators. I collected KURAMOCHI protein samples for proteomic analysis and performed most of the comparative analysis, functional annotation, and enrichment analysis. Dr Nijhuis and I worked together to generate the ID8-*Trp53*$^{-/-}$ samples for proteomics. Dr Nijhuis also contributed to the generation of all RNA samples at 24 hours. RNA-sequencing was outsourced to the Imperial Biomedical Research Centre (BRC) genomic centre and Mr Michael Gruet performed the alternative splicing analysis using the SpliceFisher as previously described (Han et al., 2017b, Nijhuis et al., 2022). I used the list of mis-spliced genes (produced by Mr Gruet) for Venn diagram comparisons and pathway enrichment analysis. Proteomic

analysis was conducted by our external collaborators (Prof Holger Kramer and Dr Alex Montoya). Dr Montoya also performed the differential expression analysis and constructed a data visualisation package in Perseus. I then used the list of differentially expressed proteins for Venn diagram comparisons, pathway enrichment analysis, and producing volcano plots.

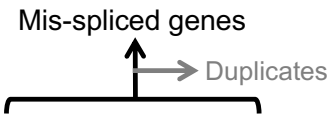
In this chapter, I aimed to answer the following research questions using the comparative analysis (Venn diagram) and pathway enrichment analysis:

1. Which pathways are preferentially affected by indisulam-mediated splicing changes (Section 6.2.1)?
2. Do splicing errors lead to reduced protein expression (Section 6.2.2)?
3. Which protein changes in indisulam-treated cells can explain the increased sensitivity to olaparib?
    a. Targeted approach – focusing on DNA repair genes (Section 6.2.3)
    b. Untargeted approach – based on literature evidence of gene expression changes that modulates PARP inhibitor sensitivity (Section 6.2.4).
4. Is the role of RBM39 on RNA splicing conserved between human and mouse (Section 6.3)?
5. Do indisulam and olaparib affect the splicing of the same genes (Section 6.4)?
6. Are there any unique protein changes when indisulam and olaparib are combined (Section 6.5)?

A



B



		Exon skipped genes	Intron retained genes	Downregulated proteins
KURAMOCHI	Indisulam (10 µM)	7904	8389	1043
	Olaparib (30 µM)	7297	7768	339
	Combination	8026	8681	1241
ID8-Trp53$^{-/-}$	Indisulam (1 µM)	5371	6283	942

Figure 6.1. Overview of the transcriptomic and proteomic analyses in human and mouse HGSOC cells.

(A) KURAMOCHI or ID8-*Trp53*$^{-/-}$ cells were treated with vehicle control (0.1% DMSO), 10 µM indisulam, 30 µM olaparib, or the combination of 10 µM indisulam and 30 µM olaparib for 24 and 48 hours. At 24 hours, total RNA was extracted for RNA-sequencing analysis; and at 48 hours, total protein was extracted for proteomic analysis. RNA-sequencing data were analysed by Michael Gruet using the SpliceFisher (Han et al., 2017b, Nijhuis et al., 2022) to detect alternative splicing events (comparing each treatment with the vehicle control). Proteomics data were analysed by Dr Alex Montoya using the MaxQuant and Perseus software platforms (comparing each treatment with the vehicle control). **(B)** Numbers of genes displayed exon skipping events or intron retention events, and the numbers of proteins significantly downregulated in the proteomics dataset.

Chapter 6

6.2. Indisulam disrupts alternative splicing of DNA repair and replication genes

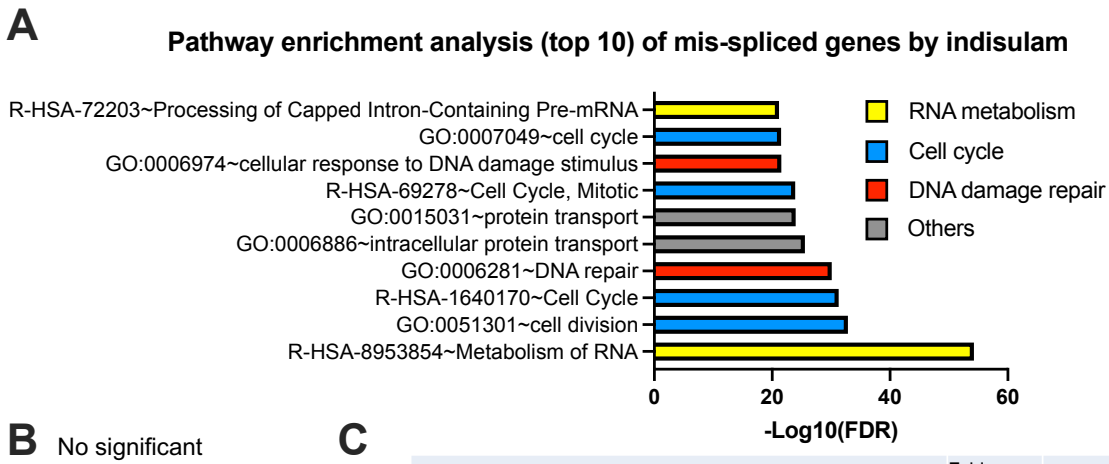
6.2.1. Indisulam treatment leads to mis-splicing in cell cycle and DNA damage repair genes

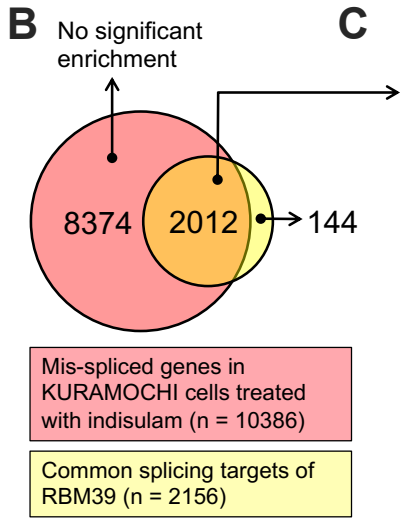
As discussed in earlier chapters (Chapter 1 and Chapter 3), RBM39 is an essential splicing factor in cancer cells mediating the splicing of many genes (Singh et al., 2021, Wang et al., 2019, Xu et al., 2020b, Lu et al., 2021b, Nijhuis et al., 2022, Mai et al., 2016b, Han et al., 2017b). The systematic analysis in Chapter 3 showed that common targets of RBM39-mediated splicing in four cancer types (neuroblastoma, melanoma, acute myeloid leukaemia, and breast cancer) are enriched in cell cycle and DNA repair genes. In addition, I validated exon skipping events of several DNA repair genes in HGSOC cells (Figure 3.2). Therefore, I speculated that the alternative splicing of cell cycle and DNA repair genes might be predominantly affected in KURAMOCHI cells upon indisulam treatment.

Alternative splicing analysis of the RNA-sequencing data in KURAMOCHI cells identified exon skipping or intron retention events (hereafter mis-splicing events) in 10386 genes following indisulam treatment. Pathway enrichment analysis found that 'Metabolism of RNA' was the most significantly enriched pathway (Figure 6.2A), which is not surprising given the involvement of RBM39 in spliceosome [reviewed in (Xu et al., 2020b)]. As expected, multiple cell cycle and DNA damage response pathways were among the top 10 significantly enriched pathways (Figure 6.2A).

When compared to the common splicing targets of RBM39 identified in the systematic literature analysis (Section 3.1.1), 93.3% (2012/2156) were aberrantly spliced in KURAMOCHI cells upon indisulam-mediated RBM39 depletion (Figure 6.2B), further confirming that the RNA splicing of a panel of genes is consistently regulated by RBM39 across multiple cancer types. These 2012 genes were significantly enriched for several cell cycle pathways and showed non-significant trends of enrichment in multiple DNA repair pathways (fold enrichment values between 1.4 to 2.1) (Figure 6.2C). Approximately 80% of exon skipped or intron retained genes (8317/10387) were KURAMOCHI-specific, and no pathway was significantly enriched within this subset (Figure 6.2B).

Overall, above findings support the hypothesis that RBM39 coordinates the splicing of cell cycle and DNA repair genes in multiple types of cancers including HGSOC.





C

Pathway enrichment analysis (Top 15)	Fold enrichment	p-value	FDR
R-HSA-380287~Centrosome maturation	2.2	1.61E-05	0.014
R-HSA-380270~Recruitment of mitotic centrosome proteins and complexes	2.2	1.61E-05	0.014
R-HSA-380320~Recruitment of NuMA to mitotic centrosomes	2.1	6.29E-05	0.036
R-HSA-8854518~AURKA Activation by TPX2	2.1	1.23E-04	0.052
R-HSA-2565942~Regulation of PLK1 Activity at G2/M Transition	2.0	1.74E-04	0.060
R-HSA-380284~Loss of proteins required for interphase microtubule organization from the centrosome	2.1	3.89E-04	0.095
R-HSA-380259~Loss of Nlp from mitotic centrosomes	2.1	3.89E-04	0.095
R-HSA-1640170~Cell Cycle	1.3	4.86E-04	0.101
R-HSA-5620912~Anchoring of the basal body to the plasma membrane	1.8	5.30E-04	0.101
hsa01240:Biosynthesis of cofactors	1.8	0.00102428	0.322
WP4016~DNA IR-damage and cellular response via ATR	1.9	0.00120691	0.652
GO:0006281~DNA repair	1.4	0.00158064	1.000
WP4148~Splicing factor NOVA regulated synaptic proteins	2.5	0.00221452	0.652
hsa03460:Fanconi anemia pathway	2.1	0.00293902	0.322
hsa01100:Metabolic pathways	1.2	0.00298537	0.322

Figure 6.2. Indisulam causes aberrant splicing in cell cycle and DNA damage repair genes.
(A) KURAMOCHI cells were treated with vehicle control or 10 µM indisulam for 24 hours before RNA sequencing and alternative splicing analysis (as shown in Figure 6.1). The mis-spliced genes (exon skipped or intron retained) were used for pathway enrichment analysis. The top 10 significantly enriched pathways were shown as bar charts and ranked based on the FDR. Closely related pathways are highlighted in the same colour. **(B)** A Venn diagram comparing the mis-spliced (exon skipped or intron retained) genes in indisulam-treated KURAMOCHI cells with previously identified common splicing targets of RBM39 (across four cancer types). **(C)** Top 15 enriched pathways of the 2012 genes identified in (b). The gene ontology biological process (GOBP), REACTOME, KEGG, and WIKIPATHWAY databases were used for enrichment analysis. All genes involved in the Venn diagram (b) were used as a background for enrichment analysis (n = 10530).

6.2.2. Most proteins downregulated by indisulam are splicing targets of RBM39

I next investigated whether the splicing errors caused by indisulam led to reduced protein expression. Among the genes mis-spliced by indisulam, 42% (4306/10386) were within the coverage of proteomics (Figure 6.3A). Proteomics analysis showed 1043 proteins were significantly downregulated by indisulam, and 91.3% (952/1043) were affected by indisulam-mediated exon skipping or intron retention events (Figure 6.3B). This finding favours the hypothesis that indisulam downregulates protein expression mainly through splicing errors and corroborates previous observations we published in neuroblastoma (Nijhuis et al., 2022).

Interestingly, among the genes mis-spliced by indisulam and downregulated at protein levels, the 'Metabolic pathways' was the only pathway significantly enriched (FDR = 0.059, fold enrichment = 1.32, Figure 6.3B), and the thymidylate synthetase (TYMS) was included within this pathway. In our recent publication, Nijhuis et al. (2022) showed that indisulam affects metabolism in neuroblastoma cells by mis-splicing and downregulating TYMS. It is possible that indisulam alters HGSOC cell metabolism also through TYMS, and future investigation is warranted.

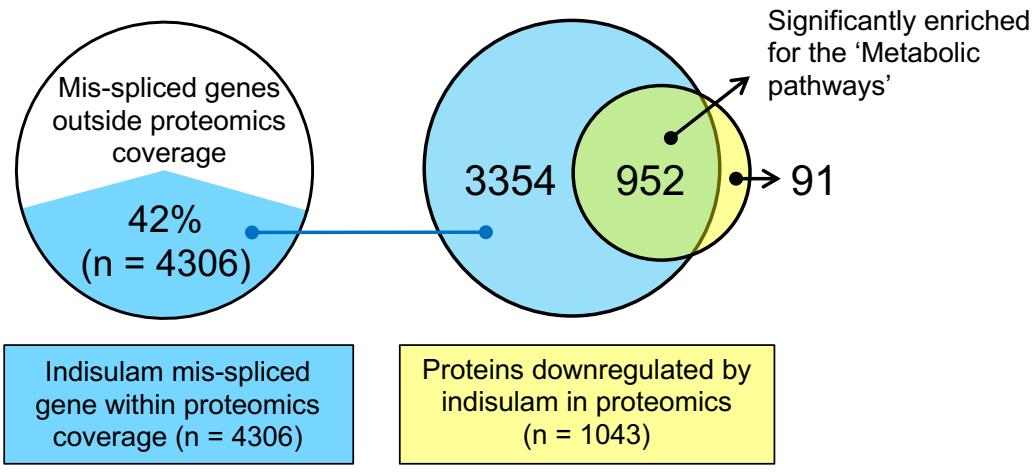


Figure 6.3. Indisulam downregulates protein expression mainly by inducing splicing errors.
(A) A pie chart showing the proportion of indisulam mis-spliced genes in KURAMOCHI cells that are also within the coverage of proteomics. **(B)** A Venn diagram showing that 952 genes mis-spliced by indisulam were also downregulated at protein levels in KURAMOCHI cells. Pathway enrichment analysis was performed using all proteins detected in the proteomics as the background (n = 5328).

6.2.3. Indisulam may increase PARP inhibitor response by downregulating DNA repair proteins

Previous data from functional assays suggested that indisulam downregulates protein expression of ATM and improves olaparib response by increasing DNA damage and replication stress (Chapter 5). Therefore, I attempted to investigate whether other DNA repair proteins may be downregulated by indisulam. Surprisingly, among the DNA repair genes mis-spliced by indisulam (based on the Reactome annotation), 44% of them (105/238) were missing in the proteomics dataset (Figure 6.4A). Proteins not reported in the proteomics data included many interesting DNA repair proteins, such as ATM, BRCA1, BRCA2, and RAD51 analogues.

Despite the limited coverage, 56% of DNA repair genes (133/238) mis-spliced by indisulam were detectable in the proteomics (Figure 6.4B). Twenty-five of them were downregulated at protein levels by indisulam, providing a list of DNA repair proteins modulated by RBM39 (Table 6.1). Functional annotation showed that these 25 DNA repair proteins have been implicated in many aspects of the genotoxic stress response, including HR repair (ERCC1, PNKP, TIM), NHEJ repair (53BP1, PNKP), nucleotide excision repair (cyclin H, ERCC1, ERCC2, TF2H1, and TF2H4), Fanconi anaemia repair (FANCI, FANCD2, ERCC1), and DNA replication stress response (claspin, FANCI, FANCD2, TIM) (Table 6.1).

I next examined the differential protein expression in KURAMOCHI cells following indisulam and olaparib treatment either alone or in combination, with a particular focus on the 25 DNA repair genes targeted by indisulam (Figure 6.5). Proteomics analysis showed that, as expected, RBM39 was one of the most depleted proteins in KURAMOCHI cells treated with indisulam and the combination therapy (Figure 6.5A and C). RBM39 level showed a small but significant reduction upon olaparib treatment, implying an intriguing possibility that RBM39 availability might be affected by PARP activities (Figure 6.5B).

Of the 25 DNA repair proteins known to be downregulated by indisulam, 84% (21/25) were also significantly downregulated in cells treated with the combination therapy of indisulam and olaparib. On the other hand, most of these DNA repair proteins were not downregulated by olaparib treatment. Instead, five of them (TIM, FANCI, UBCH8, claspin, and PNKP) were significantly upregulated by olaparib, suggesting that they may contribute to the adaptive response to PARP inhibitors. With the exception of UBCH8 (*UBE2L6*), depletion of TIM

(*TIMLESS*), FANCI (*FANCI*), claspin (*CLSPN*), and PNKP (*PNKP*) have been shown to increase PARP inhibitor response in previous CRISPR loss-of-function screens (Fugger et al., 2021, DeWeirdt et al., 2020, Blanck et al., 2020, Jamal et al., 2022, Hewitt et al., 2021, Tsujino et al., 2022, Zimmermann et al., 2018, Su et al., 2020, Noordermeer et al., 2018). UBCH8 (E2 ubiquitin-conjugating enzyme L6) regulates p21 stability and modulates DNA damage response upon radiation (Shibata et al., 2011), but its involvement in PARP inhibitor response is still unclear.

In summary, these findings show that indisulam downregulates a panel of DNA repair genes, predominantly through splicing errors, including several factors known to increase sensitivity to PARP inhibitors.

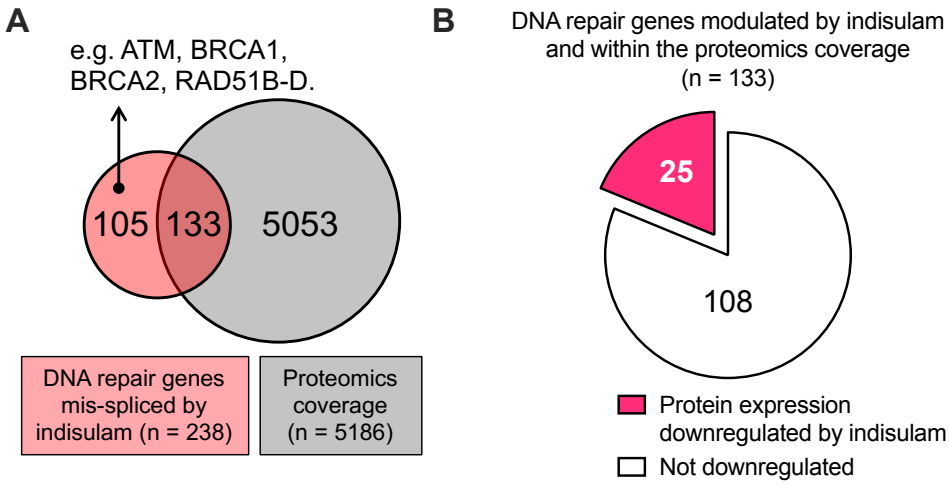


Figure 6.4. Many DNA repair genes modulated by indisulam are outside the proteomics coverage. **(A)** A Venn diagram showing that only 133 out of 238 DNA repair genes (that were mis-spliced by indisulam) were detectable in the proteomics dataset of KURAMOCHI cells. Mis-spliced genes refer to the genes with exon skipping or intron retention events. **(B)** A pie chart shows the proportion of the 133 DNA repair genes in (a) downregulated by indisulam at protein levels (pink).

Chapter 6

Table 6.1. Functional annotation of the 25 DNA repair genes mis-spliced and downregulated (at protein levels) by indisulam.

Protein name	Gene Symbol	Involvement in DNA damage repair response	References
activating signal cointegrator 1 complex subunit 2 (ASCC2)	*ASCC2*	Repairs alkylated DNA.	(Brickner et al., 2017)
activating signal cointegrator 1 complex subunit 3 (ASCC3)	*ASCC3*	DNA helicase. Promotes repairs alkylated DNA.	(Dango et al., 2011)
cyclin H	*CCNH*	Implicated in nucleotide excision repair.	(Santos et al., 2013, Wang et al., 2007)
cyclin dependent kinase 7 (CDK7)	*CDK7*	Transcriptional regulation of DNA repair genes.	(Veo et al., 2021)
chromodomain helicase DNA binding protein 1 like (CHD1L)	*CHD1L*	Oncogene. DNA helicase. Interacts with PARP1. Remodels chromatin for DNA damage.	(Verma et al., 2021, Singh et al., 2017, Juhász et al., 2020, Hewitt et al., 2021, Ahel et al., 2009).
Claspin	*CLSPN*	Mediates DNA damage and replication checkpoint. Interacts with ATR, Chk1 and BRCA1.	(Sørensen et al., 2004, Lin et al., 2004, Chini and Chen, 2003)
damage specific DNA binding protein 1 (DDB1)	*DDB1*	Repairs DNA damage by UV.	Reviewed in (Iovine et al., 2011)
ERCC excision repair 1, endonuclease non-catalytic subunit (ERCC1)	*ERCC1*	Implicated in nucleotide excision repair, Fanconi anaemia and HR repair.	(Kuraoka et al., 2000, Ahmad et al., 2008, Sijbers et al., 1996)
ERCC excision repair 2, TFIIH core complex helicase subunit (ERCC2)	*ERCC2*	An DNA helicase contributes to TFIIH-complex mediated nucleotide excision repair.	(Li et al., 2019)
FA complementation group D2 (FANCD2)	*FANCD2*	Involved in Fanconi anaemia repair and replication stress response.	(Okamoto et al., 2019, Liang et al., 2019, Smogorzewska et al., 2007)
FA complementation group I (FANCI)	*FANCI*	Involved in Fanconi anaemia repair and replication stress response.	(Liang et al., 2019, Smogorzewska et al., 2007)
general transcription factor IIH subunit 1 (TF2H1)	*GTF2H1*	Contributes to TFIIH-complex mediated nucleotide excision repair.	Reviewed in (Rimel and Taatjes, 2018)
general transcription factor IIH subunit 4 (TF2H4)	*GTF2H4*	Contributes to TFIIH-complex mediated nucleotide excision repair.	Reviewed in (Rimel and Taatjes, 2018)

HECT and RLD domain containing E3 ubiquitin protein ligase 2 (HERC2)	*HERC2*	An E3 ubiquitin ligase promoting DNA repair factor assembly to DNA damage sites. Modulates BRCA1 stability.	(Bekker-Jensen et al., 2010, Wu et al., 2010)
O-6-methylguanine-DNA methyltransferase (MGMT)	*MGMT*	Repairs methylated guanine and thymine. Contributes to temozolomide-resistance.	Reviewed in (Fan et al., 2013)
mutL homolog 1 (MLH1)	*MLH1*	Involved in DNA mis-match repair.	(Kadyrov et al., 2006)
polynucleotide kinase 3'-phosphatase	*PNKP*	Involved in DSB repair via NHEJ and HR	(Jilani et al., 1999, Aceytuno et al., 2017)
RNA polymerase II subunit A (RPB1)	*POLR2A*	Required for transcription and nuclear abundance affects cell survival upon UV-induced DNA damage.	(Tufegdžić Vidaković et al., 2020)
RNA polymerase II subunit I (RPB9)	*POLR2I*	Associated with cisplatin resistance.	(Gaponova et al., 2017)
timeless circadian regulator (TIM)	*TIMELESS*	Binds PARP1. Important for DNA replication stress response, DNA repair and S phase checkpoint.	(Xie et al., 2015, Unsal-Kaçmaz et al., 2007, Leman et al., 2010, Young et al., 2015)
tumor protein p53 binding protein 1 (53BP1)	*TP53BP1*	Crucial for NHEJ and counteracts BRCA1-mediated HR repair.	Reviewed in (Panier and Boulton, 2014)
tripartite motif containing 25 (TRIM25)	*TRIM25*	E3 ubiquitin ligase that degrades RBM39. Regulates expression of some DNA repair gene such as Ku80.	(Chen et al., 2022, Tong et al., 2019)
ubiquitin conjugating enzyme E2 L6 (UBCH8)	*UBE2L6*	Implicated in repairing UV-induced DNA damage.	(Shibata et al., 2011)
UBX domain protein 1 (UBXN1)	*UBXN1*	Involvement in DNA repair is unclear. Regulates HR-independentBRCA1 activity by ubiquitination.	(Wu-Baer et al., 2010)
X-ray repair cross complementing 1 (XRCC1)	*XRCC1*	Involved in SSBs repair.	(Brem and Hall, 2005)

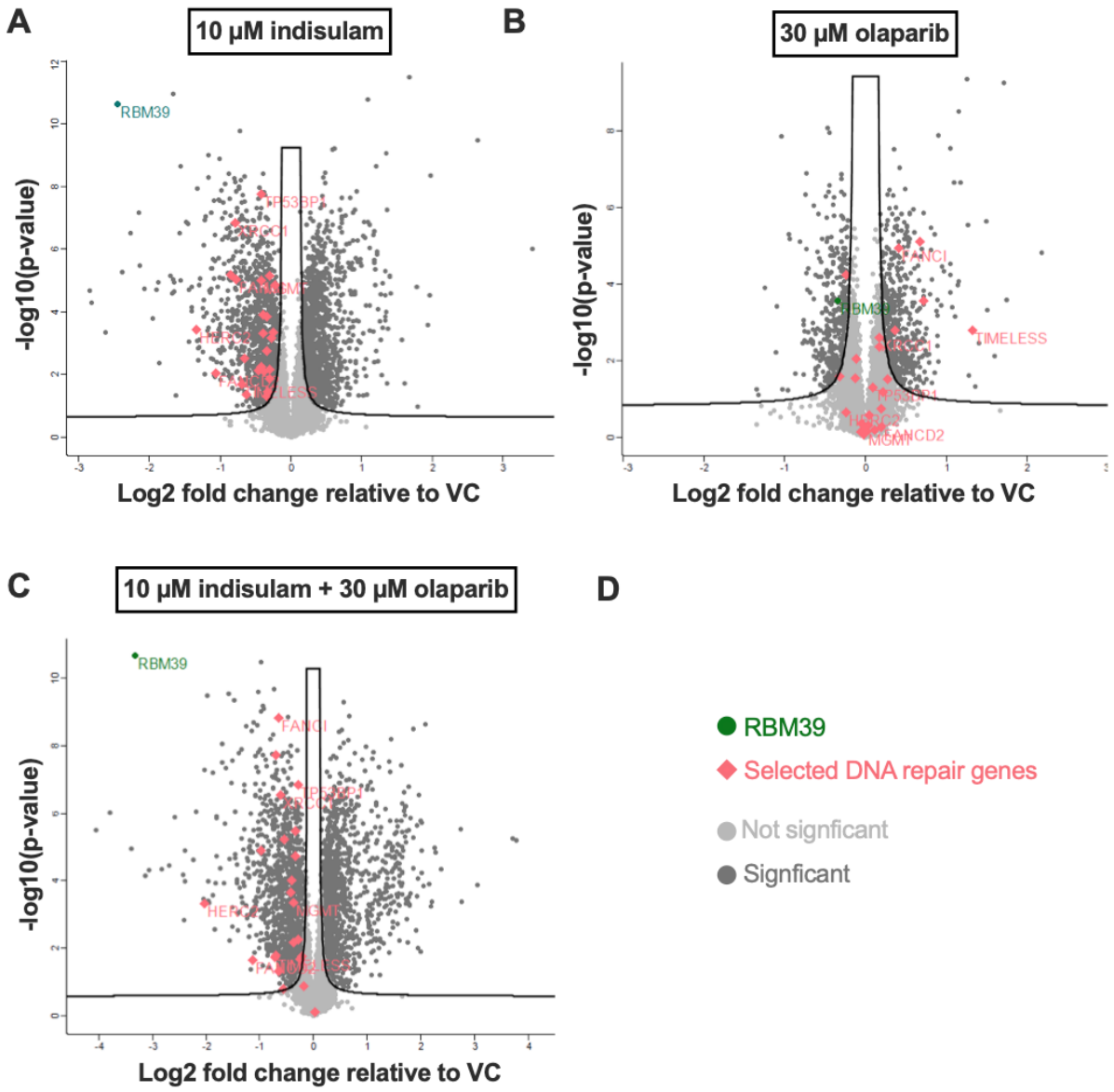


Figure 6.5. Indisulam downregulates protein expression of multiple DNA repair genes.
Volcano plots showing protein expression changes (relative to vehicle control, VC) in KURAMOCHI cells treated with 10 μM indisulam **(A)**, 30 μM olaparib **(B)**, or the combination of indisulam and olaparib **(C)** for 48 hours. The scale of axes is different between volcano plots. Proteins are shown in gene names. **(D)** Legends of the volcano plot. RBM39 and the 25 DNA repair genes both mis-spliced and downregulated by indisulam are highlighted in (a-c). Differential protein expression analysis was performed by Dr Alex Montoya using the Perseus software platform. Significant protein changes were determined by two-tailed t-test and the cut-off was set as FDR < 0.05 and S0 = 0.1.

6.2.4. Indisulam downregulates protein expression of genes modulating PARP inhibitor sensitivity – an untargeted analysis

Recent publications have reported several CRISPR-Cas9 loss-of-function screens and identified genes that increase PARP inhibitor response when knocked out (Fugger et al., 2021, DeWeirdt et al., 2020, Blanck et al., 2020, Jamal et al., 2022, Hewitt et al., 2021, Tsujino et al., 2022, Zimmermann et al., 2018, Su et al., 2020, Noordermeer et al., 2018, Clements et al., 2020, Fang et al., 2019a, Juhász et al., 2020, Olivieri et al., 2020, Verma et al., 2021). In other words, these genes maintain cell viability upon PARP inhibitor treatment. Comparison of these modulators of PARP inhibitor sensitivity versus proteins downregulated by indisulam provides an untargeted approach to uncover novel insights into the synergy between indisulam and olaparib.

To this end, I did a systematic literature analysis to identify genes that were detected in at least two independent CRISPR loss-of-function screens (using cells treated with PARP inhibitors, Figure 6.6). I started the analysis by performing PubMed searches using the keywords: ("PARPi" or "PARP inhibitor") and "sensitivity" and "CRISPR" and "screen". After removing two review articles and 15 articles without a PARP inhibitor sensitivity screen, I found six eligible articles (Zimmermann et al., 2018, Verma et al., 2021, Su et al., 2020, Juhász et al., 2020, Hewitt et al., 2021, Fang et al., 2019a). Another eight articles containing CRISPR-based PARP inhibitor sensitivity screen were included in the analysis, including six articles suggested by Schleicher and Moldovan (2021) and Jamal et al. (2022) and two articles (Jamal et al., 2022, Tsujino et al., 2022) identified by the MRes student Bertina Dragunaite who performed similar searches on bioRxiv.

In total, 14 articles containing 21 CRISPR knockout screens were included in this systematic analysis (Table 6.2). A total of 2065 genes were detected as high-confidence modulators for PARP inhibitor sensitivity in at least two independent screens, including several well-known genes such as *BRCA1/2* (Bryant et al., 2005, Farmer et al., 2005), *RAD51* (Cruz et al., 2018, Suwaki et al., 2011, Liu et al., 2017), *ATM* (Riches et al., 2020, Pike et al., 2018Lloyd, 2020 #377, Wang et al., 2017, Hong et al., 2016), and *CHD1L* (Verma et al., 2021, Singh et al., 2017, Juhász et al., 2020, Hewitt et al., 2021, Ahel et al., 2009).

Comparative analysis with the proteomics analysis showed that 215 high-confidence modulators of PARP inhibitor sensitivity were downregulated by indisulam, and 73% (158/215) were also downregulated when indisulam was combined with olaparib (Figure 6.7A). Pathway enrichment analysis showed that these 215 genes are significantly enriched in the pathways related to the following processes: S phase progression, G1/S transition, DNA replication, and RNA metabolism (Figure 6.7B). These observations are in line with previous findings that the synergy between indisulam and olaparib involves cell cycle arrest, DNA damage accumulation, and elevated replication stress (Chapter 5).

A trend of enrichment in the DNA repair pathway was also observed, but it did not pass the multiple comparisons test (fold enrichment = 2.7, p-value < 0.001, FDR = 0.13, Figure 6.7B). This is probably due to the under-representation of DNA repair proteins in proteomics, as discussed earlier (Figure 6.4).

Overall, above findings indicate that indisulam may improve PARP inhibitor response by negatively affecting cell cycle progression, DNA replication, and DNA repair pathways.

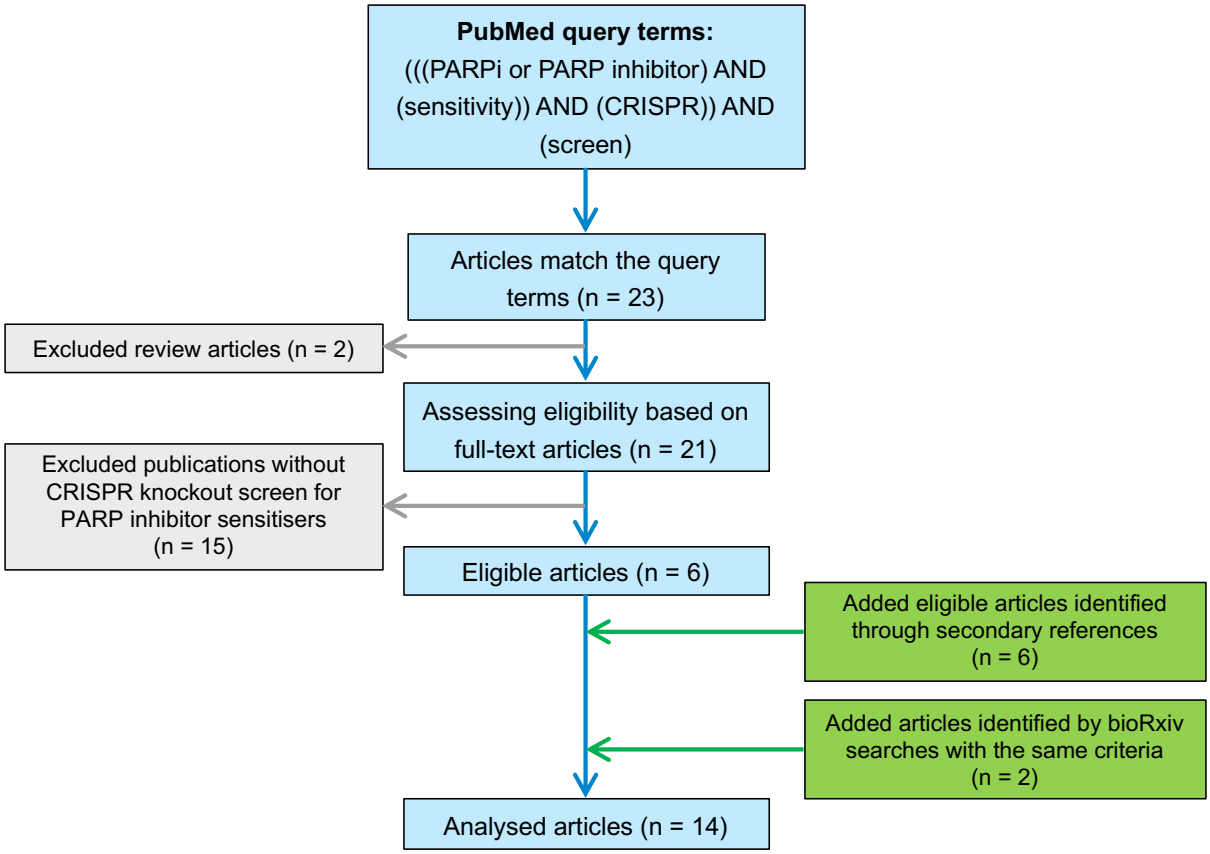


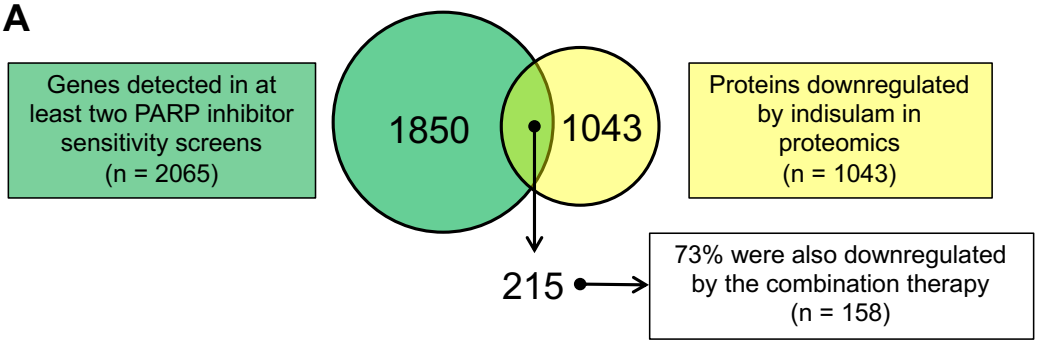
Figure 6.6. Process of identifying articles for the systematic literature review.
Flow chart showing the systematic literature searches. Inclusion criteria were articles reporting CRISPR-based PARP inhibitor sensitivity screens and contained the list of candidate genes that sensitise cells to PARP inhibitors when depleted. The bioRxiv searches were performed by previous MRes student Bertina Dragunaite.

Table 6.2. Characteristics of dropout CRISPR screens included for the systematic review.

	First author	Year	Cell line(s)	Origin	PARP inhibitor	Reference
1	Noordermeer	2018	RPE1 SUM149PT	Retina Breast cancer	Olaparib Olaparib	(Noordermeer et al., 2018)
2	Zimmermann	2018	HeLa RPE1 SUM149PT	Cervical cancer Retina Breast cancer	Olaparib Olaparib Olaparib	(Zimmermann et al., 2018)
3	Fang	2019	A2780	Ovarian cancer	Olaparib	(Fang et al., 2019a)
4	Clements	2020	HeLa	Cervical cancer	Olaparib	(Clements et al., 2020)
5	Blanck	2020	HT-90	Colorectal cancer	Olaparib	(Blanck et al., 2020)
6	Olivieri	2020	RPE1	Retina	Olaparib	(Olivieri et al., 2020)
7	Su	2020	HEK293A	Kidney	Olaparib	(Su et al., 2020)
8	DeWeirdt	2020	OVCAR8 A375 HAP1	Ovarian cancer Melanoma Leukaemia	Olaparib Olaparib Talazoparib	(DeWeirdt et al., 2020)
9	Juhász	2020	HeLa	Cervical cancer	Olaparib	(Juhász et al., 2020)
10	Verma	2021	UWB1.289 SUM149PT CAPAN-1	Ovarian cancer Breast cancer Pancreatic cancer	Olaparib Olaparib Olaparib	(Verma et al., 2021)
11	Hewitt	2021	HAP1	Leukaemia	Olaparib	(Hewitt et al., 2021)
12	Fugger	2021	HAP1	Leukaemia	Olaparib	(Fugger et al., 2021)
13	Tsujino	2022	Multiple*	Prostate cancer	Olaparib	(Tsujino et al., 2022)
14	Jamal	2022	Multiple*	Multiple	Olaparib	(Jamal et al., 2022)

Note: *Multiple cell lines were used for the CRISPR knockout screen and the authors provided a list of high-confidence candidate genes (detected in at least two cell lines). The lists of high-confidence genes were used for the systematic analysis in this study.

A



B **Pathway enrichment analysis** (n = 215)

Enriched pathways	Fold enrichment	False discovery rate
S phase or G1/S transition	2.9 – 8.6	< 0.05
Cell cycle	2.2 – 5.3	< 0.05
DNA replication	3.3 – 11.8	< 0.05
RNA metabolism	4 – 6.7	< 0.05
DNA repair	2.7	0.13 (p-value < 0.001)

Figure 6.7. Indisulam downregulates genes known to increase PARP inhibitor response upon depletion.
(A) A Venn diagram showing the overlaps between PARP inhibitor sensitivity determinants (high-confidence candidate genes, detected in at least two independent CRISPR-based PARP inhibitor sensitivity screens) with genes downregulated at protein levels by indisulam. It shows that 215 genes downregulated by indisulam may contribute to increased PARP inhibitor response. Most of them (73%) were also downregulated when indisulam was combined with olaparib. **(B)** Pathway enrichment analysis of the 215 genes identified in (a). The GOBP, REACTOME, KEGG, and WIKIPATHWAY databases were used, and all proteins detected in the proteomics were used as a background for enrichment analysis. Related pathway terms are grouped and the minimum and maximum fold enrichment values are shown.

Chapter 6

6.3. The ID8 model recapitulates indisulam-mediated splicing and proteomic changes in human HGSOC cells

The HR-proficient model of murine HGSOC cell line ID8-*Trp53*$^{-/-}$ has shown similar responses to the combination of indisulam and olaparib as the human HGSOC cell lines *in vitro* (Chapters 3 and 4). Indisulam also improved olaparib response in mice bearing ID8-*Trp53*$^{-/-}$ cells (Chapter 4). With the recent RNA-sequencing and proteomics data, it is now possible to assess the validity of the ID8-*Trp53*$^{-/-}$ clone as a model for human HGSOC from the level of transcriptomic and proteomic changes.

In ID8-*Trp53*$^{-/-}$ cells treated with indisulam, proteomics analysis identified 942 downregulated proteins. Approximately 82% (770/942) were also targets of indisulam-mediated exon skipping or intron retention (Figure 6.8A), implying that indisulam modulates murine gene expression through splicing errors – the same way as we observed in human cells.

To evaluate whether indisulam causes similar splicing changes in ID8 cells as in KURAMOCHI cells, I converted the mouse gene names to their human gene homologs based on the homology class data downloaded from the Mouse Genome Informatics (http://www.informatics.jax.org). Because not all mouse genes are found in human, this conversion led to slight differences in the total number of genes or proteins used for comparative analysis (as noted in Figure 6.8).

I found that 6159 genes were commonly mis-spliced by ID8-*Trp53*$^{-/-}$ and KURAMOCHI cells in response to indisulam, accounting for 80% (6159/7681) of all mis-spliced genes in the ID8 clone (Figure 6.8B). In addition, 233 proteins downregulated by indisulam in KURAMOCHI cells were also downregulated by indisulam in ID8-*Trp53*$^{-/-}$ cells, which included six DNA repair proteins: Xrcc1, Fanci, Mlh1, 53bp1, Mgmt, and Pnkp (Figure 6.8C and Figure 6.9). Of the six DNA repair proteins commonly modulated by indisulam, Xrcc1, Fanci and Pnkp are known to improve PARP inhibitor sensitivity upon depletion (Clements et al., 2020, Blanck et al., 2020, Olivieri et al., 2020, Su et al., 2020, DeWeirdt et al., 2020, Juhász et al., 2020, Jamal et al., 2022, Tsujino et al., 2022, Noordermeer et al., 2018, Zimmermann et al., 2018, Fugger et al., 2021). Thus, these three DNA repair genes are more likely to contribute to the synergy between indisulam and olaparib.

Overall, indisulam showed similar impacts on ID8 transcriptome and proteome as that of KURAMOCHI cells, strengthening the argument that the ID8 model is a valuable model for HGSOC. Above findings also indicate that many of the splicing targets of RBM39 are evolutionally conserved between mouse and human.

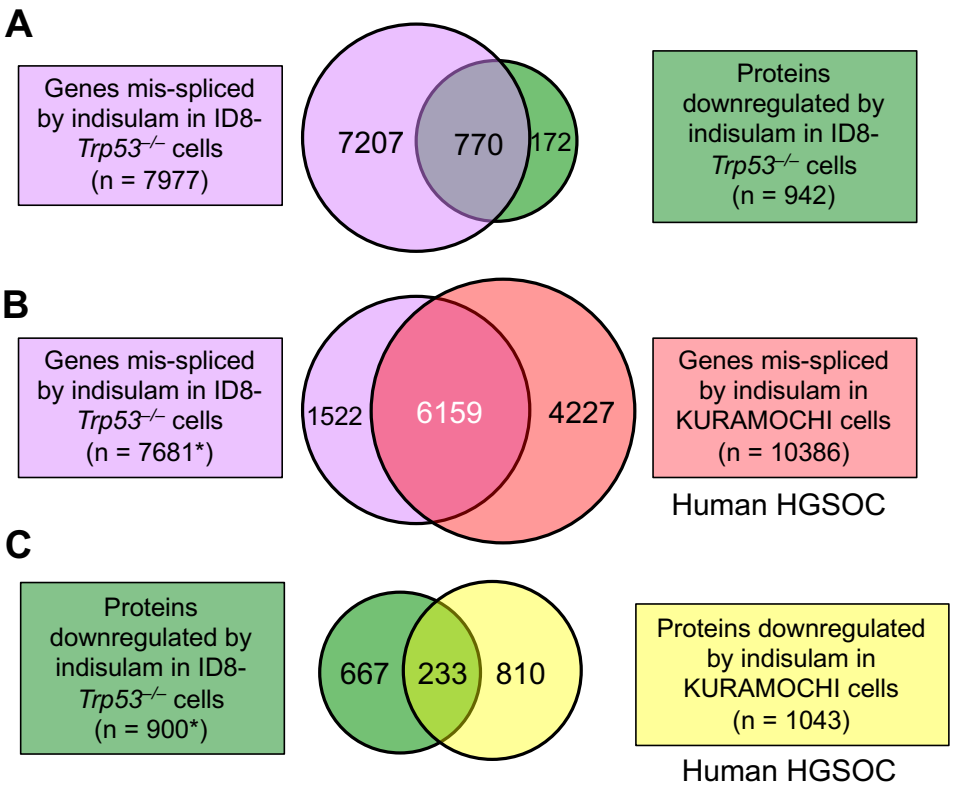


Figure 6.8. Indisulam causes similar effects in murine HGSOC cells as in human HGSOC cells.
(A) Venn diagram highlighting that 770 genes were downregulated at protein levels, which are also targets of indisulam-mediated mis-splicing in the ID8-*Trp53*$^{-/-}$ cells. **(B)** Venn diagram highlighting that 6159 genes were mis-spliced by indisulam in both KURAMOCHI and ID8-*Trp53*$^{-/-}$ cells. **(C)** Venn diagram showing 233 proteins were commonly downregulated by indisulam in mouse and human cells. Mis-splicing events in (a-b) only considered exon skipping and intron retention events. *Mouse genes were converted to their human gene equivalent before inter-species comparisons, and a small subset of mouse genes had no equivalent in the human genome.

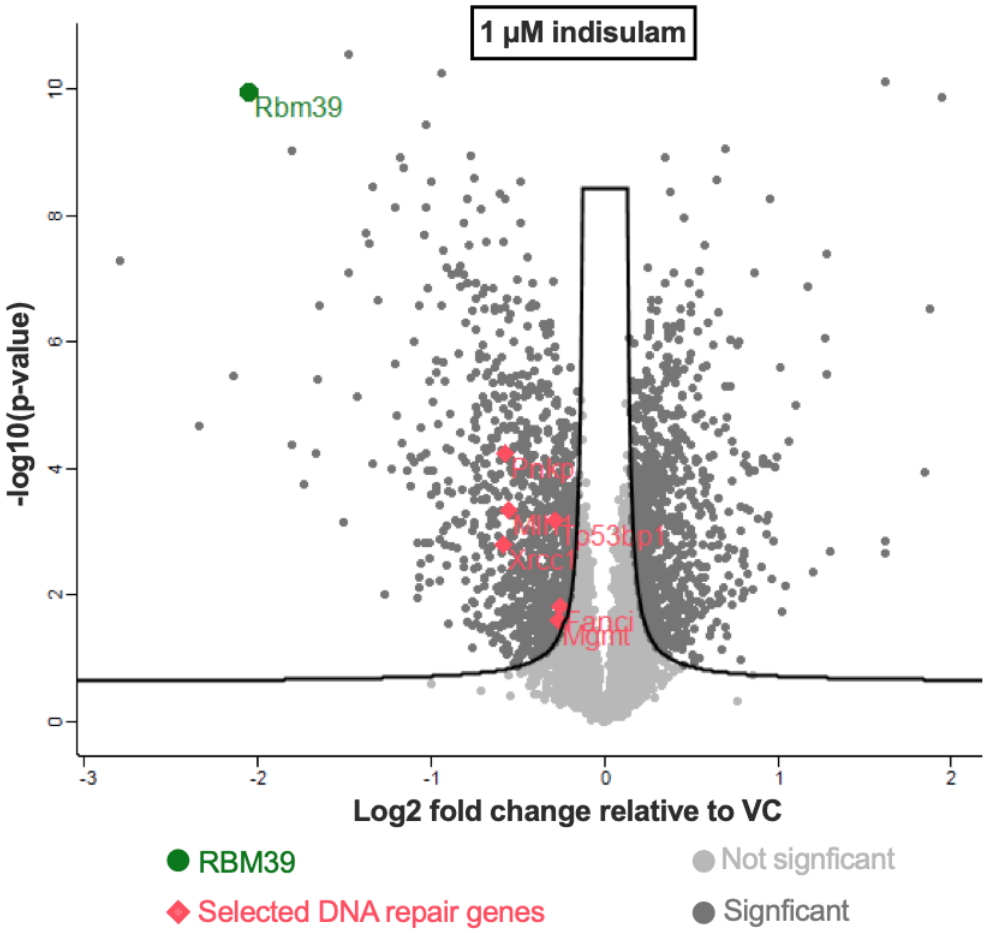


Figure 6.9. Indisulam downregulates six key DNA repair genes in ID8-*Trp53*$^{-/-}$ cells.
Volcano plot showing protein changes in ID8-*Trp53*$^{-/-}$ cells after 48-hour treatment of 10 µM indisulam. The x-axis indicates log2 fold change relative to vehicle control. RBM39 and six DNA repair proteins (consistently downregulated by indisulam in ID8 and KURAMOCHI cells) were highlighted. Proteins are shown in gene names. Differential protein expression analysis was performed by Dr Alex Montoya (two-tailed t-test, FDR < 0.05, S0 = 0.1).

Chapter 6

6.4. Olaparib may also modulate protein expression through splicing changes

Previous studies have implicated PARP1 in RNA splicing (Matveeva et al., 2016, Matveeva et al., 2019b, Matveeva et al., 2019a), and depleting PARP1 causes extensive splicing defects (Matveeva et al., 2016, Ke et al., 2021). This motivated me to investigate the impact of olaparib on alternative splicing in HGSOC cells.

Alternative splicing analysis of the RNA-sequencing data found exon skipping or intron retention events impacting 10073 genes in KURAMOCHI cells treated with olaparib, suggesting that olaparib disrupts PARP-mediated RNA splicing. Around 30% of the mis-spliced genes (3013/10073) were detectable in the proteomics, and 225 of them were downregulated at protein levels, contributing to 66% of all proteins downregulated by olaparib (Figure 6.10A). This finding suggests that olaparib may affect protein expression through splicing abnormalities, although the effect is weaker than indisulam (Figure 6.3B). Pathway enrichment analysis of the 225 genes mis-spliced and downregulated by olaparib found that 'translation factors' was the only significantly enriched pathway (fold enrichment = 6.46), suggesting a possibility that PARP may modulate the expression of translation factors.

Notably, 8534 genes were commonly mis-spliced by olaparib and indisulam (Figure 6.10B), indicating that PARP and RBM39 may cooperate in regulating alternative splicing. Examples of shared splicing targets include *ATM* and *TP53BP1*. To investigate if olaparib promotes RBM39-mediated splicing errors, I studied the splicing patterns of *ATM* (exons 52-53 skipping) and *TP53BP1* (exon 17 skipping) in KURAMOCHI cells following treatment of indisulam and olaparib individually or in combination. PCR analysis showed that the indisulam-mediated exon skipping variants of *ATM* and *TP53BP1* had the same abundance in the absence or presence of olaparib (Figure 6.11). This observation implies that PARP and RBM39 may independently modulate alternative splicing of the same gene or mediate RNA splicing of different regions within the same gene.

Overall, above findings demonstrate that olaparib may modulate gene expression through alternative splicing.

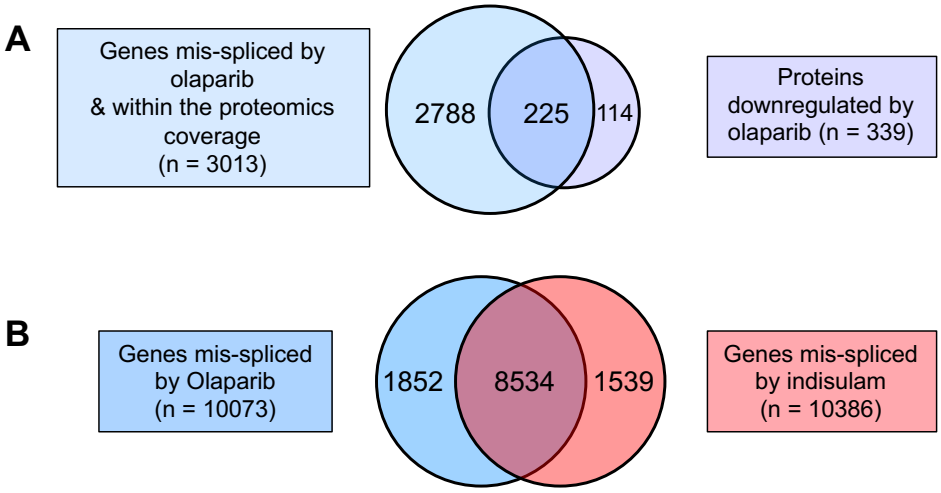


Figure 6.10. Overlap in genes where splicing is disrupted by olaparib and indisulam.
(A) A Venn diagram shows the overlaps between genes mis-spliced by olaparib (also within the proteomics coverage) and genes downregulated at protein levels upon olaparib treatment. **(B)** A Venn diagram showing the shared splicing targets between indisulam and olaparib. Only genes with exon skipping or intron retention events were included in (a-b).

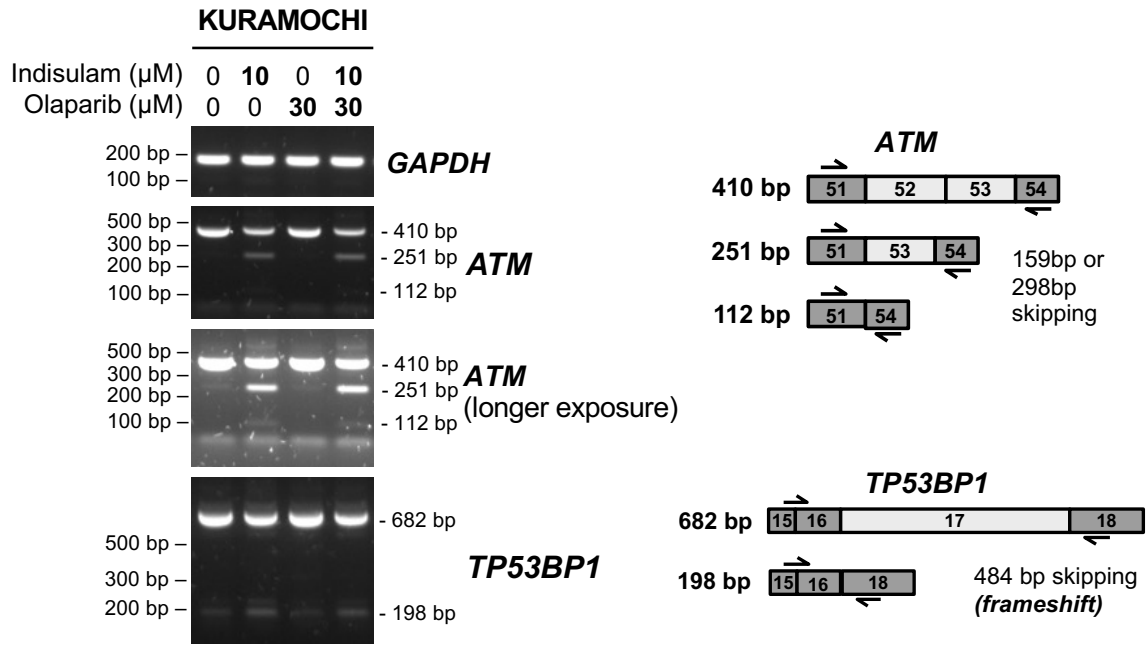


Figure 6.11. Olaparib and indisulam regulate different splicing events within the same gene target.
KURAMOCHI cells were treated with indicated drugs for 24 hours before PCR-based alternative splicing analysis (n = 1). Exon skipping of *ATM* and *TP53BP1* was detected by primers flanking the site of exon skipping (diagrams shown on the right). The same changes were also observed at 6, 24 and 72 hours (Appendix Figure 1B).

Chapter 6

6.5. Protein changes exclusive to the combination of indisulam and olaparib.

Another possible mechanism of synergy is that indisulam and olaparib may interact with each other and induce novel impacts on genes or pathways, leading to increased anti-cancer activities. To identify such protein changes, I compared the lists of proteins downregulated by indisulam, olaparib, and the combination of indisulam and olaparib. I found that 349 proteins were uniquely downregulated by the combination therapy (Figure 6.12A). Interestingly, 89 of them have been identified as modulators for PARP inhibitor sensitivity in previous dropout CRISPR screens (Figure 6.12A), providing a list of proteins that may contribute to the synergy between indisulam and olaparib. Pathway enrichment analysis showed that these 89 genes are significantly enriched for 'mRNA processing', implying that dual inhibition of PARP- and RBM39-mediated RNA splicing may cause excess stress on RNA metabolism.

Meanwhile, Chk1 depletion in KURAMOCHI cells treated with the combination of indisulam and olaparib was confirmed in the proteomics data and verified by western blot (Figure 6.12B-C). However, it is worth noting that in the initial data analysis by our collaborators, Chk1 was not listed as a significantly downregulated protein. This discrepancy was due to technical limitations in the analysis pipeline. Chk1 expression was too low to be detected in three out of five biological replicates, leading to it being excluded by the software before differential expression analysis. Therefore, detecting proteins behaving like Chk1 would require optimising the current pipeline of proteomics analysis.

In summary, above observations indicate that the action of indisulam and olaparib are not mutually exclusive, and they may alter the cancer cell proteome synergistically.

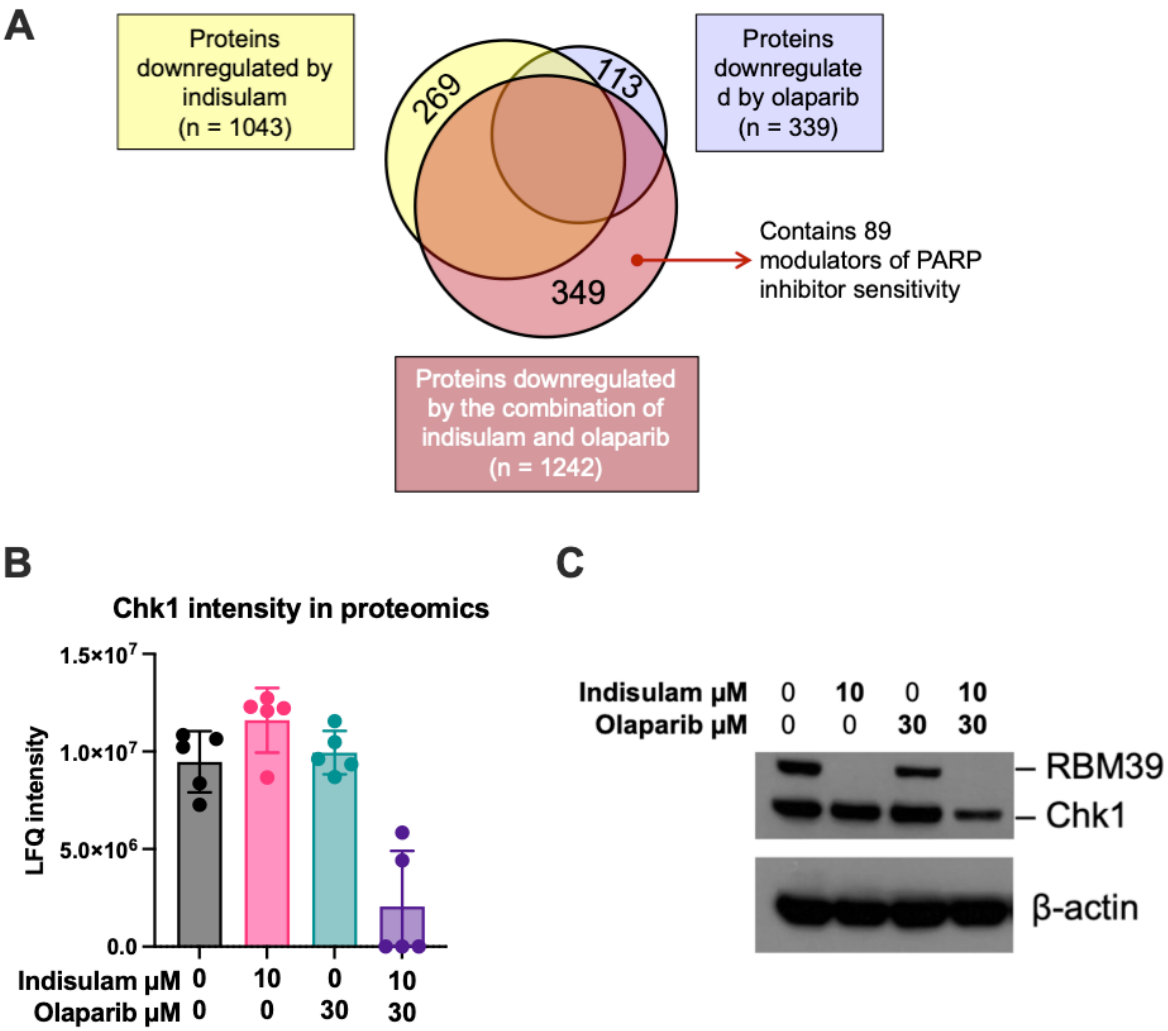


Figure 6.12. Identification of proteins exclusively downregulated by the combination of indisulam and olaparib including Chk1.

(A) A Venn diagram highlighting the number of proteins exclusively downregulated by the combination of indisulam and olaparib, but not by either monotherapy (n = 349). The 349 exclusively downregulated protein was compared with the previously identified modulators of PARP inhibitor sensitivity (Section 6.2.4). **(B)** Raw label-free quantification (LFQ) intensity of Chk1 detected in proteomics. KURAMOCHI cells were treated with indicated drugs for 48 hours before proteomics analysis. The error bars indicate SD. **(C)** Western blot verification of RBM39 and Chk1 expression levels within proteomics samples. All five biological replicates showed the same trend of changes and representative blots are shown here.

Chapter 6

6.6. Discussion

RBM39 is an essential splicing factor mediating the 3' splice site recognition during pre-mRNA splicing [reviewed in (Xu et al., 2020b)]. The genome-wide impact of RBM39 on alternative splicing has been characterised in multiple types of cancers (Mai et al., 2016a, Faherty et al., 2016, Han et al., 2017b, Kralovicova et al., 2018, Wang et al., 2019, Ting et al., 2019, Puvvula et al., 2021, Nijhuis et al., 2022, Lu et al., 2021b, Singh et al., 2021, Uehara et al., 2017), but not yet in ovarian cancer. With the help from other group members and external collaborators, we conducted global RNA sequencing and proteomics analyses using HGSOC cells treated with indisulam, olaparib, and the combination of these two agents, which provided valuable insights into the role of RBM39 in ovarian cancer and how depleting RBM39 might sensitise cells to PARP inhibitors.

In this chapter, I have shown that the splicing errors caused by indisulam preferentially disrupt cell cycle and DNA repair pathways. The same patterns of splicing changes have been found in other cancer types, including neuroblastoma (Singh et al., 2021, Nijhuis et al., 2022), acute myeloid leukaemia (Wang et al., 2019), melanoma (Lu et al., 2021b), and breast cancer (Mai et al., 2016a), suggesting a possible pan-cancer role of RBM39 in modulating splicing of cell cycle and DNA repair genes. Meanwhile, I found that over 90% of proteins downregulated in indisulam-treated cells showed splicing errors in corresponding genes, suggesting that alternative pre-mRNA splicing may be the main mechanism for RBM39 to modulate protein expression. It is plausible that indisulam reduces the abundance of canonical transcripts and increases the proportion of splicing variants with frameshifts or poison exons, thereby introducing premature stop codons and activating the nonsense-mediated decay (Pervouchine et al., 2019, Wang and Aifantis, 2020), eventually leading to lower protein expression.

Conceivably, some splicing defects may disrupt protein function without leading to protein level changes, in which case the defective protein may impair the activity of functional proteins achieving a dominant negative effect. In addition, a single pre-mRNA molecule may experience multiple alternative splicing events, and thus, the collective effect of all splicing changes in the transcript, rather than individual events, determines the fate and the function of the novel splicing variants. These research questions cannot be answered with the current

short-read RNA sequencing data alone. To address this issue, our laboratory has scheduled a long-read RNA sequencing analysis using sample-matched KURAMOCHI cells, which allows the identification of full-length splice variants and enable computational prediction of their functions. In addition, splice isoforms will be used to establish a KURAMOCHI-specific reference proteome, and the proteomics data will be reanalysed based on this customised database. This approach of proteogenomics is expected to uncover novel protein isoforms and/or neo-peptides that may contribute to anti-cancer activities of indisulam, as previously described (Miller et al., 2022, Lu et al., 2021b).

In the previous chapter (Chapter 5), I have shown that the combination of indisulam and olaparib involves cell cycle arrest at S and G2/M phases, DNA damage accumulation, and replication fork abnormalities. Here in this chapter, I employed targeted (focusing on DNA repair proteins) and untargeted approaches (comparison with previous PARP inhibitor sensitivity screen data) to identify protein changes potentially driving the synergy. I found that indisulam negatively regulates the expression of cell cycle, DNA repair, and DNA replication genes, most of which have shown synthetic lethal interaction with olaparib in the literature. Besides the evidence from CRISPR loss-of-function screens for PARP inhibitor sensitivity (Fugger et al., 2021, DeWeirdt et al., 2020, Blanck et al., 2020, Jamal et al., 2022, Hewitt et al., 2021, Tsujino et al., 2022, Zimmermann et al., 2018, Su et al., 2020, Noordermeer et al., 2018, Clements et al., 2020, Fang et al., 2019a, Juhász et al., 2020, Olivieri et al., 2020, Verma et al., 2021), PARP inhibitors have shown synergy with various inhibitors targeting cell cycle, DNA repair and DNA replication. Examples include the CDK4/6 inhibitor palbociclib (Yi et al., 2019, Zhu et al., 2021), WEE1 inhibitors (Ha et al., 2020, Fang et al., 2019b), Chk1/2 inhibitors (Brill et al., 2017, Smith et al., 2020, Anderson et al., 2011), ATR inhibitor AZD6738 (Lloyd et al., 2020), ATM inhibitors (Riches et al., 2020, Hong et al., 2016, Pike et al., 2018, Wang et al., 2017), and PARG inhibitors (Chen and Yu, 2019, Coulson-Gilmer et al., 2021, Pillay et al., 2019). Thus, indisulam might partially recapitulate the effect of these inhibitors, and the combined effect contributes to increased olaparib response in PARP-inhibitor-resistant HGSOC cells *in vitro* and *in vivo*. Collectively, above evidence favours the hypothesis that indisulam sensitises cells to PARP inhibitors by targeting the splicing of cell cycle, DNA repair, and DNA replication genes.

RNA sequencing data also suggest that the role of RBM39 seems conserved between human and mouse, because over 80% of the genes mis-spliced in the ID8 murine HGSOC cells (ID8-*Trp53*$^{-/-}$) were also mis-spliced in human HGSOC cells (KURAMOCHI). Similar findings have been reported in melanoma. Lu et al. (2021b) reported that two-thirds of genes mis-spliced by indisulam in mouse melanoma cells were also mis-spliced in human melanoma cells. The conserved role of RBM39 in both species may be attributed to the high sequence homology of RBM39 and the conserved splicing mechanisms. Murine Rbm39 is almost identical to the human RBM39 (Kang et al., 2015), and up to 74% of intron-exon junctions are conserved between human and mouse genomes (Thanaraj et al., 2003). Therefore, the similar splicing changes following indisulam treatment may be the reason why the synergy between indisulam and olaparib is effective in both human and murine HGSOC cells (Chapters 3 and 4).

Among the shared splicing targets of RBM39 in human and murine HGSOC cells, I identified a subset of genes commonly mis-spliced and downregulated by indisulam. These genes are more likely to explain the synergy between indisulam and olaparib than those only detected in one species. An outstanding candidate is FANCI because it is involved in both DNA damage repair and DNA replications stress. In addition to mediating the Fanconi anaemia repair of DNA inter-strand crosslinks (Smogorzewska et al., 2007), FANCI has been implicated in modulating replication origin firing, restarting stalled replication forks, and removing genotoxic DNA-RNA hybrids (R-loops) (Liang et al., 2019, Chen et al., 2015, Thompson et al., 2017). Knockdown or knockout of FANCI leads to an increase in stalled replication fork upon replication stress (Chen et al., 2015, Liang et al., 2019) and sensitises cells to PARP inhibitors (Blanck et al., 2020, DeWeirdt et al., 2020, Jamal et al., 2022, Su et al., 2020, Tsujino et al., 2022, Zimmermann et al., 2018, Noordermeer et al., 2018), which are phenotypically similar to the effect of indisulam. Preliminary data from our laboratory have validated indisulam-mediated exon skipping of FANCI (Dr Anke Nijhuis and Chiharu Wickremesinghe, personal communication, 18 August 2022) in KURAMOCHI cells and its involvement in the synergy between indisulam and olaparib will be studied in the future. In addition, it is important to examine splicing changes in a wider range of human and murine HGSOC cell models to understand how differences in genetic background, such as *BRCA*-deficiency and splicing factor mutations, may influence RBM39-modulated RNA splicing.

Chapter 6

A growing number of studies have implicated PARP1 in alternative splicing of pre-mRNAs. In *Drosophila* cells, Matveeva et al. (2016) found that PARP1 is co-immunoprecipitated with the core splicing factor SF3B1 and preferentially binds to the exon-intron boundaries. The authors also showed that knockdown or pharmacological inhibition of PARP1 caused alternative splicing in a broad range of genes (Matveeva et al., 2016). Recently, Ke et al. (2021) confirmed that PARP1 mediates alternative splicing in human cells. RNA sequencing data from this chapter provide additional evidence that PARP1 modulates alternative splicing in human cells, demonstrated by genome-wide splicing defects in KURAMOCHI cells. In another in-house RNA sequencing analysis, olaparib-mediated splicing abnormalities were detected in the human HGSOC cell line COV318 (unpublished data from Michael Gruet, personal communication, 6 October 2022).

Interestingly, I noticed that the majority of genes mis-spliced by olaparib were also mis-spliced by indisulam, suggesting a possibility that PARP1 and RBM39 might have converging roles in RNA splicing. Previous data suggests PARP1 and RBM39 may be in proximity in cells because immunoprecipitating RBM39 also pulled down PARP1 (Wang et al., 2019), and both of them physically interact with the core spliceosome component SF3B1 (Matveeva et al., 2016, Tari et al., 2019, Stepanyuk et al., 2016, Loerch et al., 2014). Furthermore, concurrent targeting multiple splicing factors is often detrimental to cancer cells. It has been reported that olaparib-sensitive cells may have increased reliance on splicing factors for cell survival (Blanck et al., 2020) and loss of splicing factor SF3B1 is synthetically lethal with olaparib treatment (Lappin et al., 2022). Indisulam is also preferentially cytotoxic to cells with existing defects in splicing factors (Han et al., 2017a, Wang et al., 2019) and acts synergistically with another splicing factor inhibitor SPHINX31, which targets the splicing factor SRSF protein kinase 1 (SRPK1) (Pogacar et al., 2022). These findings lead to an intriguing hypothesis that RBM39 and PARP1 may be in the same spliceosome complex, and simultaneous disruption of RBM39- and PARP1-mediated RNA splicing is synthetically lethal. In line with this hypothesis, DeWeirdt et al. (2020) reported that in the OVCAR8 ovarian cancer cells, loss of RBM39 is synthetically lethal with PARP inhibition or knockout. In the future, the interaction between RBM39 and PARP1 can be assessed using immunofluorescence and reciprocal immunoprecipitation. Analysing the KURAMOCHI RNA sequencing data at the level of individual splicing events will uncover shared splicing targets of RBM39 and PARP1, and

determine whether the combination of indisulam and olaparib causes more deleterious splicing defects than monotherapies.

Current proteomics data has two main limitations that can be improved in the future. Firstly, many DNA repair proteins, such as ATM, BRCA1 and RAD51 analogous, were not detected in the proteomics. The impact of RBM39 on DNA repair proteins was therefore underestimated in the pathway enrichment analysis. Another issue is that a subset of biologically meaningful protein changes, such as Chk1 depletion, were not included in the differential expression analysis due to very low abundance in some samples. The undesirable exclusion of these proteins would bias our interpretation of the proteomics data. To address these issues, the analysis pipeline will be reviewed and optimised to re-evaluate the coverage and to include all biologically relevant protein changes.

Overall, the RNA sequencing and proteomics data provide valuable insights into the anti-cancer effects of indisulam and olaparib individually or in combination. My findings favour the hypothesis that indisulam synergises with PARP inhibitors by causing splicing errors and reducing protein expression of DNA replication and repair genes. It is also possible that dual targeting of alternative splicing caused by RBM39 and PARP1 is synthetically lethal.

Chapter 7

Chapter 7. Final discussion and future directions

7.1. Current model for the synergy between indisulam and PARP inhibitor

High-grade serous ovarian cancer is one of the most aggressive subtypes of ovarian cancer with a poor survival rate and limited therapeutic options (ESMO, 2017, Cancer-research-UK, 2022b). Since the first approval in 2014 (FDA, 2014), PARP inhibitors have shown remarkable clinical benefits by delaying disease relapse and prolonging overall patient survival (reviewed in Section 1.2.3, Chapter 1). However, emerging drug resistance is a big challenge for PARP inhibitors. In patients with HR-deficient tumours, clinical studies have documented acquired drug resistance through reversion mutations (Barber et al., 2013, Gornstein et al., 2018, Kondrashova et al., 2017, Quigley et al., 2017, Weigelt et al., 2017, Goodall et al., 2017, Mayor et al., 2017, Lin et al., 2019, Christie et al., 2017, Wang et al., 2016) or expression of novel splice isoforms (Wang et al., 2016) that restore the HR repair. Several other resistance mechanisms have been identified in preclinical studies (reviewed in Section 1.2.5, Chapter 1). Despite active research to overcome PARP inhibitor resistance, no effective therapy has been approved for clinical use.

In this thesis, I present evidence that targeting RBM39-mediated RNA splicing is a promising strategy for enhancing PARP inhibitor response in HGSOC cells. My data suggest a model that RBM39 coordinates pre-mRNA splicing of many DNA repair and replication genes, thereby contributing to the adaptive response to PARP inhibitors (Figure 7.1A). Pharmacological depletion of RBM39 reduces the expression of these genes and weakens the DNA damage repair and replication stress response, accelerating the accumulation of genotoxic stress and conferring higher sensitivity to PARP inhibitors (Figure 7.1). This model is supported by recent data from a CRISPR screen that loss of RBM39 is synthetically lethal with PARP1 knockout or olaparib in OVCAR8 cells (DeWeirdt et al., 2020).

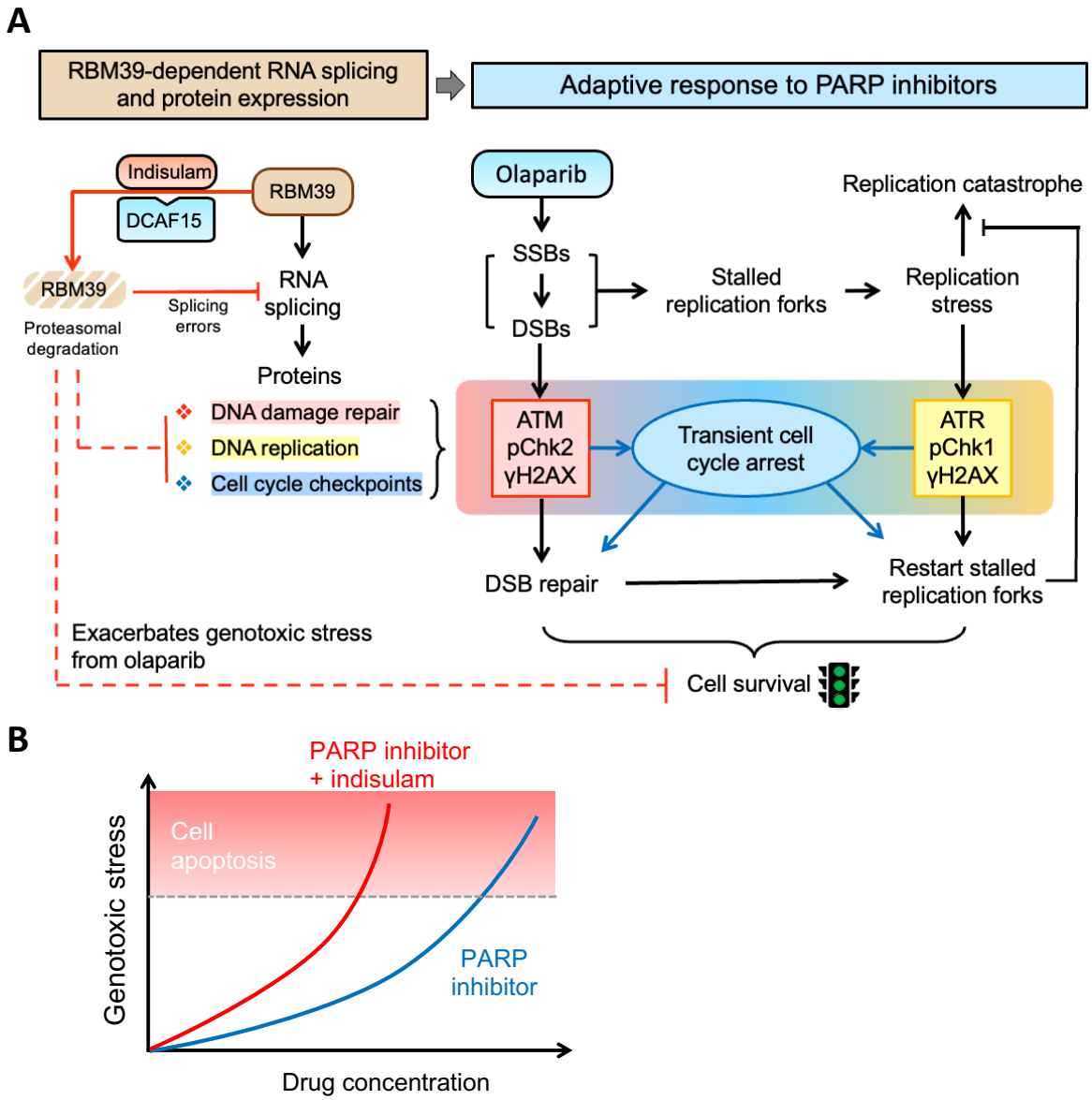


Figure 7.1. Indisulam increases PARP inhibitor response by disrupting RBM39-mediated splicing. **(A)** A working model for the synergy between indisulam and PARP inhibitor olaparib. RBM39 coordinates the splicing of many genes involved in DNA damage repair, DNA replication, and cell cycle checkpoints. Genes in these three pathways contribute to the adaptive response to olaparib by repairing DNA damage, resolving replication stress, and preventing premature cell cycle progression. In the presence of indisulam, RBM39 is degraded through the DCAF15-associated E3 ubiquitin ligase complex, leading to abnormal pre-mRNA splicing in DNA repair, DNA replication, and cell cycle genes. The splicing errors translate to reduced protein expression and a weaker adaptive response to olaparib, thereby causing synergistic growth inhibition and apoptosis. Dashed lines indicate indirect effects. **(B)** A simplified model for the synergy between indisulam and PARP inhibitor (taken from Figure 5.12 in Chapter 5). In comparison with olaparib monotherapy, the combination of indisulam and olaparib accelerates the accumulation of genotoxic stress (DNA damage and replication fork abnormalities) and cell apoptosis.

Chapter 7

RBM39 is selectively degraded by a panel of molecular glues such as indisulam (Uehara et al., 2017, Ting et al., 2019, Han et al., 2017b). I have shown that indisulam improves PARP inhibitor response in HGSOC cells *in vitro* and *in vivo* (Chapters 3 and 4). In comparison with olaparib monotherapy, the combination of indisulam and olaparib led to synergistic growth inhibition (Figure 3.4), cell apoptosis (Figure 3.4), and reduced colony growth (Figure 3.5). Furthermore, the addition of indisulam considerably enhanced the survival benefits of olaparib in mice bearing HR-proficient HGSOC tumours, and a small proportion of mice experienced complete tumour regression, which was not observed when olaparib was used alone (Figure 4.7). These findings suggest that indisulam in combination with olaparib is an effective combination strategy for HR-proficient HGSOC.

The proposed model of the synergy (Figure 7.1) is best exemplified in the KURAMOCHI cell line, a highly representative *BRCA2*-deficient HGSOC cell line (Domcke et al., 2013) with intrinsic PARP inhibitor resistance (Figure 3.2) (Coulson-Gilmer et al., 2021, Pillay et al., 2019, Kim et al., 2020). In KURAMOCHI cells, olaparib (30 μM for 48 hours) was enough to increase DNA damage (Figures 5.4 and 5.5), but was not sufficient to cause replication fork abnormalities (Figure 5.9) and cell apoptosis (Figure 3.4), suggesting that cells were able to resolve or tolerate olaparib-induced DNA damage. In the presence of indisulam, olaparib caused severe genotoxic stress, shown by significantly higher levels of DNA damage and replication fork abnormalities (Figures 5.4, 5.7, and 5.9), followed by a substantial increase in cell apoptosis (Figure 3.4).

Mechanistically, DCAF15-mediated RBM39 degradation is a key event driving the synergy between indisulam and olaparib, because CRISPR-Cas9-mediated knockout of *DCAF15* in PEO1 cells abrogated the synergistic growth inhibition and the effect of indisulam was recapitulated by E7820, another RBM39 degrader (Figure 3.8). RBM39 degradation was detected in tumour samples, confirming the target engagement of indisulam *in vivo* (Figure 4.4D). Transcriptome-wide alternative splicing analysis demonstrated that indisulam-mediated RBM39 degradation causes preferential splicing errors in DNA damage repair, DNA replication, and cell cycle genes, correlating with lower protein expression in proteomics (Chapter 6). According to recent CRISPR sensitivity screens (summarised in Table 6.2), many of the indisulam-modulated genes are involved in the adaptive response PARP inhibitor response and depleting these genes sensitises cells to PARP inhibitors (Figure 6.5 and Table

6.1). I have validated indisulam-induced exon skipping of several key DNA repair genes (Figure 3.2), including *ATM*, *TP53BP1*, *RIF1*, *BRCA1*, and *RAD51D*, and downregulation of ATM *in vitro* and *in vivo* (Figures 5.2 and 5.11). Western blot analysis indicates that indisulam attenuates olaparib-induced activation of the ATM-Chk2 and Chk1 pathways (Figure 5.2), followed by increased DNA damage (Figures 5.4, 5.5, and 5.7), slower DNA replication (Figure 5.8C), unscheduled firing of replication origins (Figure 5.9), and cell cycle arrests in S and G2/M phases (Figure 5.8). The synergistic induction of γH2AX expression in HGSOC cell lines and in tumour samples (Figures 5.5 and 5.11) further demonstrates that the combination therapy increases overall genotoxic stress level.

It is worth highlighting that indisulam synergised with olaparib in multiple HGSOC cell lines (both human and the murine ID8 models) irrespective of *BRCA* status (Figure 3.7 and 4.2). The independence of *BRCA* status may be partially explained by the finding that indisulam downregulates the expression of DNA repair proteins upstream of BRCA-mediated HR repair such as ATM (Figures 5.2, 5.11, and 6.5). In addition, indisulam disrupts other genotoxic stress response pathways, such as 53BP1-mediated NHEJ and replication stress response, which may also lead to BRCA-independent synergy with PARP inhibitors (Figure 6.5). For example, inhibitors targeting NHEJ or replication stress response, such as DNA-PK inhibitor AZD7648 (Fok et al., 2019), ATR inhibitor AZD6738 (Gralewska et al., 2020, Lloyd et al., 2020), and Chk1 inhibitor MK8776 (Gralewska et al., 2020), have shown synergistic interaction with PARP inhibitors regardless HR proficiency in preclinical studies.

Indisulam also synergised with other PARP inhibitors, including the least potent PARP trapper veliparib (Figure 3.6C) (Murai et al., 2012, Murai et al., 2014, Hopkins et al., 2015). Therefore, a potent PARP trapping ability may not be essential for the synergistic interaction with indisulam.

Taken together, these data indicate that a wide range of ovarian cancer patients may benefit from the combination therapy irrespective of their *BRCA* status and regardless of which PARP inhibitor they are taking. Nonetheless, from a clinical perspective, patients with DCAF15-amplified and HR-deficient tumours may have a larger therapeutic window for this combination therapy, because the synergistic benefit can be achieved with lower doses of indisulam and PARP inhibitors.

Chapter 7

7.2. Gaps and future directions

7.2.1. What markers may predict the response of indisulam and its synergy with PARP inhibitors?

Identifying markers that predict the therapeutic response is vital for precision medicine. Although PARP trapping efficacy (Murai et al., 2012, Murai et al., 2014, Hopkins et al., 2019, Hopkins et al., 2015) and HR proficiency (Bryant et al., 2005, Farmer et al., 2005) both correlate with PARP inhibitor toxicity, they did not predict the synergistic interaction between indisulam and PARP inhibitor, as discussed in Section 7.1.

On the other hand, I have shown that DCAF15 expression is necessary for indisulam cytotoxicity and the synergy with PARP inhibitors, but whether DCAF15 abundance is sufficient to predict indisulam sensitivity is still unclear. Several preclinical studies demonstrate that DCAF15 levels positively correlate to indisulam sensitivity in neuroblastoma (Singh et al., 2021, Nijhuis et al., 2022) and in blood cancer cells (Han et al., 2017b). However, a recent study reported that, in patient-derived acute myeloid leukaemia cells, higher *DCAF15* mRNA expression did not lead to faster RBM39 degradation by indisulam (Hsiehchen et al., 2020). Hsiehchen et al. (2020) proposed that RBM39 degradation kinetics and the occurrence of splicing defects might be better markers for indisulam sensitivity. Little evidence is available in the context of HGSOC, and whether DCAF15 predicts indisulam sensitivity in HGSOC cell lines and in patient samples should be studied in the future. More importantly, future studies are needed to assess whether higher DCAF15 expression leads to increased efficacy of the synergy between indisulam and PARP inhibitor.

Expression and mutational status of spliceosome components are also candidates for predictive markers for indisulam-based therapies. Splicing factors often have redundant roles in alternative splicing (Hastings et al., 2007). Mai et al. (2016a) reported that RBM39 and U2AF65 share more than 20% of splicing targets, and they recognise a consensus intronic motif. Redundance between RBM39 and PUF60 has also been documented (Kralovicova et al., 2018). Notably, cancer cells with splicing factor mutations are more sensitive to indisulam-mediated RBM39 depletion (Wang et al., 2019). Collectively, these observations suggest a possibility that RBM39 dependency and indisulam toxicity are affected by other spliceosome components. Thus, how other splicing factors affect sensitivity to indisulam-based therapies

is worth investigating in the future, which may uncover novel markers for patient stratification.

It is worth noting that the Chou-Talalay method used in this study does not allow direct comparisons of synergy potency between drug combinations and across genetic backgrounds, which limits the discovery of biomarkers for combination therapies. This is because the CI index only indicates drug-drug interaction at selected dose combinations and cannot be generalised to all combination doses (Chou and Martin, 2005, Chou, 2010). Thus, future studies should seek alternative synergy models that quantify the synergy efficacy of drug combinations. One good alternative is the BRAID synergy model (Twarog et al., 2016). It not only measures synergy potency, but also allows prediction of the therapeutic window using the IAE index (discussed in Appendix Discussion), which is more clinically relevant (Twarog et al., 2016, Twarog et al., 2020).

7.2.2. Does indisulam reduce DNA damage repair capacity?

I have shown that indisulam treatment causes splicing errors in DNA repair genes, attenuates the ATM-Chk2 signalling, and increases DNA damage gradually, implying that indisulam-treated cells may have impaired DNA damage repair response. However, I have not directly confirmed that indisulam-treated cells had reduced DNA damage repair capacity. This can be tested by quantifying cellular DNA repair activity using *I-SceI*-based reporter assays, as discussed in Section 5.4.4. The neutral COMET assay should also be optimised in the future to determine if indisulam promotes olaparib-induced DSB formation. Alternatively, cells can be pre-treated with indisulam before pulsing with irradiation. Repair of radiation damage at slower kinetics would indicate indisulam-treated cells have defective DNA damage response.

7.2.3. Does the combination of indisulam and olaparib cause replication catastrophe?

Another weak point in my thesis is the limited research on replication stress. Firstly, the DNA fibre analysis should be repeated to ascertain my findings. Secondly, the possibility that replication catastrophe contributes to the synergy between indisulam and olaparib is worth investigating. This hypothesis is based on the observation that the addition of indisulam to olaparib inhibited the Chk1 signalling and caused excessive new origin firing, which might result in RPA exhaustion and accelerated replication catastrophe (Toledo et al., 2017, Toledo et al., 2013). As replication catastrophe leads to cell death in the S phase (Toledo et al., 2013),

cell cycle analysis can be coupled with either γH2AX staining or Annexin V staining. A pan-nuclear colocalization of γH2AX and RPA in immunofluorescence would also indicate replication catastrophe (Toledo et al., 2017, Toledo et al., 2013). The involvement of RPA exhaustion can be ascertained by investigating whether overexpression of RPA subunits protects cells from replication catastrophe (Toledo et al., 2013). Finally, the cell cycle progression of individual cells can be tracked using time-lapse imaging techniques such as the IncuCyte, as previously described (Pillay et al., 2019, Coulson-Gilmer et al., 2021). This would differentiate prolonged cell cycle arrests from transient cell cycle arrests and provide direct evidence of replication catastrophe.

7.2.4. How important are ATM and Chk1 changes in the synergy?

The splicing errors caused by indisulam seem to affect a wide range of genes, and many of them might have contributed to increased olaparib sensitivity. However, it is possible that some splicing changes are more important than others. Given the pivotal roles of ATM and Chk1 in DNA repair and replication fork protection, respectively, it is reasonable to deduce that downregulated expression of ATM and Chk1 may be driving factors for the synergy between indisulam and olaparib. However, I have not acquired direct evidence showing that protein changes of ATM and Chk1 contribute to higher levels of DNA damage and replication stress. A rescue experiment is therefore needed to validate if restoring ATM and/or Chk1 expression confers (at least partial) resistance to the combination therapy of indisulam and olaparib. Transfecting cells with plasmids containing cDNAs of target genes should bypass the indisulam-caused splicing errors and restores protein expression. A partial rescue would indicate the involvement of other genes, and additional rescue experiments should be conducted to examine their importance in the synergy.

Notably, if mis-splicing of *ATM* and *Chk1* is indeed vital for the indisulam to synergise with PARP inhibitors, the level of deleterious splicing variants of *ATM* and *Chk1* may qualify as biomarkers for the combination therapy response.

7.2.5. Does indisulam-induced splicing errors generate novel protein isoforms and neoantigens?

As mentioned in Chapter 6 (Section 6.6.), a proteogenomics project has been scheduled to identify splicing variants and corresponding protein isoforms in HGSOC cells following drug

treatment. This project is an integrated analysis utilising sample-matched long-read RNA sequencing data (work in progress), short-read RNA sequencing data (Chapter 6), and the proteomics data (Chapter 6), to identify mRNA variants, computationally construct a cell-specific proteomics reference library, and determine the expression of protein isoforms by re-mapping peptides detected in the proteomics analysis. This project was inspired by the proteogenomics research of Dr Gloria Sheynkman (Sheynkman et al., 2016, Miller et al., 2022). This approach should facilitate the identification of novel splice variants and protein isoforms that may contribute to anti-cancer activities of indisulam, olaparib, and the combination therapy.

Moreover, the proteogenomics project may uncover indisulam-dependent expression of immunogenic peptides. Recently, Lu et al. (2021b) demonstrated that splicing errors induced by indisulam lead to the production of neoepitopes that are sufficiently immunogenic to trigger a T cell response in mice. Notably, indisulam may trigger an immune response independent of RBM39. Pech et al. (2019) reported that indisulam alters the substrate specificity of DCAF15 and increases the expression of surface antigen presenting molecules, leading to enhanced recognition and killing by natural killer cells. Thus, it is possible that, in the immuno-proficient ID8 HGSOC model, the substantial improvement of overall survival by indisulam might involve increased expression of neo-epitopes and enhanced anti-tumour immune response. This hypothesis will be tested in the future with the help of our collaborators, who specialise in immunology.

7.2.6. Does RBM39 interact directly with PARP1?

Literature evidence implies an intriguing possibility that RBM39 may directly interact with PARP1 (Wang et al., 2019). In the future, immunostaining, DUOlink proximity ligation assay, and reciprocal immunoprecipitation techniques can be used to assess the physical interaction between RBM39 and PARP1. Even if RBM39 and PARP1 do not interact directly, they may cooperate in modulating pre-mRNA splicing, as indicated by a large proportion of common splicing targets in the transcriptome-wide RNA sequencing analysis (Figure 6.10). Therefore, it is important to characterise the impact of olaparib on pre-mRNA splicing in the presence and absence of indisulam. With the help of the proteogenomics analysis (Section 7.2.5), novel

splicing variants can be identified, which may have contributed to the unique protein changes or phenotypes in cells receiving the combination therapy (indisulam plus olaparib).

7.2.7. Could indisulam increase PARP inhibitor response by depleting the nucleotide pool?

Although I found abundant evidence suggesting that indisulam impacts mis-splicing of DNA damage and replication stress response, I cannot rule out the involvement of other splicing changes in the combination therapy response. In our recent publication, Nijhuis et al. (2022) demonstrated that indisulam depletes nucleotide pools in neuroblastoma cells through DCAF15-mediated RBM39 degradation. In my analysis, I also found that splicing and expression of metabolic pathways were negatively affected by indisulam (Figure 6.3). Furthermore, our untargeted analysis on the RNA sequencing data by Dr Marc P. Lorentzen highlighted that indisulam may affect mRNA expression of metabolic genes more than DNA damage repair genes (unpublished data, personal communications, 02 December 2022). This observation suggests a possibility that indisulam may sensitise cells to PARP inhibitors by modulating cell metabolism. This new hypothesis does not contradict my primary hypothesis because metabolic changes can disrupt DNA damage repair and increase PARP inhibitor response (Bajrami et al., 2012). In the future, the impact of indisulam and olaparib on cell metabolism can be quantified using LC-MS. Alternative splicing and expression of key metabolic genes should also be validated.

Alternatively, indisulam may alter cell metabolism by depleting the nucleotide pool and sequestering nucleotides in defective splicing products. This is an intriguing hypothesis worth investigating in the future. Drugs targeting the nucleotide metabolism have shown synergistic interaction with PARP inhibitors in early studies (Bajrami et al., 2012) and in our laboratory (unpublished data from Michael Gruet). The effect of indisulam on nucleotide availability can be quantified by measuring the nucleotide pools in cells using LC-MS. A nucleotide rescue experiment can be conducted to assess if an exogenous source of nucleotides protects cells from indisulam and the combination therapy of indisulam and olaparib.

7.2.8. Does the synergy involve RBM39 as a transcriptional coregulator?

Although RBM39 is often seen as a splicing factor, it also functions as a transcriptional coactivator promoting the activity of multiple transcription factors, as discussed in my recent review article (Xu et al., 2020b). By degrading RBM39, indisulam may reduce activities of

RBM39-interacting transcription factor, contributing to some of the protein changes in the proteomics. This field is still poorly understood, mostly due to the difficulty of uncoupling RBM39-mediated alternative splicing from transcriptional coactivation. However, this is not entirely impossible. RBM39-derived competitive peptides have been developed recently, which disrupt the interaction of RBM39 with selected targets without affecting RBM39-mediated pre-mRNA splicing (Chilewski et al., 2020, Puvvula et al., 2021). Following this approach, future studies may be able to differentiate the effect of RBM39 on transcriptional coregulation from RNA splicing.

7.2.9. Other limitations and future works

One caveat in this project is that most of the mechanistic investigation, such as quantification of DNA damage, cell cycle distribution, and replication stress, was conducted in KURAMOCHI cells, a cell line with uncharacterised resistance mechanisms to PARP inhibitors. Since KURAMOCHI cells tolerated olaparib-induced DNA damage without triggering cell apoptosis, activation of alternative DNA repair pathways or increased tolerance of DNA damage are plausible resistance mechanisms [reviewed in (Ghosal and Chen, 2013)]. Besides investigating the resistance mechanism in KURAMOCHI cells, it is important to repeat the cell cycle and DNA fibre analysis in other cell lines to ascertain that the observations in KURAMOCHI cells are reproducible in other HGSOC cell lines.

Another limitation is that a comprehensive pharmacodynamic analysis has not been conducted to assess the impact of indisulam, olaparib, and the combination of indisulam and olaparib *in vivo*. Future analysis should examine the target engagement of indisulam and olaparib in tumours using immunohistochemistry or immunofluorescence. Mis-splicing of key targets, such as *ATM*, should also be validated in tumour samples. Anti-tumour activities can be assessed using the proliferation marker Ki67, as previously described (Walton et al., 2016). Since indisulam caused unexpected toxicity in mice, future animal studies should characterise the safety profiles of indisulam to inform the design of safe dosing schedules.

Although the ID8 HGSOC model used in this study faithfully recapitulated peritoneal metastasis of human HGSOC in immune-competent mice, it did not originate from the fallopian tube as most human HGSOC did (Roby et al., 2000, Walton et al., 2016). Therefore, the combination therapy of indisulam and olaparib should be tested using additional animal

models of HGSOC and possibly in patient-derived xenografts or organoids, as discussed in Section 4.4.

7.3. Concluding remarks

In recent years, alternative splicing has been recognised as a valuable target in cancer, but most spliceosome components have no enzymatic activities and are very challenging to drug with conventional inhibitors. The recent rediscovery of anti-cancer aryl sulphonamides as molecular glues targeting the splicing factor RBM39 provides a promising approach to disrupting pre-mRNA splicing in cancer cells.

This thesis presents evidence that RBM39 modulates alternative splicing of DNA repair genes across multiple cancer types and mediates the adaptive response to PARP inhibitors via coordinating correct RNA splicing. These findings provide novel insights into the role of RBM39 in cancer cells. Importantly, indisulam-mediated RBM39 degradation improves PARP inhibitor response by inhibiting the expression of DNA repair genes and suppressing the olaparib-induced activation of ATM-Chk2 and Chk1 signalling pathways. As a result, concomitant exposure to indisulam and olaparib leads to DNA damage accumulation, replication abnormalities, and cell cycle arrests. Using a series of HGSOC models, I demonstrate that the combination therapy causes synergistic growth inhibition and cell apoptosis *in vitro* and significantly prolongs the overall survival of mice with HGSOC tumours *in vivo*. Collectively, these findings support RBM39 as a valuable therapeutic target in cancer, and pharmacological depletion of RBM39 sensitises cells to PARP inhibitors in HGSOC. Adding RBM39 degrader to PARP inhibitor maintenance therapy may benefit a wide range of ovarian cancer patients, especially those with high *DCAF15* expression.

Since the safety profiles and pharmacokinetics of indisulam have been characterised in multiple clinical trials, the combination of indisulam and olaparib could progress rapidly into advanced clinical trials. Other cancer types, such as colorectal cancer, *MYCN*-amplified neuroblastoma, and acute myeloid leukaemia, may also benefit from the combination therapy of indisulam and olaparib because of high RBM39-dependency. Additionally, this project suggests several other strategies worth investigating in the future, such as combining indisulam with platinum agents, topoisomerase inhibitors, or immunotherapy. Overall, this

thesis highlights the promising therapeutic value of splicing factors as cancer targets. Developing indisulam-derived molecular glues or proteolysis-targeted chimaeras may provide additional tools to target splicing factors besides RBM39.

References

ABAL, M., ANDREU, J. M. & BARASOAIN, I. 2003. Taxanes: microtubule and centrosome targets, and cell cycle dependent mechanisms of action. *Curr Cancer Drug Targets,* 3**,** 193-203.

ABBATE, F., CASINI, A., OWA, T., SCOZZAFAVA, A. & SUPURAN, C. T. 2004. Carbonic anhydrase inhibitors: E7070, a sulfonamide anticancer agent, potently inhibits cytosolic isozymes I and II, and transmembrane, tumor-associated isozyme IX. *Bioorg Med Chem Lett,* 14**,** 217-23.

ACEYTUNO, R. D., PIETT, C. G., HAVALI-SHAHRIARI, Z., EDWARDS, R. A., REY, M., YE, R., JAVED, F., FANG, S., MANI, R., WEINFELD, M., HAMMEL, M., TAINER, J. A., SCHRIEMER, D. C., LEES-MILLER, S. P. & GLOVER, J. N. M. 2017. Structural and functional characterization of the PNKP-XRCC4-LigIV DNA repair complex. *Nucleic Acids Res,* 45**,** 6238-6251.

AFANAS'EVA, K. S., ZAZHITSKAIA, M. O. & SIVOLOB, A. V. 2009. [Mechanisms of DNA exit during neutral and alkaline comet assay]. *Tsitol Genet,* 43**,** 3-7. English version: https://biology.univ.kiev.ua/images/stories/Upload/Genetiky/mechanisms%20of%20dna%20exit%20during%20neutral%20and%20alkaline%20comet%20assay.pdf.

AGUILAR-QUESADA, R., MUÑOZ-GÁMEZ, J. A., MARTÍN-OLIVA, D., PERALTA, A., VALENZUELA, M. T., MATÍNEZ-ROMERO, R., QUILES-PÉREZ, R., MURCIA, J. M.-D., DE MURCIA, G., DE ALMODÓVAR, M. R. & OLIVER, F. J. 2007. Interaction between ATM and PARP-1 in response to DNA damage and sensitization of ATM deficient cells through PARP inhibition. *BMC Molecular Biology,* 8**,** 29.

AHEL, D., HOREJSÍ, Z., WIECHENS, N., POLO, S. E., GARCIA-WILSON, E., AHEL, I., FLYNN, H., SKEHEL, M., WEST, S. C., JACKSON, S. P., OWEN-HUGHES, T. & BOULTON, S. J. 2009. Poly(ADP-ribose)-dependent regulation of DNA repair by the chromatin remodeling enzyme ALC1. *Science,* 325**,** 1240-3.

AHMAD, A., ROBINSON, A. R., DUENSING, A., VAN DRUNEN, E., BEVERLOO, H. B., WEISBERG, D. B., HASTY, P., HOEIJMAKERS, J. H. & NIEDERNHOFER, L. J. 2008. ERCC1-XPF endonuclease facilitates DNA double-strand break repair. *Mol Cell Biol,* 28**,** 5082-92.

AHN, J. Y., SCHWARZ, J. K., PIWNICA-WORMS, H. & CANMAN, C. E. 2000. Threonine 68 phosphorylation by ataxia telangiectasia mutated is required for efficient activation of Chk2 in response to ionizing radiation. *Cancer Res,* 60**,** 5934-6.

ALEMASOVA, E. E. & LAVRIK, O. I. 2019. Poly(ADP-ribosyl)ation by PARP1: reaction mechanism and regulatory proteins. *Nucleic acids research,* 47**,** 3811-3827.

ALKEMA, N. G., TOMAR, T., VAN DER ZEE, A. G., EVERTS, M., MEERSMA, G. J., HOLLEMA, H., DE JONG, S., VAN VUGT, M. A. & WISMAN, G. B. 2014. Checkpoint kinase 2 (Chk2) supports sensitivity to platinum-based treatment in high grade serous ovarian cancer. *Gynecol Oncol,* 133**,** 591-8.

AMATA, I., MAFFEI, M. & PONS, M. 2014. Phosphorylation of unique domains of Src family kinases. *Front Genet,* 5**,** 181.

AN, J., HUANG, Y.-C., XU, Q.-Z., ZHOU, L.-J., SHANG, Z.-F., HUANG, B., WANG, Y., LIU, X.-D., WU, D.-C. & ZHOU, P.-K. 2010. DNA-PKcs plays a dominant role in the regulation of

References

H2AX phosphorylation in response to DNA damage and cell cycle progression. *BMC Molecular Biology,* 11**,** 18.

ANDERSON, V. E., WALTON, M. I., EVE, P. D., BOXALL, K. J., ANTONI, L., CALDWELL, J. J., AHERNE, W., PEARL, L. H., OLIVER, A. W., COLLINS, I. & GARRETT, M. D. 2011. CCT241533 is a potent and selective inhibitor of CHK2 that potentiates the cytotoxicity of PARP inhibitors. *Cancer research,* 71**,** 463-472.

ANTOLIN, A. A., AMERATUNGA, M., BANERJI, U., CLARKE, P. A., WORKMAN, P. & AL-LAZIKANI, B. 2020. The kinase polypharmacology landscape of clinical PARP inhibitors. *Scientific Reports,* 10**,** 2585.

ANTOLÍN, A. A. & MESTRES, J. 2014. Linking off-target kinase pharmacology to the differential cellular effects observed among PARP inhibitors. *Oncotarget,* 5.

ASTRAZENECA. 2014. *LYNPARZA™ approved by the US food and drug administration for the treatment of advanced ovarian cancer in patients with germline BRCA-mutations* [Online]. US: AstraZeneca. Available: https://www.astrazeneca.com/media-centre/press-releases/2014/lynparza-approved-us-fda-brca-mutated-ovarian-cancer-treatment-19122014.html# [Accessed 15 July 2022].

ASTRAZENECA. 2019. *Lynparza approved in China as a 1st-line maintenance therapy in BRCA-mutated advanced ovarian cancer* [Online]. US: AstraZeneca. Available: https://www.astrazeneca.com/media-centre/press-releases/2019/lynparza-approved-in-china-as-a-1st-line-maintenance-therapy-in-brca-mutated-advanced-ovarian-cancer.html#! [Accessed 15 July 2022].

AU - CECCHINI, M. J., AU - AMIRI, M. & AU - DICK, F. A. 2012. Analysis of Cell Cycle Position in Mammalian Cells. *JoVE***,** e3491.

AU - NOWSHEEN, S., AU - XIA, F. & AU - YANG, E. S. 2012. Assaying DNA Damage in Hippocampal Neurons Using the Comet Assay. *JoVE***,** e50049.

AWASTHI, P., FOIANI, M. & KUMAR, A. 2015. ATM and ATR signaling at a glance. *Journal of Cell Science,* 128**,** 4255-4262.

BAJRAMI, I., FRANKUM, J. R., KONDE, A., MILLER, R. E., REHMAN, F. L., BROUGH, R., CAMPBELL, J., SIMS, D., RAFIQ, R., HOOPER, S., CHEN, L., KOZAREWA, I., ASSIOTIS, I., FENWICK, K., NATRAJAN, R., LORD, C. J. & ASHWORTH, A. 2014. Genome-wide profiling of genetic synthetic lethality identifies CDK12 as a novel determinant of PARP1/2 inhibitor sensitivity. *Cancer Res,* 74**,** 287-97.

BAJRAMI, I., KIGOZI, A., VAN WEVERWIJK, A., BROUGH, R., FRANKUM, J., LORD, C. J. & ASHWORTH, A. 2012. Synthetic lethality of PARP and NAMPT inhibition in triple-negative breast cancer cells. *EMBO Mol Med,* 4**,** 1087-96.

BANERJEE, S., MOORE, K. N., COLOMBO, N., SCAMBIA, G., KIM, B. G., OAKNIN, A., FRIEDLANDER, M., LISYANSKAYA, A., FLOQUET, A., LEARY, A., SONKE, G. S., GOURLEY, C., OZA, A., GONZÁLEZ-MARTÍN, A., AGHAJANIAN, C., BRADLEY, W. H., HOLMES, E., LOWE, E. S. & DISILVESTRO, P. 2021. Maintenance olaparib for patients with newly diagnosed advanced ovarian cancer and a BRCA mutation (SOLO1/GOG 3004): 5-year follow-up of a randomised, double-blind, placebo-controlled, phase 3 trial. *Lancet Oncol,* 22**,** 1721-1731.

References

BARBER, E. & MATEI, D. 2021. Immunotherapy in ovarian cancer: we are not there yet. *Lancet Oncol,* 22**,** 903-905.

BARBER, L. J., SANDHU, S., CHEN, L., CAMPBELL, J., KOZAREWA, I., FENWICK, K., ASSIOTIS, I., RODRIGUES, D. N., REIS FILHO, J. S., MORENO, V., MATEO, J., MOLIFE, L. R., DE BONO, J., KAYE, S., LORD, C. J. & ASHWORTH, A. 2013. Secondary mutations in BRCA2 associated with clinical resistance to a PARP inhibitor. *J Pathol,* 229**,** 422-9.

BEKKER-JENSEN, S., RENDTLEW DANIELSEN, J., FUGGER, K., GROMOVA, I., NERSTEDT, A., LUKAS, C., BARTEK, J., LUKAS, J. & MAILAND, N. 2010. HERC2 coordinates ubiquitin-dependent assembly of DNA repair factors on damaged chromosomes. *Nat Cell Biol,* 12**,** 80-6; sup pp 1-12.

BELL, D., BERCHUCK, A., BIRRER, M., CHIEN, J., CRAMER, D. W., DAO, F., DHIR, R., DISAIA, P., GABRA, H., GLENN, P., GODWIN, A. K., GROSS, J., HARTMANN, L., HUANG, M., HUNTSMAN, D. G., IACOCCA, M., IMIELINSKI, M., KALLOGER, S., KARLAN, B. Y., LEVINE, D. A., MILLS, G. B., MORRISON, C., MUTCH, D., OLVERA, N., ORSULIC, S., PARK, K., PETRELLI, N., RABENO, B., RADER, J. S., SIKIC, B. I., SMITH-MCCUNE, K., SOOD, A. K., BOWTELL, D., PENNY, R., TESTA, J. R., CHANG, K., CREIGHTON, C. J., DINH, H. H., DRUMMOND, J. A., FOWLER, G., GUNARATNE, P., HAWES, A. C., KOVAR, C. L., LEWIS, L. R., MORGAN, M. B., NEWSHAM, I. F., SANTIBANEZ, J., REID, J. G., TREVINO, L. R., WU, Y. Q., WANG, M., MUZNY, D. M., WHEELER, D. A., GIBBS, R. A., GETZ, G., LAWRENCE, M. S., CIBULSKIS, K., SIVACHENKO, A. Y., SOUGNEZ, C., VOET, D., WILKINSON, J., BLOOM, T., ARDLIE, K., FENNELL, T., BALDWIN, J., NICHOL, R., FISHER, S., GABRIEL, S., LANDER, E. S., DING, L., FULTON, R. S., KOBOLDT, D. C., MCLELLAN, M. D., WYLIE, T., WALKER, J., O'LAUGHLIN, M., DOOLING, D. J., FULTON, L., ABBOTT, R., DEES, N. D., ZHANG, Q., KANDOTH, C., WENDL, M., SCHIERDING, W., SHEN, D., HARRIS, C. C., SCHMIDT, H., KALICKI, J., DELEHAUNTY, K. D., FRONICK, C. C., DEMETER, R., COOK, L., WALLIS, J. W., LIN, L., MAGRINI, V. J., HODGES, J. S., ELDRED, J. M., SMITH, S. M., POHL, C. S., VANDIN, F., et al. 2011. Integrated genomic analyses of ovarian carcinoma. *Nature,* 474**,** 609-615.

BENNARDO, N., CHENG, A., HUANG, N. & STARK, J. M. 2008. Alternative-NHEJ is a mechanistically distinct pathway of mammalian chromosome break repair. *PLoS Genet,* 4**,** e1000110.

BETERMIER, M., BERTRAND, P. & LOPEZ, B. S. 2014. Is non-homologous end-joining really an inherently error-prone process? *PLoS Genet,* 10**,** e1004086.

BEUCHER, A., BIRRAUX, J., TCHOUANDONG, L., BARTON, O., SHIBATA, A., CONRAD, S., GOODARZI, A. A., KREMPLER, A., JEGGO, P. A. & LOBRICH, M. 2009. ATM and Artemis promote homologous recombination of radiation-induced DNA double-strand breaks in G2. *Embo j,* 28**,** 3413-27.

BINDRA, R. S., GIBSON, S. L., MENG, A., WESTERMARK, U., JASIN, M., PIERCE, A. J., BRISTOW, R. G., CLASSON, M. K. & GLAZER, P. M. 2005. Hypoxia-induced down-regulation of BRCA1 expression by E2Fs. *Cancer Res,* 65**,** 11597-604.

BINDRA, R. S., SCHAFFER, P. J., MENG, A., WOO, J., MÅSEIDE, K., ROTH, M. E., LIZARDI, P., HEDLEY, D. W., BRISTOW, R. G. & GLAZER, P. M. 2004. Down-regulation of Rad51 and decreased homologous recombination in hypoxic cancer cells. *Mol Cell Biol,* 24**,** 8504-18.

References

BIRKBAK, N. J., KOCHUPURAKKAL, B., IZARZUGAZA, J. M., EKLUND, A. C., LI, Y., LIU, J., SZALLASI, Z., MATULONIS, U. A., RICHARDSON, A. L., IGLEHART, J. D. & WANG, Z. C. 2013. Tumor mutation burden forecasts outcome in ovarian cancer with BRCA1 or BRCA2 mutations. *PLoS One,* 8**,** e80023.

BJORGE, J. D., JAKYMIW, A. & FUJITA, D. J. 2000. Selected glimpses into the activation and function of Src kinase. *Oncogene,* 19**,** 5620-35.

BLACKFORD, A. N. & JACKSON, S. P. 2017. ATM, ATR, and DNA-PK: The Trinity at the Heart of the DNA Damage Response. *Mol Cell,* 66**,** 801-817.

BLANCK, M., BUDNIK-ZAWILSKA, M. B., LENGER, S. R., MCGONIGLE, J. E., MARTIN, G. R. A., LE SAGE, C., LAWO, S., PEMBERTON, H. N., TIWANA, G. S., SORRELL, D. A. & CROSS, B. C. S. 2020. A Flexible, Pooled CRISPR Library for Drug Development Screens. *Crispr j,* 3**,** 211-222.

BLISS, C. I. 1939. The toxicity of poisons applied jointly. *Annals of applied biology,* 26**,** 585-615.

BONADIO, R. C. & ESTEVEZ-DIZ, M. D. P. 2021. Perspectives on PARP Inhibitor Combinations for Ovarian Cancer. *Front Oncol,* 11**,** 754524.

BOTHMER, A., ROBBIANI, D. F., DI VIRGILIO, M., BUNTING, S. F., KLEIN, I. A., FELDHAHN, N., BARLOW, J., CHEN, H. T., BOSQUE, D., CALLEN, E., NUSSENZWEIG, A. & NUSSENZWEIG, M. C. 2011. Regulation of DNA end joining, resection, and immunoglobulin class switch recombination by 53BP1. *Mol Cell,* 42**,** 319-29.

BOUWMAN, P., ALY, A., ESCANDELL, J. M., PIETERSE, M., BARTKOVA, J., VAN DER GULDEN, H., HIDDINGH, S., THANASOULA, M., KULKARNI, A., YANG, Q., HAFFTY, B. G., TOMMISKA, J., BLOMQVIST, C., DRAPKIN, R., ADAMS, D. J., NEVANLINNA, H., BARTEK, J., TARSOUNAS, M., GANESAN, S. & JONKERS, J. 2010. 53BP1 loss rescues BRCA1 deficiency and is associated with triple-negative and BRCA-mutated breast cancers. *Nature Structural & Molecular Biology,* 17**,** 688-695.

BOWTELL, D. D., BÖHM, S., AHMED, A. A., ASPURIA, P. J., BAST, R. C., JR., BERAL, V., BEREK, J. S., BIRRER, M. J., BLAGDEN, S., BOOKMAN, M. A., BRENTON, J. D., CHIAPPINELLI, K. B., MARTINS, F. C., COUKOS, G., DRAPKIN, R., EDMONDSON, R., FOTOPOULOU, C., GABRA, H., GALON, J., GOURLEY, C., HEONG, V., HUNTSMAN, D. G., IWANICKI, M., KARLAN, B. Y., KAYE, A., LENGYEL, E., LEVINE, D. A., LU, K. H., MCNEISH, I. A., MENON, U., NAROD, S. A., NELSON, B. H., NEPHEW, K. P., PHAROAH, P., POWELL, D. J., JR., RAMOS, P., ROMERO, I. L., SCOTT, C. L., SOOD, A. K., STRONACH, E. A. & BALKWILL, F. R. 2015. Rethinking ovarian cancer II: reducing mortality from high-grade serous ovarian cancer. *Nat Rev Cancer,* 15**,** 668-79.

BRANDL, A. & PRABHU, A. 2020. Intraperitoneal chemotherapy in the treatment of gastric cancer peritoneal metastases: an overview of common therapeutic regimens. *Journal of Gastrointestinal Oncology***,** S32-S44.

BREM, R. & HALL, J. 2005. XRCC1 is required for DNA single-strand break repair in human cells. *Nucleic Acids Research,* 33**,** 2512-2520.

BRICKNER, J. R., SOLL, J. M., LOMBARDI, P. M., VÅGBØ, C. B., MUDGE, M. C., OYENIRAN, C., RABE, R., JACKSON, J., SULLENDER, M. E., BLAZOSKY, E., BYRUM, A. K., ZHAO, Y., CORBETT, M. A., GÉCZ, J., FIELD, M., VINDIGNI, A., SLUPPHAUG, G., WOLBERGER, C. &

References

MOSAMMAPARAST, N. 2017. A ubiquitin-dependent signalling axis specific for ALKBH-mediated DNA dealkylation repair. *Nature,* 551**,** 389-393.

BRILL, E., YOKOYAMA, T., NAIR, J., YU, M., AHN, Y. R. & LEE, J. M. 2017. Prexasertib, a cell cycle checkpoint kinases 1 and 2 inhibitor, increases in vitro toxicity of PARP inhibition by preventing Rad51 foci formation in BRCA wild type high-grade serous ovarian cancer. *Oncotarget,* 8**,** 111026-111040.

BRYANT, H. E. & HELLEDAY, T. 2006. Inhibition of poly (ADP-ribose) polymerase activates ATM which is required for subsequent homologous recombination repair. *Nucleic Acids Research,* 34**,** 1685-1691.

BRYANT, H. E., PETERMANN, E., SCHULTZ, N., JEMTH, A.-S., LOSEVA, O., ISSAEVA, N., JOHANSSON, F., FERNANDEZ, S., MCGLYNN, P. & HELLEDAY, T. 2009. PARP is activated at stalled forks to mediate Mre11-dependent replication restart and recombination. *The EMBO Journal,* 28**,** 2601-2615.

BRYANT, H. E., SCHULTZ, N., THOMAS, H. D., PARKER, K. M., FLOWER, D., LOPEZ, E., KYLE, S., MEUTH, M., CURTIN, N. J. & HELLEDAY, T. 2005. Specific killing of BRCA2-deficient tumours with inhibitors of poly(ADP-ribose) polymerase. *Nature,* 434**,** 913-7.

BUNTING, S. F., CALLÉN, E., WONG, N., CHEN, H.-T., POLATO, F., GUNN, A., BOTHMER, A., FELDHAHN, N., FERNANDEZ-CAPETILLO, O., CAO, L., XU, X., DENG, C.-X., FINKEL, T., NUSSENZWEIG, M., STARK, J. M. & NUSSENZWEIG, A. 2010. 53BP1 Inhibits Homologous Recombination in Brca1-Deficient Cells by Blocking Resection of DNA Breaks. *Cell,* 141**,** 243-254.

BURDAK-ROTHKAMM, S., SHORT, S. C., FOLKARD, M., ROTHKAMM, K. & PRISE, K. M. 2007. ATR-dependent radiation-induced gamma H2AX foci in bystander primary human astrocytes and glioma cells. *Oncogene,* 26**,** 993-1002.

BURMA, S., CHEN, B. P., MURPHY, M., KURIMASA, A. & CHEN, D. J. 2001. ATM phosphorylates histone H2AX in response to DNA double-strand breaks. *J Biol Chem,* 276**,** 42462-7.

BUSSIERE, D. E., XIE, L., SRINIVAS, H., SHU, W., BURKE, A., BE, C., ZHAO, J., GODBOLE, A., KING, D., KARKI, R. G., HORNAK, V., XU, F., COBB, J., CARTE, N., FRANK, A. O., FROMMLET, A., GRAFF, P., KNAPP, M., FAZAL, A., OKRAM, B., JIANG, S., MICHELLYS, P. Y., BECKWITH, R., VOSHOL, H., WIESMANN, C., SOLOMON, J. M. & PAULK, J. 2020. Structural basis of indisulam-mediated RBM39 recruitment to DCAF15 E3 ligase complex. *Nat Chem Biol,* 16**,** 15-23.

CAI, Z., LIU, C., CHANG, C., SHEN, C., YIN, Y., YIN, X., JIANG, Z., ZHAO, Z., MU, M., CAO, D., ZHANG, L. & ZHANG, B. 2021. Comparative safety and tolerability of approved PARP inhibitors in cancer: A systematic review and network meta-analysis. *Pharmacological Research,* 172**,** 105808.

CAMPBELL, M. C., PONTIGGIA, L., RUSSELL, A. Y., SCHWARTING, R., CAMACHO, J., JASMIN, J. F. & MERCIER, I. 2018. CAPER as a therapeutic target for triple negative breast cancer. *Oncotarget,* 9**,** 30340-30354.

CANCER-RESEARCH-UK. 2022a. *Ovarian cancer statistics* [Online]. Cancer Research UK. Available: https://www.cancerresearchuk.org/health-professional/cancer-statistics/statistics-by-cancer-type/ovarian-cancer#heading-Zero [Accessed 20 July 2022].

References

CANCER-RESEARCH-UK. 2022b. *Ovarian cancer survival statistics* [Online]. Cancer Research UK. Available: https://www.cancerresearchuk.org/health-professional/cancer-statistics/statistics-by-cancer-type/ovarian-cancer/survival#heading-Three [Accessed 20 July 2022].

CARGNELLO, M. & ROUX, P. P. 2011. Activation and function of the MAPKs and their substrates, the MAPK-activated protein kinases. *Microbiol Mol Biol Rev,* 75**,** 50-83.

CARNEY, B., KOSSATZ, S., LOK, B. H., SCHNEEBERGER, V., GANGANGARI, K. K., PILLARSETTY, N. V. K., WEBER, W. A., RUDIN, C. M., POIRIER, J. T. & REINER, T. 2018. Target engagement imaging of PARP inhibitors in small-cell lung cancer. *Nature Communications,* 9**,** 176.

CERAMI, E., GAO, J., DOGRUSOZ, U., GROSS, B. E., SUMER, S. O., AKSOY, B. A., JACOBSEN, A., BYRNE, C. J., HEUER, M. L., LARSSON, E., ANTIPIN, Y., REVA, B., GOLDBERG, A. P., SANDER, C. & SCHULTZ, N. 2012. The cBio Cancer Genomics Portal: An Open Platform for Exploring Multidimensional Cancer Genomics Data. *Cancer Discovery,* 2**,** 401-404.

CHAI, Y., LIU, X., DAI, L., LI, Y., LIU, M. & ZHANG, J.-Y. 2014. Overexpression of HCC1/CAPERα may play a role in lung cancer carcinogenesis. *Tumour biology : the journal of the International Society for Oncodevelopmental Biology and Medicine,* 35**,** 6311-6317.

CHAND, S. N., ZAREI, M., SCHIEWER, M. J., KAMATH, A. R., ROMEO, C., LAL, S., COZZITORTO, J. A., NEVLER, A., SCOLARO, L., LONDIN, E., JIANG, W., MEISNER-KOBER, N., PISHVAIAN, M. J., KNUDSEN, K. E., YEO, C. J., PASCAL, J. M., WINTER, J. M. & BRODY, J. R. 2017. Posttranscriptional Regulation of PARG mRNA by HuR Facilitates DNA Repair and Resistance to PARP Inhibitors. *Cancer Res,* 77**,** 5011-5025.

CHANOUX, R. A., YIN, B., URTISHAK, K. A., ASARE, A., BASSING, C. H. & BROWN, E. J. 2009. ATR and H2AX cooperate in maintaining genome stability under replication stress. *J Biol Chem,* 284**,** 5994-6003.

CHAPMAN, J. R., BARRAL, P., VANNIER, J. B., BOREL, V., STEGER, M., TOMAS-LOBA, A., SARTORI, A. A., ADAMS, I. R., BATISTA, F. D. & BOULTON, S. J. 2013. RIF1 is essential for 53BP1-dependent nonhomologous end joining and suppression of DNA double-strand break resection. *Mol Cell,* 49**,** 858-71.

CHARAN, J. & KANTHARIA, N. D. 2013. How to calculate sample size in animal studies? *J Pharmacol Pharmacother,* 4**,** 303-6.

CHARKHCHI, P., CYBULSKI, C., GRONWALD, J., WONG, F. O., NAROD, S. A. & AKBARI, M. R. 2020. CA125 and Ovarian Cancer: A Comprehensive Review. *Cancers,* 12**,** 3730.

CHEN, S. H. & YU, X. 2019. Targeting dePARylation selectively suppresses DNA repair-defective and PARP inhibitor-resistant malignancies. *Sci Adv,* 5**,** eaav4340.

CHEN, Y., ZHAO, Y., YANG, X., REN, X., HUANG, S., GONG, S., TAN, X., LI, J., HE, S., LI, Y., HONG, X., LI, Q., DING, C., FANG, X., MA, J. & LIU, N. 2022. USP44 regulates irradiation-induced DNA double-strand break repair and suppresses tumorigenesis in nasopharyngeal carcinoma. *Nat Commun,* 13**,** 501.

CHEN, Y. H., JONES, M. J., YIN, Y., CRIST, S. B., COLNAGHI, L., SIMS, R. J., 3RD, ROTHENBERG, E., JALLEPALLI, P. V. & HUANG, T. T. 2015. ATR-mediated phosphorylation of FANCI regulates dormant origin firing in response to replication stress. *Mol Cell,* 58**,** 323-38.

References

CHENG, Z., MIRZA, H., ENNIS, D. P., SMITH, P., MORRILL GAVARRÓ, L., SOKOTA, C., GIANNONE, G., GORANOVA, T., BRADLEY, T., PISKORZ, A., LOCKLEY, M., INVESTIGATORS, F. T. B.-., KAUR, B., SINGH, N., TOOKMAN, L. A., KRELL, J., MCDERMOTT, J., MACINTYRE, G., MARKOWETZ, F., BRENTON, J. D. & MCNEISH, I. A. 2022. The Genomic Landscape of Early-Stage Ovarian High-Grade Serous Carcinoma. *Clinical Cancer Research,* 28**,** 2911-2922.

CHILEWSKI, S. D., BHOSALE, D., DEES, S., HUTCHINSON, I., TRIMBLE, R., PONTIGGIA, L., MERCIER, I. & JASMIN, J.-F. 2020. Development of CAPER peptides for the treatment of triple negative breast cancer. *Cell Cycle,* 19**,** 432-447.

CHINI, C. C. & CHEN, J. 2003. Human claspin is required for replication checkpoint control. *J Biol Chem,* 278**,** 30057-62.

CHOI, M., KIPPS, T. & KURZROCK, R. 2016. ATM Mutations in Cancer: Therapeutic Implications. *Mol Cancer Ther,* 15**,** 1781-91.

CHOU, T. C. 2006. Theoretical basis, experimental design, and computerized simulation of synergism and antagonism in drug combination studies. *Pharmacol Rev,* 58**,** 621-81.

CHOU, T. C. 2010. Drug combination studies and their synergy quantification using the Chou-Talalay method. *Cancer Res,* 70**,** 440-6.

CHOU, T. C. & HAYBALL, M. P. 1997. CalcuSyn for Windows: multiple-drug dose- effect analyzer and manual. Cambridge (UK): Biosoft.

CHOU, T. C. & MARTIN, N. 2005. CompuSyn for drug combinations: A Computer Program for Quantitation of Synergism and Antagonism in Drug Combinations, and the Determination of IC50 and ED50 Values. New York, USA: ComboSyn, Inc.

CHOU, T. C. & TALALAY, P. 1984. Quantitative analysis of dose-effect relationships: the combined effects of multiple drugs or enzyme inhibitors. *Adv Enzyme Regul,* 22**,** 27-55.

CHRISTIE, E. L., FEREDAY, S., DOIG, K., PATTNAIK, S., DAWSON, S.-J. & BOWTELL, D. D. L. 2017. Reversion of BRCA1/2 Germline Mutations Detected in Circulating Tumor DNA From Patients With High-Grade Serous Ovarian Cancer. *Journal of Clinical Oncology,* 35**,** 1274-1280.

CHRISTIE, E. L., PATTNAIK, S., BEACH, J., COPELAND, A., RASHOO, N., FEREDAY, S., HENDLEY, J., ALSOP, K., BRADY, S. L., LAMB, G., PANDEY, A., DEFAZIO, A., THORNE, H., BILD, A. & BOWTELL, D. D. L. 2019. Multiple ABCB1 transcriptional fusions in drug resistant high-grade serous ovarian and breast cancer. *Nature Communications,* 10.

CHUN, J., BUECHELMAIER, E. S. & POWELL, S. N. 2013. Rad51 paralog complexes BCDX2 and CX3 act at different stages in the BRCA1-BRCA2-dependent homologous recombination pathway. *Molecular and cellular biology,* 33**,** 387-395.

CLEAVER, J. E. 2011. γH2Ax: Biomarker of Damage or Functional Participant in DNA Repair "All that Glitters Is not Gold!". *Photochemistry and Photobiology,* 87**,** 1230-1239.

CLEMENTS, K. E., SCHLEICHER, E. M., THAKAR, T., HALE, A., DHOONMOON, A., TOLMAN, N. J., SHARMA, A., LIANG, X., IMAMURA KAWASAWA, Y., NICOLAE, C. M., WANG, H.-G., DE, S. & MOLDOVAN, G.-L. 2020. Identification of regulators of poly-ADP-ribose

polymerase inhibitor response through complementary CRISPR knockout and activation screens. *Nature Communications,* 11**,** 6118.

COLEMAN, R. L., FLEMING, G. F., BRADY, M. F., SWISHER, E. M., STEFFENSEN, K. D., FRIEDLANDER, M., OKAMOTO, A., MOORE, K. N., EFRAT BEN-BARUCH, N., WERNER, T. L., CLOVEN, N. G., OAKNIN, A., DISILVESTRO, P. A., MORGAN, M. A., NAM, J.-H., LEATH, C. A., NICUM, S., HAGEMANN, A. R., LITTELL, R. D., CELLA, D., BARON-HAY, S., GARCIA-DONAS, J., MIZUNO, M., BELL-MCGUINN, K., SULLIVAN, D. M., BACH, B. A., BHATTACHARYA, S., RATAJCZAK, C. K., ANSELL, P. J., DINH, M. H., AGHAJANIAN, C. & BOOKMAN, M. A. 2019. Veliparib with First-Line Chemotherapy and as Maintenance Therapy in Ovarian Cancer. *New England Journal of Medicine,* 381**,** 2403-2415.

COLLINS, A. R. 2004. The comet assay for DNA damage and repair: principles, applications, and limitations. *Mol Biotechnol,* 26**,** 249-61.

CONG, K., PENG, M., KOUSHOLT, A. N., LEE, W. T. C., LEE, S., NAYAK, S., KRAIS, J., VANDERVERE-CAROZZA, P. S., PAWELCZAK, K. S., CALVO, J., PANZARINO, N. J., TURCHI, J. J., JOHNSON, N., JONKERS, J., ROTHENBERG, E. & CANTOR, S. B. 2021. Replication gaps are a key determinant of PARP inhibitor synthetic lethality with BRCA deficiency. *Mol Cell,* 81**,** 3128-3144.e7.

COOMAR, S., PENSON, A., SCHWALLER, J., ABDEL-WAHAB, O. & GILLINGHAM, D. 2021. Arylsulfonamide mediated RBM39 degradation causes aberrant splicing of mitotic kinesins. *bioRxiv***,** 2021.02.01.428819.

COULSON-GILMER, C., MORGAN, R. D., NELSON, L., BARNES, B. M., TIGHE, A., WARDENAAR, R., SPIERINGS, D. C. J., SCHLECHT, H., BURGHEL, G. J., FOIJER, F., DESAI, S., MCGRAIL, J. C. & TAYLOR, S. S. 2021. Replication catastrophe is responsible for intrinsic PAR glycohydrolase inhibitor-sensitivity in patient-derived ovarian cancer models. *J Exp Clin Cancer Res,* 40**,** 323.

CRUZ, C., CASTROVIEJO-BERMEJO, M., GUTIÉRREZ-ENRÍQUEZ, S., LLOP-GUEVARA, A., IBRAHIM, Y. H., GRIS-OLIVER, A., BONACHE, S., MORANCHO, B., BRUNA, A., RUEDA, O. M., LAI, Z., POLANSKA, U. M., JONES, G. N., KRISTEL, P., DE BUSTOS, L., GUZMAN, M., RODRÍGUEZ, O., GRUESO, J., MONTALBAN, G., CARATÚ, G., MANCUSO, F., FASANI, R., JIMÉNEZ, J., HOWAT, W. J., DOUGHERTY, B., VIVANCOS, A., NUCIFORO, P., SERRES-CRÉIXAMS, X., RUBIO, I. T., OAKNIN, A., CADOGAN, E., BARRETT, J. C., CALDAS, C., BASELGA, J., SAURA, C., CORTÉS, J., ARRIBAS, J., JONKERS, J., DÍEZ, O., O'CONNOR, M. J., BALMAÑA, J. & SERRA, V. 2018. RAD51 foci as a functional biomarker of homologous recombination repair and PARP inhibitor resistance in germline BRCA-mutated breast cancer. *Ann Oncol,* 29**,** 1203-1210.

DALE REIN, I., SOLBERG LANDSVERK, K., MICCI, F., PATZKE, S. & STOKKE, T. 2015. Replication-induced DNA damage after PARP inhibition causes G2 delay, and cell line-dependent apoptosis, necrosis and multinucleation. *Cell Cycle,* 14**,** 3248-60.

DALTON, W. B., HELMENSTINE, E., PIETERSE, L., LI, B., GOCKE, C. D., DONALDSON, J., XIAO, Z., GONDEK, L. P., GHIAUR, G., GOJO, I., SMITH, B. D., LEVIS, M. J. & DEZERN, A. E. 2020. The K666N mutation in SF3B1 is associated with increased progression of MDS and distinct RNA splicing. *Blood Adv,* 4**,** 1192-1196.

References

DANGO, S., MOSAMMAPARAST, N., SOWA, M. E., XIONG, L. J., WU, F., PARK, K., RUBIN, M., GYGI, S., HARPER, J. W. & SHI, Y. 2011. DNA unwinding by ASCC3 helicase is coupled to ALKBH3-dependent DNA alkylation repair and cancer cell proliferation. *Mol Cell,* 44**,** 373-84.

DARMAN, R. B., SEILER, M., AGRAWAL, A. A., LIM, K. H., PENG, S., AIRD, D., BAILEY, S. L., BHAVSAR, E. B., CHAN, B., COLLA, S., CORSON, L., FEALA, J., FEKKES, P., ICHIKAWA, K., KEANEY, G. F., LEE, L., KUMAR, P., KUNII, K., MACKENZIE, C., MATIJEVIC, M., MIZUI, Y., MYINT, K., PARK, E. S., PUYANG, X., SELVARAJ, A., THOMAS, M. P., TSAI, J., WANG, J. Y., WARMUTH, M., YANG, H., ZHU, P., GARCIA-MANERO, G., FURMAN, R. R., YU, L., SMITH, P. G. & BUONAMICI, S. 2015. Cancer-Associated SF3B1 Hotspot Mutations Induce Cryptic 3' Splice Site Selection through Use of a Different Branch Point. *Cell Rep,* 13**,** 1033-45.

DASARI, S. & TCHOUNWOU, P. B. 2014. Cisplatin in cancer therapy: molecular mechanisms of action. *Eur J Pharmacol,* 740**,** 364-78.

DE FERAUDY, S., REVET, I., BEZROOKOVE, V., FEENEY, L. & CLEAVER, J. E. 2010. A minority of foci or pan-nuclear apoptotic staining of gammaH2AX in the S phase after UV damage contain DNA double-strand breaks. *Proc Natl Acad Sci U S A,* 107**,** 6870-5.

DEBOEVER, C., GHIA, E. M., SHEPARD, P. J., RASSENTI, L., BARRETT, C. L., JEPSEN, K., JAMIESON, C. H., CARSON, D., KIPPS, T. J. & FRAZER, K. A. 2015. Transcriptome sequencing reveals potential mechanism of cryptic 3' splice site selection in SF3B1-mutated cancers. *PLoS Comput Biol,* 11**,** e1004105.

DEL PRETE, S., ANGELI, A., GHOBRIL, C., HITCE, J., CLAVAUD, C., MARAT, X., SUPURAN, C. T. & CAPASSO, C. 2020. Sulfonamide Inhibition Profile of the β-Carbonic Anhydrase from Malassezia restricta, An Opportunistic Pathogen Triggering Scalp Conditions. *Metabolites,* 10**,** 39.

DEMPSTER, J. M., ROSSEN, J., KAZACHKOVA, M., PAN, J., KUGENER, G., ROOT, D. E. & TSHERNIAK, A. 2019. Extracting Biological Insights from the Project Achilles Genome-Scale CRISPR Screens in Cancer Cell Lines. *bioRxiv***,** 720243.

DENG, C., ZHANG, P., HARPER, J. W., ELLEDGE, S. J. & LEDER, P. 1995. Mice lacking p21CIP1/WAF1 undergo normal development, but are defective in G1 checkpoint control. *Cell,* 82**,** 675-84.

DENG, M., QIN, K., LI, Y., JIANG, Y., JIN, W. & SHEN, Z. 2022. Abstract 5338: Pamiparib as a non-P-glycoprotein substrate PARP inhibitor can overcome ABCB1-mediated multidrug resistance in ovarian cancer cells. *Cancer Research,* 82**,** 5338-5338.

DEPMAP. 2020. *Broad (2020): DepMap 20Q2 Public. figshare. Dataset.* [Online]. Available: https://doi.org/10.6084/m9.figshare.12280541.v4. [Accessed 25 June 2020 2020].

DEV, H., CHIANG, T.-W. W., LESCALE, C., DE KRIJGER, I., MARTIN, A. G., PILGER, D., COATES, J., SCZANIECKA-CLIFT, M., WEI, W., OSTERMAIER, M., HERZOG, M., LAM, J., SHEA, A., DEMIR, M., WU, Q., YANG, F., FU, B., LAI, Z., BALMUS, G., BELOTSERKOVSKAYA, R., SERRA, V., O'CONNOR, M. J., BRUNA, A., BELI, P., PELLEGRINI, L., CALDAS, C., DERIANO, L., JACOBS, J. J. L., GALANTY, Y. & JACKSON, S. P. 2018. Shieldin complex promotes DNA end-joining and counters homologous recombination in BRCA1-null cells. *Nature Cell Biology,* 20**,** 954-965.

References

DEWEIRDT, P. C., SANGREE, A. K., HANNA, R. E., SANSON, K. R., HEGDE, M., STRAND, C., PERSKY, N. S. & DOENCH, J. G. 2020. Genetic screens in isogenic mammalian cell lines without single cell cloning. *Nature Communications,* 11**,** 752.

DI GIULIO, S., COLICCHIA, V., PASTORINO, F., PEDRETTI, F., FABRETTI, F., NICOLIS DI ROBILANT, V., RAMPONI, V., SCAFETTA, G., MORETTI, M., LICURSI, V., BELARDINILLI, F., PERUZZI, G., INFANTE, P., GOFFREDO, B. M., COPPA, A., CANETTIERI, G., BARTOLAZZI, A., PONZONI, M., GIANNINI, G. & PETRONI, M. 2021. A combination of PARP and CHK1 inhibitors efficiently antagonizes MYCN-driven tumors. *Oncogene,* 40**,** 6143-6152.

DI, L. & KERNS, E. H. 2016. Chapter 41 - Formulation. *In:* DI, L. & KERNS, E. H. (eds.) *Drug-Like Properties (Second Edition).* Boston: Academic Press.

DIETLEIN, F., THELEN, L. & REINHARDT, H. C. 2014. Cancer-specific defects in DNA repair pathways as targets for personalized therapeutic approaches. *Trends Genet,* 30**,** 326-39.

DING, L., KIM, H. J., WANG, Q., KEARNS, M., JIANG, T., OHLSON, C. E., LI, B. B., XIE, S., LIU, J. F., STOVER, E. H., HOWITT, B. E., BRONSON, R. T., LAZO, S., ROBERTS, T. M., FREEMAN, G. J., KONSTANTINOPOULOS, P. A., MATULONIS, U. A. & ZHAO, J. J. 2018. PARP Inhibition Elicits STING-Dependent Antitumor Immunity in Brca1-Deficient Ovarian Cancer. *Cell Rep,* 25**,** 2972-2980.e5.

DISIS, M. L., TAYLOR, M. H., KELLY, K., BECK, J. T., GORDON, M., MOORE, K. M., PATEL, M. R., CHAVES, J., PARK, H. & MITA, A. C. 2019. Efficacy and safety of avelumab for patients with recurrent or refractory ovarian cancer: phase 1b results from the JAVELIN solid tumor trial. *JAMA oncology,* 5**,** 393-401.

DOMCHEK, S. M., AGHAJANIAN, C., SHAPIRA-FROMMER, R., SCHMUTZLER, R. K., AUDEH, M. W., FRIEDLANDER, M., BALMAÑA, J., MITCHELL, G., FRIED, G., STEMMER, S. M., HUBERT, A., ROSENGARTEN, O., LOMAN, N., ROBERTSON, J. D., MANN, H. & KAUFMAN, B. 2016. Efficacy and safety of olaparib monotherapy in germline BRCA1/2 mutation carriers with advanced ovarian cancer and three or more lines of prior therapy. *Gynecol Oncol,* 140**,** 199-203.

DOMCKE, S., SINHA, R., LEVINE, D. A., SANDER, C. & SCHULTZ, N. 2013. Evaluating cell lines as tumour models by comparison of genomic profiles. *Nat Commun,* 4**,** 2126.

DOWHAN, D. H., HONG, E. P., AUBOEUF, D., DENNIS, A. P., WILSON, M. M., BERGET, S. M. & O'MALLEY, B. W. 2005. Steroid hormone receptor coactivation and alternative RNA splicing by U2AF65-related proteins CAPERalpha and CAPERbeta. *Mol Cell,* 17**,** 429-39.

DREGALLA, R. C., ZHOU, J., IDATE, R. R., BATTAGLIA, C. L., LIBER, H. L. & BAILEY, S. M. 2010. Regulatory roles of tankyrase 1 at telomeres and in DNA repair: suppression of T-SCE and stabilization of DNA-PKcs. *Aging (Albany NY),* 2**,** 691-708.

DU, X., VOLKOV, O. A., CZERWINSKI, R. M., TAN, H., HUERTA, C., MORTON, E. R., RIZZI, J. P., WEHN, P. M., XU, R., NIJHAWAN, D. & WALLACE, E. M. 2019. Structural Basis and Kinetic Pathway of RBM39 Recruitment to DCAF15 by a Sulfonamide Molecular Glue E7820. *Structure,* 27**,** 1625-1633 e3.

DUARTE, A. A., GOGOLA, E., SACHS, N., BARAZAS, M., ANNUNZIATO, S., R DE RUITER, J., VELDS, A., BLATTER, S., HOUTHUIJZEN, J. M., VAN DE VEN, M., CLEVERS, H., BORST, P.,

References

JONKERS, J. & ROTTENBERG, S. 2018. BRCA-deficient mouse mammary tumor organoids to study cancer-drug resistance. *Nature Methods,* 15**,** 134-140.

DURKACZ, B. W., OMIDIJI, O., GRAY, D. A. & SHALL, S. 1980. (ADP-ribose)n participates in DNA excision repair. *Nature,* 283**,** 593-6.

EL MARABTI, E. & YOUNIS, I. 2018. The Cancer Spliceome: Reprograming of Alternative Splicing in Cancer. *Frontiers in Molecular Biosciences,* 5.

ELIAS, K. M., EMORI, M. M., PAPP, E., MACDUFFIE, E., KONECNY, G. E., VELCULESCU, V. E. & DRAPKIN, R. 2015. Beyond genomics: critical evaluation of cell line utility for ovarian cancer research. *Gynecol Oncol,* 139**,** 97-103.

ELLIS, J. D., LLÈRES, D., DENEGRI, M., LAMOND, A. I. & CÁCERES, J. F. 2008. Spatial mapping of splicing factor complexes involved in exon and intron definition. *The Journal of cell biology,* 181**,** 921-934.

EMA. 2014. *Lynparza recomended for approval in ovarian cancer* [Online]. European Medicines Agency. Available: https://www.ema.europa.eu/en/news/lynparza-recommended-approval-ovarian-cancer [Accessed 15 July 2022].

EMA. 2018. *Rubraca (rucaparib)* [Online]. European Medicines Agency. Available: https://www.ema.europa.eu/en/medicines/human/EPAR/rubraca#assessment-history-section [Accessed 15 July 2022].

EMA. 2019a. *Summary of opinion (post authorisation) Lynparza Olaparib* [Online]. European Medicines Agency. Available: https://www.ema.europa.eu/en/documents/smop/chmp-post-authorisation-summary-positive-opinion-lynparza-ii-23_en.pdf [Accessed 15 July 2022].

EMA. 2019b. *Talzenna (talazoparib)* [Online]. European Medicines Agency. Available: https://www.ema.europa.eu/en/medicines/human/EPAR/talzenna [Accessed 15 July 2022].

EMA. 2020. *Orphan Maintenance Assessment Report - Zejula (niraparib) treatment of ovarian cancer* [Online]. European Medicines Agency. Available: https://www.ema.europa.eu/en/documents/orphan-maintenance-report-post/zejula-orphan-maintenance-assessment-report-post-authorisation-ii-019_en.pdf [Accessed 15 July 2022].

ESCRIBANO-DÍAZ, C., ORTHWEIN, A., FRADET-TURCOTTE, A., XING, M., YOUNG, J. T., TKÁČ, J., COOK, M. A., ROSEBROCK, A. P., MUNRO, M., CANNY, M. D., XU, D. & DUROCHER, D. 2013. A cell cycle-dependent regulatory circuit composed of 53BP1-RIF1 and BRCA1-CtIP controls DNA repair pathway choice. *Mol Cell,* 49**,** 872-83.

ESFAHANI, K., ROUDAIA, L., BUHLAIGA, N., DEL RINCON, S. V., PAPNEJA, N. & MILLER, W. H., JR. 2020. A review of cancer immunotherapy: from the past, to the present, to the future. *Current oncology (Toronto, Ont.),* 27**,** S87-S97.

ESKENS, F. A. L. M., RAMOS, F. J., BURGER, H., O'BRIEN, J. P., PIERA, A., DE JONGE, M. J. A., MIZUI, Y., WIEMER, E. A. C., CARRERAS, M. J., BASELGA, J. & TABERNERO, J. 2013. Phase I Pharmacokinetic and Pharmacodynamic Study of the First-in-Class Spliceosome Inhibitor E7107 in Patients with Advanced Solid Tumors. *Clinical Cancer Research,* 19**,** 6296-6304.

References

ESMO. 2017. *Ovarian cancer - an ESMO guide for patients* [Online]. ESMO. Available: https://www.esmo.org/for-patients/patient-guides/ovarian-cancer [Accessed 01 July 2017 2022].

FAHERTY, N., BENSON, M., SHARMA, E., LEE, A., HOWARTH, A., LOCKSTONE, H., EBNER, D. & BHATTACHARYA, S. 2016. Negative autoregulation of BMP dependent transcription by SIN3B splicing reveals a role for RBM39. *Sci Rep,* 6**,** 28210.

FALCK, J., MAILAND, N., SYLJUÅSEN, R. G., BARTEK, J. & LUKAS, J. 2001. The ATM-Chk2-Cdc25A checkpoint pathway guards against radioresistant DNA synthesis. *Nature,* 410**,** 842-7.

FAN, C. H., LIU, W. L., CAO, H., WEN, C., CHEN, L. & JIANG, G. 2013. O6-methylguanine DNA methyltransferase as a promising target for the treatment of temozolomide-resistant gliomas. *Cell Death & Disease,* 4**,** e876-e876.

FANALE, D., BAZAN, V., CARUSO, S., CASTIGLIA, M., BRONTE, G., ROLFO, C., CICERO, G. & RUSSO, A. 2013. Hypoxia and human genome stability: downregulation of BRCA2 expression in breast cancer cell lines. *Biomed Res Int,* 2013**,** 746858.

FANG, P., DE SOUZA, C., MINN, K. & CHIEN, J. 2019a. Genome-scale CRISPR knockout screen identifies TIGAR as a modifier of PARP inhibitor sensitivity. *Commun Biol,* 2**,** 335.

FANG, Y., MCGRAIL, D. J., SUN, C., LABRIE, M., CHEN, X., ZHANG, D., JU, Z., VELLANO, C. P., LU, Y., LI, Y., JEONG, K. J., DING, Z., LIANG, J., WANG, S. W., DAI, H., LEE, S., SAHNI, N., MERCADO-URIBE, I., KIM, T.-B., CHEN, K., LIN, S.-Y., PENG, G., WESTIN, S. N., LIU, J., O'CONNOR, M. J., YAP, T. A. & MILLS, G. B. 2019b. Sequential Therapy with PARP and WEE1 Inhibitors Minimizes Toxicity while Maintaining Efficacy. *Cancer Cell,* 35**,** 851-867.e7.

FARMER, H., MCCABE, N., LORD, C. J., TUTT, A. N., JOHNSON, D. A., RICHARDSON, T. B., SANTAROSA, M., DILLON, K. J., HICKSON, I., KNIGHTS, C., MARTIN, N. M., JACKSON, S. P., SMITH, G. C. & ASHWORTH, A. 2005. Targeting the DNA repair defect in BRCA mutant cells as a therapeutic strategy. *Nature,* 434**,** 917-21.

FAUST, T. B., YOON, H., NOWAK, R. P., DONOVAN, K. A., LI, Z., CAI, Q., ELEUTERI, N. A., ZHANG, T., GRAY, N. S. & FISCHER, E. S. 2020. Structural complementarity facilitates E7820-mediated degradation of RBM39 by DCAF15. *Nat Chem Biol,* 16**,** 7-14.

FDA. 2014. *FDA-Approved Drugs LYNPARZA (OLAPARIB)* [Online]. USA: U.S. Food & Drug Administration. Available: https://www.accessdata.fda.gov/scripts/cder/daf/index.cfm?event=overview.process&ApplNo=206162 [Accessed 15 July 2022].

FDA. 2016. *RUBRACA (rucaparib) label* [Online]. USA: U.S. Food & Drug Administration. Available: https://www.accessdata.fda.gov/drugsatfda_docs/label/2016/209115s000lbl.pdf [Accessed 15 July 2022].

FDA. 2018a. *FDA-Approved Drugs LYNPARZA (OLAPARIB)* [Online]. USA: U.S. Food & Drug Administration. Available: https://www.accessdata.fda.gov/drugsatfda_docs/label/2018/208558s006lbl.pdf [Accessed 15 July 2022].

References

FDA. 2018b. *FDA-Approved Drugs Talzenna Talazoparib tosylate* [Online]. USA: U.S. Food & Drug Administration. Available: https://www.accessdata.fda.gov/drugsatfda_docs/label/2018/211651s000lbl.pdf [Accessed 15 July 2022].

FDA. 2020. *ZEJULA (niraparib) label* [Online]. USA: U.S. Food & Drug Administration. Available: https://www.accessdata.fda.gov/drugsatfda_docs/label/2020/208447s015s017lbledt.pdf [Accessed 15 July 2022].

FOK, J. H. L., RAMOS-MONTOYA, A., VAZQUEZ-CHANTADA, M., WIJNHOVEN, P. W. G., FOLLIA, V., JAMES, N., FARRINGTON, P. M., KARMOKAR, A., WILLIS, S. E., CAIRNS, J., NIKKILÄ, J., BEATTIE, D., LAMONT, G. M., FINLAY, M. R. V., WILSON, J., SMITH, A., O'CONNOR, L. O., LING, S., FAWELL, S. E., O'CONNOR, M. J., HOLLINGSWORTH, S. J., DEAN, E., GOLDBERG, F. W., DAVIES, B. R. & CADOGAN, E. B. 2019. AZD7648 is a potent and selective DNA-PK inhibitor that enhances radiation, chemotherapy and olaparib activity. *Nature Communications,* 10**,** 5065.

FONTANA, G. A., REINERT, J. K., THOMÄ, N. H. & RASS, U. 2018. Shepherding DNA ends: Rif1 protects telomeres and chromosome breaks. *Microb Cell,* 5**,** 327-343.

FORD, C. E., WERNER, B., HACKER, N. F. & WARTON, K. 2020. The untapped potential of ascites in ovarian cancer research and treatment. *British Journal of Cancer,* 123**,** 9-16.

FRANKENBERG-SCHWAGER, M., KIRCHERMEIER, D., GREIF, G., BAER, K., BECKER, M. & FRANKENBERG, D. 2005. Cisplatin-mediated DNA double-strand breaks in replicating but not in quiescent cells of the yeast Saccharomyces cerevisiae. *Toxicology,* 212**,** 175-84.

FU, X., TIAN, M., GU, J., CHENG, T., MA, D., FENG, L. & XIN, X. 2017. SF3B1 mutation is a poor prognostic indicator in luminal B and progesterone receptor-negative breast cancer patients. *Oncotarget,* 8.

FUEGER, B. J., CZERNIN, J., HILDEBRANDT, I., TRAN, C., HALPERN, B. S., STOUT, D., PHELPS, M. E. & WEBER, W. A. 2006. Impact of animal handling on the results of 18F-FDG PET studies in mice. *J Nucl Med,* 47**,** 999-1006.

FUGGER, K., BAJRAMI, I., SILVA DOS SANTOS, M., YOUNG, S. J., KUNZELMANN, S., KELLY, G., HEWITT, G., PATEL, H., GOLDSTONE, R., CARELL, T., BOULTON, S. J., MACRAE, J., TAYLOR, I. A. & WEST, S. C. 2021. Targeting the nucleotide salvage factor DNPH1 sensitizes BRCA-deficient cells to PARP inhibitors. *Science,* 372**,** 156-165.

FUKUOKA, K., USUDA, J., IWAMOTO, Y., FUKUMOTO, H., NAKAMURA, T., YONEDA, T., NARITA, N., SAIJO, N. & NISHIO, K. 2001. Mechanisms of action of the novel sulfonamide anticancer agent E7070 on cell cycle progression in human non-small cell lung cancer cells. *Invest New Drugs,* 19**,** 219-27.

FUNAHASHI, Y., SUGI, N. H., SEMBA, T., YAMAMOTO, Y., HAMAOKA, S., TSUKAHARA-TAMAI, N., OZAWA, Y., TSURUOKA, A., NARA, K., TAKAHASHI, K., OKABE, T., KAMATA, J., OWA, T., UEDA, N., HANEDA, T., YONAGA, M., YOSHIMATSU, K. & WAKABAYASHI, T. 2002. Sulfonamide derivative, E7820, is a unique angiogenesis inhibitor suppressing an expression of integrin alpha2 subunit on endothelium. *Cancer Res,* 62**,** 6116-23.

References

GAGOU, M. E., ZUAZUA-VILLAR, P. & MEUTH, M. 2010. Enhanced H2AX phosphorylation, DNA replication fork arrest, and cell death in the absence of Chk1. *Molecular biology of the cell,* 21**,** 739-752.

GAILLARD, H., GARCÍA-MUSE, T. & AGUILERA, A. 2015. Replication stress and cancer. *Nature Reviews Cancer,* 15**,** 276-289.

GAO, H., YAMASAKI, E. F., CHAN, K. K., SHEN, L. L. & SNAPKA, R. M. 2000. Chloroquinoxaline sulfonamide (NSC 339004) is a topoisomerase IIalpha/beta poison. *Cancer Res,* 60**,** 5937-40.

GAO, H., YAMASAKI, E. F., CHAN, K. K., SHEN, L. L. & SNAPKA, R. M. 2003. DNA sequence specificity for topoisomerase II poisoning by the quinoxaline anticancer drugs XK469 and CQS. *Mol Pharmacol,* 63**,** 1382-8.

GAO, J., AKSOY, B. A., DOGRUSOZ, U., DRESDNER, G., GROSS, B., SUMER, S. O., SUN, Y., JACOBSEN, A., SINHA, R., LARSSON, E., CERAMI, E., SANDER, C. & SCHULTZ, N. 2013. Integrative analysis of complex cancer genomics and clinical profiles using the cBioPortal. *Sci Signal,* 6**,** pl1.

GAPONOVA, A. V., DENEKA, A. Y., BECK, T. N., LIU, H., ANDRIANOV, G., NIKONOVA, A. S., NICOLAS, E., EINARSON, M. B., GOLEMIS, E. A. & SEREBRIISKII, I. G. 2017. Identification of evolutionarily conserved DNA damage response genes that alter sensitivity to cisplatin. *Oncotarget,* 8**,** 19156-19171.

GARCIA, A. & SINGH, H. 2013. Bevacizumab and ovarian cancer. *Therapeutic advances in medical oncology,* 5**,** 133-141.

GE, X. Q. & BLOW, J. J. 2010. Chk1 inhibits replication factory activation but allows dormant origin firing in existing factories. *J Cell Biol,* 191**,** 1285-97.

GE, X. Q., JACKSON, D. A. & BLOW, J. J. 2007. Dormant origins licensed by excess Mcm2-7 are required for human cells to survive replicative stress. *Genes Dev,* 21**,** 3331-41.

GHOSAL, G. & CHEN, J. 2013. DNA damage tolerance: a double-edged sword guarding the genome. *Transl Cancer Res,* 2**,** 107-129.

GOGOLA, E., DUARTE, A. A., DE RUITER, J. R., WIEGANT, W. W., SCHMID, J. A., DE BRUIJN, R., JAMES, D. I., GUERRERO LLOBET, S., VIS, D. J., ANNUNZIATO, S., VAN DEN BROEK, B., BARAZAS, M., KERSBERGEN, A., VAN DE VEN, M., TARSOUNAS, M., OGILVIE, D. J., VAN VUGT, M., WESSELS, L. F. A., BARTKOVA, J., GROMOVA, I., ANDUJAR-SANCHEZ, M., BARTEK, J., LOPES, M., VAN ATTIKUM, H., BORST, P., JONKERS, J. & ROTTENBERG, S. 2018. Selective Loss of PARG Restores PARylation and Counteracts PARP Inhibitor-Mediated Synthetic Lethality. *Cancer Cell,* 33**,** 1078-1093.e12.

GONZALEZ-MARTIN, A., POTHURI, B., VERGOTE, I., DEPONT CHRISTENSEN, R., GRAYBILL, W., MIRZA, M. R., MCCORMICK, C., LORUSSO, D., HOSKINS, P., FREYER, G., BAUMANN, K., JARDON, K., REDONDO, A., MOORE, R. G., VULSTEKE, C., O'CEARBHAILL, R. E., LUND, B., BACKES, F., BARRETINA-GINESTA, P., HAGGERTY, A. F., RUBIO-PEREZ, M. J., SHAHIN, M. S., MANGILI, G., BRADLEY, W. H., BRUCHIM, I., SUN, K., MALINOWSKA, I. A., LI, Y., GUPTA, D. & MONK, B. J. 2019. Niraparib in Patients with Newly Diagnosed Advanced Ovarian Cancer. *N Engl J Med*.

References

GOODALL, J., MATEO, J., YUAN, W., MOSSOP, H., PORTA, N., MIRANDA, S., PEREZ-LOPEZ, R., DOLLING, D., ROBINSON, D. R., SANDHU, S., FOWLER, G., EBBS, B., FLOHR, P., SEED, G., RODRIGUES, D. N., BOYSEN, G., BERTAN, C., ATKIN, M., CLARKE, M., CRESPO, M., FIGUEIREDO, I., RIISNAES, R., SUMANASURIYA, S., RESCIGNO, P., ZAFEIRIOU, Z., SHARP, A., TUNARIU, N., BIANCHINI, D., GILLMAN, A., LORD, C. J., HALL, E., CHINNAIYAN, A. M., CARREIRA, S. & DE BONO, J. S. 2017. Circulating Cell-Free DNA to Guide Prostate Cancer Treatment with PARP Inhibition. *Cancer Discov,* 7**,** 1006-1017.

GORNSTEIN, E. L., SANDEFUR, S., CHUNG, J. H., GAY, L. M., HOLMES, O., ERLICH, R. L., SOMAN, S., MARTIN, L. K., ROSE, A. V., STEPHENS, P. J., ROSS, J. S., MILLER, V. A., ALI, S. M. & BLAU, S. 2018. BRCA2 Reversion Mutation Associated With Acquired Resistance to Olaparib in Estrogen Receptor-positive Breast Cancer Detected by Genomic Profiling of Tissue and Liquid Biopsy. *Clin Breast Cancer,* 18**,** 184-188.

GRALEWSKA, P., GAJEK, A., MARCZAK, A., MIKUŁA, M., OSTROWSKI, J., ŚLIWIŃSKA, A. & ROGALSKA, A. 2020. PARP Inhibition Increases the Reliance on ATR/CHK1 Checkpoint Signaling Leading to Synthetic Lethality-An Alternative Treatment Strategy for Epithelial Ovarian Cancer Cells Independent from HR Effectiveness. *Int J Mol Sci,* 21.

GRAVELLS, P., GRANT, E., SMITH, K. M., JAMES, D. I. & BRYANT, H. E. 2017. Specific killing of DNA damage-response deficient cells with inhibitors of poly(ADP-ribose) glycohydrolase. *DNA Repair,* 52**,** 81-91.

GRECHKO, N., SKARBOVA, V., TOMASZEWSKA-KIECANA, M., RAMLAU, R., CENTKOWSKI, P., DREW, Y., DZIADZIUSZKO, R., ZEMANOVA, M., BELTMAN, J., NASH, E., HABECK, J., LIAO, M. & XIAO, J. 2021. Pharmacokinetics and safety of rucaparib in patients with advanced solid tumors and hepatic impairment. *Cancer Chemotherapy and Pharmacology,* 88**,** 259-270.

GRECO, W. R., BRAVO, G. & PARSONS, J. C. 1995. The search for synergy: a critical review from a response surface perspective. *Pharmacological Reviews,* 47**,** 331.

GRUVER, A. M., YARD, B. D., MCINNES, C., RAJESH, C. & PITTMAN, D. L. 2009. Functional characterization and identification of mouse Rad51d splice variants. *BMC molecular biology,* 10**,** 27-27.

GUNN, A. & STARK, J. M. 2012. I-SceI-based assays to examine distinct repair outcomes of mammalian chromosomal double strand breaks. *Methods Mol Biol,* 920**,** 379-91.

GUO, C., KUMAGAI, A., SCHLACHER, K., SHEVCHENKO, A., SHEVCHENKO, A. & DUNPHY, W. G. 2015. Interaction of Chk1 with Treslin negatively regulates the initiation of chromosomal DNA replication. *Mol Cell,* 57**,** 492-505.

GUPTA, R., SOMYAJIT, K., NARITA, T., MASKEY, E., STANLIE, A., KREMER, M., TYPAS, D., LAMMERS, M., MAILAND, N., NUSSENZWEIG, A., LUKAS, J. & CHOUDHARY, C. 2018. DNA Repair Network Analysis Reveals Shieldin as a Key Regulator of NHEJ and PARP Inhibitor Sensitivity. *Cell,* 173**,** 972-988.e23.

GUSEV, A., LAWRENSON, K., LIN, X., LYRA, P. C., JR., KAR, S., VAVRA, K. C., SEGATO, F., FONSECA, M. A. S., LEE, J. M., PEJOVIC, T., LIU, G., KARLAN, B. Y., FREEDMAN, M. L., NOUSHMEHR, H., MONTEIRO, A. N., PHAROAH, P. D. P., PASANIUC, B. & GAYTHER, S. A. 2019. A transcriptome-wide association study of high-grade serous epithelial

ovarian cancer identifies new susceptibility genes and splice variants. *Nat Genet,* 51**,** 815-823.

HA, D.-H., MIN, A., KIM, S., JANG, H., KIM, S. H., KIM, H.-J., RYU, H. S., KU, J.-L., LEE, K.-H. & IM, S.-A. 2020. Antitumor effect of a WEE1 inhibitor and potentiation of olaparib sensitivity by DNA damage response modulation in triple-negative breast cancer. *Scientific Reports,* 10**,** 9930.

HADDAD, R. I., WEINSTEIN, L. J., WIECZOREK, T. J., BHATTACHARYA, N., RAFTOPOULOS, H., OSTER, M. W., ZHANG, X., LATHAM, V. M., JR., COSTELLO, R., FAUCHER, J., DEROSA, C., YULE, M., MILLER, L. P., LODA, M., POSNER, M. R. & SHAPIRO, G. I. 2004. A phase II clinical and pharmacodynamic study of E7070 in patients with metastatic, recurrent, or refractory squamous cell carcinoma of the head and neck: modulation of retinoblastoma protein phosphorylation by a novel chloroindolyl sulfonamide cell cycle inhibitor. *Clin Cancer Res,* 10**,** 4680-7.

HAN, J., RUAN, C., HUEN, M. S. Y., WANG, J., XIE, A., FU, C., LIU, T. & HUANG, J. 2017a. BRCA2 antagonizes classical and alternative nonhomologous end-joining to prevent gross genomic instability. *Nat Commun,* 8**,** 1470.

HAN, T., GORALSKI, M., GASKILL, N., CAPOTA, E., KIM, J., TING, T. C., XIE, Y., WILLIAMS, N. S. & NIJHAWAN, D. 2017b. Anticancer sulfonamides target splicing by inducing RBM39 degradation via recruitment to DCAF15. *Science,* 356.

HANASOGE, S. & LJUNGMAN, M. 2007. H2AX phosphorylation after UV irradiation is triggered by DNA repair intermediates and is mediated by the ATR kinase. *Carcinogenesis,* 28**,** 2298-2304.

HANZLIKOVA, H., KALASOVA, I., DEMIN, A. A., PENNICOTT, L. E., CIHLAROVA, Z. & CALDECOTT, K. W. 2018. The Importance of Poly(ADP-Ribose) Polymerase as a Sensor of Unligated Okazaki Fragments during DNA Replication. *Mol Cell,* 71**,** 319-331.e3.

HAO, J., LIU, Y., ZHANG, T., HE, J., ZHAO, H., AN, R. & XUE, Y. 2021. Efficacy and safety of PARP inhibitors in the treatment of advanced ovarian cancer: An updated systematic review and meta-analysis of randomized controlled trials. *Critical Reviews in Oncology/Hematology,* 157**,** 103145.

HARDING, S. M., COACKLEY, C. & BRISTOW, R. G. 2011. ATM-dependent phosphorylation of 53BP1 in response to genomic stress in oxic and hypoxic cells. *Radiother Oncol,* 99**,** 307-12.

HARITUNIANS, T., GUELLER, S., O'KELLY, J., ILARIA, R., JR. & KOEFFLER, H. P. 2008. Novel acyl sulfonamide LY573636-sodium: effect on hematopoietic malignant cells. *Oncol Rep,* 20**,** 1237-42.

HARRISION, D., GRAVELLS, P., THOMPSON, R. & BRYANT, H. E. 2020. Poly(ADP-Ribose) Glycohydrolase (PARG) vs. Poly(ADP-Ribose) Polymerase (PARP) - Function in Genome Maintenance and Relevance of Inhibitors for Anti-cancer Therapy. *Front Mol Biosci,* 7**,** 191.

HASTINGS, M. L., ALLEMAND, E., DUELLI, D. M., MYERS, M. P. & KRAINER, A. R. 2007. Control of Pre-mRNA Splicing by the General Splicing Factors PUF60 and U2AF65. *PLOS ONE,* 2**,** e538.

References

HE, Y. J., MEGHANI, K., CARON, M.-C., YANG, C., RONATO, D. A., BIAN, J., SHARMA, A., MOORE, J., NIRAJ, J., DETAPPE, A., DOENCH, J. G., LEGUBE, G., ROOT, D. E., D'ANDREA, A. D., DRANÉ, P., DE, S., KONSTANTINOPOULOS, P. A., MASSON, J.-Y. & CHOWDHURY, D. 2018. DYNLL1 binds to MRE11 to limit DNA end resection in BRCA1-deficient cells. *Nature,* 563**,** 522-526.

HELT, C. E., CLIBY, W. A., KENG, P. C., BAMBARA, R. A. & O'REILLY, M. A. 2005. Ataxia telangiectasia mutated (ATM) and ATM and Rad3-related protein exhibit selective target specificities in response to different forms of DNA damage. *J Biol Chem,* 280**,** 1186-92.

HEWITT, G., BOREL, V., SEGURA-BAYONA, S., TAKAKI, T., RUIS, P., BELLELLI, R., LEHMANN, L. C., SOMMEROVA, L., VANCEVSKA, A., TOMAS-LOBA, A., ZHU, K., COOPER, C., FUGGER, K., PATEL, H., GOLDSTONE, R., SCHNEIDER-LUFTMAN, D., HERBERT, E., STAMP, G., BROUGH, R., PETTITT, S., LORD, C. J., WEST, S. C., AHEL, I., AHEL, D., CHAPMAN, J. R., DEINDL, S. & BOULTON, S. J. 2021. Defective ALC1 nucleosome remodeling confers PARPi sensitization and synthetic lethality with HRD. *Mol Cell,* 81**,** 767-783.e11.

HONG, D. S., KURZROCK, R., NAING, A., WHELER, J. J., FALCHOOK, G. S., SCHIFFMAN, J. S., FAULKNER, N., PILAT, M. J., O'BRIEN, J. & LORUSSO, P. 2014. A phase I, open-label, single-arm, dose-escalation study of E7107, a precursor messenger ribonucleic acid (pre-mRNA) splicesome inhibitor administered intravenously on days 1 and 8 every 21 days to patients with solid tumors. *Invest New Drugs,* 32**,** 436-44.

HONG, R., MA, F., ZHANG, W., YU, X., LI, Q., LUO, Y., ZHU, C., JIANG, W. & XU, B. 2016. 53BP1 depletion causes PARP inhibitor resistance in ATM-deficient breast cancer cells. *BMC Cancer,* 16**,** 725.

HOOGDUIJN, M. J., VAN DEN BEUKEL, J. C., WIERSMA, L. C. & IJZER, J. 2013. Morphology and size of stem cells from mouse and whale: observational study. *Bmj,* 347**,** f6833.

HOPKINS, T. A., AINSWORTH, W. B., ELLIS, P. A., DONAWHO, C. K., DIGIAMMARINO, E. L., PANCHAL, S. C., ABRAHAM, V. C., ALGIRE, M. A., SHI, Y., OLSON, A. M., JOHNSON, E. F., WILSBACHER, J. L. & MAAG, D. 2019. PARP1 Trapping by PARP Inhibitors Drives Cytotoxicity in Both Cancer Cells and Healthy Bone Marrow. *Molecular Cancer Research,* 17**,** 409-419.

HOPKINS, T. A., SHI, Y., RODRIGUEZ, L. E., SOLOMON, L. R., DONAWHO, C. K., DIGIAMMARINO, E. L., PANCHAL, S. C., WILSBACHER, J. L., GAO, W., OLSON, A. M., STOLARIK, D. F., OSTERLING, D. J., JOHNSON, E. F. & MAAG, D. 2015. Mechanistic Dissection of PARP1 Trapping and the Impact on In Vivo Tolerability and Efficacy of PARP Inhibitors. *Mol Cancer Res,* 13**,** 1465-77.

HSIEHCHEN, D., GORALSKI, M., KIM, J., XIE, Y. & NIJHAWAN, D. 2020. Biomarkers for RBM39 degradation in acute myeloid leukemia. *Leukemia*.

HSU, P.-C., GOPINATH, R. K., HSUEH, Y.-A. & SHIEH, S.-Y. 2019. CHK2-mediated regulation of PARP1 in oxidative DNA damage response. *Oncogene,* 38**,** 1166-1182.

HU, D., GUO, E., YANG, B., QIN, X., FU, Y., FAN, J., ZHUANG, X., YAO, Q., LU, F., LI, W., XIAO, R., WU, X., YANG, X., WANG, Z., LIU, C., YOU, L., ZANG, R., ZHOU, Q., ZHAO, W., CHEN, G. & SUN, C. 2022. Mutation profiles in circulating cell-free DNA predict acquired resistance to olaparib in high-grade serous ovarian carcinoma. *Cancer Sci*.

References

HUANG DA, W., SHERMAN, B. T. & LEMPICKI, R. A. 2009. Systematic and integrative analysis of large gene lists using DAVID bioinformatics resources. *Nat Protoc,* 4**,** 44-57.

HUANG, S. C., ZHANG, H. S., YU, B., MCMAHON, E., NGUYEN, D. T., YU, F. H., OU, A. C., OU, J. P. & BENZ, E. J., JR. 2017. Protein 4.1R Exon 16 3' Splice Site Activation Requires Coordination among TIA1, Pcbp1, and RBM39 during Terminal Erythropoiesis. *Mol Cell Biol,* 37.

HÜLSKAMP, M. D., KRONENBERG, D. & STANGE, R. 2021. The small-molecule protein ligand interface stabiliser E7820 induces differential cell line specific responses of integrin α2 expression. *BMC Cancer,* 21**,** 571.

HURLEY, R. M., WAHNER HENDRICKSON, A. E., VISSCHER, D. W., ANSELL, P., HARRELL, M. I., WAGNER, J. M., NEGRON, V., GOERGEN, K. M., MAURER, M. J., OBERG, A. L., MENG, X. W., FLATTEN, K. S., DE JONGE, M. J. A., VAN HERPEN, C. D., GIETEMA, J. A., KOORNSTRA, R. H. T., JAGER, A., DEN HOLLANDER, M. W., DUDLEY, M., SHEPHERD, S. P., SWISHER, E. M. & KAUFMANN, S. H. 2019. 53BP1 as a potential predictor of response in PARP inhibitor-treated homologous recombination-deficient ovarian cancer. *Gynecol Oncol,* 153**,** 127-134.

HYUN, S. Y. & JANG, Y. J. 2015. p53 activates G_1 checkpoint following DNA damage by doxorubicin during transient mitotic arrest. *Oncotarget,* 6**,** 4804-15.

IBRAHIM, Y. H., GARCÍA-GARCÍA, C., SERRA, V., HE, L., TORRES-LOCKHART, K., PRAT, A., ANTON, P., COZAR, P., GUZMÁN, M., GRUESO, J., RODRÍGUEZ, O., CALVO, M. T., AURA, C., DÍEZ, O., RUBIO, I. T., PÉREZ, J., RODÓN, J., CORTÉS, J., ELLISEN, L. W., SCALTRITI, M. & BASELGA, J. 2012. PI3K Inhibition Impairs BRCA1/2 Expression and Sensitizes BRCA-Proficient Triple-Negative Breast Cancer to PARP Inhibition. *Cancer Discovery,* 2**,** 1036-1047.

INGHAM, S. L., WARWICK, J., BUCHAN, I., SAHIN, S., O'HARA, C., MORAN, A., HOWELL, A. & EVANS, D. G. 2013. Ovarian cancer among 8,005 women from a breast cancer family history clinic: no increased risk of invasive ovarian cancer in families testing negative for BRCA1 and BRCA2. *J Med Genet,* 50**,** 368-72.

IOVINE, B., IANNELLA, M. L. & BEVILACQUA, M. A. 2011. Damage-specific DNA binding protein 1 (DDB1): a protein with a wide range of functions. *Int J Biochem Cell Biol,* 43**,** 1664-7.

JAMAL, K., GALBIATI, A., ARMENIA, J., ILLUZZI, G., HALL, J., BENTOUATI, S., BARRELL, D., AHDESMAKI, M., O'CONNOR, M. J., LEO, E. & FORMENT, J. V. 2022. Drug-gene interaction screens coupled to tumour data analyses identify the most clinically-relevant cancer vulnerabilities driving sensitivity to PARP inhibition. *Cancer Research Communications*.

JASPERS, J. E., KERSBERGEN, A., BOON, U., SOL, W., VAN DEEMTER, L., ZANDER, S. A., DROST, R., WIENTJENS, E., JI, J., ALY, A., DOROSHOW, J. H., CRANSTON, A., MARTIN, N. M., LAU, A., O'CONNOR, M. J., GANESAN, S., BORST, P., JONKERS, J. & ROTTENBERG, S. 2013. Loss of 53BP1 causes PARP inhibitor resistance in Brca1-mutated mouse mammary tumors. *Cancer Discov,* 3**,** 68-81.

JASPERS, J. E., SOL, W., KERSBERGEN, A., SCHLICKER, A., GUYADER, C., XU, G., WESSELS, L., BORST, P., JONKERS, J. & ROTTENBERG, S. 2015. BRCA2-deficient sarcomatoid mammary tumors exhibit multidrug resistance. *Cancer Research,* 75**,** 732-741.

References

JILANI, A., RAMOTAR, D., SLACK, C., ONG, C., YANG, X. M., SCHERER, S. W. & LASKO, D. D. 1999. Molecular cloning of the human gene, PNKP, encoding a polynucleotide kinase 3'-phosphatase and evidence for its role in repair of DNA strand breaks caused by oxidative damage. *J Biol Chem,* 274**,** 24176-86.

JUHÁSZ, S., SMITH, R., SCHAUER, T., SPEKHARDT, D., MAMAR, H., ZENTOUT, S., CHAPUIS, C., HUET, S. & TIMINSZKY, G. 2020. The chromatin remodeler ALC1 underlies resistance to PARP inhibitor treatment. *Sci Adv,* 6.

JUNG, D. J., NA, S. Y., NA, D. S. & LEE, J. W. 2002. Molecular cloning and characterization of CAPER, a novel coactivator of activating protein-1 and estrogen receptors. *J Biol Chem,* 277**,** 1229-34.

JUNGMICHEL, S., ROSENTHAL, F., ALTMEYER, M., LUKAS, J., HOTTIGER, M. O. & NIELSEN, M. L. 2013. Proteome-wide identification of poly(ADP-Ribosyl)ation targets in different genotoxic stress responses. *Mol Cell,* 52**,** 272-85.

KADYROV, F. A., DZANTIEV, L., CONSTANTIN, N. & MODRICH, P. 2006. Endonucleolytic function of MutLalpha in human mismatch repair. *Cell,* 126**,** 297-308.

KANAGAL-SHAMANNA, R., MONTALBAN-BRAVO, G., SASAKI, K., DARBANIYAN, F., JABBOUR, E., BUESO-RAMOS, C., WEI, Y., CHIEN, K., KADIA, T., RAVANDI, F., BORTHAKUR, G., SOLTYSIAK, K. A., ROUTBORT, M., PATEL, K., PIERCE, S., MEDEIROS, L. J., KANTARJIAN, H. M. & GARCIA-MANERO, G. 2021. Only SF3B1 mutation involving K700E independently predicts overall survival in myelodysplastic syndromes. *Cancer,* 127**,** 3552-3565.

KANG, Y. K., PUTLURI, N., MAITY, S., TSIMELZON, A., ILKAYEVA, O., MO, Q., LONARD, D., MICHAILIDIS, G., SREEKUMAR, A., NEWGARD, C. B., WANG, M., TSAI, S. Y., TSAI, M.-J. & O'MALLEY, B. W. 2015. CAPER Is Vital for Energy and Redox Homeostasis by Integrating Glucose-Induced Mitochondrial Functions via ERR-α-Gabpa and Stress-Induced Adaptive Responses via NF-κB-cMYC. *PLOS Genetics,* 11**,** e1005116.

KAPLAN, A. R., GUEBLE, S. E., LIU, Y., OECK, S., KIM, H., YUN, Z. & GLAZER, P. M. 2019. Cediranib suppresses homology-directed DNA repair through down-regulation of BRCA1/2 and RAD51. *Sci Transl Med,* 11.

KARAKASHEV, S., FUKUMOTO, T., ZHAO, B., LIN, J., WU, S., FATKHUTDINOV, N., PARK, P. H., SEMENOVA, G., JEAN, S., CADUNGOG, M. G., BOROWSKY, M. E., KOSSENKOV, A. V., LIU, Q. & ZHANG, R. 2020. EZH2 Inhibition Sensitizes CARM1-High, Homologous Recombination Proficient Ovarian Cancers to PARP Inhibition. *Cancer Cell,* 37**,** 157-167.e6.

KARAKASHEV, S., ZHU, H., YOKOYAMA, Y., ZHAO, B., FATKHUTDINOV, N., KOSSENKOV, A. V., WILSON, A. J., SIMPKINS, F., SPEICHER, D., KHABELE, D., BITLER, B. G. & ZHANG, R. 2017. BET Bromodomain Inhibition Synergizes with PARP Inhibitor in Epithelial Ovarian Cancer. *Cell Rep,* 21**,** 3398-3405.

KAUFMAN, B., SHAPIRA-FROMMER, R., SCHMUTZLER, R. K., AUDEH, M. W., FRIEDLANDER, M., BALMANA, J., MITCHELL, G., FRIED, G., STEMMER, S. M., HUBERT, A., ROSENGARTEN, O., STEINER, M., LOMAN, N., BOWEN, K., FIELDING, A. & DOMCHEK, S. M. 2015. Olaparib monotherapy in patients with advanced cancer and a germline BRCA1/2 mutation. *J Clin Oncol,* 33**,** 244-50.

References

KE, J., LIU, F., TU, Y., CAI, Z., LUO, Y. & WU, X. 2021. PARP1–RNA interaction analysis: PARP1 regulates the expression of extracellular matrix-related genes in HK-2 renal proximal tubular epithelial cells. *FEBS Letters,* 595**,** 1375-1387.

KIM, C., KIM, I. H., KIM, S. I., KIM, Y. S., KANG, S. H., MOON, S. H., KIM, T. S. & KIM, S. K. 2011. Comparison of the Intraperitoneal, Retroorbital and per Oral Routes for F-18 FDG Administration as Effective Alternatives to Intravenous Administration in Mouse Tumor Models Using Small Animal PET/CT Studies. *Nucl Med Mol Imaging,* 45**,** 169-76.

KIM, E., GOREN, A. & AST, G. 2008. Insights into the connection between cancer and alternative splicing. *Trends Genet,* 24**,** 7-10.

KIM, G., ISON, G., MCKEE, A. E., ZHANG, H., TANG, S., GWISE, T., SRIDHARA, R., LEE, E., TZOU, A., PHILIP, R., CHIU, H. J., RICKS, T. K., PALMBY, T., RUSSELL, A. M., LADOUCEUR, G., PFUMA, E., LI, H., ZHAO, L., LIU, Q., VENUGOPAL, R., IBRAHIM, A. & PAZDUR, R. 2015. FDA Approval Summary: Olaparib Monotherapy in Patients with Deleterious Germline BRCA-Mutated Advanced Ovarian Cancer Treated with Three or More Lines of Chemotherapy. *Clin Cancer Res,* 21**,** 4257-61.

KIM, H., GEORGE, E., RAGLAND, R., RAFAIL, S., ZHANG, R., KREPLER, C., MORGAN, M., HERLYN, M., BROWN, E. & SIMPKINS, F. 2017. Targeting the ATR/CHK1 Axis with PARP Inhibition Results in Tumor Regression in BRCA-Mutant Ovarian Cancer Models. *Clin Cancer Res,* 23**,** 3097-3108.

KIM, H., XU, H., GEORGE, E., HALLBERG, D., KUMAR, S., JAGANNATHAN, V., MEDVEDEV, S., KINOSE, Y., DEVINS, K., VERMA, P., LY, K., WANG, Y., GREENBERG, R. A., SCHWARTZ, L., JOHNSON, N., SCHARPF, R. B., MILLS, G. B., ZHANG, R., VELCULESCU, V. E., BROWN, E. J. & SIMPKINS, F. 2020. Combining PARP with ATR inhibition overcomes PARP inhibitor and platinum resistance in ovarian cancer models. *Nature Communications,* 11**,** 3726.

KIM, M. K. 2018. Novel insight into the function of tankyrase. *Oncol Lett,* 16**,** 6895-6902.

KLAUDE, M., ERIKSSON, S., NYGREN, J. & AHNSTRÖM, G. 1996. The comet assay: mechanisms and technical considerations. *Mutat Res,* 363**,** 89-96.

KNEZEVIC, C. E., WRIGHT, G., RIX, L. L. R., KIM, W., KUENZI, B. M., LUO, Y., WATTERS, J. M., KOOMEN, J. M., HAURA, E. B., MONTEIRO, A. N., RADU, C., LAWRENCE, H. R. & RIX, U. 2016. Proteome-wide Profiling of Clinical PARP Inhibitors Reveals Compound-Specific Secondary Targets. *Cell Chem Biol,* 23**,** 1490-1503.

KONDRASHOVA, O., NGUYEN, M., SHIELD-ARTIN, K., TINKER, A. V., TENG, N. N. H., HARRELL, M. I., KUIPER, M. J., HO, G. Y., BARKER, H., JASIN, M., PRAKASH, R., KASS, E. M., SULLIVAN, M. R., BRUNETTE, G. J., BERNSTEIN, K. A., COLEMAN, R. L., FLOQUET, A., FRIEDLANDER, M., KICHENADASSE, G., O'MALLEY, D. M., OZA, A., SUN, J., ROBILLARD, L., MALONEY, L., BOWTELL, D., GIORDANO, H., WAKEFIELD, M. J., KAUFMANN, S. H., SIMMONS, A. D., HARDING, T. C., RAPONI, M., MCNEISH, I. A., SWISHER, E. M., LIN, K. K. & SCOTT, C. L. 2017. Secondary Somatic Mutations Restoring RAD51C and RAD51D Associated with Acquired Resistance to the PARP Inhibitor Rucaparib in High-Grade Ovarian Carcinoma. *Cancer Discov,* 7**,** 984-998.

References

KONECNY, G. E. & KRISTELEIT, R. S. 2016. PARP inhibitors for BRCA1/2-mutated and sporadic ovarian cancer: current practice and future directions. *Br J Cancer,* 115**,** 1157-1173.

KONSTANTINOPOULOS, P. A., WAGGONER, S., VIDAL, G. A., MITA, M., MORONEY, J. W., HOLLOWAY, R., VAN LE, L., SACHDEV, J. C., CHAPMAN-DAVIS, E., COLON-OTERO, G., PENSON, R. T., MATULONIS, U. A., KIM, Y. B., MOORE, K. N., SWISHER, E. M., FÄRKKILÄ, A., D'ANDREA, A., STRINGER-REASOR, E., WANG, J., BUERSTATTE, N., ARORA, S., GRAHAM, J. R., BOBILEV, D., DEZUBE, B. J. & MUNSTER, P. 2019. Single-Arm Phases 1 and 2 Trial of Niraparib in Combination With Pembrolizumab in Patients With Recurrent Platinum-Resistant Ovarian Carcinoma. *JAMA Oncology,* 5**,** 1141-1149.

KOZLOV, S. V., GRAHAM, M. E., PENG, C., CHEN, P., ROBINSON, P. J. & LAVIN, M. F. 2006. Involvement of novel autophosphorylation sites in ATM activation. *The EMBO journal,* 25**,** 3504-3514.

KRAJEWSKA, M., HEIJINK, A. M., BISSELINK, Y. J., SEINSTRA, R. I., SILLJÉ, H. H., DE VRIES, E. G. & VAN VUGT, M. A. 2013. Forced activation of Cdk1 via wee1 inhibition impairs homologous recombination. *Oncogene,* 32**,** 3001-8.

KRALOVICOVA, J., SEVCIKOVA, I., STEJSKALOVA, E., OBUCA, M., HILLER, M., STANEK, D. & VORECHOVSKY, I. 2018. PUF60-activated exons uncover altered 3' splice-site selection by germline missense mutations in a single RRM. *Nucleic Acids Res,* 46**,** 6166-6187.

KRISHAN, A. & HAMELIK, R. M. 2010. Click-iT proliferation assay with improved DNA histograms. *Curr Protoc Cytom,* Chapter 7**,** Unit7.36.

KUMAR, V., TIWARI, A., PANDITA, R., HUNT, C. & PANDITA, T. 2020. Role of HP1β during spermatogenesis and DNA replication. *Chromosoma,* 129.

KURAOKA, I., KOBERTZ, W. R., ARIZA, R. R., BIGGERSTAFF, M., ESSIGMANN, J. M. & WOOD, R. D. 2000. Repair of an interstrand DNA cross-link initiated by ERCC1-XPF repair/recombination nuclease. *J Biol Chem,* 275**,** 26632-6.

KURMAN, R. J. 2013. Origin and molecular pathogenesis of ovarian high-grade serous carcinoma. *Ann Oncol,* 24 Suppl 10**,** x16-21.

KURMAN, R. J. & SHIH IE, M. 2008. Pathogenesis of ovarian cancer: lessons from morphology and molecular biology and their clinical implications. *Int J Gynecol Pathol,* 27**,** 151-60.

KURMAN, R. J. & SHIH IE, M. 2011. Molecular pathogenesis and extraovarian origin of epithelial ovarian cancer--shifting the paradigm. *Hum Pathol,* 42**,** 918-31.

KURMAN, R. J. & SHIH IE, M. 2016. The Dualistic Model of Ovarian Carcinogenesis: Revisited, Revised, and Expanded. *Am J Pathol,* 186**,** 733-47.

LANE, D., MATTE, I., LAPLANTE, C., GARDE-GRANGER, P., CARIGNAN, A., BESSETTE, P., RANCOURT, C. & PICHÉ, A. 2016. CCL18 from ascites promotes ovarian cancer cell migration through proline-rich tyrosine kinase 2 signaling. *Mol Cancer,* 15**,** 58.

LANGDON, S. P., LAWRIE, S. S., HAY, F. G., HAWKES, M. M., MCDONALD, A., HAYWARD, I. P., SCHOL, D. J., HILGERS, J., LEONARD, R. C. & SMYTH, J. F. 1988. Characterization and properties of nine human ovarian adenocarcinoma cell lines. *Cancer Res,* 48**,** 6166-72.

LAPPIN, K. M., BARROS, E. M., JHUJH, S. S., IRWIN, G. W., MCMILLAN, H., LIBERANTE, F. G., LATIMER, C., LA BONTE, M. J., MILLS, K. I., HARKIN, D. P., STEWART, G. S. & SAVAGE,

References

K. I. 2022. Cancer-Associated SF3B1 Mutations Confer a BRCA-Like Cellular Phenotype and Synthetic Lethality to PARP Inhibitors. *Cancer Res,* 82**,** 819-830.

LATTANZIO, R., IEZZI, M., SALA, G., TINARI, N., FALASCA, M., ALBERTI, S., BUGLIONI, S., MOTTOLESE, M., PERRACCHIO, L., NATALI, P. G. & PIANTELLI, M. 2019. PLC-gamma-1 phosphorylation status is prognostic of metastatic risk in patients with early-stage Luminal-A and -B breast cancer subtypes. *BMC Cancer,* 19**,** 747.

LAWLOR, D., MARTIN, P., BUSSCHOTS, S., THERY, J., O'LEARY, J. J., HENNESSY, B. T. & STORDAL, B. 2014. PARP Inhibitors as P-glyoprotein Substrates. *Journal of Pharmaceutical Sciences,* 103**,** 1913-1920.

LAWRENSON, K., FONSECA, M. A. S., LIU, A. Y., SEGATO DEZEM, F., LEE, J. M., LIN, X., CORONA, R. I., ABBASI, F., VAVRA, K. C., DINH, H. Q., GILL, N. K., SEO, J.-H., COETZEE, S., LIN, Y. G., PEJOVIC, T., MHAWECH-FAUCEGLIA, P., ROWAT, A. C., DRAPKIN, R., KARLAN, B. Y., HAZELETT, D. J., FREEDMAN, M. L., GAYTHER, S. A. & NOUSHMEHR, H. 2019. A Study of High-Grade Serous Ovarian Cancer Origins Implicates the SOX18 Transcription Factor in Tumor Development. *Cell Reports,* 29**,** 3726-3735.e4.

LEDERMANN, J., HARTER, P., GOURLEY, C., FRIEDLANDER, M., VERGOTE, I., RUSTIN, G., SCOTT, C., MEIER, W., SHAPIRA-FROMMER, R., SAFRA, T., MATEI, D., MACPHERSON, E., WATKINS, C., CARMICHAEL, J. & MATULONIS, U. 2012. Olaparib maintenance therapy in platinum-sensitive relapsed ovarian cancer. *N Engl J Med,* 366**,** 1382-92.

LEDERMANN, J., HARTER, P., GOURLEY, C., FRIEDLANDER, M., VERGOTE, I., RUSTIN, G., SCOTT, C. L., MEIER, W., SHAPIRA-FROMMER, R., SAFRA, T., MATEI, D., FIELDING, A., SPENCER, S., DOUGHERTY, B., ORR, M., HODGSON, D., BARRETT, J. C. & MATULONIS, U. 2014. Olaparib maintenance therapy in patients with platinum-sensitive relapsed serous ovarian cancer: a preplanned retrospective analysis of outcomes by BRCA status in a randomised phase 2 trial. *Lancet Oncol,* 15**,** 852-61.

LEMAN, A. R., NOGUCHI, C., LEE, C. Y. & NOGUCHI, E. 2010. Human Timeless and Tipin stabilize replication forks and facilitate sister-chromatid cohesion. *J Cell Sci,* 123**,** 660-70.

LI, Q., DAMISH, A. W., FRAZIER, Z., LIU, D., REZNICHENKO, E., KAMBUROV, A., BELL, A., ZHAO, H., JORDAN, E. J., GAO, S. P., MA, J., ABBOSH, P. H., BELLMUNT, J., PLIMACK, E. R., LAZARO, J. B., SOLIT, D. B., BAJORIN, D., ROSENBERG, J. E., D'ANDREA, A. D., RIAZ, N., VAN ALLEN, E. M., IYER, G. & MOUW, K. W. 2019. ERCC2 Helicase Domain Mutations Confer Nucleotide Excision Repair Deficiency and Drive Cisplatin Sensitivity in Muscle-Invasive Bladder Cancer. *Clin Cancer Res,* 25**,** 977-988.

LIANG, Z., LIANG, F., TENG, Y., CHEN, X., LIU, J., LONGERICH, S., RAO, T., GREEN, A. M., COLLINS, N. B., XIONG, Y., LAN, L., SUNG, P. & KUPFER, G. M. 2019. Binding of FANCI-FANCD2 Complex to RNA and R-Loops Stimulates Robust FANCD2 Monoubiquitination. *Cell Rep,* 26**,** 564-572.e5.

LIAO, J. B., OVENELL, K. J., CURTIS, E. E., CECIL, D. L., KOEHNLEIN, M. R., RASTETTER, L. R., GAD, E. A. & DISIS, M. L. 2015. Preservation of tumor-host immune interactions with luciferase-tagged imaging in a murine model of ovarian cancer. *J Immunother Cancer,* 3**,** 16.

LIN, K. K., HARRELL, M. I., OZA, A. M., OAKNIN, A., RAY-COQUARD, I., TINKER, A. V., HELMAN, E., RADKE, M. R., SAY, C., VO, L. T., MANN, E., ISAACSON, J. D., MALONEY, L., O'MALLEY,

References

D. M., CHAMBERS, S. K., KAUFMANN, S. H., SCOTT, C. L., KONECNY, G. E., COLEMAN, R. L., SUN, J. X., GIORDANO, H., BRENTON, J. D., HARDING, T. C., MCNEISH, I. A. & SWISHER, E. M. 2019. BRCA Reversion Mutations in Circulating Tumor DNA Predict Primary and Acquired Resistance to the PARP Inhibitor Rucaparib in High-Grade Ovarian Carcinoma. *Cancer Discov,* 9**,** 210-219.

LIN, Q., LIU, W., XU, S., SHANG, H., LI, J., GUO, Y. & TONG, J. 2021. PARP inhibitors as maintenance therapy in newly diagnosed advanced ovarian cancer: a meta‐analysis. *BJOG: An International Journal of Obstetrics & Gynaecology,* 128**,** 485-493.

LIN, S. Y., LI, K., STEWART, G. S. & ELLEDGE, S. J. 2004. Human Claspin works with BRCA1 to both positively and negatively regulate cell proliferation. *Proc Natl Acad Sci U S A,* 101**,** 6484-9.

LINDAHL, T., SATOH, M. S., POIRIER, G. G. & KLUNGLAND, A. 1995. Post-translational modification of poly(ADP-ribose) polymerase induced by DNA strand breaks. *Trends Biochem Sci,* 20**,** 405-11.

LISIO, M.-A., FU, L., GOYENECHE, A., GAO, Z.-H. & TELLERIA, C. 2019. High-Grade Serous Ovarian Cancer: Basic Sciences, Clinical and Therapeutic Standpoints. *International Journal of Molecular Sciences,* 20**,** 952.

LIU, J., LV, D., WANG, X., WANG, R. & LI, X. 2021. Systematic Profiling of Alternative Splicing Events in Ovarian Cancer. *Front Oncol,* 11**,** 622805.

LIU, J. F., BARRY, W. T., BIRRER, M., LEE, J.-M., BUCKANOVICH, R. J., FLEMING, G. F., RIMEL, B. J., BUSS, M. K., NATTAM, S., HURTEAU, J., LUO, W., QUY, P., WHALEN, C., OBERMAYER, L., LEE, H., WINER, E. P., KOHN, E. C., IVY, S. P. & MATULONIS, U. A. 2014. Combination cediranib and olaparib versus olaparib alone for women with recurrent platinum-sensitive ovarian cancer: a randomised phase 2 study. *The Lancet Oncology,* 15**,** 1207-1214.

LIU, P., BARKLEY, L. R., DAY, T., BI, X., SLATER, D. M., ALEXANDROW, M. G., NASHEUER, H.-P. & VAZIRI, C. 2006. The Chk1-mediated S-phase Checkpoint Targets Initiation Factor Cdc45 via a Cdc25A/Cdk2-independent Mechanism*. *Journal of Biological Chemistry,* 281**,** 30631-30644.

LIU, Q., GUNTUKU, S., CUI, X. S., MATSUOKA, S., CORTEZ, D., TAMAI, K., LUO, G., CARATTINI-RIVERA, S., DEMAYO, F., BRADLEY, A., DONEHOWER, L. A. & ELLEDGE, S. J. 2000. Chk1 is an essential kinase that is regulated by Atr and required for the G(2)/M DNA damage checkpoint. *Genes Dev,* 14**,** 1448-59.

LIU, Y., BURNESS, M. L., MARTIN-TREVINO, R., GUY, J., BAI, S., HAROUAKA, R., BROOKS, M. D., SHANG, L., FOX, A., LUTHER, T. K., DAVIS, A., BAKER, T. L., COLACINO, J., CLOUTHIER, S. G., SHAO, Z.-M., WICHA, M. S. & LIU, S. 2017. RAD51 Mediates Resistance of Cancer Stem Cells to PARP Inhibition in Triple-Negative Breast Cancer. *Clinical Cancer Research,* 23**,** 514-522.

LLOYD, R. L., WIJNHOVEN, P. W. G., RAMOS-MONTOYA, A., WILSON, Z., ILLUZZI, G., FALENTA, K., JONES, G. N., JAMES, N., CHABBERT, C. D., STOTT, J., DEAN, E., LAU, A. & YOUNG, L. A. 2020. Combined PARP and ATR inhibition potentiates genome instability and cell death in ATM-deficient cancer cells. *Oncogene,* 39**,** 4869-4883.

References

LOERCH, S., MAUCUER, A., MANCEAU, V., GREEN, M. R. & KIELKOPF, C. L. 2014. Cancer-relevant splicing factor CAPERalpha engages the essential splicing factor SF3b155 in a specific ternary complex. *J Biol Chem,* 289**,** 17325-37.

LOEWE, S. 1953. The problem of synergism and antagonism of combined drugs. *Arzneimittelforschung,* 3**,** 285-290.

LOMBARD, A. P., LIU, C., ARMSTRONG, C. M., D'ABRONZO, L. S., LOU, W., CHEN, H., DALL'ERA, M., GHOSH, P. M., EVANS, C. P. & GAO, A. C. 2019. Overexpressed ABCB1 Induces Olaparib-Taxane Cross-Resistance in Advanced Prostate Cancer. *Translational Oncology,* 12**,** 871-878.

LORUSSO, D., MALTESE, G., SABATUCCI, I., CRESTA, S., MATTEO, C., CERUTI, T., D'INCALCI, M., ZUCCHETTI, M., RASPAGLIESI, F., SONETTO, C., SINNO, V., RONZULLI, D., GIOLITTO, S. & DE BRAUD, F. 2021. Phase I Study of Rucaparib in Combination with Bevacizumab in Ovarian Cancer Patients: Maximum Tolerated Dose and Pharmacokinetic Profile. *Target Oncol,* 16**,** 59-68.

LU, C., ZHU, F., CHO, Y. Y., TANG, F., ZYKOVA, T., MA, W. Y., BODE, A. M. & DONG, Z. 2006. Cell apoptosis: requirement of H2AX in DNA ladder formation, but not for the activation of caspase-3. *Mol Cell,* 23**,** 121-32.

LU, J., JIANG, H., LI, D., CHEN, T., WANG, Y., PU, Z. & XU, G. 2021a. Proximity Labeling, Quantitative Proteomics, and Biochemical Studies Revealed the Molecular Mechanism for the Inhibitory Effect of Indisulam on the Proliferation of Gastric Cancer Cells. *Journal of Proteome Research,* 20**,** 4462-4474.

LU, S. X., DE NEEF, E., THOMAS, J. D., SABIO, E., ROUSSEAU, B., GIGOUX, M., KNORR, D. A., GREENBAUM, B., ELHANATI, Y., HOGG, S. J., CHOW, A., GHOSH, A., XIE, A., ZAMARIN, D., CUI, D., ERICKSON, C., SINGER, M., CHO, H., WANG, E., LU, B., DURHAM, B. H., SHAH, H., CHOWELL, D., GABEL, A. M., SHEN, Y., LIU, J., JIN, J., RHODES, M. C., TAYLOR, R. E., MOLINA, H., WOLCHOK, J. D., MERGHOUB, T., DIAZ, L. A., JR., ABDEL-WAHAB, O. & BRADLEY, R. K. 2021b. Pharmacologic modulation of RNA splicing enhances anti-tumor immunity. *Cell,* 184**,** 4032-4047.e31.

LU, Y., LIU, Y. & YANG, C. 2017. Evaluating In Vitro DNA Damage Using Comet Assay. *J Vis Exp*.

LUO, J., OU, S., WEI, H., QIN, X. & JIANG, Q. 2022. Comparative Efficacy and Safety of Poly (ADP-Ribose) Polymerase Inhibitors in Patients With Ovarian Cancer: A Systematic Review and Network Meta-Analysis. *Front Oncol,* 12**,** 815265.

LUSK, H., BURDETTE, J. E. & SANCHEZ, L. M. 2021. Models for measuring metabolic chemical changes in the metastasis of high grade serous ovarian cancer: fallopian tube, ovary, and omentum. *Mol Omics,* 17**,** 819-832.

LUTZE, J., WARRINGTON, S. E. & KRON, S. J. 2022. TdT-dUTP DSB End Labeling (TUDEL), for Specific, Direct In Situ Labeling of DNA Double Strand Breaks. *Methods Mol Biol,* 2394**,** 299-317.

LYKKE-ANDERSEN, S. & JENSEN, T. H. 2015. Nonsense-mediated mRNA decay: an intricate machinery that shapes transcriptomes. *Nature Reviews Molecular Cell Biology,* 16**,** 665-677.

References

MAI, S., QU, X., LI, P., MA, Q., CAO, C. & LIU, X. 2016a. Global regulation of alternative RNA splicing by the SR-rich protein RBM39. *Biochim Biophys Acta,* 1859**,** 1014-24.

MAI, S., QU, X., LI, P., MA, Q., LIU, X. & CAO, C. 2016b. Functional interaction between nonreceptor tyrosine kinase c-Abl and SR-Rich protein RBM39. *Biochem Biophys Res Commun,* 473**,** 355-360.

MANEK, R., PAKZAMIR, E., MHAWECH-FAUCEGLIA, P., PEJOVIC, T., SOWTER, H., GAYTHER, S. A. & LAWRENSON, K. 2016. Targeting Src in endometriosis-associated ovarian cancer. *Oncogenesis,* 5**,** e251-e251.

MANIATI, E., BERLATO, C., GOPINATHAN, G., HEATH, O., KOTANTAKI, P., LAKHANI, A., MCDERMOTT, J., PEGRUM, C., DELAINE-SMITH, R. M., PEARCE, O. M. T., HIRANI, P., JOY, J. D., SZABOVA, L., PERETS, R., SANSOM, O. J., DRAPKIN, R., BAILEY, P. & BALKWILL, F. R. 2020. Mouse Ovarian Cancer Models Recapitulate the Human Tumor Microenvironment and Patient Response to Treatment. *Cell Rep,* 30**,** 525-540.e7.

MARHEINEKE, K., HYRIEN, O. & KRUDE, T. 2005. Visualization of bidirectional initiation of chromosomal DNA replication in a human cell free system. *Nucleic Acids Res,* 33**,** 6931-41.

MATSUOKA, S., HUANG, M. & ELLEDGE, S. J. 1998. Linkage of ATM to cell cycle regulation by the Chk2 protein kinase. *Science,* 282**,** 1893-7.

MATSUOKA, S., ROTMAN, G., OGAWA, A., SHILOH, Y., TAMAI, K. & ELLEDGE, S. J. 2000. Ataxia telangiectasia-mutated phosphorylates Chk2 in vivo and in vitro. *Proc Natl Acad Sci U S A,* 97**,** 10389-94.

MATULONIS, U. A. 2018. Management of newly diagnosed or recurrent ovarian cancer. *Clin Adv Hematol Oncol,* 16**,** 426-437.

MATVEEVA, E., MAIORANO, J., ZHANG, Q., ETELEEB, A. M., CONVERTINI, P., CHEN, J., INFANTINO, V., STAMM, S., WANG, J., ROUCHKA, E. C. & FONDUFE-MITTENDORF, Y. N. 2016. Involvement of PARP1 in the regulation of alternative splicing. *Cell Discov,* 2**,** 15046.

MATVEEVA, E. A., AL-TINAWI, Q. M. H., ROUCHKA, E. C. & FONDUFE-MITTENDORF, Y. N. 2019a. Coupling of PARP1-mediated chromatin structural changes to transcriptional RNA polymerase II elongation and cotranscriptional splicing. *Epigenetics & Chromatin,* 12**,** 15.

MATVEEVA, E. A., MATHBOUT, L. F. & FONDUFE-MITTENDORF, Y. N. 2019b. PARP1 is a versatile factor in the regulation of mRNA stability and decay. *Scientific Reports,* 9**,** 3722.

MAVADDAT, N., PEOCK, S., FROST, D., ELLIS, S., PLATTE, R., FINEBERG, E., EVANS, D. G., IZATT, L., EELES, R. A., ADLARD, J., DAVIDSON, R., ECCLES, D., COLE, T., COOK, J., BREWER, C., TISCHKOWITZ, M., DOUGLAS, F., HODGSON, S., WALKER, L., PORTEOUS, M. E., MORRISON, P. J., SIDE, L. E., KENNEDY, M. J., HOUGHTON, C., DONALDSON, A., ROGERS, M. T., DORKINS, H., MIEDZYBRODZKA, Z., GREGORY, H., EASON, J., BARWELL, J., MCCANN, E., MURRAY, A., ANTONIOU, A. C. & EASTON, D. F. 2013. Cancer risks for BRCA1 and BRCA2 mutation carriers: results from prospective analysis of EMBRACE. *J Natl Cancer Inst,* 105**,** 812-22.

References

MAYA-MENDOZA, A., MOUDRY, P., MERCHUT-MAYA, J. M., LEE, M., STRAUSS, R. & BARTEK, J. 2018. High speed of fork progression induces DNA replication stress and genomic instability. *Nature,* 559**,** 279-284.

MAYOR, P., GAY, L. M., LELE, S. & ELVIN, J. A. 2017. BRCA1 reversion mutation acquired after treatment identified by liquid biopsy. *Gynecol Oncol Rep,* 21**,** 57-60.

MCFARLAND, J. M., HO, Z. V., KUGENER, G., DEMPSTER, J. M., MONTGOMERY, P. G., BRYAN, J. G., KRILL-BURGER, J. M., GREEN, T. M., VAZQUEZ, F., BOEHM, J. S., GOLUB, T. R., HAHN, W. C., ROOT, D. E. & TSHERNIAK, A. 2018. Improved estimation of cancer dependencies from large-scale RNAi screens using model-based normalization and data integration. *Nature Communications,* 9**,** 4610.

MCINTOSH, D. & BLOW, J. J. 2012. Dormant origins, the licensing checkpoint, and the response to replicative stresses. *Cold Spring Harb Perspect Biol,* 4.

MEIER, T., UHLIK, M., CHINTHARLAPALLI, S., DOWLESS, M., VAN HORN, R., STEWART, J., BLOSSER, W., COOK, J., YOUNG, D., YE, X., EVANS, G., CREDILLE, K., BALLARD, D., HUBER, L., CAPEN, A., CHEDID, M., ILARIA, R., JR., SMITH, M. C. & STANCATO, L. 2011. Tasisulam sodium, an antitumor agent that inhibits mitotic progression and induces vascular normalization. *Mol Cancer Ther,* 10**,** 2168-78.

MENG, X., YANG, S. & CAMP, V. J. A. 2019. The Interplay Between the DNA Damage Response, RNA Processing and Extracellular Vesicles. *Front Oncol,* 9**,** 1538.

MERCIER, I., CASIMIRO, M. C., ZHOU, J., WANG, C., PLYMIRE, C., BRYANT, K. G., DAUMER, K. M., SOTGIA, F., BONUCCELLI, G., WITKIEWICZ, A. K., LIN, J., TRAN, T. H., MILLIMAN, J., FRANK, P. G., JASMIN, J. F., RUI, H., PESTELL, R. G. & LISANTI, M. P. 2009. Genetic ablation of caveolin-1 drives estrogen-hypersensitivity and the development of DCIS-like mammary lesions. *Am J Pathol,* 174**,** 1172-90.

MERCIER, I., GONZALES, D. M., QUANN, K., PESTELL, T. G., MOLCHANSKY, A., SOTGIA, F., HULIT, J., GANDARA, R., WANG, C., PESTELL, R. G., LISANTI, M. P. & JASMIN, J.-F. 2014. CAPER, a novel regulator of human breast cancer progression. *Cell cycle (Georgetown, Tex.),* 13**,** 1256-1264.

MEYER, C. T., WOOTEN, D. J., LOPEZ, C. F. & QUARANTA, V. 2020. Charting the Fragmented Landscape of Drug Synergy. *Trends Pharmacol Sci,* 41**,** 266-280.

MEYER, C. T., WOOTEN, D. J., PAUDEL, B. B., BAUER, J., HARDEMAN, K. N., WESTOVER, D., LOVLY, C. M., HARRIS, L. A., TYSON, D. R. & QUARANTA, V. 2019. Quantifying Drug Combination Synergy along Potency and Efficacy Axes. *Cell Syst,* 8**,** 97-108.e16.

MEYERS, R. M., BRYAN, J. G., MCFARLAND, J. M., WEIR, B. A., SIZEMORE, A. E., XU, H., DHARIA, N. V., MONTGOMERY, P. G., COWLEY, G. S., PANTEL, S., GOODALE, A., LEE, Y., ALI, L. D., JIANG, G., LUBONJA, R., HARRINGTON, W. F., STRICKLAND, M., WU, T., HAWES, D. C., ZHIVICH, V. A., WYATT, M. R., KALANI, Z., CHANG, J. J., OKAMOTO, M., STEGMAIER, K., GOLUB, T. R., BOEHM, J. S., VAZQUEZ, F., ROOT, D. E., HAHN, W. C. & TSHERNIAK, A. 2017. Computational correction of copy number effect improves specificity of CRISPR-Cas9 essentiality screens in cancer cells. *Nat Genet,* 49**,** 1779-1784.

MILLER, R. M., JORDAN, B. T., MEHLFERBER, M. M., JEFFERY, E. D., CHATZIPANTSIOU, C., KAUR, S., MILLIKIN, R. J., DAI, Y., TIBERI, S., CASTALDI, P. J., SHORTREED, M. R., LUCKEY, C. J., CONESA, A., SMITH, L. M., DESLATTES MAYS, A. & SHEYNKMAN, G. M. 2022.

References

Enhanced protein isoform characterization through long-read proteogenomics. *Genome Biology,* 23**,** 69.

MITRA, A. K., DAVIS, D. A., TOMAR, S., ROY, L., GURLER, H., XIE, J., LANTVIT, D. D., CARDENAS, H., FANG, F., LIU, Y., LOUGHRAN, E., YANG, J., SHARON STACK, M., EMERSON, R. E., COWDEN DAHL, K. D., V BARBOLINA, M., NEPHEW, K. P., MATEI, D. & BURDETTE, J. E. 2015. In vivo tumor growth of high-grade serous ovarian cancer cell lines. *Gynecologic oncology,* 138**,** 372-377.

MOEGLIN, E., DESPLANCQ, D., CONIC, S., OULAD-ABDELGHANI, M., STOESSEL, A., CHIPER, M., VIGNERON, M., DIDIER, P., TORA, L. & WEISS, E. 2019. Uniform Widespread Nuclear Phosphorylation of Histone H2AX Is an Indicator of Lethal DNA Replication Stress. *Cancers (Basel),* 11.

MONTEILHET, C., PERRIN, A., THIERRY, A., COLLEAUX, L. & DUJON, B. 1990. Purification and characterization of the in vitro activity of I-Sce I, a novel and highly specific endonuclease encoded by a group I intron. *Nucleic Acids Res,* 18**,** 1407-13.

MOORE, K., COLOMBO, N., SCAMBIA, G., KIM, B.-G., OAKNIN, A., FRIEDLANDER, M., LISYANSKAYA, A., FLOQUET, A., LEARY, A., SONKE, G. S., GOURLEY, C., BANERJEE, S., OZA, A., GONZÁLEZ-MARTÍN, A., AGHAJANIAN, C., BRADLEY, W., MATHEWS, C., LIU, J., LOWE, E. S., BLOOMFIELD, R. & DISILVESTRO, P. 2018. Maintenance Olaparib in Patients with Newly Diagnosed Advanced Ovarian Cancer. *New England Journal of Medicine,* 379**,** 2495-2505.

MOORE, K. N., BOOKMAN, M., SEHOULI, J., MILLER, A., ANDERSON, C., SCAMBIA, G., MYERS, T., TASKIRAN, C., ROBISON, K., MÄENPÄÄ, J., WILLMOTT, L., COLOMBO, N., THOMES-PEPIN, J., LIONTOS, M., GOLD, M. A., GARCIA, Y., SHARMA, S. K., DARUS, C. J., AGHAJANIAN, C., OKAMOTO, A., WU, X., SAFIN, R., WU, F., MOLINERO, L., MAIYA, V., KHOR, V. K., LIN, Y. G. & PIGNATA, S. 2021. Atezolizumab, Bevacizumab, and Chemotherapy for Newly Diagnosed Stage III or IV Ovarian Cancer: Placebo-Controlled Randomized Phase III Trial (IMagyn050/GOG 3015/ENGOT-OV39). *J Clin Oncol,* 39**,** 1842-1855.

MORTUSEWICZ, O., AMÉ, J. C., SCHREIBER, V. & LEONHARDT, H. 2007. Feedback-regulated poly(ADP-ribosyl)ation by PARP-1 is required for rapid response to DNA damage in living cells. *Nucleic Acids Res,* 35**,** 7665-75.

MUKHERJEE, B., KESSINGER, C., KOBAYASHI, J., CHEN, B. P., CHEN, D. J., CHATTERJEE, A. & BURMA, S. 2006. DNA-PK phosphorylates histone H2AX during apoptotic DNA fragmentation in mammalian cells. *DNA Repair (Amst),* 5**,** 575-90.

MURAI, J., HUANG, S.-Y. N., RENAUD, A., ZHANG, Y., JI, J., TAKEDA, S., MORRIS, J., TEICHER, B., DOROSHOW, J. H. & POMMIER, Y. 2014. Stereospecific PARP Trapping by BMN 673 and Comparison with Olaparib and Rucaparib. *Molecular Cancer Therapeutics,* 13**,** 433.

MURAI, J., HUANG, S. Y., DAS, B. B., RENAUD, A., ZHANG, Y., DOROSHOW, J. H., JI, J., TAKEDA, S. & POMMIER, Y. 2012. Trapping of PARP1 and PARP2 by Clinical PARP Inhibitors. *Cancer Res,* 72**,** 5588-99.

MURAI, J. & POMMIER, Y. 2019. PARP Trapping Beyond Homologous Recombination and Platinum Sensitivity in Cancers. *Annual Review of Cancer Biology,* 3**,** 131-150.

References

MURRAY, J., THOMAS, H., BERRY, P., KYLE, S., PATTERSON, M., JONES, C., LOS, G., HOSTOMSKY, Z., PLUMMER, E. R., BODDY, A. V. & CURTIN, N. J. 2014. Tumour cell retention of rucaparib, sustained PARP inhibition and efficacy of weekly as well as daily schedules. *British Journal of Cancer,* 110**,** 1977-1984.

MUSACCHIO, L., CICALA, C. M., CAMARDA, F., GHIZZONI, V., GIUDICE, E., CARBONE, M. V., RICCI, C., PERRI, M. T., TRONCONI, F., GENTILE, M., SALUTARI, V., SCAMBIA, G. & LORUSSO, D. 2022. Combining PARP inhibition and immune checkpoint blockade in ovarian cancer patients: a new perspective on the horizon? *ESMO Open,* 7**,** 100536.

NAGY, Z., KALOUSI, A., FURST, A., KOCH, M., FISCHER, B. & SOUTOGLOU, E. 2016. Tankyrases Promote Homologous Recombination and Check Point Activation in Response to DSBs. *PLoS Genet,* 12**,** e1005791.

NIEMINUSZCZY, J., SCHWAB, R. A. & NIEDZWIEDZ, W. 2016. The DNA fibre technique – tracking helicases at work. *Methods,* 108**,** 92-98.

NIIDA, H., TSUGE, S., KATSUNO, Y., KONISHI, A., TAKEDA, N. & NAKANISHI, M. 2005. Depletion of Chk1 Leads to Premature Activation of Cdc2-cyclin B and Mitotic Catastrophe*. *Journal of Biological Chemistry,* 280**,** 39246-39252.

NIJHUIS, A., SIKKA, A., YOGEV, O., HERENDI, L., BALCELLS, C., MA, Y., POON, E., ECKOLD, C., VALBUENA, G. N., XU, Y., LIU, Y., DA COSTA, B. M., GRUET, M., WICKREMESINGHE, C., BENITO, A., KRAMER, H., MONTOYA, A., CARLING, D., WANT, E. J., JAMIN, Y., CHESLER, L. & KEUN, H. C. 2022. Indisulam targets RNA splicing and metabolism to serve as a therapeutic strategy for high-risk neuroblastoma. *Nature Communications,* 13**,** 1380.

NITISS, J. L. 2009. Targeting DNA topoisomerase II in cancer chemotherapy. *Nat Rev Cancer,* 9**,** 338-50.

NMPA. 2021. *国家药监局附条件批准帕米帕利胶囊上市/Pamiparib is approved by NMPA for prescription* [Online]. (China) National Medical Products Administration. Available: https://www.nmpa.gov.cn/directory/web/nmpa/yaowen/ypjgyw/20210507094042167.html [Accessed 15 July 2022].

NOORDERMEER, S. M., ADAM, S., SETIAPUTRA, D., BARAZAS, M., PETTITT, S. J., LING, A. K., OLIVIERI, M., ÁLVAREZ-QUILÓN, A., MOATTI, N., ZIMMERMANN, M., ANNUNZIATO, S., KRASTEV, D. B., SONG, F., BRANDSMA, I., FRANKUM, J., BROUGH, R., SHERKER, A., LANDRY, S., SZILARD, R. K., MUNRO, M. M., MCEWAN, A., GOULLET DE RUGY, T., LIN, Z.-Y., HART, T., MOFFAT, J., GINGRAS, A.-C., MARTIN, A., VAN ATTIKUM, H., JONKERS, J., LORD, C. J., ROTTENBERG, S. & DUROCHER, D. 2018. The shieldin complex mediates 53BP1-dependent DNA repair. *Nature,* 560**,** 117-121.

NOORDERMEER, S. M. & VAN ATTIKUM, H. 2019. PARP Inhibitor Resistance: A Tug-of-War in BRCA-Mutated Cells. *Trends Cell Biol,* 29**,** 820-834.

ODA, Y., OWA, T., SATO, T., BOUCHER, B., DANIELS, S., YAMANAKA, H., SHINOHARA, Y., YOKOI, A., KUROMITSU, J. & NAGASU, T. 2003. Quantitative chemical proteomics for identifying candidate drug targets. *Anal Chem,* 75**,** 2159-65.

OKAMOTO, Y., ABE, M., ITAYA, A., TOMIDA, J., ISHIAI, M., TAKAORI-KONDO, A., TAOKA, M., ISOBE, T. & TAKATA, M. 2019. FANCD2 protects genome stability by recruiting RNA processing enzymes to resolve R-loops during mild replication stress. *Febs j,* 286**,** 139-150.

References

OLIVE, P. L. & BANÁTH, J. P. 2006. The comet assay: a method to measure DNA damage in individual cells. *Nature Protocols,* 1**,** 23-29.

OLIVE, P. L., WLODEK, D. & BANÁTH, J. P. 1991. DNA double-strand breaks measured in individual cells subjected to gel electrophoresis. *Cancer Res,* 51**,** 4671-6.

OLIVEROS, J. C. 2007. VENNY. An interactive tool for comparing lists with Venn Diagrams. *http://bioinfogp. cnb. csic. es/tools/venny/index. html*.

OLIVIERI, M., CHO, T., ÁLVAREZ-QUILÓN, A., LI, K., SCHELLENBERG, M. J., ZIMMERMANN, M., HUSTEDT, N., ROSSI, S. E., ADAM, S., MELO, H., HEIJINK, A. M., SASTRE-MORENO, G., MOATTI, N., SZILARD, R. K., MCEWAN, A., LING, A. K., SERRANO-BENITEZ, A., UBHI, T., FENG, S., PAWLING, J., DELGADO-SAINZ, I., FERGUSON, M. W., DENNIS, J. W., BROWN, G. W., CORTÉS-LEDESMA, F., WILLIAMS, R. S., MARTIN, A., XU, D. & DUROCHER, D. 2020. A Genetic Map of the Response to DNA Damage in Human Cells. *Cell,* 182**,** 481-496.e21.

OUYANG, Y., XIA, K., YANG, X., ZHANG, S., WANG, L., REN, S., ZHOU, H., LIU, Y. & TANG, F. 2021. Alternative splicing acts as an independent prognosticator in ovarian carcinoma. *Scientific Reports,* 11**,** 10413.

OWA, T., YOSHINO, H., OKAUCHI, T., YOSHIMATSU, K., OZAWA, Y., SUGI, N. H., NAGASU, T., KOYANAGI, N. & KITOH, K. 1999. Discovery of novel antitumor sulfonamides targeting G1 phase of the cell cycle. *J Med Chem,* 42**,** 3789-99.

OZAWA, Y., KUSANO, K., OWA, T., YOKOI, A., ASADA, M. & YOSHIMATSU, K. 2012. Therapeutic potential and molecular mechanism of a novel sulfonamide anticancer drug, indisulam (E7070) in combination with CPT-11 for cancer treatment. *Cancer Chemother Pharmacol,* 69**,** 1353-62.

OZAWA, Y., SUGI, N. H., NAGASU, T., OWA, T., WATANABE, T., KOYANAGI, N., YOSHINO, H., KITOH, K. & YOSHIMATSU, K. 2001. E7070, a novel sulphonamide agent with potent antitumour activity in vitro and in vivo. *Eur J Cancer,* 37**,** 2275-82.

PALOZOLA, K. C., DONAHUE, G., LIU, H., GRANT, G. R., BECKER, J. S., COTE, A., YU, H., RAJ, A. & ZARET, K. S. 2017. Mitotic transcription and waves of gene reactivation during mitotic exit. *Science,* 358**,** 119-122.

PANIER, S. & BOULTON, S. J. 2014. Double-strand break repair: 53BP1 comes into focus. *Nat Rev Mol Cell Biol,* 15**,** 7-18.

PANNUNZIO, N. R., WATANABE, G. & LIEBER, M. R. 2018. Nonhomologous DNA end-joining for repair of DNA double-strand breaks. *J Biol Chem,* 293**,** 10512-10523.

PARK, E. J., CHAN, D. W., PARK, J. H., OETTINGER, M. A. & KWON, J. 2003. DNA-PK is activated by nucleosomes and phosphorylates H2AX within the nucleosomes in an acetylation-dependent manner. *Nucleic Acids Res,* 31**,** 6819-27.

PARMAR, K., KOCHUPURAKKAL, B. S., LAZARO, J.-B., WANG, Z. C., PALAKURTHI, S., KIRSCHMEIER, P. T., YANG, C., SAMBEL, L. A., FÄRKKILÄ, A., REZNICHENKO, E., REAVIS, H. D., DUNN, C. E., ZOU, L., DO, K. T., KONSTANTINOPOULOS, P. A., MATULONIS, U. A., LIU, J. F., D'ANDREA, A. D. & SHAPIRO, G. I. 2019. The CHK1 Inhibitor Prexasertib Exhibits Monotherapy Activity in High-Grade Serous Ovarian Cancer Models and Sensitizes to PARP inhibition. *Clinical Cancer Research***,** clincanres.0448.2019.

References

PASQUIER, J., GOSSET, M., GEYL, C., HOARAU-VÉCHOT, J., CHEVROT, A., POCARD, M., MIRSHAHI, M., LIS, R., RAFII, A. & TOUBOUL, C. 2018. CCL2/CCL5 secreted by the stroma induce IL-6/PYK2 dependent chemoresistance in ovarian cancer. *Mol Cancer,* 17**,** 47.

PAUL, B. T., BLANCHARD, Z., RIDGWAY, M. & ELSHAMY, W. M. 2015. BRCA1-IRIS inactivation sensitizes ovarian tumors to cisplatin. *Oncogene,* 34**,** 3036-52.

PECH, M., FONG, L. E., VILLALTA, J. E., CHAN, L. J., KHARBANDA, S., O'BRIEN, J. J., MCALLISTER, F. E., FIRESTONE, A. J., JAN, C. H. & SETTLEMAN, J. 2019. Systematic identification of cancer cell vulnerabilities to natural killer cell-mediated immune surveillance. *Elife,* 8.

PERVOUCHINE, D., POPOV, Y., BERRY, A., BORSARI, B., FRANKISH, A. & GUIGO, R. 2019. Integrative transcriptomic analysis suggests new autoregulatory splicing events coupled with nonsense-mediated mRNA decay. *Nucleic Acids Res,* 47**,** 5293-5306.

PETERMANN, E., MAYA-MENDOZA, A., ZACHOS, G., GILLESPIE, D. A., JACKSON, D. A. & CALDECOTT, K. W. 2006. Chk1 requirement for high global rates of replication fork progression during normal vertebrate S phase. *Mol Cell Biol,* 26**,** 3319-26.

PETERMANN, E., ORTA, M. L., ISSAEVA, N., SCHULTZ, N. & HELLEDAY, T. 2010. Hydroxyurea-stalled replication forks become progressively inactivated and require two different RAD51-mediated pathways for restart and repair. *Mol Cell,* 37**,** 492-502.

PETTITT, S. J., KRASTEV, D. B., BRANDSMA, I., DRÉAN, A., SONG, F., ALEKSANDROV, R., HARRELL, M. I., MENON, M., BROUGH, R., CAMPBELL, J., FRANKUM, J., RANES, M., PEMBERTON, H. N., RAFIQ, R., FENWICK, K., SWAIN, A., GUETTLER, S., LEE, J.-M., SWISHER, E. M., STOYNOV, S., YUSA, K., ASHWORTH, A. & LORD, C. J. 2018. Genome-wide and high-density CRISPR-Cas9 screens identify point mutations in PARP1 causing PARP inhibitor resistance. *Nature Communications,* 9**,** 1849.

PIERCE, A. J., JOHNSON, R. D., THOMPSON, L. H. & JASIN, M. 1999. XRCC3 promotes homology-directed repair of DNA damage in mammalian cells. *Genes Dev,* 13**,** 2633-8.

PIKE, K. G., BARLAAM, B., CADOGAN, E., CAMPBELL, A., CHEN, Y., COLCLOUGH, N., DAVIES, N. L., DE-ALMEIDA, C., DEGORCE, S. L., DIDELOT, M., DISHINGTON, A., DUCRAY, R., DURANT, S. T., HASSALL, L. A., HOLMES, J., HUGHES, G. D., MACFAUL, P. A., MULHOLLAND, K. R., MCGUIRE, T. M., OUVRY, G., PASS, M., ROBB, G., STRATTON, N., WANG, Z., WILSON, J., ZHAI, B., ZHAO, K. & AL-HUNITI, N. 2018. The Identification of Potent, Selective, and Orally Available Inhibitors of Ataxia Telangiectasia Mutated (ATM) Kinase: The Discovery of AZD0156 (8-{6-[3-(Dimethylamino)propoxy]pyridin-3-yl}-3-methyl-1-(tetrahydro-2H-pyran-4-yl)-1,3-dihydro-2H-imidazo[4,5-c]quinolin-2-one). *Journal of Medicinal Chemistry,* 61**,** 3823-3841.

PILLA REDDY, V., BUI, K., SCARFE, G., ZHOU, D. & LEAROYD, M. 2018. Physiologically Based Pharmacokinetic Modeling for Olaparib Dosing Recommendations: Bridging Formulations, Drug Interactions, and Patient Populations: PBPK modeling for olaparib dosing recommendations. *Clinical Pharmacology & Therapeutics,* 105.

PILLAY, N., TIGHE, A., NELSON, L., LITTLER, S., COULSON-GILMER, C., BAH, N., GOLDER, A., BAKKER, B., SPIERINGS, D. C. J., JAMES, D. I., SMITH, K. M., JORDAN, A. M., MORGAN, R. D., OGILVIE, D. J., FOIJER, F., JACKSON, D. A. & TAYLOR, S. S. 2019. DNA Replication

References

Vulnerabilities Render Ovarian Cancer Cells Sensitive to Poly(ADP-Ribose) Glycohydrolase Inhibitors. *Cancer Cell,* 35**,** 519-533.e8.

POGACAR, Z., GROOT, K., JOCHEMS, F., DOS SANTOS DIAS, M., MULERO-SÁNCHEZ, A., MORRIS, B., ROOSEN, M., WARDAK, L., DE CONTI, G., VELDS, A., LIEFTINK, C., THIJSSEN, B., BEIJERSBERGEN, R. L., BERNARDS, R. & LEITE DE OLIVEIRA, R. 2022. Genetic and compound screens uncover factors modulating cancer cell response to indisulam. *Life Sci Alliance,* 5.

POVEDA, A., FLOQUET, A., LEDERMANN, J. A., ASHER, R., PENSON, R. T., OZA, A. M., KORACH, J., HUZARSKI, T., PIGNATA, S. & FRIEDLANDER, M. 2021. Olaparib tablets as maintenance therapy in patients with platinum-sensitive relapsed ovarian cancer and a BRCA1/2 mutation (SOLO2/ENGOT-Ov21): a final analysis of a double-blind, randomised, placebo-controlled, phase 3 trial. *The Lancet Oncology,* 22**,** 620-631.

POVEDA, A., FLOQUET, A., LEDERMANN, J. A., ASHER, R., PENSON, R. T., OZA, A. M., KORACH, J., HUZARSKI, T., PIGNATA, S., FRIEDLANDER, M., BALDONI, A., PARK-SIMON, T.-W., SONKE, G. S., LISYANSKAYA, A. S., KIM, J.-H., FILHO, E. A., VERGOTE, I., ROWE, P. & PUJADE-LAURAINE, E. 2020. Final overall survival (OS) results from SOLO2/ENGOT-ov21: A phase III trial assessing maintenance olaparib in patients (pts) with platinum-sensitive, relapsed ovarian cancer and a BRCA mutation. *Journal of Clinical Oncology,* 38**,** 6002-6002.

PRIGGE, J. R., IVERSON, S. V., SIDERS, A. M. & SCHMIDT, E. E. 2009. Interactome for auxiliary splicing factor U2AF(65) suggests diverse roles. *Biochimica et biophysica acta,* 1789**,** 487-492.

PU, X., STORR, S. J., AHMAD, N. S., RAKHA, E. A., GREEN, A. R., ELLIS, I. O. & MARTIN, S. G. 2018. High nuclear MSK1 is associated with longer survival in breast cancer patients. *J Cancer Res Clin Oncol,* 144**,** 509-517.

PUJADE-LAURAINE, E., FUJIWARA, K., LEDERMANN, J. A., OZA, A. M., KRISTELEIT, R., RAY-COQUARD, I. L., RICHARDSON, G. E., SESSA, C., YONEMORI, K., BANERJEE, S., LEARY, A., TINKER, A. V., JUNG, K. H., MADRY, R., PARK, S. Y., ANDERSON, C. K., ZOHREN, F., STEWART, R. A., WEI, C., DYCHTER, S. S. & MONK, B. J. 2021. Avelumab alone or in combination with chemotherapy versus chemotherapy alone in platinum-resistant or platinum-refractory ovarian cancer (JAVELIN Ovarian 200): an open-label, three-arm, randomised, phase 3 study. *Lancet Oncol,* 22**,** 1034-1046.

PUJADE-LAURAINE, E., LEDERMANN, J. A., SELLE, F., GEBSKI, V., PENSON, R. T., OZA, A. M., KORACH, J., HUZARSKI, T., POVEDA, A., PIGNATA, S., FRIEDLANDER, M., COLOMBO, N., HARTER, P., FUJIWARA, K., RAY-COQUARD, I., BANERJEE, S., LIU, J., LOWE, E. S., BLOOMFIELD, R. & PAUTIER, P. 2017. Olaparib tablets as maintenance therapy in patients with platinum-sensitive, relapsed ovarian cancer and a BRCA1/2 mutation (SOLO2/ENGOT-Ov21): a double-blind, randomised, placebo-controlled, phase 3 trial. *Lancet Oncol,* 18**,** 1274-1284.

PUVVULA, P. K., YU, Y., SULLIVAN, K. R., EYOB, H., ROSENBERG, J., WELM, A., HUFF, C. & MOON, A. M. 2021. Inhibiting an RBM39/MLL1 epigenomic regulatory complex with dominant-negative peptides disrupts cancer cell transcription and proliferation. *Cell Rep,* 35**,** 109156.

References

QUIGLEY, D., ALUMKAL, J. J., WYATT, A. W., KOTHARI, V., FOYE, A., LLOYD, P., AGGARWAL, R., KIM, W., LU, E., SCHWARTZMAN, J., BEJA, K., ANNALA, M., DAS, R., DIOLAITI, M., PRITCHARD, C., THOMAS, G., TOMLINS, S., KNUDSEN, K., LORD, C. J., RYAN, C., YOUNGREN, J., BEER, T. M., ASHWORTH, A., SMALL, E. J. & FENG, F. Y. 2017. Analysis of Circulating Cell-Free DNA Identifies Multiclonal Heterogeneity of BRCA2 Reversion Mutations Associated with Resistance to PARP Inhibitors. *Cancer Discov,* 7**,** 999-1005.

QUINET, A., CARVAJAL-MALDONADO, D., LEMACON, D. & VINDIGNI, A. 2017. DNA Fiber Analysis: Mind the Gap! *Methods Enzymol,* 591**,** 55-82.

RAHMUTULLA, B., MATSUSHITA, K. & NOMURA, F. 2014. Alternative splicing of DNA damage response genes and gastrointestinal cancers. *World J Gastroenterol,* 20**,** 17305-13.

RAPPOLD, I., IWABUCHI, K., DATE, T. & CHEN, J. 2001. Tumor suppressor p53 binding protein 1 (53BP1) is involved in DNA damage-signaling pathways. *J Cell Biol,* 153**,** 613-20.

RAY CHAUDHURI, A., CALLEN, E., DING, X., GOGOLA, E., DUARTE, A. A., LEE, J.-E., WONG, N., LAFARGA, V., CALVO, J. A., PANZARINO, N. J., JOHN, S., DAY, A., CRESPO, A. V., SHEN, B., STARNES, L. M., RUITER, J. R. D., DANIEL, J. A., KONSTANTINOPOULOS, P. A., CORTEZ, D., CANTOR, S. B., FERNANDEZ-CAPETILLO, O., GE, K., JONKERS, J., ROTTENBERG, S., SHARAN, S. K. & NUSSENZWEIG, A. 2016. Replication fork stability confers chemoresistance in BRCA-deficient cells. *Nature,* 535**,** 382-387.

RAY-COQUARD, I., PAUTIER, P., PIGNATA, S., PÉROL, D., GONZÁLEZ-MARTÍN, A., BERGER, R., FUJIWARA, K., VERGOTE, I., COLOMBO, N., MÄENPÄÄ, J., SELLE, F., SEHOULI, J., LORUSSO, D., GUERRA ALÍA, E. M., REINTHALLER, A., NAGAO, S., LEFEUVRE-PLESSE, C., CANZLER, U., SCAMBIA, G., LORTHOLARY, A., MARMÉ, F., COMBE, P., DE GREGORIO, N., RODRIGUES, M., BUDERATH, P., DUBOT, C., BURGES, A., YOU, B., PUJADE-LAURAINE, E. & HARTER, P. 2019. Olaparib plus Bevacizumab as First-Line Maintenance in Ovarian Cancer. *New England Journal of Medicine,* 381**,** 2416-2428.

REARDON, J. T., VAISMAN, A., CHANEY, S. G. & SANCAR, A. 1999. Efficient nucleotide excision repair of cisplatin, oxaliplatin, and Bis-aceto-ammine-dichloro-cyclohexylamine-platinum(IV) (JM216) platinum intrastrand DNA diadducts. *Cancer Res,* 59**,** 3968-71.

REES, M. G., SEASHORE-LUDLOW, B., CHEAH, J. H., ADAMS, D. J., PRICE, E. V., GILL, S., JAVAID, S., COLETTI, M. E., JONES, V. L. & BODYCOMBE, N. E. 2016. Correlating chemical sensitivity and basal gene expression reveals mechanism of action. *Nature chemical biology,* 12**,** 109-116.

RICHES, L. C., TRINIDAD, A. G., HUGHES, G., JONES, G. N., HUGHES, A. M., THOMASON, A. G., GAVINE, P., CUI, A., LING, S., STOTT, J., CLARK, R., PEEL, S., GILL, P., GOODWIN, L. M., SMITH, A., PIKE, K. G., BARLAAM, B., PASS, M., O'CONNOR, M. J., SMITH, G. & CADOGAN, E. B. 2020. Pharmacology of the ATM Inhibitor AZD0156: Potentiation of Irradiation and Olaparib Responses Preclinically. *Mol Cancer Ther,* 19**,** 13-25.

RIMEL, J. K. & TAATJES, D. J. 2018. The essential and multifunctional TFIIH complex. *Protein Sci,* 27**,** 1018-1037.

ROBY, K. F., TAYLOR, C. C., SWEETWOOD, J. P., CHENG, Y., PACE, J. L., TAWFIK, O., PERSONS, D. L., SMITH, P. G. & TERRANOVA, P. F. 2000. Development of a syngeneic mouse model for events related to ovarian cancer. *Carcinogenesis,* 21**,** 585-91.

References

ROELL, K. R., REIF, D. M. & MOTSINGER-REIF, A. A. 2017. An Introduction to Terminology and Methodology of Chemical Synergy-Perspectives from Across Disciplines. *Front Pharmacol,* 8**,** 158.

ROGAKOU, E. P., NIEVES-NEIRA, W., BOON, C., POMMIER, Y. & BONNER, W. M. 2000. Initiation of DNA fragmentation during apoptosis induces phosphorylation of H2AX histone at serine 139. *J Biol Chem,* 275**,** 9390-5.

RONDINELLI, B., GOGOLA, E., YÜCEL, H., DUARTE, A. A., VAN DE VEN, M., VAN DER SLUIJS, R., KONSTANTINOPOULOS, P. A., JONKERS, J., CECCALDI, R., ROTTENBERG, S. & D'ANDREA, A. D. 2017. EZH2 promotes degradation of stalled replication forks by recruiting MUS81 through histone H3 trimethylation. *Nature Cell Biology,* 19**,** 1371-1378.

RONSON, G. E., PIBERGER, A. L., HIGGS, M. R., OLSEN, A. L., STEWART, G. S., MCHUGH, P. J., PETERMANN, E. & LAKIN, N. D. 2018. PARP1 and PARP2 stabilise replication forks at base excision repair intermediates through Fbh1-dependent Rad51 regulation. *Nature Communications,* 9**,** 746.

ROSE, M., BURGESS, J. T., O'BYRNE, K., RICHARD, D. J. & BOLDERSON, E. 2020. PARP Inhibitors: Clinical Relevance, Mechanisms of Action and Tumor Resistance. *Front Cell Dev Biol,* 8**,** 564601.

ROTH, J., PEER, C. J., MANNARGUDI, B., SWAISLAND, H., LEE, J.-M., KOHN, E. C. & FIGG, W. D. 2014. A Sensitive and Robust Ultra HPLC Assay with Tandem Mass Spectrometric Detection for the Quantitation of the PARP Inhibitor Olaparib (AZD2281) in Human Plasma for Pharmacokinetic Application. *Chromatography,* 1**,** 82-95.

ROTTENBERG, S., JASPERS, J. E., KERSBERGEN, A., BURG, E. V. D., NYGREN, A. O. H., ZANDER, S. A. L., DERKSEN, P. W. B., BRUIN, M. D., ZEVENHOVEN, J., LAU, A., BOULTER, R., CRANSTON, A., O'CONNOR, M. J., MARTIN, N. M. B., BORST, P. & JONKERS, J. 2008. High sensitivity of BRCA1-deficient mammary tumors to the PARP inhibitor AZD2281 alone and in combination with platinum drugs. *Proceedings of the National Academy of Sciences,* 105**,** 17079-17084.

ROULEAU, M., PATEL, A., HENDZEL, M. J., KAUFMANN, S. H. & POIRIER, G. G. 2010. PARP inhibition: PARP1 and beyond. *Nature reviews. Cancer,* 10**,** 293-301.

SAHIN, I. D., JÖNSSON, J.-M. & HEDENFALK, I. 2019. Crizotinib and PARP inhibitors act synergistically by triggering apoptosis in high-grade serous ovarian cancer. *Oncotarget,* 10.

SAKAI, W., SWISHER, E. M., JACQUEMONT, C., CHANDRAMOHAN, K. V., COUCH, F. J., LANGDON, S. P., WURZ, K., HIGGINS, J., VILLEGAS, E. & TANIGUCHI, T. 2009. Functional restoration of BRCA2 protein by secondary BRCA2 mutations in BRCA2-mutated ovarian carcinoma. *Cancer Res,* 69**,** 6381-6.

SAKAI, W., SWISHER, E. M., KARLAN, B. Y., AGARWAL, M. K., HIGGINS, J., FRIEDMAN, C., VILLEGAS, E., JACQUEMONT, C., FARRUGIA, D. J., COUCH, F. J., URBAN, N. & TANIGUCHI, T. 2008. Secondary mutations as a mechanism of cisplatin resistance in BRCA2-mutated cancers. *Nature,* 451**,** 1116-20.

SALEH-GOHARI, N., BRYANT, H. E., SCHULTZ, N., PARKER, K. M., CASSEL, T. N. & HELLEDAY, T. 2005. Spontaneous homologous recombination is induced by collapsed replication

forks that are caused by endogenous DNA single-strand breaks. *Mol Cell Biol,* 25**,** 7158-69.

SALLMANN, F. R., VODENICHAROV, M. D., WANG, Z. Q. & POIRIER, G. G. 2000. Characterization of sPARP-1. An alternative product of PARP-1 gene with poly(ADP-ribose) polymerase activity independent of DNA strand breaks. *J Biol Chem,* 275**,** 15504-11.

SALVADOR, S., GILKS, B., KOBEL, M., HUNTSMAN, D., ROSEN, B. & MILLER, D. 2009. The fallopian tube: primary site of most pelvic high-grade serous carcinomas. *Int J Gynecol Cancer,* 19**,** 58-64.

SANDHU, D., ANTOLIN, A. A., COX, A. R. & JONES, A. M. 2022. Identification of different side effects between PARP inhibitors and their polypharmacological multi-target rationale. *Br J Clin Pharmacol,* 88**,** 742-752.

SANTOS, L. S., GOMES, B. C., GOUVEIA, R., SILVA, S. N., AZEVEDO, A. P., CAMACHO, V., MANITA, I., GIL, O. M., FERREIRA, T. C., LIMBERT, E., RUEFF, J. & GASPAR, J. F. 2013. The role of CCNH Val270Ala (rs2230641) and other nucleotide excision repair polymorphisms in individual susceptibility to well-differentiated thyroid cancer. *Oncol Rep,* 30**,** 2458-66.

SARFARAZI, A., LEE, G., MIRJALILI, S. A., PHILLIPS, A. R. J., WINDSOR, J. A. & TREVASKIS, N. L. 2019. Therapeutic delivery to the peritoneal lymphatics: Current understanding, potential treatment benefits and future prospects. *Int J Pharm,* 567**,** 118456.

SAVAGE, K. I., GORSKI, J. J., BARROS, E. M., IRWIN, G. W., MANTI, L., POWELL, A. J., PELLAGATTI, A., LUKASHCHUK, N., MCCANCE, D. J., MCCLUGGAGE, W. G., SCHETTINO, G., SALTO-TELLEZ, M., BOULTWOOD, J., RICHARD, D. J., MCDADE, S. S. & HARKIN, D. P. 2014. Identification of a BRCA1-mRNA splicing complex required for efficient DNA repair and maintenance of genomic stability. *Mol Cell,* 54**,** 445-59.

SCHLEICHER, E. M. & MOLDOVAN, G. L. 2021. CRISPR screens guide the way for PARP and ATR inhibitor biomarker discovery. *FEBS J,* n/a.

SCHOENFELD, D. A. 1983. Sample-size formula for the proportional-hazards regression model. *Biometrics,* 39**,** 499-503.

SCIARRILLO, R., WOJTUSZKIEWICZ, A., ASSARAF, Y. G., JANSEN, G., KASPERS, G. J. L., GIOVANNETTI, E. & CLOOS, J. 2020. The role of alternative splicing in cancer: From oncogenesis to drug resistance. *Drug Resistance Updates,* 53**,** 100728.

SCULLY, R., PANDAY, A., ELANGO, R. & WILLIS, N. A. 2019. DNA double-strand break repair-pathway choice in somatic mammalian cells. *Nature Reviews Molecular Cell Biology,* 20**,** 698-714.

SEDELNIKOVA, O. A., ROGAKOU, E. P., PANYUTIN, I. G. & BONNER, W. M. 2002. Quantitative detection of (125)IdU-induced DNA double-strand breaks with gamma-H2AX antibody. *Radiat Res,* 158**,** 486-92.

SEILER, M., PENG, S., AGRAWAL, A. A., PALACINO, J., TENG, T., ZHU, P., SMITH, P. G., BUONAMICI, S. & YU, L. 2018. Somatic Mutational Landscape of Splicing Factor Genes and Their Functional Consequences across 33 Cancer Types. *Cell Rep,* 23**,** 282-296.e4.

References

SEMBA, T., FUNAHASHI, Y., ONO, N., YAMAMOTO, Y., SUGI, N. H., ASADA, M., YOSHIMATSU, K. & WAKABAYASHI, T. 2004. An Angiogenesis Inhibitor E7820 Shows Broad-Spectrum Tumor Growth Inhibition in a Xenograft Model: Possible Value of Integrin α2 on Platelets as a Biological Marker. *Clinical Cancer Research,* 10**,** 1430-1438.

SETTE, C. & PARONETTO, M. P. 2022. Somatic Mutations in Core Spliceosome Components Promote Tumorigenesis and Generate an Exploitable Vulnerability in Human Cancer. *Cancers,* 14**,** 1827.

SHAPIRO, G. I., KRISTELEIT, R. S., BURRIS, H. A., LORUSSO, P., PATEL, M. R., DREW, Y., GIORDANO, H., MALONEY, L., WATKINS, S., GOBLE, S., JAW-TSAI, S. & XIAO, J. J. 2019. Pharmacokinetic Study of Rucaparib in Patients With Advanced Solid Tumors. *Clin Pharmacol Drug Dev,* 8**,** 107-118.

SHARMA, A., SINGH, K. & ALMASAN, A. 2012. Histone H2AX phosphorylation: a marker for DNA damage. *Methods Mol Biol,* 920**,** 613-26.

SHEN, J., ZHAO, W., JU, Z., WANG, L., PENG, Y., LABRIE, M., YAP, T. A., MILLS, G. B. & PENG, G. 2019. PARPi Triggers the STING-Dependent Immune Response and Enhances the Therapeutic Efficacy of Immune Checkpoint Blockade Independent of BRCAness. *Cancer Res,* 79**,** 311-319.

SHERMAN, B. T., HAO, M., QIU, J., JIAO, X., BASELER, M. W., LANE, H. C., IMAMICHI, T. & CHANG, W. 2022. DAVID: a web server for functional enrichment analysis and functional annotation of gene lists (2021 update). *Nucleic Acids Res,* 50**,** W216-21.

SHEYNKMAN, G. M., SHORTREED, M. R., CESNIK, A. J. & SMITH, L. M. 2016. Proteogenomics: Integrating Next-Generation Sequencing and Mass Spectrometry to Characterize Human Proteomic Variation. *Annu Rev Anal Chem (Palo Alto Calif),* 9**,** 521-45.

SHIBATA, A. & JEGGO, P. A. 2021. ATM's Role in the Repair of DNA Double-Strand Breaks. *Genes (Basel),* 12.

SHIBATA, E., ABBAS, T., HUANG, X., WOHLSCHLEGEL, J. A. & DUTTA, A. 2011. Selective ubiquitylation of p21 and Cdt1 by UBCH8 and UBE2G ubiquitin-conjugating enzymes via the CRL4Cdt2 ubiquitin ligase complex. *Mol Cell Biol,* 31**,** 3136-45.

SHIEH, W. M., AME, J. C., WILSON, M. V., WANG, Z. Q., KOH, D. W., JACOBSON, M. K. & JACOBSON, E. L. 1998. Poly(ADP-ribose) polymerase null mouse cells synthesize ADP-ribose polymers. *J Biol Chem,* 273**,** 30069-72.

SIEGL, T., PETZKE, L., WELLE, E. & LUZHETSKYY, A. 2010. I-SceI endonuclease: a new tool for DNA repair studies and genetic manipulations in streptomyces. *Appl Microbiol Biotechnol,* 87**,** 1525-32.

SIJBERS, A. M., DE LAAT, W. L., ARIZA, R. R., BIGGERSTAFF, M., WEI, Y. F., MOGGS, J. G., CARTER, K. C., SHELL, B. K., EVANS, E., DE JONG, M. C., RADEMAKERS, S., DE ROOIJ, J., JASPERS, N. G., HOEIJMAKERS, J. H. & WOOD, R. D. 1996. Xeroderma pigmentosum group F caused by a defect in a structure-specific DNA repair endonuclease. *Cell,* 86**,** 811-22.

SILLARS-HARDEBOL, A. H., CARVALHO, B., TIJSSEN, M., BELIËN, J. A., DE WIT, M., DELIS-VAN DIEMEN, P. M., PONTÉN, F., VAN DE WIEL, M. A., FIJNEMAN, R. J. & MEIJER, G. A. 2012.

References

TPX2 and AURKA promote 20q amplicon-driven colorectal adenoma to carcinoma progression. *Gut,* 61**,** 1568-75.

SINGH, H. R., NARDOZZA, A. P., MÖLLER, I. R., KNOBLOCH, G., KISTEMAKER, H. A. V., HASSLER, M., HARRER, N., BLESSING, C., EUSTERMANN, S., KOTTHOFF, C., HUET, S., MUELLER-PLANITZ, F., FILIPPOV, D. V., TIMINSZKY, G., RAND, K. D. & LADURNER, A. G. 2017. A Poly-ADP-Ribose Trigger Releases the Auto-Inhibition of a Chromatin Remodeling Oncogene. *Mol Cell,* 68**,** 860-871.e7.

SINGH, S., QUARNI, W., GORALSKI, M., WAN, S., JIN, H., VELDE, L.-A. V. D., FANG, J., WU, Q., ABU-ZAID, A., WANG, T., SINGH, R., CRAFT, D., FAN, Y., CONFER, T., JOHNSON, M., AKERS, W. J., WANG, R., MURRAY, P. J., THOMAS, P. G., NIJHAWAN, D., DAVIDOFF, A. M. & YANG, J. 2021. Targeting the spliceosome through RBM39 degradation results in exceptional responses in high-risk neuroblastoma models. *Science Advances,* 7**,** eabj5405.

SIRBU, B. M., COUCH, F. B., FEIGERLE, J. T., BHASKARA, S., HIEBERT, S. W. & CORTEZ, D. 2011. Analysis of protein dynamics at active, stalled, and collapsed replication forks. *Genes Dev,* 25**,** 1320-7.

ŠKUBNÍK, J., PAVLÍČKOVÁ, V., RUML, T. & RIMPELOVÁ, S. 2021. Current Perspectives on Taxanes: Focus on Their Bioactivity, Delivery and Combination Therapy. *Plants (Basel),* 10.

SMITH, H. L., PRENDERGAST, L. & CURTIN, N. J. 2020. Exploring the Synergy between PARP and CHK1 Inhibition in Matched BRCA2 Mutant and Corrected Cells. *Cancers (Basel),* 12.

SMOGORZEWSKA, A., MATSUOKA, S., VINCIGUERRA, P., MCDONALD, E. R., 3RD, HUROV, K. E., LUO, J., BALLIF, B. A., GYGI, S. P., HOFMANN, K., D'ANDREA, A. D. & ELLEDGE, S. J. 2007. Identification of the FANCI protein, a monoubiquitinated FANCD2 paralog required for DNA repair. *Cell,* 129**,** 289-301.

SO, S., DAVIS, A. J. & CHEN, D. J. 2009. Autophosphorylation at serine 1981 stabilizes ATM at DNA damage sites. *Journal of Cell Biology,* 187**,** 977-990.

SONG, G., CHEN, L., ZHANG, B., SONG, Q., YU, Y., MOORE, C., WANG, T. L., SHIH, I. M., ZHANG, H., CHAN, D. W., ZHANG, Z. & ZHU, H. 2019. Proteome-wide Tyrosine Phosphorylation Analysis Reveals Dysregulated Signaling Pathways in Ovarian Tumors. *Mol Cell Proteomics,* 18**,** 448-460.

SONG, Y., GUO, Y., LI, X., SUN, R., ZHU, M., SHI, J., TAN, Z., ZHANG, L. & HUANG, J. 2021. RBM39 Alters Phosphorylation of c-Jun and Binds to Viral RNA to Promote PRRSV Proliferation. *Frontiers in Immunology,* 12.

SOPIK, V., IQBAL, J., ROSEN, B. & NAROD, S. A. 2015. Why have ovarian cancer mortality rates declined? Part II. Case-fatality. *Gynecol Oncol,* 138**,** 750-6.

SØRENSEN, C. S., SYLJUÅSEN, R. G., LUKAS, J. & BARTEK, J. 2004. ATR, Claspin and the Rad9-Rad1-Hus1 complex regulate Chk1 and Cdc25A in the absence of DNA damage. *Cell Cycle,* 3**,** 941-5.

STANLEY, R. F. & ABDEL-WAHAB, O. 2022. Dysregulation and therapeutic targeting of RNA splicing in cancer. *Nature Cancer,* 3**,** 536-546.

References

STANOJCIC, S., KUK, N., ULLAH, I., STERKERS, Y. & MERRICK, C. J. 2017. Single-molecule analysis reveals that DNA replication dynamics vary across the course of schizogony in the malaria parasite Plasmodium falciparum. *Scientific Reports,* 7**,** 4003.

STAROPOLI, N., CILIBERTO, D., DEL GIUDICE, T., IULIANO, E., CUCÈ, M., GRILLONE, F., SALVINO, A., BARBIERI, V., RUSSO, A., TASSONE, P. & TAGLIAFERRI, P. 2018. The Era of PARP inhibitors in ovarian cancer: "Class Action" or not? A systematic review and meta-analysis. *Critical Reviews in Oncology/Hematology,* 131**,** 83-89.

STEENSMA, D. P., WERMKE, M., KLIMEK, V. M., GREENBERG, P. L., FONT, P., KOMROKJI, R. S., YANG, J., BRUNNER, A. M., CARRAWAY, H. E., ADES, L., AL-KALI, A., ALONSO-DOMINGUEZ, J. M., ALFONSO-PIÉROLA, A., COOMBS, C. C., DEEG, H. J., FLINN, I., FORAN, J. M., GARCIA-MANERO, G., MARIS, M. B., MCMASTERS, M., MICOL, J.-B., DE OTEYZA, J. P., THOL, F., WANG, E. S., WATTS, J. M., TAYLOR, J., STONE, R., GOURINENI, V., MARINO, A. J., YAO, H., DESTENAVES, B., YUAN, X., YU, K., DAR, S., OHANJANIAN, L., KUIDA, K., XIAO, J., SCHOLZ, C., GUALBERTO, A. & PLATZBECKER, U. 2021. Phase I First-in-Human Dose Escalation Study of the oral SF3B1 modulator H3B-8800 in myeloid neoplasms. *Leukemia,* 35**,** 3542-3550.

STEPANYUK, G. A., SERRANO, P., PERALTA, E., FARR, C. L., AXELROD, H. L., GERALT, M., DAS, D., CHIU, H. J., JAROSZEWSKI, L., DEACON, A. M., LESLEY, S. A., ELSLIGER, M. A., GODZIK, A., WILSON, I. A., WUTHRICH, K., SALOMON, D. R. & WILLIAMSON, J. R. 2016. UHM-ULM interactions in the RBM39-U2AF65 splicing-factor complex. *Acta Crystallogr D Struct Biol,* 72**,** 497-511.

STEVENS, M. & OLTEAN, S. 2019. Modulation of the Apoptosis Gene Bcl-x Function Through Alternative Splicing. *Front Genet,* 10**,** 804.

STEWART, C., RALYEA, C. & LOCKWOOD, S. 2019. Ovarian Cancer: An Integrated Review. *Seminars in Oncology Nursing,* 35**,** 151-156.

STIFF, T., O'DRISCOLL, M., RIEF, N., IWABUCHI, K., LÖBRICH, M. & JEGGO, P. A. 2004. ATM and DNA-PK function redundantly to phosphorylate H2AX after exposure to ionizing radiation. *Cancer Res,* 64**,** 2390-6.

STOLZ, A., ERTYCH, N. & BASTIANS, H. 2011. Tumor Suppressor CHK2: Regulator of DNA Damage Response and Mediator of Chromosomal Stability. *Clinical Cancer Research,* 17**,** 401-405.

STRICKLAND, K. C., HOWITT, B. E., SHUKLA, S. A., RODIG, S., RITTERHOUSE, L. L., LIU, J. F., GARBER, J. E., CHOWDHURY, D., WU, C. J., D'ANDREA, A. D., MATULONIS, U. A. & KONSTANTINOPOULOS, P. A. 2016. Association and prognostic significance of BRCA1/2-mutation status with neoantigen load, number of tumor-infiltrating lymphocytes and expression of PD-1/PD-L1 in high grade serous ovarian cancer. *Oncotarget,* 7.

SU, D., FENG, X., COLIC, M., WANG, Y., ZHANG, C., WANG, C., TANG, M., HART, T. & CHEN, J. 2020. CRISPR/CAS9-based DNA damage response screens reveal gene-drug interactions. *DNA Repair (Amst),* 87**,** 102803.

SUNG, C. O., SONG, I. H. & SOHN, I. 2014. A distinctive ovarian cancer molecular subgroup characterized by poor prognosis and somatic focal copy number amplifications at chromosome 19. *Gynecol Oncol,* 132**,** 343-50.

References

SUWAKI, N., KLARE, K. & TARSOUNAS, M. 2011. RAD51 paralogs: roles in DNA damage signalling, recombinational repair and tumorigenesis. *Semin Cell Dev Biol,* 22**,** 898-905.

TAGLIALATELA, A., ALVAREZ, S., LEUZZI, G., SANNINO, V., RANJHA, L., HUANG, J. W., MADUBATA, C., ANAND, R., LEVY, B., RABADAN, R., CEJKA, P., COSTANZO, V. & CICCIA, A. 2017. Restoration of Replication Fork Stability in BRCA1- and BRCA2-Deficient Cells by Inactivation of SNF2-Family Fork Remodelers. *Mol Cell,* 68**,** 414-430.e8.

TANG, J., WENNERBERG, K. & AITTOKALLIO, T. 2015. What is synergy? The Saariselkä agreement revisited. *Front Pharmacol,* 6**,** 181.

TANIKAWA, M., SANJIV, K., HELLEDAY, T., HERR, P. & MORTUSEWICZ, O. 2016. The spliceosome U2 snRNP factors promote genome stability through distinct mechanisms; transcription of repair factors and R-loop processing. *Oncogenesis,* 5**,** e280.

TARI, M., MANCEAU, V., DE MATHA SALONE, J., KOBAYASHI, A., PASTRE, D. & MAUCUER, A. 2019. U2AF(65) assemblies drive sequence-specific splice site recognition. *EMBO Rep,* 20**,** e47604.

TEIXEIRA, S. A., VIAPIANO, M. S., ANDRADE, A. F., NANDHU, M. S., PEZUK, J. A., BIDINOTTO, L. T., SUAZO, V. K., NEDER, L., CARLOTTI, C. G., BECKER, A. P., TONE, L. G. & SCRIDELI, C. A. 2021. The Carbonic Anhydrase Inhibitor E7070 Sensitizes Glioblastoma Cells to Radio- and Chemotherapy and Reduces Tumor Growth. *Molecular Neurobiology,* 58**,** 4520-4534.

TELATAR, M., TERAOKA, S., WANG, Z., CHUN, H. H., LIANG, T., CASTELLVI-BEL, S., UDAR, N., BORRESEN-DALE, A. L., CHESSA, L., BERNATOWSKA-MATUSZKIEWICZ, E., PORRAS, O., WATANABE, M., JUNKER, A., CONCANNON, P. & GATTI, R. A. 1998. Ataxia-telangiectasia: identification and detection of founder-effect mutations in the ATM gene in ethnic populations. *Am J Hum Genet,* 62**,** 86-97.

THANARAJ, T. A., CLARK, F. & MUILU, J. 2003. Conservation of human alternative splice events in mouse. *Nucleic Acids Res,* 31**,** 2544-52.

THOMPSON, E. L., YEO, J. E., LEE, E.-A., KAN, Y., RAGHUNANDAN, M., WIEK, C., HANENBERG, H., SCHÄRER, O. D., HENDRICKSON, E. A. & SOBECK, A. 2017. FANCI and FANCD2 have common as well as independent functions during the cellular replication stress response. *Nucleic Acids Research,* 45**,** 11837-11857.

TING, T. C., GORALSKI, M., KLEIN, K., WANG, B., KIM, J., XIE, Y. & NIJHAWAN, D. 2019. Aryl Sulfonamides Degrade RBM39 and RBM23 by Recruitment to CRL4-DCAF15. *Cell Rep,* 29**,** 1499-1510 e6.

TKÁČ, J., XU, G., ADHIKARY, H., YOUNG, J. T. F., GALLO, D., ESCRIBANO-DÍAZ, C., KRIETSCH, J., ORTHWEIN, A., MUNRO, M., SOL, W., AL-HAKIM, A., LIN, Z.-Y., JONKERS, J., BORST, P., BROWN, G. W., GINGRAS, A.-C., ROTTENBERG, S., MASSON, J.-Y. & DUROCHER, D. 2016. HELB Is a Feedback Inhibitor of DNA End Resection. *Molecular Cell,* 61**,** 405-418.

TOBALINA, L., ARMENIA, J., IRVING, E., O'CONNOR, M. J. & FORMENT, J. V. 2021. A meta-analysis of reversion mutations in BRCA genes identifies signatures of DNA end-joining repair mechanisms driving therapy resistance. *Annals of Oncology,* 32**,** 103-112.

References

TOLEDO, L., NEELSEN, K. J. & LUKAS, J. 2017. Replication Catastrophe: When a Checkpoint Fails because of Exhaustion. *Molecular Cell,* 66**,** 735-749.

TOLEDO, L. I., ALTMEYER, M., RASK, M. B., LUKAS, C., LARSEN, D. H., POVLSEN, L. K., BEKKER-JENSEN, S., MAILAND, N., BARTEK, J. & LUKAS, J. 2013. ATR prohibits replication catastrophe by preventing global exhaustion of RPA. *Cell,* 155**,** 1088-103.

TOMAO, F., BARDHI, E., DI PINTO, A., SASSU, C. M., BIAGIOLI, E., PETRELLA, M. C., PALAIA, I., MUZII, L., COLOMBO, N. & PANICI, P. B. 2019. Parp inhibitors as maintenance treatment in platinum sensitive recurrent ovarian cancer: An updated meta-analysis of randomized clinical trials according to BRCA mutational status. *Cancer Treatment Reviews,* 80**,** 101909.

TONG, J., XU, X., ZHANG, Z., MA, C., XIANG, R., LIU, J., XU, W., WU, C., LI, J., ZHAN, F., WU, Y. & YAN, H. 2019. Hypoxia-induced long non-coding RNA DARS-AS1 regulates RBM39 stability to promote myeloma malignancy. *Haematologica*.

TORRE, L. A., TRABERT, B., DESANTIS, C. E., MILLER, K. D., SAMIMI, G., RUNOWICZ, C. D., GAUDET, M. M., JEMAL, A. & SIEGEL, R. L. 2018. Ovarian cancer statistics, 2018. *CA: a cancer journal for clinicians,* 68**,** 284-296.

TRISCIUOGLIO, D., TUPONE, M. G., DESIDERI, M., DI MARTILE, M., GABELLINI, C., BUGLIONI, S., PALLOCCA, M., ALESSANDRINI, G., D'AGUANNO, S. & DEL BUFALO, D. 2017. BCL-XL overexpression promotes tumor progression-associated properties. *Cell Death & Disease,* 8**,** 3216.

TSIBULAK, I., ZEIMET, A. G. & MARTH, C. 2019. Hopes and failures in front-line ovarian cancer therapy. *Crit Rev Oncol Hematol,* 143**,** 14-19.

TSUJINO, T., TAKAI, T., HINOHARA, K., GUI, F., TSUTSUMI, T., BAI, X., MIAO, C., FENG, C., GUI, B., SZTUPINSZKI, Z., SIMONEAU, A., XIE, N., FAZLI, L., DONG, X., AZUMA, H., CHOUDHURY, A. D., MOUW, K. W., SZALLASI, Z., ZOU, L., KIBEL, A. S. & JIA, L. 2022. CRISPR screens reveal genetic determinants of PARP inhibitor sensitivity and resistance in prostate cancer. *bioRxiv***,** 2022.04.13.488115.

TUFEGDŽIĆ VIDAKOVIĆ, A., MITTER, R., KELLY, G. P., NEUMANN, M., HARREMAN, M., RODRÍGUEZ-MARTÍNEZ, M., HERLIHY, A., WEEMS, J. C., BOEING, S., ENCHEVA, V., GAUL, L., MILLIGAN, L., TOLLERVEY, D., CONAWAY, R. C., CONAWAY, J. W., SNIJDERS, A. P., STEWART, A. & SVEJSTRUP, J. Q. 2020. Regulation of the RNAPII Pool Is Integral to the DNA Damage Response. *Cell,* 180**,** 1245-1261.e21.

TUMIATI, M., HIETANEN, S., HYNNINEN, J., PIETILÄ, E., FÄRKKILÄ, A., KAIPIO, K., ROERING, P., HUHTINEN, K., ALKODSI, A., LI, Y., LEHTONEN, R., ERKAN, E. P., TUOMINEN, M. M., LEHTI, K., HAUTANIEMI, S. K., VÄHÄRAUTIO, A., GRÉNMAN, S., CARPÉN, O. & KAUPPI, L. 2018. A Functional Homologous Recombination Assay Predicts Primary Chemotherapy Response and Long-Term Survival in Ovarian Cancer Patients. *Clin Cancer Res,* 24**,** 4482-4493.

TWAROG, N. R., CONNELLY, M. & SHELAT, A. A. 2020. A critical evaluation of methods to interpret drug combinations. *Sci Rep,* 10**,** 5144.

TWAROG, N. R., STEWART, E., HAMMILL, C. V. & SHELAT, A. A. 2016. BRAID: A Unifying Paradigm for the Analysis of Combined Drug Action. *Sci Rep,* 6**,** 25523.

References

UEHARA, T., MINOSHIMA, Y., SAGANE, K., SUGI, N. H., MITSUHASHI, K. O., YAMAMOTO, N., KAMIYAMA, H., TAKAHASHI, K., KOTAKE, Y., UESUGI, M., YOKOI, A., INOUE, A., YOSHIDA, T., MABUCHI, M., TANAKA, A. & OWA, T. 2017. Selective degradation of splicing factor CAPERalpha by anticancer sulfonamides. *Nat Chem Biol,* 13**,** 675-680.

UNSAL-KAÇMAZ, K., CHASTAIN, P. D., QU, P. P., MINOO, P., CORDEIRO-STONE, M., SANCAR, A. & KAUFMANN, W. K. 2007. The human Tim/Tipin complex coordinates an Intra-S checkpoint response to UV that slows replication fork displacement. *Mol Cell Biol,* 27**,** 3131-42.

VAIDYANATHAN, A., SAWERS, L., GANNON, A.-L., CHAKRAVARTY, P., SCOTT, A. L., BRAY, S. E., FERGUSON, M. J. & SMITH, G. 2016. ABCB1 (MDR1) induction defines a common resistance mechanism in paclitaxel- and olaparib-resistant ovarian cancer cells. *British Journal of Cancer,* 115**,** 431-441.

VARGA, A., PIHA-PAUL, S., OTT, P. A., MEHNERT, J. M., BERTON-RIGAUD, D., MOROSKY, A., YANG, P., RUMAN, J. & MATEI, D. 2019. Pembrolizumab in patients with programmed death ligand 1-positive advanced ovarian cancer: Analysis of KEYNOTE-028. *Gynecol Oncol,* 152**,** 243-250.

VENERIS, J. T., MATULONIS, U. A., LIU, J. F. & KONSTANTINOPOULOS, P. A. 2020. Choosing wisely: Selecting PARP inhibitor combinations to promote anti-tumor immune responses beyond BRCA mutations. *Gynecol Oncol,* 156**,** 488-497.

VEO, B., DANIS, E., PIERCE, A., WANG, D., FOSMIRE, S., SULLIVAN, K. D., JOSHI, M., KHANAL, S., DAHL, N. & KARAM, S. 2021. Transcriptional control of DNA repair networks by CDK7 regulates sensitivity to radiation in MYC-driven medulloblastoma. *Cell Reports,* 35**,** 109013.

VERMA, P., ZHOU, Y., CAO, Z., DERASKA, P. V., DEB, M., ARAI, E., LI, W., SHAO, Y., PUENTES, L., LI, Y., PATANKAR, S., MACH, R. H., FARYABI, R. B., SHI, J. & GREENBERG, R. A. 2021. ALC1 links chromatin accessibility to PARP inhibitor response in homologous recombination-deficient cells. *Nature Cell Biology,* 23**,** 160-171.

VICHAI, V. & KIRTIKARA, K. 2006. Sulforhodamine B colorimetric assay for cytotoxicity screening. *Nature Protocols,* 1**,** 1112-1116.

VYAS, S., MATIC, I., UCHIMA, L., ROOD, J., ZAJA, R., HAY, R. T., AHEL, I. & CHANG, P. 2014. Family-wide analysis of poly(ADP-ribose) polymerase activity. *Nat Commun,* 5**,** 4426.

WAHLBERG, E., KARLBERG, T., KOUZNETSOVA, E., MARKOVA, N., MACCHIARULO, A., THORSELL, A. G., POL, E., FROSTELL, A., EKBLAD, T., ONCU, D., KULL, B., ROBERTSON, G. M., PELLICCIARI, R., SCHULER, H. & WEIGELT, J. 2012. Family-wide chemical profiling and structural analysis of PARP and tankyrase inhibitors. *Nat Biotechnol,* 30**,** 283-8.

WALTON, J., BLAGIH, J., ENNIS, D., LEUNG, E., DOWSON, S., FARQUHARSON, M., TOOKMAN, L. A., ORANGE, C., ATHINEOS, D., MASON, S., STEVENSON, D., BLYTH, K., STRATHDEE, D., BALKWILL, F. R., VOUSDEN, K., LOCKLEY, M. & MCNEISH, I. A. 2016. CRISPR/Cas9-Mediated Trp53 and Brca2 Knockout to Generate Improved Murine Models of Ovarian High-Grade Serous Carcinoma. *Cancer Res,* 76**,** 6118-6129.

WALTON, J. B., FARQUHARSON, M., MASON, S., PORT, J., KRUSPIG, B., DOWSON, S., STEVENSON, D., MURPHY, D., MATZUK, M., KIM, J., COFFELT, S., BLYTH, K. & MCNEISH, I. A. 2017. CRISPR/Cas9-derived models of ovarian high grade serous carcinoma

targeting Brca1, Pten and Nf1, and correlation with platinum sensitivity. *Sci Rep,* 7**,** 16827.

WANG, C., JETTE, N., MOUSSIENKO, D., BEBB, D. G. & LEES-MILLER, S. P. 2017. ATM-Deficient Colorectal Cancer Cells Are Sensitive to the PARP Inhibitor Olaparib. *Translational Oncology,* 10**,** 190-196.

WANG, D. & LIPPARD, S. J. 2005. Cellular processing of platinum anticancer drugs. *Nat Rev Drug Discov,* 4**,** 307-20.

WANG, E. & AIFANTIS, I. 2020. RNA Splicing and Cancer. *Trends Cancer,* 6**,** 631-644.

WANG, E., LU, S. X., PASTORE, A., CHEN, X., IMIG, J., CHUN-WEI LEE, S., HOCKEMEYER, K., GHEBRECHRISTOS, Y. E., YOSHIMI, A., INOUE, D., KI, M., CHO, H., BITNER, L., KLOETGEN, A., LIN, K. T., UEHARA, T., OWA, T., TIBES, R., KRAINER, A. R., ABDEL-WAHAB, O. & AIFANTIS, I. 2019. Targeting an RNA-Binding Protein Network in Acute Myeloid Leukemia. *Cancer Cell,* 35**,** 369-384.e7.

WANG, E. T., SANDBERG, R., LUO, S., KHREBTUKOVA, I., ZHANG, L., MAYR, C., KINGSMORE, S. F., SCHROTH, G. P. & BURGE, C. B. 2008. Alternative isoform regulation in human tissue transcriptomes. *Nature,* 456**,** 470-476.

WANG, H., WU, M., LIU, H., ZHOU, H., ZHAO, Y., GENG, Y., JIANG, B., ZHANG, K., ZHANG, B., HAN, Z. & DU, X. 2021a. Comparison of the Efficacy and Safety of PARP Inhibitors as a Monotherapy for Platinum-Sensitive Recurrent Ovarian Cancer: A Network Meta-Analysis. *Front Oncol,* 11**,** 785102.

WANG, H., ZHANG, S., SONG, L., QU, M. & ZOU, Z. 2020. Synergistic lethality between PARP-trapping and alantolactone-induced oxidative DNA damage in homologous recombination-proficient cancer cells. *Oncogene*.

WANG, S., WANG, Z., LI, J., QIN, J., SONG, J., LI, Y., ZHAO, L., ZHANG, X., GUO, H., SHAO, C., KONG, B. & LIU, Z. 2021b. Splicing factor USP39 promotes ovarian cancer malignancy through maintaining efficient splicing of oncogenic HMGA2. *Cell Death & Disease,* 12**,** 294.

WANG, Y., BERNHARDY, A. J., CRUZ, C., KRAIS, J. J., NACSON, J., NICOLAS, E., PERI, S., VAN DER GULDEN, H., VAN DER HEIJDEN, I., O'BRIEN, S. W., ZHANG, Y., HARRELL, M. I., JOHNSON, S. F., CANDIDO DOS REIS, F. J., PHAROAH, P. D., KARLAN, B., GOURLEY, C., LAMBRECHTS, D., CHENEVIX-TRENCH, G., OLSSON, H., BENITEZ, J. J., GREENE, M. H., GORE, M., NUSSBAUM, R., SADETZKI, S., GAYTHER, S. A., KJAER, S. K., D'ANDREA, A. D., SHAPIRO, G. I., WIEST, D. L., CONNOLLY, D. C., DALY, M. B., SWISHER, E. M., BOUWMAN, P., JONKERS, J., BALMAÑA, J., SERRA, V. & JOHNSON, N. 2016. The BRCA1-Δ11q Alternative Splice Isoform Bypasses Germline Mutations and Promotes Therapeutic Resistance to PARP Inhibition and Cisplatin. *Cancer Res,* 76**,** 2778-90.

WANG, Y., SPITZ, M. R., LEE, J. J., HUANG, M., LIPPMAN, S. M. & WU, X. 2007. Nucleotide excision repair pathway genes and oral premalignant lesions. *Clin Cancer Res,* 13**,** 3753-8.

WARD, I. M. & CHEN, J. 2001. Histone H2AX is phosphorylated in an ATR-dependent manner in response to replicational stress. *J Biol Chem,* 276**,** 47759-62.

References

WARD, I. M., MINN, K. & CHEN, J. 2004. UV-induced ataxia-telangiectasia-mutated and Rad3-related (ATR) activation requires replication stress. *J Biol Chem,* 279**,** 9677-80.

WARD, I. M., MINN, K., JORDA, K. G. & CHEN, J. 2003. Accumulation of checkpoint protein 53BP1 at DNA breaks involves its binding to phosphorylated histone H2AX. *J Biol Chem,* 278**,** 19579-82.

WEIGELT, B., COMINO-MENDEZ, I., DE BRUIJN, I., TIAN, L., MEISEL, J. L., GARCIA-MURILLAS, I., FRIBBENS, C., CUTTS, R., MARTELOTTO, L. G., NG, C. K. Y., LIM, R. S., SELENICA, P., PISCUOGLIO, S., AGHAJANIAN, C., NORTON, L., MURALI, R., HYMAN, D. M., BORSU, L., ARCILA, M. E., KONNER, J., REIS-FILHO, J. S., GREENBERG, R. A., ROBSON, M. E. & TURNER, N. C. 2017. Diverse BRCA1 and BRCA2 Reversion Mutations in Circulating Cell-Free DNA of Therapy-Resistant Breast or Ovarian Cancer. *Clin Cancer Res,* 23**,** 6708-6720.

WETHINGTON, S. L., WAHNER-HENDRICKSON, A. E., SWISHER, E. M., KAUFMANN, S. H., KARLAN, B. Y., FADER, A. N. & DOWDY, S. C. 2021. PARP inhibitor maintenance for primary ovarian cancer - A missed opportunity for precision medicine. *Gynecol Oncol,* 163**,** 11-13.

WOODWARD, A. M., GÖHLER, T., LUCIANI, M. G., OEHLMANN, M., GE, X., GARTNER, A., JACKSON, D. A. & BLOW, J. J. 2006. Excess Mcm2-7 license dormant origins of replication that can be used under conditions of replicative stress. *J Cell Biol,* 173**,** 673-83.

WU, Q., XUAN, Y. F., SU, A. L., BAO, X. B., MIAO, Z. H. & WANG, Y. Q. 2022. TNKS inhibitors potentiate proliferative inhibition of BET inhibitors via reducing β-Catenin in colorectal cancer cells. *Am J Cancer Res,* 12**,** 1069-1087.

WU, W., SATO, K., KOIKE, A., NISHIKAWA, H., KOIZUMI, H., VENKITARAMAN, A. R. & OHTA, T. 2010. HERC2 is an E3 ligase that targets BRCA1 for degradation. *Cancer Res,* 70**,** 6384-92.

WU, X., CAI, J., ZUO, Z. & LI, J. 2019. Collagen facilitates the colorectal cancer stemness and metastasis through an integrin/PI3K/AKT/Snail signaling pathway. *Biomed Pharmacother,* 114**,** 108708.

WU-BAER, F., LUDWIG, T. & BAER, R. 2010. The UBXN1 protein associates with autoubiquitinated forms of the BRCA1 tumor suppressor and inhibits its enzymatic function. *Mol Cell Biol,* 30**,** 2787-98.

XIAO, Z., CHEN, Z., GUNASEKERA, A. H., SOWIN, T. J., ROSENBERG, S. H., FESIK, S. & ZHANG, H. 2003. Chk1 Mediates S and G2 Arrests through Cdc25A Degradation in Response to DNA-damaging Agents*. *Journal of Biological Chemistry,* 278**,** 21767-21773.

XIE, S., MORTUSEWICZ, O., MA, H. T., HERR, P., POON, R. Y., HELLEDAY, T. & QIAN, C. 2015. Timeless Interacts with PARP-1 to Promote Homologous Recombination Repair. *Mol Cell,* 60**,** 163-76.

XIONG, Y., GUO, Y., LIU, Y., WANG, H., GONG, W., LIU, Y., WANG, X., GAO, Y., YU, F., SU, D., WANG, F., ZHU, Y., ZHAO, Y., WU, Y., QIN, Z., SUN, X., REN, B., JIANG, B., JIN, W., SHEN, Z., TANG, Z., SONG, X., WANG, L., LIU, X., ZHOU, C. & JIANG, B. 2020. Pamiparib is a potent and selective PARP inhibitor with unique potential for the treatment of brain tumor. *Neoplasia,* 22**,** 431-440.

References

XU, Y., DING, L., TIAN, Y., BI, M., HAN, N. & WANG, L. 2020a. Comparative Efficacy and Safety of PARP Inhibitors as Maintenance Therapy in Platinum Sensitive Recurrent Ovarian Cancer: A Network Meta-Analysis. *Front Oncol,* 10**,** 573801.

XU, Y., NIJHUIS, A. & KEUN, H. C. 2020b. RNA-binding motif protein 39 (RBM39): An emerging cancer target. *Br J Pharmacol,* 179**,** 2795-2812.

XU, Z., VANDENBERG, C. J., LIESCHKE, E., DI RAGO, L., SCOTT, C. L. & MAJEWSKI, I. J. 2021. CHK2 Inhibition Provides a Strategy to Suppress Hematologic Toxicity from PARP Inhibitors. *Molecular Cancer Research,* 19**,** 1350-1360.

YAMAMOTO, N., NOKIHARA, H., YAMADA, Y., GOTO, Y., TANIOKA, M., SHIBATA, T., YAMADA, K., ASAHINA, H., KAWATA, T., SHI, X. & TAMURA, T. 2012. A Phase I, dose-finding and pharmacokinetic study of olaparib (AZD2281) in Japanese patients with advanced solid tumors. *Cancer Sci,* 103**,** 504-9.

YANG, H., NOVICK, S. J. & ZHAO, W. 2015. Drug combination synergy. *In:* BYRON JONES, J.-P. L., KARL E. PEACE; BRUCE W. TURNBULL (ed.) *Chapman & Hall/CRC biostatistics series.* USA: Boca Raton : CRC Press, [2015] ©2015.

YANG, Y., DU, N., XIE, L., JIANG, J., MO, J., HONG, J., MAO, D., NG, D. M. & SHI, H. 2020. The efficacy and safety of the addition of poly ADP-ribose polymerase (PARP) inhibitors to therapy for ovarian cancer: a systematic review and meta-analysis. *World Journal of Surgical Oncology,* 18**,** 151.

YAO, S., YUAN, C., SHI, Y., QI, Y., SRIDHA, R., DAI, M. & CAI, H. 2022. Alternative Splicing: A New Therapeutic Target for Ovarian Cancer. *Technology in cancer research & treatment,* 21**,** 15330338211067911-15330338211067911.

YI, J., LIU, C., TAO, Z., WANG, M., JIA, Y., SANG, X., SHEN, L., XUE, Y., JIANG, K., LUO, F., LIU, P. & CHENG, H. 2019. MYC status as a determinant of synergistic response to Olaparib and Palbociclib in ovarian cancer. *EBioMedicine,* 43**,** 225-237.

YI, Y. W., PARK, J.-S., KWAK, S.-J. & SEONG, Y.-S. 2015. Co-treatment with BEZ235 Enhances Sensitivity of BRCA1-negative Breast Cancer Cells to Olaparib. *Anticancer Research,* 35**,** 3829-3838.

YING, S., HAMDY, F. C. & HELLEDAY, T. 2012. Mre11-dependent degradation of stalled DNA replication forks is prevented by BRCA2 and PARP1. *Cancer Res,* 72**,** 2814-21.

YOKOI, A., KUROMITSU, J., KAWAI, T., NAGASU, T., SUGI, N. H., YOSHIMATSU, K., YOSHINO, H. & OWA, T. 2002. Profiling novel sulfonamide antitumor agents with cell-based phenotypic screens and array-based gene expression analysis. *Mol Cancer Ther,* 1**,** 275-86.

YOUNG, L. M., MARZIO, A., PEREZ-DURAN, P., REID, D. A., MEREDITH, D. N., ROBERTI, D., STAR, A., ROTHENBERG, E., UEBERHEIDE, B. & PAGANO, M. 2015. TIMELESS Forms a Complex with PARP1 Distinct from Its Complex with TIPIN and Plays a Role in the DNA Damage Response. *Cell Rep,* 13**,** 451-459.

YUE, C., ZHAO, T., ZHANG, S., LIU, Y., ZHENG, G. & ZHANG, Y. 2022. Comprehensive characterization of 11 prognostic alternative splicing events in ovarian cancer interacted with the immune microenvironment. *Scientific Reports,* 12**,** 980.

References

ZAILAB. 2020. *Zai Lab Announces NMPA Approval of ZEJULA® (Niraparib) for First-Line Maintenance Treatment of Ovarian Cancer in China* [Online]. GlobeNewswire. Available: https://www.globenewswire.com/news-release/2020/09/10/2091603/0/en/Zai-Lab-Announces-NMPA-Approval-of-ZEJULA-Niraparib-for-First-Line-Maintenance-Treatment-of-Ovarian-Cancer-in-China.html [Accessed 18 July 2022].

ZANDARASHVILI, L., LANGELIER, M.-F., VELAGAPUDI, U. K., HANCOCK, M. A., STEFFEN, J. D., BILLUR, R., HANNAN, Z. M., WICKS, A. J., KRASTEV, D. B., PETTITT, S. J., LORD, C. J., TALELE, T. T., PASCAL, J. M. & BLACK, B. E. 2020. Structural basis for allosteric PARP-1 retention on DNA breaks. *Science,* 368**,** eaax6367.

ZANNINI, L., DELIA, D. & BUSCEMI, G. 2014. CHK2 kinase in the DNA damage response and beyond. *Journal of molecular cell biology,* 6**,** 442-457.

ZHANG, D., ZOU, D., DENG, Y. & YANG, L. 2021a. Systematic analysis of the relationship between ovarian cancer prognosis and alternative splicing. *Journal of Ovarian Research,* 14**,** 120.

ZHANG, J., LIAN, H., CHEN, K., PANG, Y., CHEN, M., HUANG, B., ZHU, L., XU, S., LIU, M. & ZHONG, C. 2021b. RECQ1 Promotes Stress Resistance and DNA Replication Progression Through PARP1 Signaling Pathway in Glioblastoma. *Front Cell Dev Biol,* 9**,** 714868.

ZHANG, P., ZHANG, P., ZHOU, M., JIANG, H., ZHANG, H., SHI, B., PAN, X., GAO, H., SUN, H. & LI, Z. 2013. Exon 4 deletion variant of epidermal growth factor receptor enhances invasiveness and cisplatin resistance in epithelial ovarian cancer. *Carcinogenesis,* 34**,** 2639-2646.

ZHANG, W. H., POH, A., FANOUS, A. A. & EASTMAN, A. 2008. DNA damage-induced S phase arrest in human breast cancer depends on Chk1, but G2 arrest can occur independently of Chk1, Chk2 or MAPKAPK2. *Cell Cycle,* 7**,** 1668-77.

ZHAO, C., LI, Y., QIU, C., CHEN, J., WU, H., WANG, Q., MA, X., SONG, K. & KONG, B. 2021. Splicing Factor DDX23, Transcriptionally Activated by E2F1, Promotes Ovarian Cancer Progression by Regulating FOXM1. *Front Oncol,* 11**,** 749144.

ZHAO, H. & PIWNICA-WORMS, H. 2001. ATR-mediated checkpoint pathways regulate phosphorylation and activation of human Chk1. *Mol Cell Biol,* 21**,** 4129-39.

ZHU, J., CHEN, Z. & YONG, L. 2018. Systematic profiling of alternative splicing signature reveals prognostic predictor for ovarian cancer. *Gynecol Oncol,* 148**,** 368-374.

ZHU, X., CHEN, L., HUANG, B., LI, X., YANG, L., HU, X., JIANG, Y., SHAO, Z. & WANG, Z. 2021. Efficacy and mechanism of the combination of PARP and CDK4/6 inhibitors in the treatment of triple-negative breast cancer. *Journal of Experimental & Clinical Cancer Research,* 40**,** 122.

ZIMMERMANN, M., LOTTERSBERGER, F., BUONOMO, S. B., SFEIR, A. & DE LANGE, T. 2013. 53BP1 regulates DSB repair using Rif1 to control 5' end resection. *Science,* 339**,** 700-4.

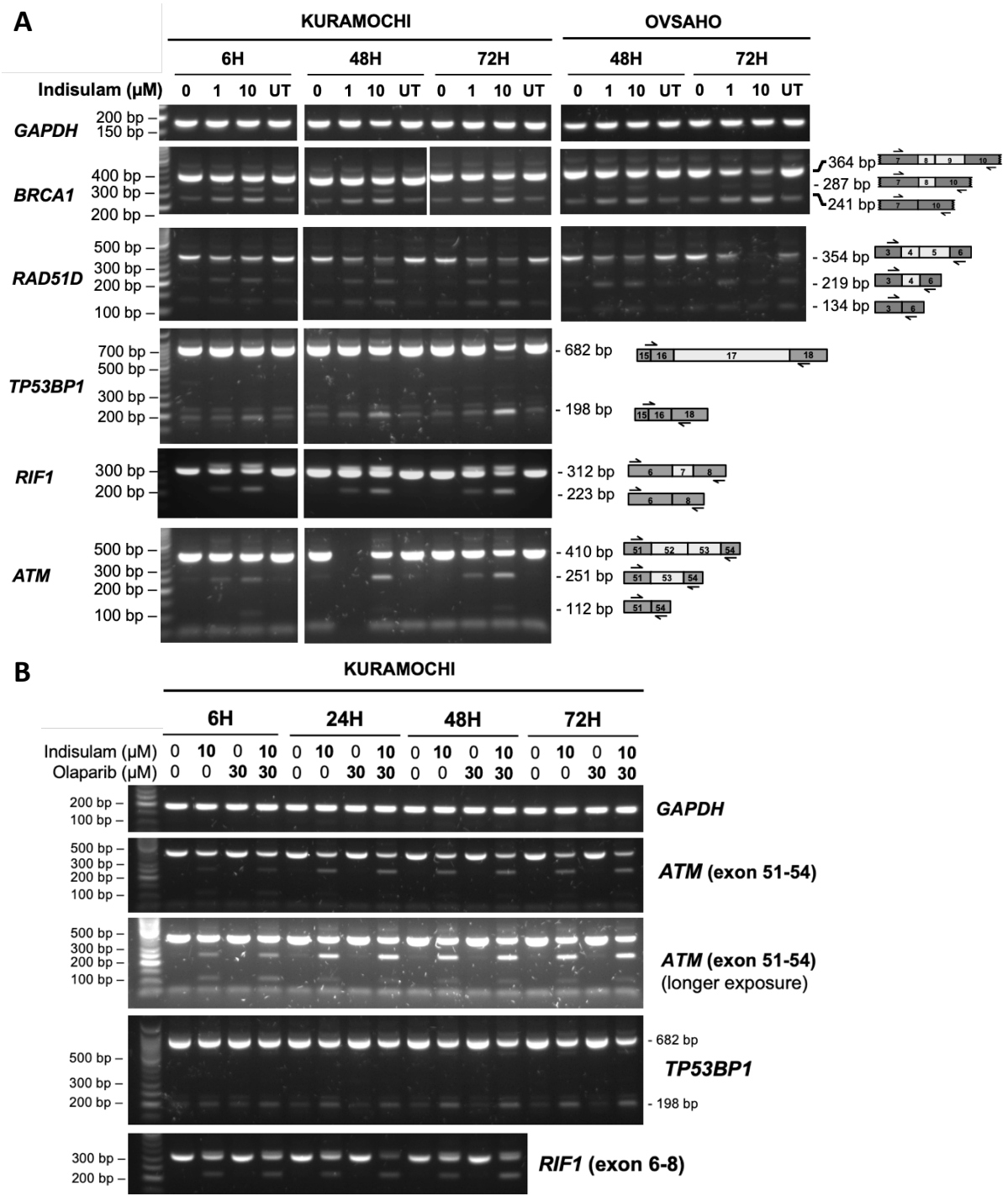
ZIMMERMANN, M., MURINA, O., REIJNS, M. A. M., AGATHANGGELOU, A., CHALLIS, R., TARNAUSKAITĖ, Ž., MUIR, M., FLUTEAU, A., AREGGER, M., MCEWAN, A., YUAN, W., CLARKE, M., LAMBROS, M. B., PANEESHA, S., MOSS, P., CHANDRASHEKHAR, M.,

References

ANGERS, S., MOFFAT, J., BRUNTON, V. G., HART, T., DE BONO, J., STANKOVIC, T., JACKSON, A. P. & DUROCHER, D. 2018. CRISPR screens identify genomic ribonucleotides as a source of PARP-trapping lesions. *Nature,* 559**,** 285-289.

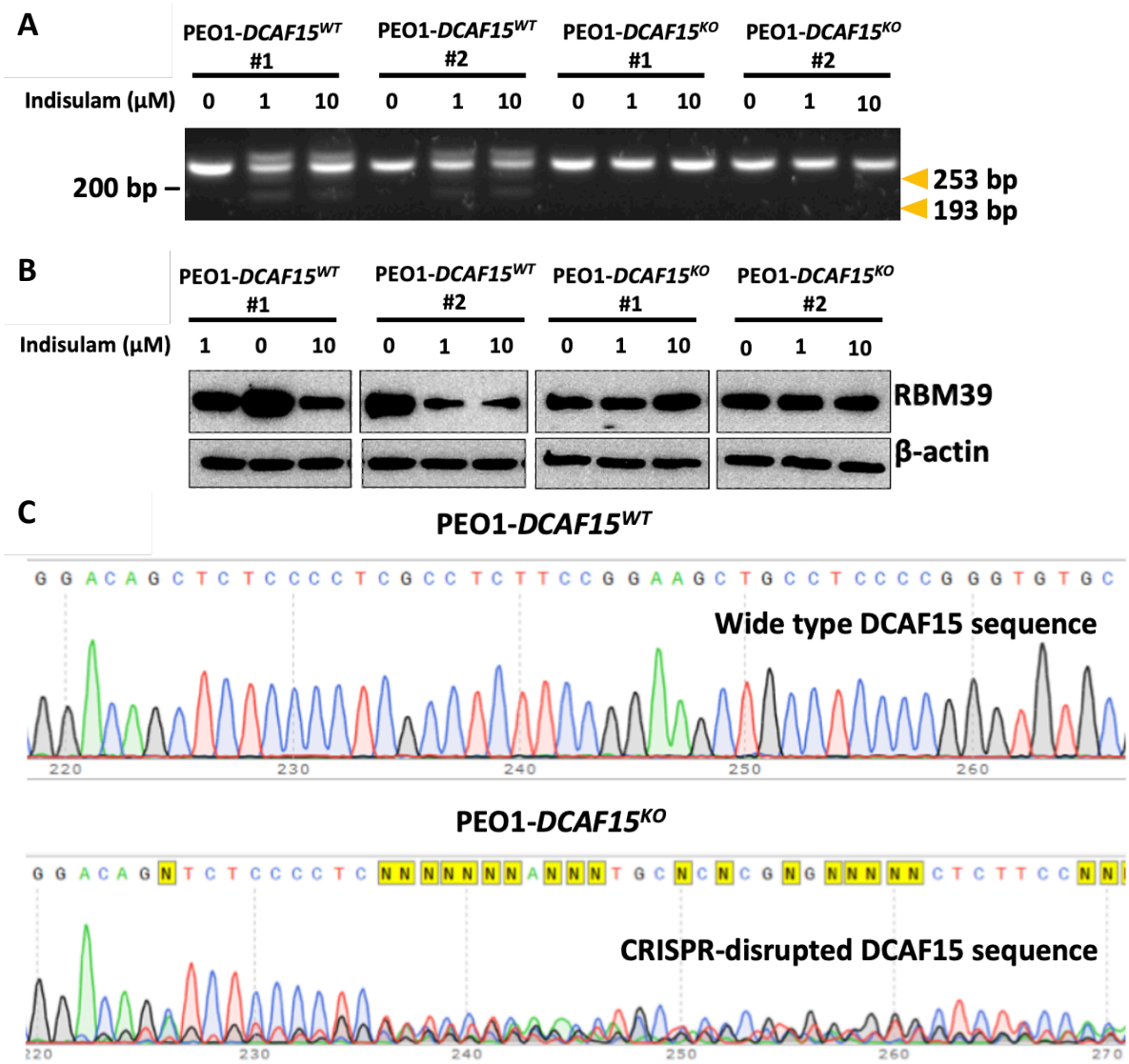
Appendix

1. Appendix Figures and Tables



Appendix Figure 1. Indisulam induces aberrant splicing DNA repair genes in HGSOC cells.
(A) KURAMOCHI (n = 1) and OVSAHO (n = 1) cells were either untreated (medium only), or treated with indicated doses of indisulam for 6, 48, and 72 hours, followed by PCR-based exon skipping analysis. Exon skipping events and expected product sizes are annotated on the right. Related to Figure 3.2. **(B)** KURAMOCHI cells were treated with indicated drugs for 6 to 72 hours before PCR-based exon skipping analysis (n = 1). The same exon skipping events as in (a) were probed. Related to Figure 6.11.

Appendix



Appendix Figure 2. Validation of DCAF15-knockout in the PEO1 clones.

Two CRISPR-edited PEO1-*DCAF15*^{KO} clones and two control clones were treated with indicated doses of indisulam for 6 hours, and total RNA and protein were extracted for PCR-based exon skipping analysis and western blot analysis. **(A)** PCR analysis showing PEO1-*DCAF15*^{KO} clones resist indisulam-induced mis-splicing of *TRIM27*, a well-established splicing targets of RBM39 (Han et al., 2017b, Nijhuis et al., 2022). **(B)** Western blot analysis showing PEO1-*DCAF15*^{KO} clones resist indisulam-mediated RBM39 degradation. These data were acquired by the previous master student Madelen Shepherd. **(C)** Genomic DNA was extracted from PEO1-*DCAF15*^{WT} (#1) and PEO1-*DCAF15*^{KO} (#1), and the CRISPR-edited region was sequenced. Sequencing results show that CRISPR-editing disrupted the target sequence of *DCAF15*, which was expected. PEO1 has increased copy numbers of DCAF15, the CRISPR-editing results were therefore heterogenous. Sequencing was done by Dr Anke Nijhuis.

Appendix

Appendix Table 1. Phospho-events detected in the human kinase array worth future investigation.

Phospho-events	Functional annotation
p-cJun (S63)	The c-Jun is a component of the activator protein-1 (AP-1) transcription factor, and an interacting partner of RBM39 (Song et al., 2021, Jung et al., 2002). Conflicting data have been reported about how RBM39 affects c-Jun activity. Mercier et al. (2014) showed that RBM39 is required for c-Jun phosphorylation (at S63 and S73), but a recent study showed that RBM39 inhibits c-Jun phosphorylation (at S73) (Song et al., 2021).
pSrc(Y419)	Src is a non-receptor tyrosine kinase and a proto-oncogene commonly upregulated in endometrioid ovarian cancer (Bjorge et al., 2000, Manek et al., 2016). Phosphorylation at Y419 activates Src (Amata et al., 2014) and it is frequently upregulated in ovarian cancer (Song et al., 2019).
pPYK2 (Y402)	Proline-rich kinase 2 (PYK2) is a tyrosine kinase and is associated with ovarian cancer metastasis (Lane et al., 2016, Pasquier et al., 2018) and chemoresistance. The Y402 phosphorylation is commonly upregulated in HGSOC (Song et al., 2019).
pPLC-γ1 (Y783)	Phospholipase C-γ1 (PLC-γ1) is an enzyme mediating hydrolysis of the phosphatidylinositol 4,5-biphosphate and is associated with higher risk of metastasis in patients with Luminal A-breast cancer (Lattanzio et al., 2019).
pMSK1/2 (S376/S360)	Mitogen- and Stress-activated protein kinases 1 and 2 downstream of the mitogen-activated protein kinases [reviewed in (Cargnello and Roux, 2011)], and higher expression of MSK1 is associated with better prognosis in breast cancer patients (Pu et al., 2018).

2. Appendix Materials and Methods

2.1. Proteomics analysis

The following methods are provided by Dr Alex Montoya.

Sample processing.

Cellular lysates containing 550µg of protein in 8M urea (in 20mM HEPES, pH 8.0), were sequentially reduced and alkylated in the dark and at room temperature with 10mM dithiothreitol (DTT) and 50mM 2-chloroacetamide (2-CAM) respectively. An initial digestion was carried out by diluting samples to 4M urea with 20mM HEPES followed by the addition of 1µg of LysC (Thermo, 90307) and incubation at 37^{o}C for 5 hours. Samples were subsequently diluted to 2M urea with 20mM HEPES. 10µg of Trypsin Gold (Promega, V5280)

was added followed by incubation at 37^{o}C over-night. Post-digestion, samples were acidified to 0.5% trifluoroacetic acid (TFA) and processed as follows:

Total protein analysis: volumes equivalent to 50µg were taken and de-salted using Glygen C18 spin-tips (Glygen Corp, TT2C18.96). Briefly, spin-tips were sequentially solvated and washed three times with 50µl of 60% acetonitrile (ACN), 0.1% formic acid (FA) and 1% ACN, 0.1% FA respectively. Peptide volumes were loaded and then de-salted with 1% ACN, 0.1% FA (3 x 50µl). Peptides were eluted with 60% ACN, 0.1% FA (3 x 50µl) and eluents then dried by vacuum centrifugation. Volumes purged between various washing and loading stages by centrifugation.

Phospho-enrichment: The remaining sample volumes (500µg of digest) were de-salted using reversed-phase solid phase extraction with OASIS HLB 10mg cartridges (Waters, 186000383) according to the manufacturer's instructions. Briefly, HLB cartridges were sequentially solvated and washed with 1ml of ACN and 1.5ml of 1% ACN, 0.1% TFA, respectively. Peptide volumes loaded and de-salted with 1.5ml 1% ACN, 0.1% TFA. Volumes purged between various washing and loading stages by centrifugation by vacuum suction. Peptides were eluted with 500µl of 1M glycolic acid in 80% acetonitrile (ACN), 5% TFA and phospho-enrichment carried out using a TiO_2 based method.

Briefly, eluents were adjusted to 1ml with 1M glycolic acid solution and then incubated with 25mg of TiO_2 (GL Sciences, PN:5020-75000, 50% slurry in 1% TFA) for 5 minutes at room temperature. After 5 minutes of incubation with mixing, the TiO_2/peptide mixture was packed into empty spin tips by centrifugation. The TiO_2 layer was then sequentially washed with 1M glycolic acid solution, 100mM ammonium acetate in 25% ACN and 10% ACN. Phosphopeptides were eluted with 4 sequential additions of a 5% NH_4OH solution in 10% ACN. Eluents were clarified with centrifugation (18,000g) for 2 minutes and clear supernatant transferred to new tubes. Samples were snap frozen on dry ice and then dried by vacuum centrifugation.

Liquid chromatography-tandem mass spectrometry (LC-MS/MS) analysis.

Phospho-enriched samples and desalted total protein digests were re-dissolved in 0.1% TFA by shaking (1,200rpm) for 30min and sonication on an ultrasonic water bath for 5min,

followed by centrifugation (13,000rpm, 5°C) for 10min. Clarified supernatant sampled and transferred into MS vials.

Total protein samples: single replicate injections for a final on-column concentration of 1500ng.

Phospho-enriched samples: single replicate injections.

LC-MS/MS analysis was performed using an Ultimate 3000 RSLC nano liquid chromatography system (Thermo Scientific) coupled to a Q-Exactive HF-X mass spectrometer (Thermo Scientific) via an EASY spray source (Thermo Scientific). Sample solutions were injected and loaded onto a trap column (Acclaim PepMap 100 C18, 100µm × 2cm) for desalting and concentration at 8µl/min in 2% acetonitrile, 0.1% TFA. Peptides were then eluted on-line to an analytical column (Acclaim Pepmap RSLC C18, 75µm × 50cm) at a flow rate of 200nl/min. Peptides were separated using a 120 minute gradient, 1-22% of buffer B for 90 minutes followed by 22-42% of buffer B for another 30 minutes (composition of buffer B – 75% acetonitrile, 20% H_20, 5% DMSO, 0.1% FA) and subsequent column conditioning and equilibration. Eluted peptides were analysed by the mass spectrometer operating in positive polarity using a data-dependent acquisition mode. Ions for fragmentation were determined from an initial MS1 survey scan at 120,000 resolution, followed by HCD (Higher Energy Collision Induced Dissociation) of the top 30 most abundant ions at 15,000 resolution. For total protein samples MS1 and MS2 scan AGC targets were set to 3e6 and 5e4 for maximum injection times of 25ms and 50ms respectively. A survey scan m/z range of 350 – 1750 was used, normalised collision energy set to 27%, charge exclusion enabled with unassigned and +1 charge states rejected and a minimal AGC target of 8e3. For phospho-enriched samples, a top 25 method was utilised, with MS1 and MS2 scan AGC targets set to 3e6 and 5e4 for maximum injection times of 25ms and 100ms respectively. Dynamic exclusion settings were 50 and 60 seconds for total protein and phospho-enriched samples respectively.

Raw data processing.

Data was processed using the MaxQuant software platform (v1.6.10.43), with database searches carried out by the in-built Andromeda search engine. Databases used were the Uniprot Mus Musculus database (version 20211018, number of entries: 55,389) and Homo

Sapiens database (version 20211019, number of entries: 78,139). A reverse decoy search approach was used at a 1% false discovery rate (FDR) for both peptide spectrum matches and protein groups. Search parameters included: maximum missed cleavages set to 3, fixed modification of cysteine carbamidomethylation, variable modifications of methionine oxidation, protein N-terminal acetylation and phospho (STY). Label-free quantification was enabled with an LFQ minimum ratio count of 1. 'Match between runs' function was used with match and alignment time limits of 0.7 and 20 minutes respectively.

3. Appendix Discussion

3.1. Rationale for drug combination therapy

Combination therapies are commonly used in the clinic for ovarian cancer patients because it has the potential to increase clinical outcomes while reducing adverse effects. Most newly diagnosed patients receive dual-agent chemotherapy consisting of carboplatin and paclitaxel (ESMO, 2017, Tsibulak et al., 2019). For some patients, the chemotherapy is supplemented with bevacizumab, a VEGF inhibitor inhibiting angiogenesis in tumours (ESMO, 2017, Tsibulak et al., 2019). Combining drugs as the first-line treatment improves patient outcomes and reduces the risk of developing drug resistance, since tumours are less likely to develop resistance to both drugs than to a single agent.

Drugs may interact with other drugs in three ways: synergistically, additively, or antagonistically. A synergistic drug combination can achieve a greater therapeutic response than the effect of two drugs working independently (additive effect). An antagonistic drug combination includes drugs that counteract each other and may lead to reduced efficacy or increased toxicities.

Multiple statistical models are available to assess the combined effect of drugs. Bliss independence (Bliss, 1939) and Loewe additivity (Loewe, 1953) are two basic synergy models commonly used in pre-clinical and clinical studies, and they have been the parental model for a series of derivative methods. The core of all synergy models is the prediction of additive effect, which defines the boundary between synergism and antagonism. Unfortunately, every method has advantages and limitations, and there is no consensus on which method is the best.

Appendix

3.2. Bliss independence model

The Bliss independence model is based on the independence probability theory. It predicts the additive effect of drug A and drug B under the assumption that these two drugs act independently from each other and combined effects were achieved by drugs acting on distinct pathways with no cross-talking (Roell et al., 2017, Greco et al., 1995).

For example:

- if drug A causes 30% inhibition on cell growth, i.e., f(A) = 30%
- and drug B causes 40% growth inhibition, i.e., f(B) = 40%

The predicted additive effect of drugs A and B in combination is:

- f(A) + f(B) – f(A)*f(B) = 30% + 40% - 30%*40% = 58% inhibition.

In other words (from the perspective of SRB readings),

- 70% cells are left after exposure to drug A, i.e., r(A) = 70%
- and 60% cells are left after exposure to drug B, i.e., r(B) = 60%

Bliss independence model predicts the additive effect as:

- r(A)*r(B) = 70% * 60% = 42% cells remaining after exposure to the drug combination of A + B, which is equivalent to the 58% growth inhibition.

A bliss score is determined by calculating the difference between the predicted additive effect and the observed effect. Drug-drug interaction is interpreted as:

- (Bliss) Synergism: observed effect > predicted additive effect
- (Bliss) Additivity: observed effect = predicted additive effect
- (Bliss) Antagonism: observed effect < predicted additive effect

This method is very intuitive and easy to use. Bliss score can be calculated with as few as one single set of drug dose pairs in monotherapies and combination. It is therefore compatible with high-throughput screens (such as the screen in Section 2.10.2) and clinical trials where testing multiple drug dose pairs are not always convenient. However, bliss independence ignores the non-linear nature of the dose-response relationship, which is often better represented as sigmoid curves. One good example to explain this issue is the ‘sham mixture’ – a drug is mixed with itself. Below is an example of a false positive (of synergism):

- Assume two batches of the same drug (A1 and A2) with the same inhibitory effect on cancer cells.
- 10 µM drug A (either A1 or A2) causes 10% growth inhibition
- 20 µM drug A causes 40% growth inhibition, which equals to a 'sham mixture' consisting of 10 µM drug A1 and 10 µM of drug A2.
- Bliss independence predicts additive effect of 10 µM A1 + 10 µM A2 as
    - $f(A1, A2) = f(A1) + f(A2) – f(A1)*f(A2) = 10\% + 10\% - 10\%*10\% = 19\%$
- The predicted additive effect (19%) is weaker than 40% inhibition observed when 10 µM drug A1 and 10 µM drug A2 are combined. Therefore, bliss synergy can be claimed theoretically.
- However, it would be wrong to conclude that the sham mixture (10 µM A1 and 10 µM A2) is more effective than 20 µM drug A, because they are equivalent of each other. Thus, this is a false positive bliss synergy.

Likewise, false negative Bliss antagonism can occur at the same rate as false positive bliss synergism (Twarog et al., 2020). As a result, increasing the number of data points and drug doses does not necessarily improve the accuracy of the Bliss model (Twarog et al., 2020). Furthermore, it is labour-intensive to calculate Bliss synergy for combinations with more than two drugs. Overall, Bliss independence is straightforward but remains as a controversial method due to its over-simplification of the drug-drug interaction (Roell et al., 2017).

3.3. Loewe additivity

The Loewe additivity model is a more intricate model than Bliss independence. It calculates the drug combination effect by determining the extent of dose reduction when a second drug is added. This method by default defines the 'sham mixture' as additive combination, and a drug can only be additive with itself. This feature is in sharp contrast to the Bliss independence (Section 3.3). For example:

- Assuming
    - 10 µM drug A causes 40% growth inhibition.
    - And dose-response curve of drug A indicates:
        - 20 µM drug A causes 50% growth inhibition
        - 30 µM drug A causes 70% growth inhibition.

    - 5 μM drug B causes 50% growth inhibition.
- Thus, 5 μM drug B is at equal potency as 20 μM drug A.
- Loewe additivity predicts additive effect of 10 μM drug A + 5 μM drug B as

  10 μM drug A + 5 μM drug B
  = 10 μM drug A + 20 μM drug A
  = 30 μM drug A
  = 70% growth inhibition.
- Synergism is claimed when the observed inhibitory effect of the drug combination is larger than 70%
- The equal potency conversion is bi-directional. The same result can be achieved by considering the drug combination as a mixture of 5 μM drug B and a dose of drug B having equal potency as 10 μM drug A.

In actual practice, Loewe additivity is often shown as combination index (CI) values [reviewed in Yang et al. (2015) and Roell et al. (2017)]:

$$Combination\ index = \frac{a}{A} + \frac{b}{B}$$

Appendix Equation 1

CI values < 1 indicates synergism; CI = 1 indicates additivity, and CI > 1 indicates antagonism. In the equation (**Error! Reference source not found.**), symbols represent:

- *a, b*: actual doses of drug A and drug B in combination
- *A*: doses of drug A required to reach the effect of combination (*a* + *b*) treatment.
- *B*: doses of drug B required to reach the effect of combination (*a* + *b*) treatment.

Compared with the Bliss independence, the Loewe additivity is less likely to produce false positive or false negative results, and the combination index can be easily expanded to cover combinations involving three or more drugs (Roell et al., 2017). The accuracy also increases as more data points are available due to the improvement in fitting dose-response curves. However, the requirement of dose-response curves limits its application in animal studies and in clinical settings because a large number of animals or participants will be needed (Chou, 2010). Meanwhile, Loewe additivity assumes a constant potency ratio between drugs, which

is a rare scenario in drug combinations. Loewe's method also tends to bias towards slight synergism when the actions of two drugs are not mutually exclusive (Chou and Talalay, 1984). Despite the above flaws, Loewe additivity is a popular reference theory for drug synergy analysis, and it is the basis of multiple more advanced synergy models.

3.4. Chou-Talalay method

The Chou-Talalay method is a more advanced version of the Loewe additivity, and it has become one of the most widely used synergy methods, attracting nearly 6000 citations (Chou and Talalay, 1984). Chou and Talalay (1984) improved Loewe additivity by integrating the median effect equation – a dose-response curve calculation approach unifying four other equations (Chou, 2006, Chou, 2010). The method adopted the concept of the combination index. For mutually exclusive drugs, the equation for combination index is the same as **Error! Reference source not found.**, with the difference that the median effect equation is used to calculate the parameters *A* and *B* – theoretical doses of individual drugs to achieve the same effect seen in the drug combination. For mutually nonexclusive drugs, the equation is as follows:

$$Combination\ index = \frac{a}{A} + \frac{b}{B} + \frac{a * b}{A * B}$$

Appendix Equation 2

In comparison with Bliss independent and Loewe additivity, the Chou-Talalay method has multiple advantages (Chou and Talalay, 1984, Chou, 2006, Chou, 2010). Firstly, the median effect equation allows a more accurate estimation of dose-response curves and, thus, more reliable combination index values. It is compatible with a wide range of scenarios, including mutually exclusive or nonexclusive drug-drug interaction, agonist or antagonistic drugs, hyperbolic or sigmoidal dose-response relationships and multiple mechanisms of enzyme inhibition (competitive, non-competitive or un-competitive inhibitors) (Chou and Talalay, 1984, Chou, 2006). The third advantage is that the Chou-Talalay method tolerates drugs with variable potency ratios, but the method performs better with constant potency ratio drugs (Chou, 2010). Nevertheless, all models have flaws, and the median effect equation is no exception. Greco et al. (1995) pointed out that Appendix Equation 2 has low accuracy for combinations involving mutually nonexclusive drugs, and it may bias toward antagonism in

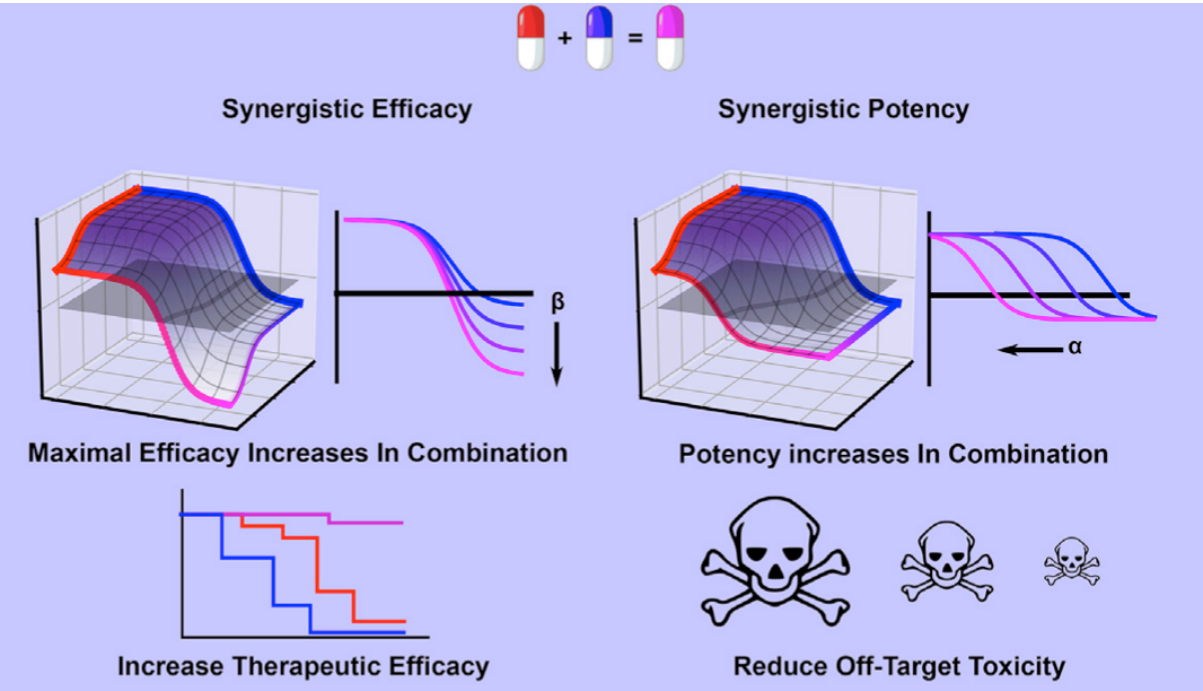
some cases (Roell et al., 2017). Variations in drug dose pairs and effect levels can also lead to fluctuation in the combination index values and complicate the data interpretation (Twarog et al., 2020).

Despite criticisms, the Chou-Talalay method remains one of the most popular models. Its success has been facilitated by the freely available software CompuSyn developed by Ting-Chao Chou and Nick Martin in 2005 (Chou and Martin, 2005). CompuSyn calculates combination index semi-automatically and generates results with customisable layout features. A fully-automated version of the software called CalcuSyn is commercially available for high-throughput analysis (Chou and Hayball, 1997).

3.5. Re-defining synergy with advanced models

Advanced mathematical models have been developed, attempting to address the limitations of conventional models. They have provided novel insights into the definition of 'synergy'. Meyer et al. (2019) proposed that synergy has two dimensions: synergistic efficacy and synergistic potency. Synergistic efficacy refers to a combination effect that increases the maximum effect of individual drugs, while synergistic potency refers to those combinations that decrease the half-maximal effect (EC50) of individual drugs (**Error! Reference source not found.**) (Meyer et al., 2019). Dissecting synergy into these two dimensions may improve the clinical translation of combination therapy (**Error! Reference source not found.**) (Meyer et al., 2019). If efficacy of a drug is sufficient to treat the target disease, a combination with synergistic potency is preferred to reduce the doses and minimise side effects. On the other hand, if the efficacy of a drug is inadequate, a combination with synergistic efficacy is preferable to improve the amplitude of clinical benefits. A multi-dimensional synergy of combinations (MuSyC) method has been developed to quantify efficacy and potency changes in drug combinations (Meyer et al., 2019).

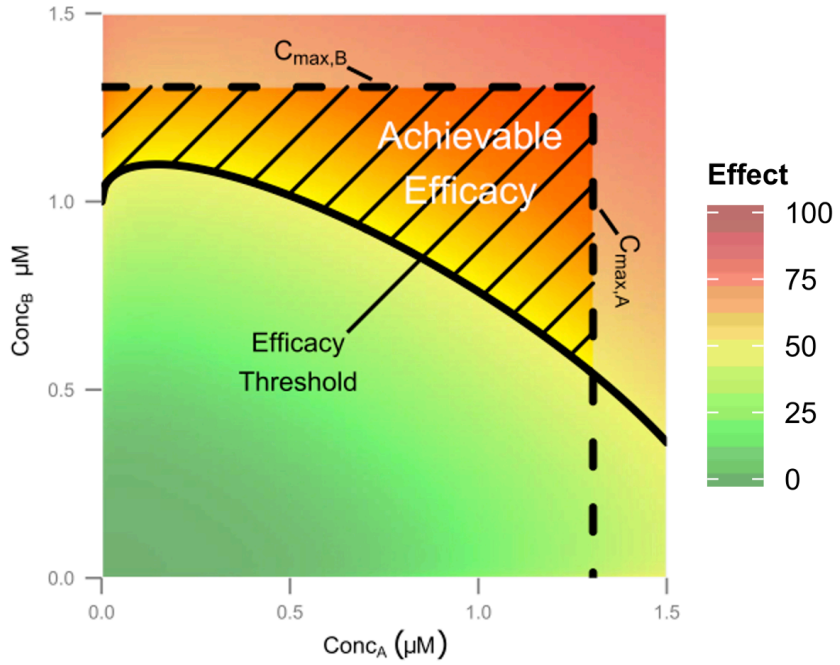
Appendix



Appendix Figure 3. Synergistic efficacy and potency.
Meyer et al. (2019) proposed that synergy has two dimensions: synergistic efficacy and synergistic potency. Synergistic efficacy describes drug combinations that increase the maximum efficacy of individual drugs without affecting the half-maximal inhibition concentration (EC50) (left panel). Synergistic potency describes drug combinations that decrease the EC50 without increasing the maximum efficacy (right panel). In the clinic, synergistically efficacious drug combinations increase maximal benefits, and synergistically potent drug combinations reduce adverse effects by dose reduction. This figure is taken from Meyer et al. (2019) with permission.

A similar theory was proposed by Twarog et al. (2020), who developed the Bivariate Response to Additive Interacting Doses (BRAID) model that distinguishes efficacy-driven synergy from potency-driven synergy (Twarog et al., 2016). Using publicly available databases, they demonstrated that these two forms of synergy are context-dependent, and the same drug combination can shift synergy types when genetic background changes (Twarog et al., 2020). Comparing the synergistic potential of drug combinations across a panel of cancer cell lines may therefore reveal novel mechanisms of action and facilitate the identification of predictive markers [examples in (Twarog et al., 2020)]. Another interesting feature of the BRAID model is the proposal of a novel parameter: the Index of achievable efficacy (IAE). IAE quantifies the therapeutic window of drug combinations by considering the maximum tolerated doses of drugs in patients (**Error! Reference source not found.**) (Twarog et al., 2016). This may improve the translation of combination therapy from lab benches to the clinic by filtering out drug combinations that require doses hardly achievable or tolerable in patients.

Appendix



Appendix Figure 4. Index of achievable efficacy by the BRAID synergy model.
Diagrams visualising the IAE proposed by Twarog et al. (2016). The x-axis indicates the concentration of drug A, the y-axis indicates the concentration of drug B, and the area within the square shows the combined effect of drugs A and B. The dark line within the square is the efficacy threshold, which indicates the boundary of desired (synergy) effect. $C_{max,A}$ and $C_{max,B}$ are the maximal achievable concentrations of drugs A and B in the clinic, respectively. IAE is calculated as the square root of the ratio between achievable efficacy (i.e. synergistic dose pairs) over all possible combinations ($C_{max,A}$ * $C_{max,B}$). Higher IAE indicates drug combinations with a wider therapeutic window. This figure is taken from Twarog et al. (2016) with permission.

Several other models have been developed [reviewed in (Meyer et al., 2020)], but most of them are still in the early stages, and professional programming software is often required to perform the calculation. Inevitably, an increase in model complexity leads to frequent misuse by users, as exemplified by Meyer et al. (2020). A simplified user interface and a detailed user guide will be necessary for complex models such as MuSyc and BRAID to surpass the popularity of traditional methods.

3.6. Challenges in synergy analysis

The biggest challenge in synergy analysis is the lack of consensus, which reflects the complex nature of drug-drug interactions. The Saariselkä conference held in 1992 failed to reach a consensus on the synergy model, but a basic agreement (The Saariselkä agreement) on good practice was made, stating that researchers are free to choose any synergy model as long as

the method is explicitly reported (Tang et al., 2015). Three decades later, a consensus on how to determine synergy still has not been reached, and the definition of 'synergy' is under frequent debate.

In the absence of consensus, the choice of synergy model should consider the nature of data types and the experimental design (Chou, 2006, Chou, 2010, Meyer et al., 2020). It is, therefore, vital to understand the theoretical basis, requirements, and limitations of each method before implementing them. The choice of software (applications, web tools or R packages) for synergy calculation is another important factor to consider because conflicting results may be obtained due to different requirements in data inputs and processing steps (Meyer et al., 2020).

4. Copyright permissions

Following figures in this thesis included illustrations from other publications, and I have been granted copyright permissions to reuse them. Below is a list of copyright permissions, and full Licenses are shown afterwards:

1. Figures 1.3A-B were adapted from Figure 1 published by Stanley and Abdel-Wahab (2022). The copyright permission was granted on 5 August 2022 by the publisher Springer Nature (License number: 5362520671491).
2. Figure 1.3C was taken from Figure 1(A) published by Wang and Aifantis (2020). The copyright permission was granted on 5 August 2022 by the publisher Elsevier (License number: 5362520856667).
3. Figures 1.4 and 1.5 were taken from Figure 1(a) and Figure 3 from the review paper I published on the British Journal of Pharmacology (Xu et al., 2020b). I was the leading author and the publisher allows me to reuse my illustrations without requesting permission formally.
4. Figure 4.1A was taken from Fig. 1 published by Lusk et al. (2021). The copyright permission was granted on 6 September by the Copyright Clearance Center, Inc. on behalf of the Royal Society of Chemistry (License ID: 1265811-1).

Appendix

5. Appendix Figure 3 was taken from the graphical abstract published by Meyer et al. (2019). The copyright permission was granted on 5 August 2022 by the publisher Elsevier (License number: 5362521087392).
6. Appendix Figure 4 was taken from Figure 7a published by Twarog et al. (2016). The copyright permission was granted on 5 August 2022 under the Creative Commons Attribution 4.0 License.

Appendix

SPRINGER NATURE LICENSE TERMS AND CONDITIONS

Aug 05, 2022

This Agreement between Mr. Yuewei Xu ("You") and Springer Nature ("Springer Nature") consists of your license details and the terms and conditions provided by Springer Nature and Copyright Clearance Center.

License Number	5362520671491
License date	Aug 05, 2022
Licensed Content Publisher	Springer Nature
Licensed Content Publication	Nature Cancer
Licensed Content Title	Dysregulation and therapeutic targeting of RNA splicing in cancer
Licensed Content Author	Robert F. Stanley et al
Licensed Content Date	May 27, 2022
Type of Use	Thesis/Dissertation
Requestor type	academic/university or research institute
Format	print and electronic
Portion	figures/tables/illustrations
Number of figures/tables/illustrations	1
High-res required	no
Will you be translating?	no
Circulation/distribution	1 - 29
Author of this Springer Nature content	no
Title	Targeting RNA splicing by indisulam (to be decided)
Institution name	n/a
Expected presentation date	Jun 2023
Order reference number	Stanley 2022, Fig 1
Portions	Figure1a and b
Requestor Location	Mr. Yuewei Xu Hammersmith Campus Du Cane Road Imperial College London London, W12 0NN United Kingdom Attn: Mr. Yuewei Xu
Total	**0.00 GBP**
Terms and Conditions	

Springer Nature Customer Service Centre GmbH
Terms and Conditions

This agreement sets out the terms and conditions of the licence (the **Licence**) between you and **Springer Nature Customer Service Centre GmbH** (the **Licensor**). By clicking 'accept' and completing the transaction for the material (**Licensed Material**), you also confirm your acceptance of these terms and conditions.

1. Grant of License

1. 1. The Licensor grants you a personal, non-exclusive, non-transferable, world-wide licence to reproduce the Licensed Material for the purpose specified in your order only. Licences are granted for the specific use requested in the order and for no other use, subject to the conditions below.

Appendix

ELSEVIER LICENSE
TERMS AND CONDITIONS

Aug 05, 2022

This Agreement between Mr. Yuewei Xu ("You") and Elsevier ("Elsevier") consists of your license details and the terms and conditions provided by Elsevier and Copyright Clearance Center.

License Number	5362520856667
License date	Aug 05, 2022
Licensed Content Publisher	Elsevier
Licensed Content Publication	Trends in Cancer
Licensed Content Title	RNA Splicing and Cancer
Licensed Content Author	Eric Wang,Iannis Aifantis
Licensed Content Date	Aug 1, 2020
Licensed Content Volume	6
Licensed Content Issue	8
Licensed Content Pages	14
Start Page	631
End Page	644
Type of Use	reuse in a thesis/dissertation

Appendix

Portion	figures/tables/illustrations
Number of figures/tables/illustrations	1
Format	both print and electronic
Are you the author of this Elsevier article?	No
Will you be translating?	No
Title	Targeting RNA splicing by indisulam (to be decided)
Institution name	n/a
Expected presentation date	Jun 2023
Order reference number	Wang 2020 Fig 1A alternative splicing
Portions	Figure 1a
Requestor Location	Mr. Yuewei Xu Hammersmith Campus Du Cane Road Imperial College London London, W12 0NN United Kingdom Attn: Mr. Yuewei Xu
Publisher Tax ID	GB 494 6272 12
Total	0.00 GBP

Appendix

CCC Marketplace

This is a License Agreement between Yuewei Xu / Imperial College London ("User") and Copyright Clearance Center, Inc. ("CCC") on behalf of the Rightsholder identified in the order details below. The license consists of the order details, the Marketplace Order General Terms and Conditions below, and any Rightsholder Terms and Conditions which are included below.

All payments must be made in full to CCC in accordance with the Marketplace Order General Terms and Conditions below.

Order Date	06-Sep-2022	Type of Use	Republish in a thesis/dissertation
Order License ID	1265811-1		
ISSN	2515-4184	Publisher	Royal Society of Chemistry
		Portion	Image/photo/illustration

LICENSED CONTENT

Publication Title	Molecular Omics	Start Page	819
Article Title	Models for measuring metabolic chemical changes in the metastasis of high grade serous ovarian cancer: Fallopian tube, ovary, and omentum	End Page	832
		Issue	6
		Volume	17
Date	01/01/2018		
Rightsholder	Royal Society of Chemistry		
Publication Type	Journal		

REQUEST DETAILS

Portion Type	Image/photo/illustration	Distribution	U.K. and Commonwealth (excluding Canada)
Number of images / photos / illustrations	1	Translation	Original language of publication
Format (select all that apply)	Print, Electronic	Copies for the disabled?	No
Who will republish the content?	Academic institution	Minor editing privileges?	No
Duration of Use	Current edition and up to 5 years	Incidental promotional use?	No
Lifetime Unit Quantity	Up to 499	Currency	GBP
Rights Requested	Main product		

NEW WORK DETAILS

Title	PhD candidate	Institution name	Imperial College London
Instructor name	Yuewei Xu	Expected presentation date	2022-12-01

ADDITIONAL DETAILS

Order reference number	HGSOC metastasis	The requesting person / organization to appear on the license	Yuewei Xu / Imperial College London

REUSE CONTENT DETAILS

Title, description or numeric reference of the portion(s)	PhD thesis	Title of the article/chapter the portion is from	Models for measuring metabolic chemical changes in the metastasis of high grade serous ovarian cancer: Fallopian tube, ovary, and omentum
Editor of portion(s)	Lusk, Hannah; Burdette, Joanna E; Sanchez, Laura Margaret	Author of portion(s)	Lusk, Hannah; Burdette, Joanna E; Sanchez, Laura Margaret
Volume of serial or monograph	17	Issue, if republishing an article from a serial	6
Page or page range of portion	819-832	Publication date of portion	2021-12-06

Appendix

ELSEVIER LICENSE
TERMS AND CONDITIONS

Aug 05, 2022

This Agreement between Mr. Yuewei Xu ("You") and Elsevier ("Elsevier") consists of your license details and the terms and conditions provided by Elsevier and Copyright Clearance Center.

License Number	5362521087392
License date	Aug 05, 2022
Licensed Content Publisher	Elsevier
Licensed Content Publication	Cell Systems
Licensed Content Title	Quantifying Drug Combination Synergy along Potency and Efficacy Axes
Licensed Content Author	Christian T. Meyer,David J. Wooten,B. Bishal Paudel,Joshua Bauer,Keisha N. Hardeman,David Westover,Christine M. Lovly,Leonard A. Harris,Darren R. Tyson,Vito Quaranta
Licensed Content Date	Feb 27, 2019
Licensed Content Volume	8
Licensed Content Issue	2
Licensed Content Pages	28

Appendix

Start Page	97
End Page	108.e16
Type of Use	reuse in a thesis/dissertation
Portion	abstract
Format	both print and electronic
Are you the author of this Elsevier article?	No
Will you be translating?	No
Title	Targeting RNA splicing by indisulam (to be decided)
Institution name	n/a
Expected presentation date	Jun 2023
Order reference number	musyc model
Requestor Location	Mr. Yuewei Xu Hammersmith Campus Du Cane Road Imperial College London London, W12 0NN United Kingdom Attn: Mr. Yuewei Xu
Publisher Tax ID	GB 494 6272 12
Total	0.00 GBP

Terms and Conditions